INTERPRETATION OF LOAD TRANSFER MECHANISM FOR PILES IN UNSATURATED EXPANSIVE SOILS

by

Yunlong Liu

Thesis submitted to the
Faculty of Graduate and Postdoctoral Studies
in partial fulfillment of the requirements
for the Doctor in Philosophy degree in Civil Engineering
Department of Civil Engineering
Faculty of Engineering
University of Ottawa
Ottawa, Ontario, Canada

© Yunlong Liu, Ottawa, Canada, 2019

ABSTRACT

Water infiltration associated with natural precipitation events or other artificial activities such as pipe leaks in expansive soils significantly influence the engineering properties; namely, coefficient of permeability, shear strength and volume change behavior. For this reason, it is challenging to design or construct geotechnical infrastructure within or with expansive soils. Several billions of dollars losses, world-wide, can be attributed to the repairing, redesigning and retrofitting of infrastructure constructed with or within expansive soils, annually. Piles are widely used as foundations in expansive soils extending conventional design procedures based on the principles of saturated soil mechanics. However, the behavior of piles in unsaturated expansive soils is significantly different from conventional non-expansive saturated soils. Three significant changes arise as water infiltrates into expansive soil around the pile. Firstly, soil volume expansion contributes to ground heave in vertical direction. Secondly, volume expansion restriction leads to development of the lateral swelling pressure resulting in an increment in the lateral earth pressure in the horizontal direction. Thirdly, pile-soil interface shear strength properties change due to variations in water content (matric suction) of the surrounding soil. These three changes are closely related to matric suction variations that arise during the water infiltration process. For this reason, a rational methodology is necessary for the pile load transfer mechanism analysis based on the mechanics of unsaturated soils.

Studies presented in this thesis are directed towards developing simple methods to predict the load transfer mechanism changes of piles in expansive soils upon infiltration. More emphasis is directed towards the prediction of the pile mechanical behavior which includes the pile head load-displacement relationship, the pile axial force (shaft friction) distribution and the pile base resistance using unsaturated mechanical as a tool. The function of matric suction as an independent stress state variable on the mechanical behavior pile is highlighted. More specifically, following studies were conducted:

(i) Previous studies on various factors influencing the load transfer mechanisms of piles in unsaturated expansive soils are summarized and discussed to give a background of current research. More specifically, state-of-the-art reviews are summarized on the application of piles in expansive soils, mobilization of lateral swelling pressure, mobilization of unsaturated pile-soil interface shear strength and methods available for the load transfer analysis of piles in expansive soils.

(ii) Employing unsaturated soil mechanics as a tool, theoretical methods are proposed for estimating the lateral earth pressure variations considering the mobilization of lateral swelling pressure. The proposed methods are verified using two large-scale laboratory studies and two field studies from published literatures.

(iii) The shear displacement method and load transfer curve methods used traditionally for pile load transfer mechanisms analysis for saturated soils were modified to extend their applications for unsaturated expansive soils. The influence of volume change characteristics and unsaturated soil properties on unsaturated expansive soils are considered in these methods. The validation of the modified shear displacement method and modified load transfer curve method were established using a large-scale model test performed in the geotechnical engineering lab of University of Ottawa and a field case study results from the published literature.

(iv) A large-scale model pile infiltration test conducted in a typical expansive soil from Regina in Canada in the geotechnical lab of University of Ottawa is presented and interpreted using the experimental data of volumetric water content suction measurements and shear strength data. The results of the comprehensive experiment studies are also used to validate the proposed modified shear displacement method and modified load transfer curve method achieving reasonable good comparisons.

The proposed modified shear displacement method and modified load transfer curve method are simple and require limited number soil properties including the soil water characteristic curve (SWCC), matric suction profile upon wetting and drying and some soil physical properties. Due to these advantages, they can be easily and conveniently applied in engineering practice for prediction of the mechanical behavior of piles in unsaturated expansive soils, which facilitate practicing engineers to produce sound design of pile foundation in unsaturated expansive soils in a simplistic manner.

LIST OF CONTENTS

LIST OF FIGURES

LIST OF TABLES

ACKNOWLEDGMENTS

Studies presented in this thesis were conducted at the Department of Civil Engineering, University of Ottawa under the supervision of Prof. Sai K. Vanapalli. I am proud to say that Dr. Vanapalli is not only my supervisor, but also my Guruji for my research as well as my life. His encouragement, insightful suggestions, and continuous supports have enlightened my way towards exploring the mysteries of unsaturated soils and have broadened my horizon and vision. His critical comments, constant encouragement and guidance have greatly enlightened me not only on the academic pursuit but also on the morals of being a human being. Without his consistent and illuminating instruction, both this thesis and I could not have reached its present stage.

The financial supports received from the China Scholarship Council (CSC) - University of Ottawa joint scholarship, the Natural Sciences and Engineering Research Council of Canada (NSERC), I really appreciate the support from my homeland and university.

My appreciations extend to my colleagues at the University of Ottawa for their friendship, company and support. These individuals include; Celestin, Won, Hana, Zhonghan, Shunchao, Mohammed, Ping, Hongyu, Junping, Penghai, Jiaying, Xueming, Xiaokun, Xiuhan.

I am extremely thankful for my parents, who wholeheartedly encouraged their only child to go Canada to pursue his studies and dreams, and supported his every decision in his life. They have been courageous in accepting several challenges during the last four years, without their grownup son at home. This thesis would not have been possible without their love, support and inspiration. I humbly dedicate this thesis to my parents.

CHAPTER ONE

INTRODUCTION

1.1 Background

Vast deposits of expansive soils are widely distributed in several countries of six of the seven continents of the world. Some of these countries include Canada and United States from North America, Argentina from South America; Sudan and Algeria from Africa, China, India and Israel from Asia; Spain and United Kingdom from Europe and Australia from Australia (Chen 1988; Al-Rawas and Qamaruddin 1998; Rao and Reddy et al. 2001). Expansive soils are typically referred to as problematic soils in the literature because their mechanical behavior is highly sensitive to the changes in their natural water content associated with environmental factors such as the infiltration and evaporation. Ground heave or settlement contribute to severe distress to various infrastructure constructed in expansive soil due to the changes in their natural water content and result in significant economic losses to building industry (Gourley et al. 1993; Jaremski 2012). Studies by Adem and Vanapalli (2016) suggest that the economic losses associated with expansive soils have been significantly increasing during the past five decades all over the world, the losses in USA alone is estimated to be several billions of dollars.

Among various choices that are available as foundations for infrastructure placed in expansive soils, pile foundations are typically preferred (Al-Rawas and Goosen 2006). Typically, piles can be used in expansive soils as micropiles in the active zone or as group pile foundations. Micropiles reduce ground heave in the top layer of expansive soil in addition to providing support as foundation to the infrastructure constructed in expansive soils (Nelson et al. 2015). Typically small diameter steel piles (75 to 250 mm in diameter) are inserted in predrilled holes of larger diameter, which are then filled with compacted sand to improve the frictional resistance of micropiles (Nusier and Alawneh 2004). Upon infiltration, heave is significantly reduced by the friction mobilized at the pile-soil interface. Micropile reinforcement technique is a rational choice to mitigate damages of lightly loaded structures on thin layer expansive soils with limited swelling potential. However, for heavy structures on thick expansive soil with high to very high swell potential, pile or group pile foundation are typically favored.

Piles with high strength and stiffness can penetrate through active zone (depth of expansive soil layer in which moisture content changes are sensitive to environmental factors associated with infiltration and evaporation) in expansive soil and are placed on rigid bedrock or lower stable soil stratum. Such a pile foundation system not only has a significant bearing capacity but also can effectively control the non-uniform settlement, even when the mechanical behavior of shallow expansive soil layer experience significant changes under extreme conditions (heave and settlement). Two kinds of pile foundations are commonly used in engineering practice; namely, single pile (drilled pile, pushing pile) (Poulos and Davis 1980; O'Neill 1988) or group pile foundation (helical pile, precast pile) (Ekshtein 1978). Pile foundation with diameters greater than 800 mm are typically cast in-situ. In some scenarios, in order to increase the bearing capacity of the pile foundation, belled pile which enlarges at the end is used. For enhancing integrity of group pile foundation, grade beams which link the pile top is set to form a pile grade beam foundation system are used. Such a pile system is more reliable to prevent the non-uniform settlement and tilt of the super structure.

The design of pile foundation are conventionally based on saturated soil mechanics assuming drained condition (effective stress). However, for most cases the soil surrounding the pile is in an unsaturated state. The in-situ matric suction of expansive soils significantly influences the mechanical behavior of the piles. The load transfer mechanism of pile foundation is sensitive to matric suction changes associated with environmental factors (i.e. infiltration and evaporation of water).

As shown in Figure 1.1, upon evaporation, the matric suction in the active zone increases due in comparison to the hydrostatic matric suction profile. On the contrary, matric suction in the active zone decreases upon infiltration.

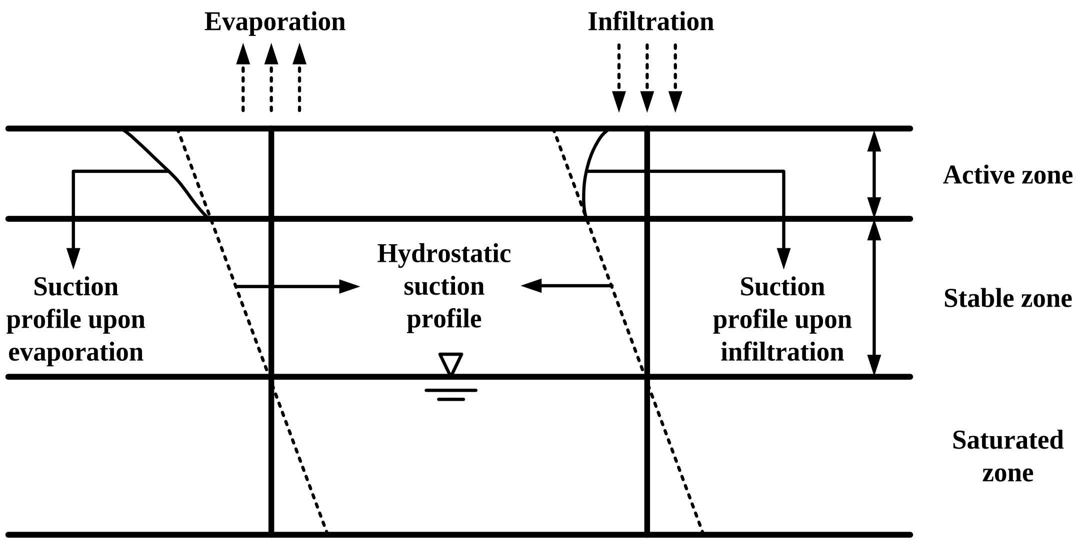

Figure 1.1 Variation of matric suction profile in a typical unsaturated expansive soil under the influence of environmental factors

For a single pile installed in expansive soil, the changes in load transfer mechanism before and after infiltration are illustrated in Figure 1.2. Prior to infiltration, positive friction is distributed along the entire length of the pile and bears the upper load along with the end bearing capacity [as shown in Figure 1.2(A)]. As water infiltrates into the active zone [as shown in Figure 1.2(B)], changes mainly occur in three aspects: in vertical direction, volume expansion of expansive soil causes ground heave. In the horizontal direction, restricted volume expansion produces lateral swelling pressure. The pile-soil interface strength properties changes due to variations in the water content (matric suction) of surrounding soil. Due to these changes, in the active zone (the depth influenced by water infiltration), uplift friction generates along the pile as a result of displacement between the pile and adjacent soil (i.e., soil swells and moves upward relative to the pile). The magnitude of the uplift friction is determined by the increasing lateral earth pressure considering the contribution of lateral swelling pressure and the water content (matric suction)-dependent interface strength properties. A pile under a light loaded structure may get uplifted due to the uplift friction contribution. Once the pile has an upward movement, negative friction generates in the stable zone and the pile base bearing capacity decreases significantly. The net contribution that arises from negative shaft friction, end bearing capacity and applied load combine to balance the increased uplift shaft friction.

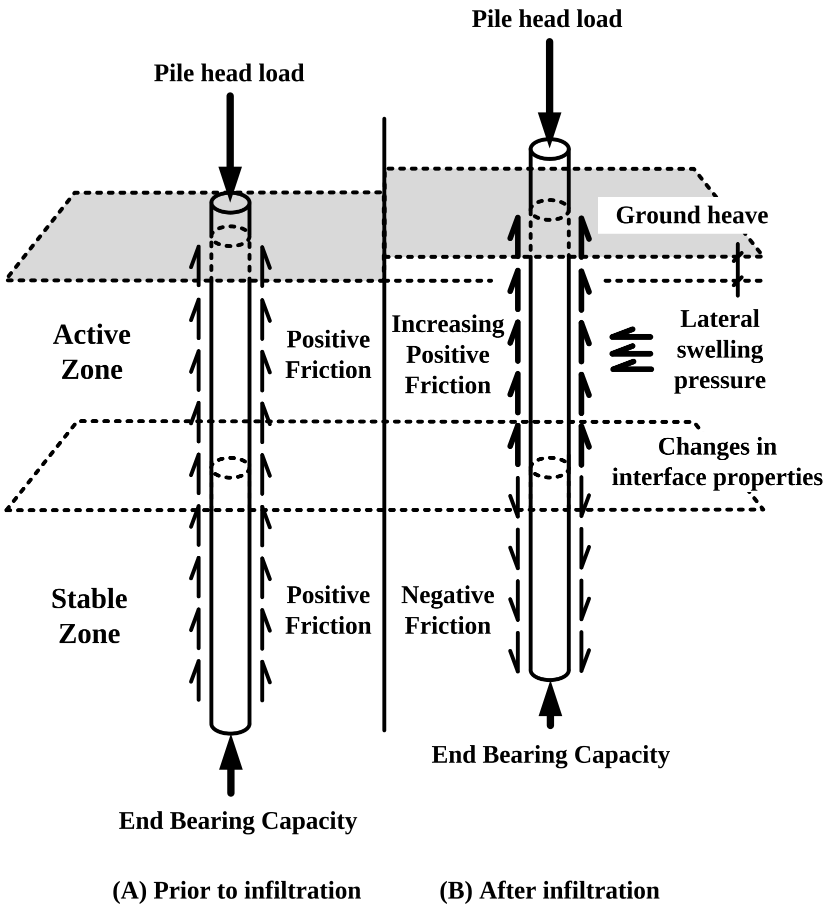

Figure 1.2 Mechanical behavior changes of a pile in expansive soil before and after infiltration

Piles as foundation typically penetrate through active zone and rest on bedrock or extend into soil layers with higher stiffness. In other words, mechanical behavior of the soil under the pile end is no longer influenced by seasonal water content changes. The variations in the load transfer mechanism of pile upon infiltration are mainly associated to the variations of shaft friction in the active zone. The shaft friction in the active zone is determined by four factors including the net normal stress (lateral earth pressure), matric suction, interface shear strength properties and the pile-soil relative displacement. In the infiltration process, mobilization of lateral swelling pressure can add an increment to the lateral earth pressure due to soil unit weight and surcharge. The pile-soil interface shear strength properties decrease with a decrease in matric suction. Ground heave also changes the pile-soil relative displacement. Considering these changes associated with the water infiltration process, the traditional shear displacement method and load transfer curve method for the analysis of the load transfer mechanism of the pile is modified to extend their application in expansive soils. Proposed methods are verified using case studies from the published literature and a large scale model pile test conducted in the geotechnical engineering laboratory of the University of Ottawa. The results of these studies suggest that there is a reasonable comparisons between the measured and predicted results. Proposed methods are simple yet powerful tools for the estimation of mechanical behaviors of single pile in expansive soil upon water infiltration, which facilitate geotechnical engineers to provide rational design of pile foundations in various regions of the world with expansive soils.

1.2 Objectives

The present study aims at developing methods based on the mechanics of unsaturated soils to rationally interpret and estimate the load transfer mechanism variations of a single pile in expansive soil upon infiltration. The traditional shear displacement method and load transfer curve method are modified for the analysis of variations in the mechanical behaviors of a single pile in expansive soil upon water infiltration. Using the matric suction profile prior to and after water infiltration, a theoretical method is proposed to estimate the mobilization of lateral swelling pressure against fixed retaining structures and pile in expansive soil. These two methods are combined used for the pile load transfer analysis. Employing the modified shear displacement method, the pile head load-displacement relationship was achieved. The modified load transfer curve method is more comprehensive which has the ability to show changes in the pile shaft friction distribution, pile end bearing capacity, pile head and end movement in the infiltration process. The proposed methods are simple in formulation and require only limited soil parameters to be determined from conventional experimental studies.

1.3 Novelty

Currently, there is limited understanding of the comprehensive behavior of piles in expansive soils (Nelson et al. 2015). For this reason, it is usually recommended to conduct in-situ tests (MOHURD 2013) or perform numerical analysis to better understand the complexities associated with the mechanical behaviors of piles in expansive soils (Ellison et al. 1971; Justo et al. 1984; Chen 1988; Nelson et al. 2015). However, in-situ pile testing is usually expensive and time-consuming while numerical analyses require complex constitutive relationships which need many soil parameters. For engineering practice applications, a quick, simple and acceptable approach is required for the analysis of mechanical behaviors of pile foundation associated with water infiltration.

The study undertaken through this thesis is a pioneering contribution to analyze load transfer mechanism extending the state-of-the-art understanding of the mechanics of unsaturated soils. The novelty of the methods that are introduced in this thesis are summarized below:

- A theoretical method is proposed for the estimation of the lateral earth pressure considering lateral swelling pressure upon water infiltration. The active and passive earth pressures are considered as the boundaries for the lateral earth pressure variations under different degree of saturation in the analysis. More importantly, the influence of soil-pile interface roughness and changes in matric suction is considered in the analyses of results extending the mechanics of unsaturated soil mechanics.

- Traditional shear displacement method is modified from two aspects: (1) By dividing the pile into several segments, the pile-soil relative displacement variations at different depth due to the ground heave are taken into account; (2) Theoretical model is proposed for the estimation of the shear modulus (G) at different matric suction condition. The modified shear displacement method is relatively simple and is found to a valuable tool to predict the pile head load displacement relationship and pile mechanical behaviors including the pile shaft friction distribution, the pile end bearing capacity, the pile head and end settlement.

- A unified load transfer curve model relating the pile shaft friction and pile-soil relative displacement are modified considering following factors: (1) the increased lateral earth pressure due to mobilization of lateral swelling pressure; (2) both peak and residual pile-soil interface shear strength corresponding to different matric suction; (3) the pile-soil relative displacement variations due to the ground heave. Extending the modified 12-step load transfer curve method, various mechanical behaviors of pile were estimated similar to the modified shear displacement method. Compared to the modified shear displacement method, the modified load transfer curve method is comprehensive; however, it is capable to provide more reliable estimations.

- A large scale pile infiltration test in expansive soils was conducted and presented for studying the variations of mechanical behaviors of a single model pile in unsaturated expansive soil upon infiltration. In the infiltration process, both the water content and matric suction variations at different depths are measured and recorded. Under a certain upper load, the pile head settlement, the pile shaft friction distribution and pile end bearing capacity are measured. Valuable experimental data was acquired from this test which well reflects the disciplines of the load transfer mechanism changes. Experimental data further validate the feasibility of the proposed modified shear displacement method and modified load transfer curve method.

1.4 Thesis lay out

In this thesis, a general introduction is presented introducing the load transfer mechanism of piles in expansive soils in Chapter 1. A comprehensive state-of-the-art literature review on the mobilization of lateral swelling pressure, shear strength behavior of pile-soil interface, methods available in the literature for load transfer analysis of piles in expansive soils are summarized and discussed in Chapter 2.

In Chapter 3, employing unsaturated soil mechanics, a theoretical method is proposed for estimating the mobilization of lateral swelling pressure with respect to a matric suction reduction. This method has been also extended to estimate the variation of lateral earth pressure taking account of the lateral swelling pressure associated with environmental factors (evaporation and infiltration). The proposed method for the evaluation of mobilized lateral swelling pressure with a matric suction reduction is verified using two large-scale laboratory studies and two field studies achieving relative good comparisons.

Chapter 4 summarizes the various factors that influence the lateral earth pressure in expansive soils. These factors include; (i) lateral earth pressure increase due to mobilization of lateral swelling pressure; (ii) variation in peak and residual pile-soil interface shear strength due to matric suction changes associated with environmental factors; (iii) the pile-soil relative displacement variations due to the ground heave. The shear displacement method and load transfer curve methods used traditionally for pile load transfer mechanisms analysis for saturated soils were modified to extend their application for unsaturated expansive soils. The validation of the modified shear displacement method and modified load transfer curve method were established using a large-scale model test and a field case study results from published literature. These methods are simple and can be used in engineering practice applications for predicting the pile mechanical behaviors including the pile head displacement and pile axial force (shaft friction) distribution.

In Chapter 5, a large-scale model pile infiltration tests performed in Regina expansive clay soils conducted in the geotechnical lab of University of Ottawa is summarized. The experimental data acquired from the pile infiltration test provides a complete profile (including suction profile, volumetric water content profile, pile head displacement, ground displacement, pile axial force and pile base resistance) of the pile load transfer mechanism changes during the infiltration process. The experiment results are discussed and analyzed using the mechanics of unsaturated soils. Experiment results are also used for the validation of proposed modified shear displacement method and modified load transfer curve method.

Various conclusions of the research undertaken in this thesis are summarized in Chapter 6. A succinct summary of the future research plans on this research topic is also included in this Chapter.

1.5 Related publications

Journal publications:

[1] **Liu, Y.,** & Vanapalli, S. K. (2017). "Influence of Lateral Swelling Pressure on the Geotechnical Infrastructure in Expansive Soils." *Journal of Geotechnical and Geoenvironmental Engineering*, 143(6), 04017006. (SCI)

[2] **Liu, Y** and Vanapalli, S.K. (2018). Discussion "Closure to "Influence of lateral swelling pressure on the geotechnical infrastructure in expansive soils"." *Journal of Geotechnical and Geoenivronmental Engineering*, 144(7), 070108016.

[3] **Liu, Y**. and Vanapalli, S.K. (2018). "Prediction of lateral swelling pressure behind retaining structure with expansive soil as." *Soils and Foundations* (Accepted for publication). /doi.org/10.1016/j.sandf.2018.10.003 (SCI)

[4] **Liu, Y.** and Vanapalli, S.K. (2018). "Load displacement analysis of a single pile in unsaturated expansive soil upon infiltration." *Computer and Geotechnics* (Accepted for publication). (SCI)

[5] **Liu, Y.** and Vanapalli, S.K. (2018). "Mechanical behaviors of geotechnical infrastructures in expansive soils considering the influence of environmental factors." *Submitted to an International Journal* (under review). (SCI)

[6] **Liu, Y.** and Vanapalli, S.K. (2017). "Simplified shear deformation method for analysis of mechanical behaviors of piles in expansive soils." *Special Issue on Unsaturated Soils in Geotechnical Engineering Journal – SEAGS & AGSSEA.*

Conference publications:

[7] **Liu, Y.** and Vanapalli, S.K. (2017). "Design of retaining wall and single pile in expansive soil using unsaturated soil mechanics as a tool." *Proceeding of PanAm-*

UNSAT 2017: Second Pan-American Conference on Unsaturated Soils (Unsaturated Soil Mechanics for Sustainable Geotechnics). Dallas, USA. (SCI)

[8] **Liu**, Y. and Vanapalli, S.K. (2015). "Estimation of uplift shaft friction of single pile in expansive soil using the mechanics of unsaturated soils.*" Proceeding of the 68th Canadian Geotechnical Conference.* Quebec, Canada

[9] **Liu, Y.**, Vanapalli, S. K. and Amina, W. (2017). "Load-deformation Analysis of a Pile in Expansive Soil upon Infiltration." *Proceedings of the 2nd World Congress on Civil, Structural, and Environmental Engineering (CSEE'17)*, Barcelona, Spain.

[10] **Liu, Y.** and Vanapalli, S.K. (2017). "Modified shear deformation method for analyzing the load-displacement response of a single pile in expansive soil upon infiltration." *Proceeding of the 70th Canadian Geotechnical Conference*. Ottawa, Canada.

[11] **Liu, Y.** and Vanapalli, S.K. (2018). "Testing of unsaturated soil-steel interface shear strength." *In proceedings of the 7th International Conference on Unsaturated soils*, Hong Kong.

CHPATER TWO

LITERATURE REVIEW

Notation

Symbols	
A_s	Pore pressure parameter which can be evaluated from triaxial testing
b_{dia}	Diameter of the pier
c_{aho}	Adhesion intercept, and can be defined as $c_{aho}=c_a'+(u_{af}-u_{wf})tan\delta^b$
c'_a	Effective interface cohesion
d_z	Calculating depth
d_{z0}	Unit depth
E	Elastic modulus with respect to net normal stress
f_H	Factor ranging from $1/\theta$ to 1 depending on degree of saturation
G	Shear modulus of soil
G_b	Shear modulus of the pile-end soil
h_i	Initial matric suction
h_f	Final matric suction
h_0	Active zone or the maximum depth that the water can be immersed into
H	Elastic modulus with respect to matric suction
K_0	Coefficient of at rest earth pressure, $K_0\approx 1-sin\phi'$ for normally consolidated soil (Jaky 1944); $K_0\approx(1-sin\phi')\text{OCR}^{sin\phi'}$ for over consolidated soil (Mayne and Kulhawy 1982)
L	Pile length
OCR	Overconsolidation ratio
P_{LS}	Lateral earth pressure considering the influence of lateral swelling pressure
P_{CNS}	Lateral earth pressure of cohesive non-swelling (CNS) material for the corresponding depth
P_{SW}	Lateral swelling pressure of oven-dry expansive soil at constant volume condition
P_0	At rest earth pressure
P_p	Passive earth pressure
P_L	Lateral swelling pressure under partially saturated condition
$P_{LS(max)}$	Maximum lateral swelling pressure from laboratory tests
P_K	Soil capillary pressure before test
r	Distance from the center of the pile

r_0	Radius of pile
r_m	Distance form pile axis to somewhere that the deformation of soil can be ignored
r_b	Radius of the pile end
S_{ult}	Ultimate shearing resistance
u_r	Radial displacement
u_φ	Circumferential displacement
u_{wf}	Water pressure at failure
u	Radius displacement
u_w	Water pressure
w	Vertical displacement
$w_{p1}(z)$	Displacement of pile
z_H	Depth of calculating point
α_{fl}	Adhesion used in Fleming et al. (2006)
α_{sh}	Adhesion used in Sharma et al. (2007)
α_J	Coefficient of water content, which is the ratio of the lateral swelling pressure at current water to the water content at maximum lateral swelling pressure
α_N	Parameter varies form 0.7 (Sapaz 2004) to 1 (Katti et al. 2002);
β_J	Coefficient of deformation, which is ratio of current deformation to the deformation at maximum lateral swelling pressure
ξ	Effective parameter of the pile radius ξ is $\ln(r_m/r_0)$
γ_σ	Mean principle stress compression index
γ_h	Matric suction compression index
γ_t	Unit weight of soil
$\Delta(u_a - u_w)$	Matric suction variation
ε_h	Horizontal swelling strain
θ	Volumetric water content
θ_s	Volumetric water content at a saturation of 100%
θ_r	Residual volumetric water content
σ_{im}	Initial values of mean principle stress
σ'_s	Effective vertical stress
σ_s	Total vertical stress
σ_{nf}	Normal stress at failure
τ_{xy}	Shear stress on the x-plane in the y-direction (i.e., $\tau_{xy} = \tau_{yx}$)
τ_{yz}	Shear stress on the y-plane in the z-direction (i.e., $\tau_{yz} = \tau_{zy}$)
τ_{zx}	Shear stress on the z-plane in the x-direction (i.e., $\tau_{zx}= \tau_{xz}$)

$\tau_{\varphi r}$	Circumferential strain
$\tau_{r\varphi}$	Radial strain
τ_{unsat}	Unsaturated interface shear strength
τ_0	Shear stress at the interface of soil-pile
τ_{sp}	Shear stress between soil and the pier
δ'	Interface friction angle with respect to net normal stress
δ^b	Interface friction angle with respect to matric suction
δ_{sh}	Angle of shearing resistance at the soil-geomembrane interface
$\delta_{relative}$	Pier soil relative displacement
χ_{sh}	A parameter whose value ranges from 0 to 1
ψ_{ihy}	Interface dilation angle
η	Effective parameters of pile-end displacement, generally η=0.5-1.0 (Xiao et al. 2003)
ϕ'	Effective internal friction angle of soil
υ	Poisson's ratio
$(\sigma_{nf} - u_{af})$	Net normal stress at failure
$(u_{af} - u_{wf})$	Matric suction at failure
$(\sigma_r - u_a)$	Net normal stress in radial direction
$(\sigma_\varphi - u_a)$	Net normal stress in circumferential direction
$(\sigma_x - u_a)$	Net normal stress in *x* direction
$(\sigma_y - u_a)$	Net normal stress in *y* direction
$(\sigma_z - u_a)$	Net normal stress in *z* direction
$(u_a - u_w)$	Matric suction

2.1 Introduction

Pile foundations as typical deep foundation are widely used in engineering practice due to its high bearing capacity and high stiffness. Piles that penetrate weak soil layers and rest on rigid bedrock or lower stable soil stratum not only provide a relatively high bearing capacity and assure non-uniform settlement. They also ensure the stability of super structure when the shallow soil layers lose their strength. In addition, these foundations safely carry the load from the superstructure including their self-weight, the horizontal load produced by wind or earthquake. Typically, the high stiffness of pile in both vertical and horizontal directions keep the structure stable and limit the non-uniform settlement and tilt within the allowable range prescribed by design codes. Due to these advantages, the pile foundation are widely chosen to combat the problems deduced by expansive soils. In this chapter, a comprehensive reviews on the use of piles in expansive soils are introduced first, followed by analysis on the mechanical behavior variations of piles in expansive soils upon water infiltration. Detailed discussions are provided on several key factors that influence the load transfer mechanism of piles in expansive soils such as the mobilization of lateral swelling pressure, the pile-soil interface shear strength and the available load transfer analysis methods collected from literatures.

2.1.1 Application of Piles in Expansive Soils

Piles in expansive soils can be classified into different categories. Based on construction method, piles in expansive soils can be classified into two types; namely, driven pile and cast in-situ pile. The precast piles greatly accelerate the construction progress of driven piles. So this technique is widely used in areas where the construction duration is limited. For example, most projects constructed on expansive soils in Africa must be completed in the dry season to avoid the possible hazards triggered by intense precipile infiltration testation during rainy season. However, the main drawback which prevents the more widely application of driven piles in expansive soils is that sometimes piles could hardly be driven to a desired design depth. Mature technology and additional measures should be undertaken to ensure the accuracy of this technique. For this reason, cast in-situ piles are typically preferred. Chen (1988) stated that one of in-situ cast piles, drilled pier, has been widely used to combat the problems associated with expansive soils in Rocky Mountain area of Colorado in USA.

Piles in expansive soils could be divided into three categories based on the depth of penetration. In the first category of piles, the whole pile is set in expansive soil layer. Both the shaft friction and the end-bearing capacity are significantly influenced by the swelling and shrinkage behaviors of expansive soils. Especially in the swelling process, uplift friction may arise along the entire pile length and lead to the upward movement of the pile. In these type of piles, the end-bearing capacity drops sharply and some scenarios it could be negligible. In the second category of piles, the pile body is set in the expansive soil layer while the pile end is on the stiff soil layer. End-bearing capacity is maintained by rigid soil layer but shaft friction is significantly influenced by volume changes of expansive soils. In the third category of piles, a major portion of pile length is in the active zone and the remainder is in the stiff soil layer. Figure 2.1(A to C) shows these three kinds of piles in expansive soils respectively.

The first category of piles is commonly used in micro-pile reinforcement technique which makes full use of shaft frictions to control the heave of expansive soils. In engineering practice, a thin sand layer is usually used to cover the pile surface to increase the friction resistance (Nusier et al. 2007). The second and the third category of piles are often used as pile foundation or pier foundation. There are mainly two features differing pier foundation from pile foundation. The pier foundation usually has a larger diameter which is typically larger than 800mm. The other difference is that piers need to be casted in-situ. However, generally piers can be treated as piles with large diameters. Piles such as the helical pile, precast pile and piers are similar to drilled piers. Piers are widely applied in engineering practice to increase the bearing capacity of the pier. For example, belled pier shown in [Figure 2.1(E)] enlarged base at the end of straight pier is often used. Also, in order to enhance the integrity of pile foundation, grade beams are usually added to pile foundations. They together form a pile grade beam foundation system [Figure 2.1(F)] which is more reliable to prevent the non-uniform settlement and tilt of the upper structures. In this study, main attention will focus on pier foundation, or large diameter single pile foundation.

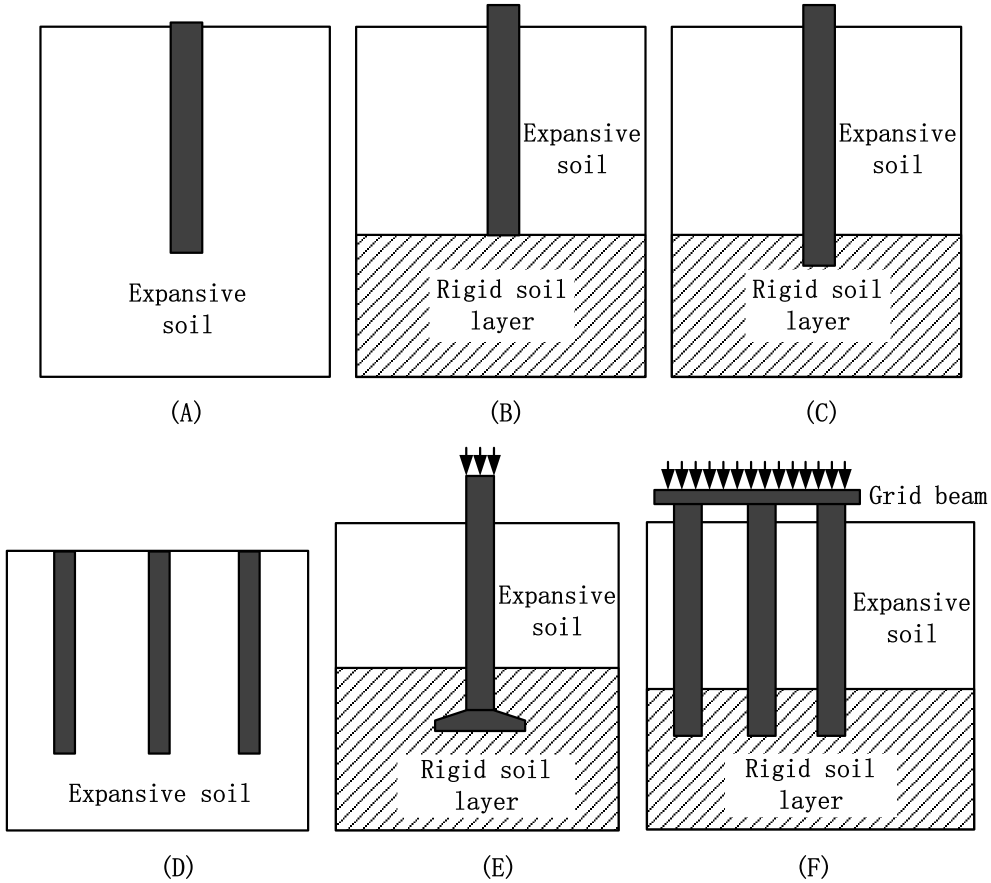

Figure 2.1 Different kinds of piles in expansive soils [(A) Whole pile in expansive soil; (B) Pile ends at rigid soil layer; (C) Part of pile in rigid soil layer; (D) Micropile reinforcement technique; (E) Belled pile foundation; (F) Pile and grad beam system]

2.1.2 Influence of water infiltration on the mechanical behaviors of pile foundations in expansive soils

In conventional soils, which are typically not expansive in nature, it is generally recognized that the total bearing capacity of pile foundation comprises end-bearing capacity and shaft friction. However, the contribution arising from end-bearing and shaft friction may vary significantly due to the influence of swelling or shrinkage behavior in expansive soils. The soil layer in which piles penetrate could also be divided into two parts; the top layer is typically active zone, which includes expansive soil layers influenced by moisture migration. The layer below this zone is considered to be stable zone including certain thickness of expansive soils which will not be affected by moisture migration.

The increasing water content in active zone may cause the bearing capacity loss of pile foundation. Mainly two factors are responsible for this phenomenon: the first factor is associated with the decrease in soil strength properties when the water content of expansive soil experiences an increase upon flooding or heavy rain. Compared with the soil with natural water content, the bearing capacity of a foundation upon flooding will reduce 1.5 to 2 times in the bearing capacity. However, this phenomenon is gradually weakened with an increase in the pile length. The second factor is associated with the uplift forces. Mostly, these uplift forces arise along the pile length contributing to an increasing positive friction. For piles totally set in expansive soil layer, end-bearing capacity will also be influenced by swelling pressure of expansive soils. It is generally recognized that uplift forces is a combined function of mobilized lateral swelling pressure, pile-soil interface shear strength properties and pile-soil relative displacement. There is a balance between the uplifting force and withholding force. To ensure the safety and stability of the upper structure, enough withholding force must be developed in pile foundations to carry the structural loads as well as the uplifting force (Poulos and Davis 1980). This goal could be achieved through a variety of methods. For instance, when thick expansive clay layers are encountered in practice, engineers could choose to protect the piles from the direct connection with the surrounding expansive clays or reduce the friction coefficient between them to overcome the net effect of uplifting force. Another solution is the application of pile and grade-beam system, this system on the one hand gains the ability to regulate the load distribution. On the other hand, by constructing the infrastructure higher than the ground surface, enough space which is referred to as crawl space is provided to accommodate the potential ground heave of the soil. If there is a provision of crawl space, there is no need to control the vertical deformation of expansive soils.

Drilled pier is a rational choice to combat problems deduced by expansive soils because of its ability to transfer the structural loads to stable material or a stable zone where moisture changes are improbable. However, the design and construction process must be carefully controlled. Drilled piers can be further divided into two categories; if they made with an enlarged base, they are commonly referred to as belled piers. However, when they are made without an enlarged base, they are referred to as straight-shaft piers. In order to increase the bearing capacity, piers drilled into the materials other than bedrock are enlarged at the bottom of the hole to increase the bearing capacity. Generally, the enlarged ends have a diameter equal to three times of the diameter of the pier.

The lateral pressure distribution along a pile in expansive soils upon infiltration is shown in Figure 2.2(A). The lateral earth pressure and the influence surcharge can be analyzed in the same way as saturated soils. Lateral swelling pressure that develops in the active zone is a function of matric suction. Due to this reason, the influence of lateral swelling pressure should be considered by taking account of the variations of matric suction reduction (i.e., from initial to a subsequent state). The typical distribution of shaft friction along a pile is illustrated in Figure 2.2(B). Positive friction in the active zone contributes to the uplift force while negative friction in the stable zone and the surcharge constitute the withholding force.

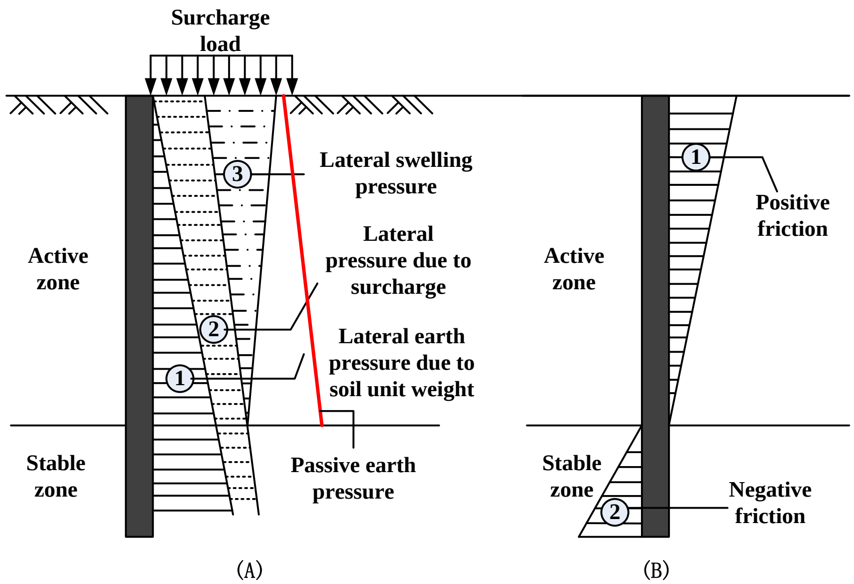

Figure 2.2 Distribution of lateral earth pressure and shaft friction along a pile upon infiltration [(A) Lateral earth pressure; (B) Shaft friction]

Figure 2.3 describes a grade beam and piers system in expansive clay. A lot of information can be extracted from this figure. It is clear that soil in this figure is divided into two layers: active zone and stable zone. Behaviors of soil in active zone are significantly affected by water infiltration. The expansive clay has a low hydraulic conductivity due to high matric suction at initial unsaturated condition. Also, the density in the soil layer at a greater depth is typically higher than the top layer at a shallow depth. Due to these two factors, soils below the active zone is in a relatively stable state as water can hardly reach this zone.

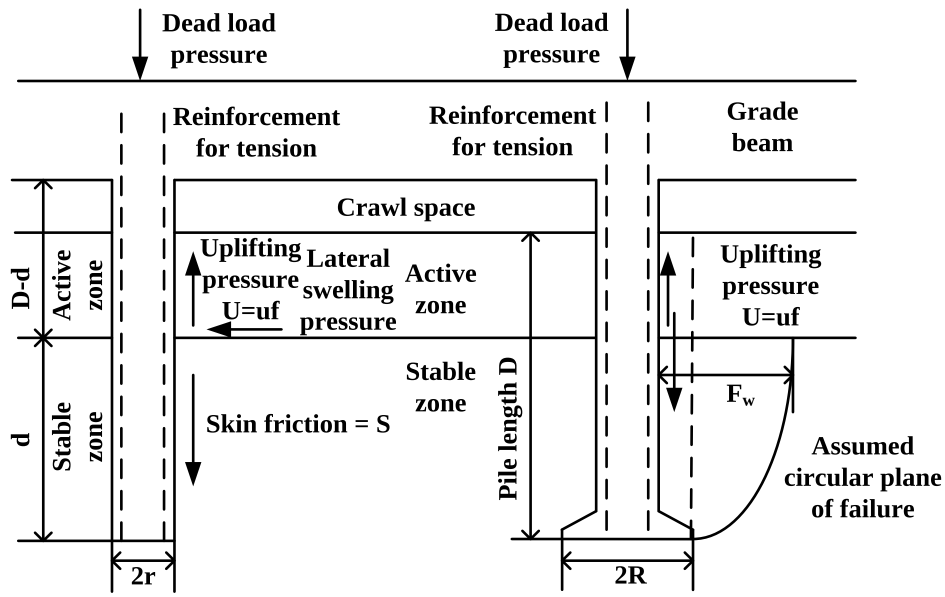

Figure 2.3 Grade beam and pier system (modified from Chen 1988)

The behaviors of pier in these two zones are totally different. If there is no water infiltration, the designs of piers in saturated soils and unsaturated soils will be the same. Also, in most cases piers in unsaturated soils have much higher bearing capacity due to the contribution of matric suction to shear strength. However, when the influence of matric suction is considered the shear strength properties of soils in active zone sharply reduces due to water infiltration. In conventional soils, for example in sandy soils, deformation in soil associated with saturation process can be neglected. The reduction in bearing capacity is only attribution to the reduction the shear strength parameters. However, in expansive clay, along with the decrease in soil strength properties, soil swells as the swelling potential is released by water infiltration. In vertical direction, soil swells freely while in horizontal directions swelling potential turns to swelling pressure as the result of restricted horizontal displacement. These two behaviors derived from soil swelling significantly change the pile behavior within the active zone. The ground heave causes an upward movement of soil surrounding the pile and results in generation of uplift friction, while the mobilization of lateral swelling pressure adds an additional component to the lateral earth pressure. Uplift force generates as the summation of upward shaft friction. End bearing capacity of straight-shaft pile does not work any longer on condition that the soil has been pulled up. Once the balance fails (i.e., the uplift force exceed the withholding force), the upward movement of piers is dangerous and may cause cracks and fractures in the superstructure. For this reason, in engineering practice, piers are typically connected by beams to form a grade-beam system. This technique is useful to reduce the displacement difference between piles. Meanwhile, a crawl space that is usually left between the grade beam system and ground surface to accommodate the potential upward movement, as discussed earlier.

2.2 Literature review on the determination of lateral swelling pressure

As shown in Figure 2.4(A), upon water infiltration, matric suction of the backfill of the retaining wall decreases significantly. As a consequence, mobilization of the lateral swelling pressure causes an increment to lateral earth pressure, which is calculated considering at rest condition prior to infiltration [as shown in Figure 2.4(B)]. However, increase in the lateral earth pressure is limited by the passive earth pressure to avoid shear failure of the soil.

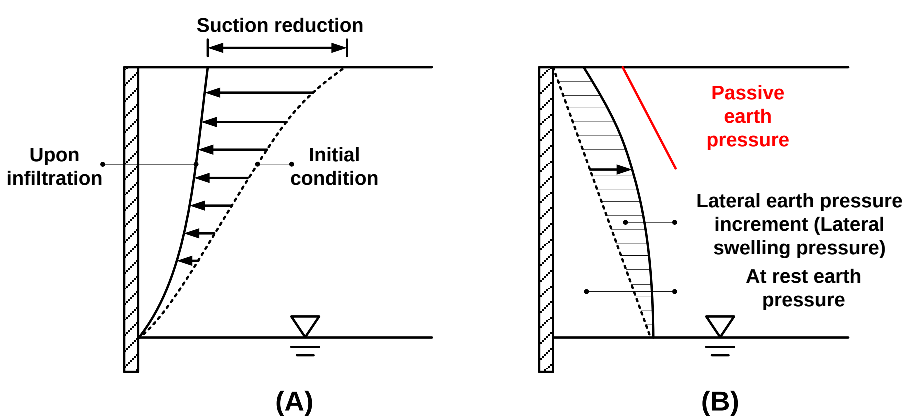

Figure 2.4 Schematic diagram of earth pressure at rest conditions during wetting process behind a retaining wall with expansive soil as backfill material: (A) Variation of matric suction; (B) Influence of lateral pressure on the variation of lateral earth pressure

Problems associated with the lateral swelling pressure of expansive soils received significant research attention over the past several decades (Kassiff and Zeitlen 1962;

Richards and Kurzeme 1973; Moza et al. 1987; Chen 1988; Puppala and Cerato 2009; Nelson et al. 2015). Both laboratory and in-situ techniques are available for determination of the lateral swelling pressure. Several investigators have proposed experimental methods to determine the lateral swelling pressure introducing modifications to the traditional odometer and hydraulic triaxial apparatus (Komornik and Zeitlen 1965; Ofer 1980; Fourie 1988; Dif and Bluemel 1991; Ertekin 1991; Windal and Shahrour 2002; Sapaz 2004; Xie et al. 2007; Sahin 2011; Abbas et al. 2015). Large scale tests and in-situ investigations were also undertaken to determine the lateral earth pressure considering influence of the lateral swelling pressure and understand its influence on the infrastructures (Robertson and Wagener 1975; Ofer 1980; Katti et al. 1983; Symons et al. 1989; Brackley and Sanders 1992; Gu 2005; Mohamed et al. 2013 and Yang et al. 2014).

Measurement of lateral swelling pressure is usually based on two approaches; namely, laboratory tests and in-situ tests (including large scale model tests). Laboratory tests are conventionally conducted using relatively small, cubic or cylindrical specimens and the experimental data are assumed to be representative of the mechanical behavior of in-situ soil. However, compared to laboratory tests, large scale model tests and in-situ tests provide more valuable information which can be used in engineering practice applications with a greater degree of confidence. In this section, details of various testing methods used both in laboratory and in-situ are discussed.

2.2.1 Laboratory Techniques for Determination of Lateral Swelling Pressure

Through decades of research, modified oedometer, triaxial apparatus and 3-D swelling-shrinkage apparatus has been widely used by various scholars in the laboratory studies for the determination of lateral swelling pressure (see Table 2.1). The modified oedometer has been widely used to monitor the development of lateral swelling pressure of unsaturated expansive soil specimens over the past 50 years. A typical modification includes a strain gage in the central portion of the oedometer ring [as shown in Figure 2.5(A)]. The lateral swelling pressure that develops is derived from the circumferential strain variation. Another modification includes a pressure sensors installed at the side of the oedometer ring [as shown in Figure 2.5(B)]. This modification enabled researchers directly measure the lateral swelling pressure.

Modified hydraulic triaxial apparatus allows stress-controlled loading on both axial and radial directions. In the test, provision is introduced for gradual infiltration of water into the cylindrical soil specimen inside the triaxial cell. Under fixed vertical boundaries, the increasing cell pressure for compensation of the radial volume expansion of the cylinder specimen is the lateral swelling pressure. An alternative test method is also used in which the test specimens are allowed to swell under the application of different confining pressures which facilitate in understanding overcompensation effects.

Besides making modifications to oedometer and hydraulic triaxial apparatus, there are also some newly and specially designed apparatus for the measurement of lateral swelling pressure. For example, Xie et al. (2007) presented a more advanced apparatus which has movable boundaries instrumented with pressure sensors to record the generating swelling pressure and dial gauges to record the strain [as shown in Figure 2.5(D)]. This apparatus facilitates measurement of swelling pressure with respect to different strains. Ikizler et al. (2012) studied the effect of EPS geofoam on the reduction of swelling pressure using a specially designed rigid steel box, which could be classified as a modified form of 3-D swelling shrinkage apparatus. The apparatus constitutes of a closed steel cubic box with porous stone placed on the steel walls along with two pressure sensors [as shown in Figure 2.5(E)] mounted on the top and on one side of the steel wall. In this test, the entire steel box is soaked into water allowing water infiltration into the soil specimen through the porous stone and swelling pressure that generates in both vertical and horizontal directions is recorded by pressure sensors.

Table 2.1 Laboratory testing apparatus for the measurement of lateral swelling pressure

Type	References	Stress path available
Modified odeometer	Komornik and Zeitlen (1965); Ofer (1981); Edil and Alanazy (1992);	Constant volume swell; Swell under surcharge; Swell and load back

	Windal and Shahrour (2002); Sapaz (2004); Azam and Wilson (2006); Agus and Schanz (2008); Saba et al. (2014)	
Modified hydraulic triaxial apparatus	Fourie (1988); Yeşil et al. (1993); Puppala et al. (2007); Al-Shamrani (2004)	Swell under different axial and radial strain
3-D swelling shrinkage apparatus	Xie et al. (2007); Ikizler et al. (2012)	Swell under different vertical and horizontal strain

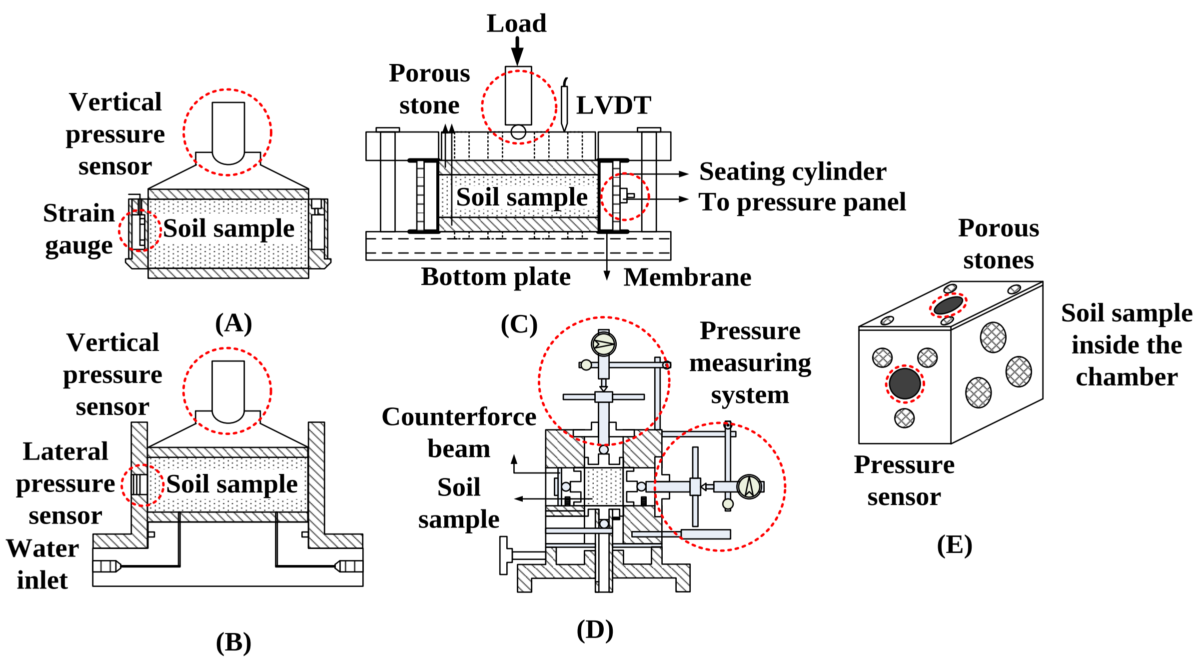

Figure 2.5 Various apparatus for the measurement of lateral earth pressure in the lab [(A) Modified odeometer with strain gauge (modified after Ofer 1981); (B) Modified odeometer with pressure sensor (modified after Saba et al. 2014); (C) Modified hydraulic triaxial apparatus (modified after Puppala et al. 2007); (D) 3-D swelling shrinkage apparatus presented by Xie et al. (2007) (Modified after Xie et al. 2007); (E) 3-D swelling shrinkage apparatus presented by Ikizler et al. (2012) (Modified after Ikizler et al. 2012)

2.2.2 Large Scale Model Tests and In-Situ Tests for Determination of Lateral Swelling Pressure

Lateral swelling pressure measurements from the conventional laboratory tests need relatively simple equipment and operation. However, in-situ and large-scale model tests are far more cumbersome to perform. Large scale model and in-situ tests usually need extensive planning, instrumentation and operation from trained personnel. Furthermore, a long period of time is required to saturate the in-situ expansive soil due to its low hydraulic conductivity of unsaturated expansive soils. In many scenarios, it is also difficult to reliably determine the soil properties because of limited number of soil specimens collected, which may not be representative. In other words, it is likely that there may be significant variations in the in-situ soil properties compared to the soil properties measured from limited number of soil specimens. However, large scale model and in-situ test results are more representative and outweigh the difficulties associated with their testing methods and their limitations.

The influence of surcharge has a significant influence on the lateral swelling pressure measured from in-situ and large scale model tests; for this reason, these tests are typically categorized as swell under surcharge tests. It is also important to note that the lateral swelling pressure measured from large scale model tests include the information of lateral earth pressure. Two different types of testing configurations are commonly used for the measurement of lateral swelling pressure in large scale model and in-situ tests. Figure 2.6 illustrates the first type of testing configuration, which includes the counterforce device, lateral earth pressure measuring and recording system and the model retaining wall. Table 2.2 summarizes some key information derived from experimental results using this type of apparatus.

Table 2.2 Measurement of lateral earth pressure considering lateral swelling pressure from retaining wall test using pressure sensors

Reference	Soil type/Resource	Time period of testing	Apparatus	Remarks

Katti et al. (1983)	Black cotton soil/Malaprabha right bank canal, India	Average 60 days	Figure 2.6(A)	Influence of different thickness cohesive non-swelling (CNS) soil layers as backfill and at the top of expansive clay as surcharge was studied on the mobilization of lateral earth pressure.
Gu (2005)	Expansive clay/Nanning, China	Around 45 to 80 minutes	Figure 2.6(B)	Centrifuge test, test terminate when the lateral earth pressure measurement is stabilized; Sand drains were installed to accelerate the infiltration process; Application of video technique to monitor ground heave.
Symons et al. (1989)	London clay/London, England	Over 20 months	Figure 2.6(C)	Sand drains were installed to accelerate the infiltration process.
Yang et a. (2014)	Expansive clay/Baise, China	5 days	Figure 2.6(D)	Sand drains were installed to accelerate the infiltration process.
Wang et al. (2008a)	Expansive clay/Nanjing, China	100days	Figure 2.6(E)	PVC infiltration pipes were used to accelerate the infiltration process.

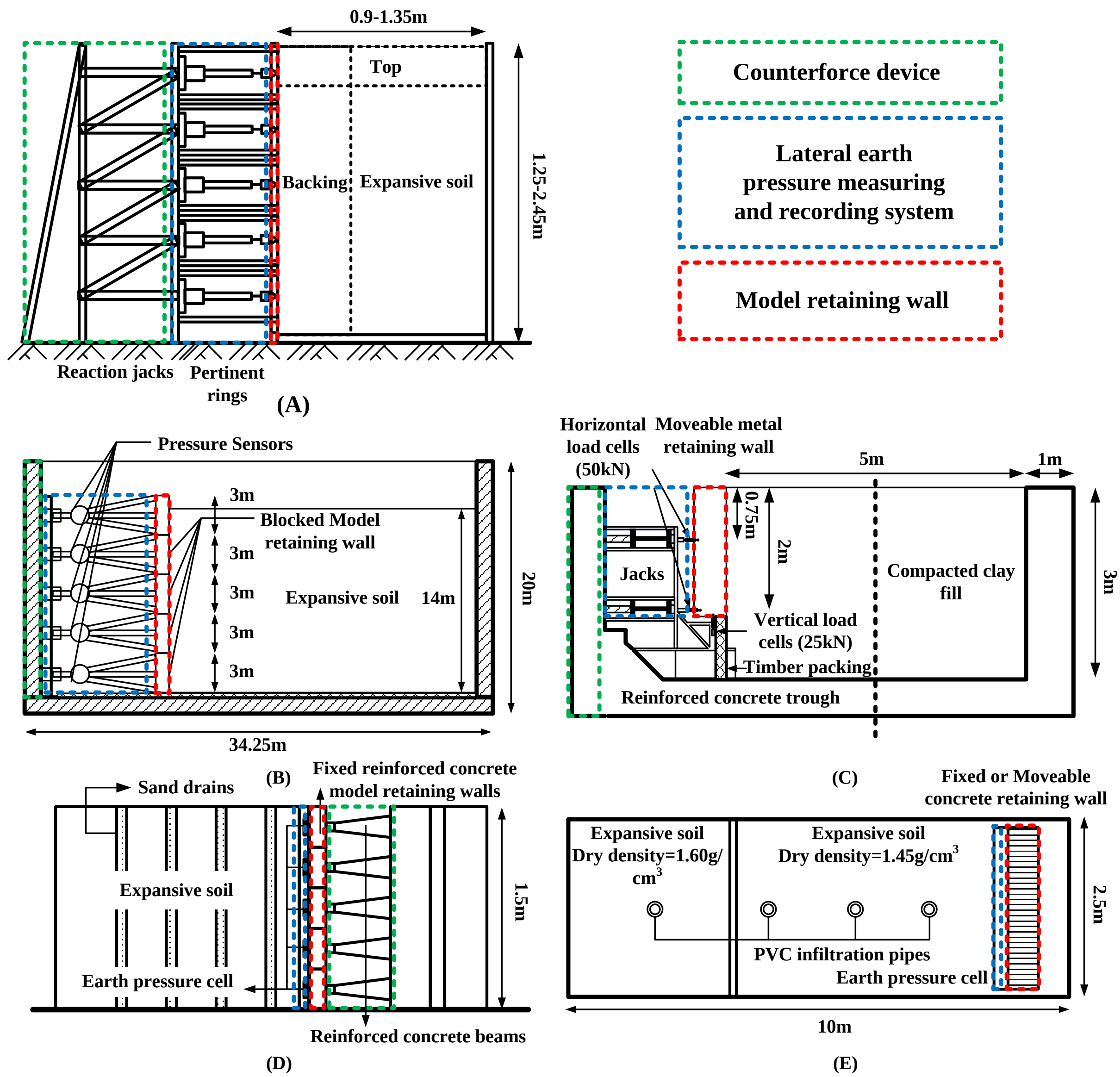

Figure 2.6 Measurement of lateral earth pressure on retaining wall with expansive soil as backfill material using different type of pressure sensors [(A) apparatus used by Katti et al. 1983 (modified after Katti et al. 1983); (B) apparatus used by Gu (2005) in a centrifuge model using enlarged dimensions (modified after Gu 2005); (C) apparatus used by Symons et al. 1989 (modified after Symons et al. 1989); (D) apparatus used by Yang et al. (2014) (modified after Yang et al. 2014); (E) apparatus used by Wang et al. (2008a) (modified after Wang et a. 2008a)]

The second type of testing configuration is shown in Figure 2.7, which only includes a vertically placed pressure sensor that is buried inside the testing pile infiltration test. One outstanding merit of this method is its simple configuration. However, for in-situ test, special measures are usually required to keep the position of the pressure sensor in the same position throughout the testing process. Disturbance can be attributed to the non-uniform volume expansion from one point to the other is associated with non-uniform conditions, soil anisotropy properties and water infiltration. Table 2.3 summarize experiments conducted using this type of testing configuration.

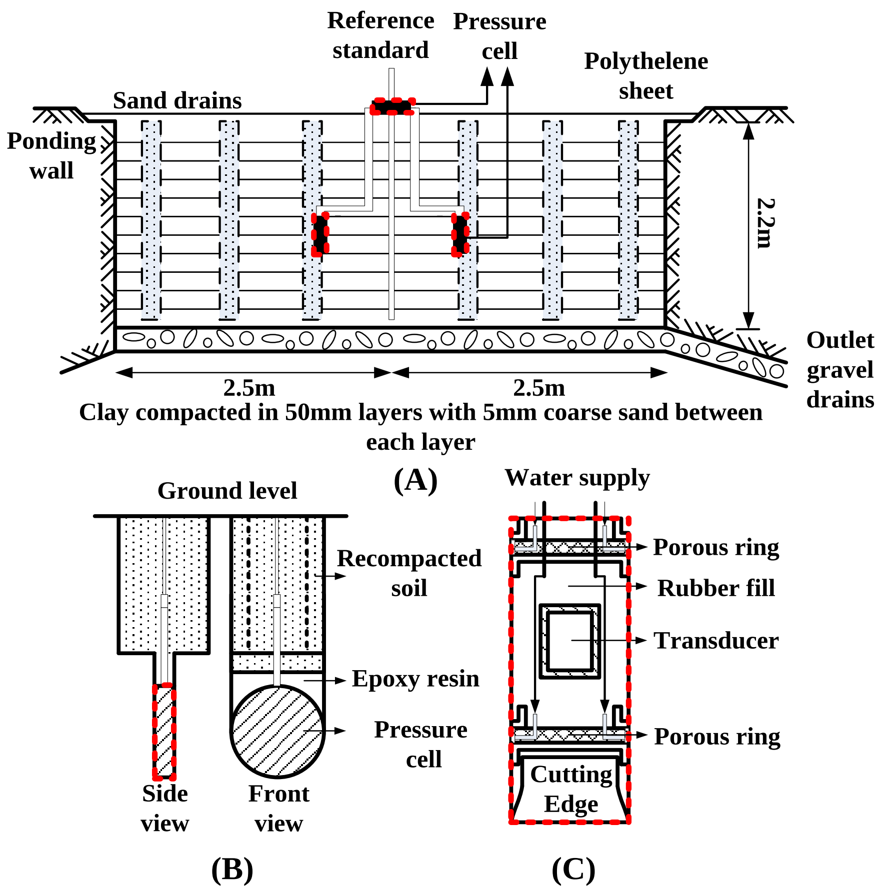

Figure 2.7 Various apparatus with buried pressure sensors for the measurement of lateral earth pressure [(A) modified after Robertson and Wagener (1975); (B) in-situ probe (modified after Ofer 1980); (C) pressure cell (modified after Brackley and Sanders (1992)]

Table 2.3 Measurement of lateral earth pressure considering lateral swelling pressure using buried pressure sensors

Reference	Soil type/Resource	Experimental period	Apparatus or experiment settings	Remarks
Robertson and Wagener (1975)	Remoulded compacted expansive clay/Newcastle South Africa	Around 10 months	Figure 2.7(A)	Sand drains were installed to accelerate the infiltration process; Lateral earth pressure and vertical swelling pressure measurement conducted by conventional pressure cells inserted in the testing pile infiltration test.
Ofer (1980)	Expansive clay/ South Africa	More than 10^4 minutes	Figure 2.7(B)	In-situ probe with ingenious designs enables the infiltration and measurement of lateral earth pressure proceed at the same time.
Brackley and Sanders (1992)	Leeuhof clay (lacustrine clay)/Vereeniging, South Africa	10 years	Figure 2.7(C)	Long term measurement; Detailed measures were introduced to ensure the soil was disturbed as little as possible in the placement of the pressure cell.

2.2.3 Estimation of Lateral Swelling Pressure or Lateral Earth Pressure Considering Lateral Swelling Pressure

The laboratory and field tests are direct methods and provide reliable information about the mobilization of lateral swelling pressure. However, these tests are complex and require assistance of trained professional services which are expensive and hence cannot be used in routine engineering practice. Also, due to the low hydraulic conductivity of expansive soil they are usually time-consuming. As shown in Table 2.4, field tests in some scenarios can be as long as 10 years Brackley and Sanders (1992). Based on experimental and theoretical studies, some investigators have proposed models for predicting lateral swelling pressure or lateral earth pressure considering lateral swelling pressure that are based on experimental and/or theoretical studies. Table 2.4 summarizes six prediction models from the literature with remarks on their advantages and limitations. All these models are capable of predicting the lateral swelling pressure mobilized under swell under surcharge boundary conditions which corresponds to the stress state of a soil element in engineering practice. However, there are only two models proposed by Jiang and Qin (1991) and Hong (2008) in the literature that consider the mobilization of lateral swelling pressure from an unsaturated state to another unsaturated state. Both these models require parameters which can only be determined from complex experiments instead of basic soil properties. These experiments in some scenarios can be more complicated than the direct measurement of lateral swelling pressure. Also, it is accepted that the volume change characteristics of expansive soil can only be better explained taking account of hydromechanical behavior considering soil attributes such as the matric suction and clay mineralogy information (Puppala et al. 2016). However, the presently available models do not incorporate the influence matric suction for lateral swelling pressure mobilization, thereby leading to poor or erroneous characterization practices.

For these reasons, a simple model has been proposed in this study which can provide reliable prediction of lateral earth pressure considering lateral swelling pressure against fixed rigid retaining structures from an initial unsaturated state to another unsaturated state based on matric suction profile variations and limited number of soil properties.

Table 2.4 Models for predicting the lateral earth pressure considering lateral swelling pressure or lateral swelling pressure in expansive soils

Reference	Equation/Description	Stress/strain boundary conditions	Saturation path	Remarks
Skempton (1961)	$P_{LS} = \sigma_s \dfrac{(P_K / \sigma_s - A_s)}{(1 - A_s)}$ (2.1)	Swell under surcharge test.	From initial water content (i.e. unsaturated condition) to fully saturated condition.	Semi-empirical equation; involving a parameter A_s which can be determined from triaxial tests.

Sudhindra and Moza (1987)	$P_{LS} = \dfrac{P_{SV}\dfrac{d_z}{d_{z0}}}{(a + b\dfrac{d_z}{d_{z0}})}$ (2.2)	Swell under surcharge test.	From initial water content (i.e. unsaturated contention) to fully saturated condition.	Empirical equation deduced from limited case studies; Two empirical parameters *a* and *b* need to be determined from complex experiments.
Katti et al. (1983)	$P_{LS} = P_{CNS} + 0.2(P_{SW} - P_{CNS})$ (2.3)	Swell under surcharge test.	From initial water content (i.e. unsaturated contention) to fully saturated condition..	Empirical equation only suitable for certain cases with CNS material filled between expansive soil and the retaining wall.
Nelson et al. (2015)	$P_{LS} = P_0 + \alpha_N P_{SV} \leq P_0 + P_p$ (2.4)	Swell under surcharge test.	From initial water content (i.e. unsaturated contention) to fully saturated condition.	Simple empirical equation involving an empirical parameter α_N which is estimated from past engineering practice experience.
Jiang and Qin (1991)	$P_{LS} = \alpha_J \beta_J P_{LS(\max)}$ (2.5)	Swell under surcharge test.	From an unsaturated state to another unsaturated state associated with matric suction reduction.	Empirical equation involving parameters α_J and β_J determined from complex experiments.
Hong (2008)	$P_{LS} = (\frac{3}{2})\sigma_{im}10^{-\frac{2\varepsilon_h}{\gamma_\sigma(1-f_H)}}(\frac{h_i}{h_f})^{\frac{\gamma_h}{\gamma_\sigma}} - \frac{\gamma_t z_H}{2}$ (2.6)	Swell under surcharge test.	From an unsaturated state to another unsaturated state associated with matric suction reduction.	Complex semi-empirical equation involving two parameters γ_σ and γ_h determined from complex experiments and one empirical parameters f_H.

where P_{LS} = lateral earth pressure considering the influence of lateral swelling pressure; σ_s = vertical effective stress; P_K = soil capillary pressure before test; A_s = pore pressure parameter which can be evaluated from triaxial testing; P_{SV} = minimum stress required to prevent vertical swelling; d_z = calculating depth; d_{z0} = unit depth; a and b are empirical parameters determined from experiment; P_{CNS} = lateral earth pressure of cohesive non-swelling (CNS) material for the corresponding depth; P_{SW} = lateral swelling pressure of oven-dry expansive soil at constant volume condition; P_0 = at rest earth pressure; P_p = passive earth pressure; α_N = parameter varies form 0.7 (Sapaz 2004) to 1 (Katti et al. 2002); P_L = lateral swelling pressure under partially saturated condition; α_J = coefficient of water content, which is the ratio of the lateral swelling pressure at current water to the water content at maximum lateral swelling pressure; β_J = coefficient of deformation, which is ratio of current deformation to the deformation at maximum lateral swelling pressure; $P_{LS(max)}$ = maximum lateral swelling pressure from laboratory tests; σ_{im} = initial values of mean principle stress; ε_h = horizontal swelling strain; γ_σ = the mean principle stress compression index; h_i = initial matric suction; h_f = final matric suction; γ_h = matric suction compression index; f_H = factor ranging from $1/\theta$ to 1 depending on degree of saturation; θ = volumetric water content; γ_t = unit weight of soil; z_H = depth of calculating point.

2.3 Various Factors Contributing to the Mobilization of Lateral Swelling Pressure

Lateral swelling pressure generates when the horizontal volumetric expansion of a soil associated with an increase in water content is restricted. Based on previous experimental investigations, various factors that contribute to the mobilization of lateral swelling pressure can be summarized and analyzed in a flow chart as shown in Figure 2.8.

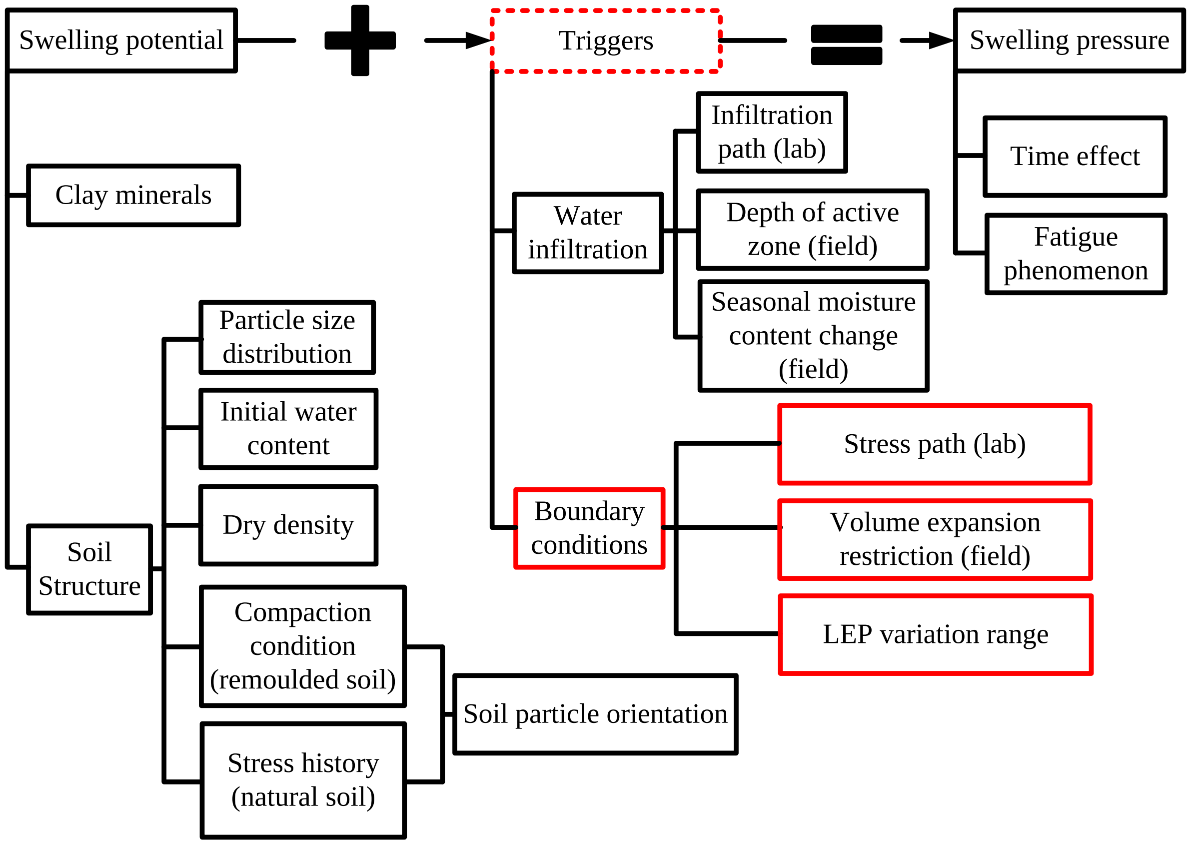

Figure 2.8 Summary of various factors that contribute to the mobilization of lateral swelling pressure in a flow chart

2.3.1 Swelling potential

Expansive soil's swelling potential is typically stored within the soil as an internal stress. This potential is dependent on the clay minerals present within the structure of the expansive soil. Montmorillonite and Illite are two key clay minerals which contribute to the swelling behavior in expansive soils. The percentage of the clay minerals present within expansive soil provides valuable information about the swelling potential. Swelling potential of an expansive soil increases with an increase in the clay content (i.e. clay fraction whose size is 2μm or less). The swelling potential within an expansive soil can be empirically estimated from its initial water content and dry density (Seed et al. 1962; Nagaraj et al. 2010; Sapaz 2004; Schanz and Al-Badran 2014). High dry density and low initial water content contribute to a high swelling potential within an expansive soil. Higher soil density is associated with a relatively larger clay fraction in a certain volume while low initial water content soil has the ability to imbibe more moisture into soil pores that enhances soil swelling. For remoulded soils, these two factors are dependent on the degree of compaction condition (i.e. compaction energy), which in turn has a significant influence on the expansive soil structure. Nature of soil structure and soil particle arrangement in soils compacted with different initial water content has been originally investigated by Lambe (1958). Soils compacted at dry of optimum water content have flocculated structure with random particle orientation (i.e. flocculated structure). However, soils compacted with water contents greater than optimum moisture content typically have their soil particles mostly oriented parallel to each other (dispersed structure). Greater swelling potential can be observed in expansive soils with plate like structures that are oriented parallel to each other and perpendicular to the swelling direction (Gokhale and Jain 1972). Komornik and Livneh (1968) suggested that the swelling potential is greater in expansive soils that have their clay mineral fraction (i.e. montmorillonite or illite) particles parallel to the direction of compaction. The swelling potential in the vertical direction is usually greater than lateral (horizontal) direction for a flat-lying deposit natural expansive soils which show strong anisotropic behavior; however, for steeply dipping deposit, it is just the opposite (Nelson et al. 2015).

2.3.2 Water infiltration

The swelling potential is a stored energy that releases when water intrusion occurs within an expansive soil. In the laboratory tests, moisture migration inside the soil specimen can be mainly attributed to thermal, capillary and osmosis action. In field tests, moisture variation is associated with many factors such as the precipile infiltration testation, ground water table variation, lawn irrigation and leakage of underground pipes lines. Influence of environmental factors along with the non-uniform soil profile makes the problem far more complex in engineering practice. Expansive soil problems can be predominantly attributed to the water content changes in the upper few meters, with deep seated heave being rare (Nelson and Miller 1992). These layers are usually referred to as zone of seasonal fluctuations or simply, active zone. Nelson et al. (2001) summarized two key characteristics for the active zone in expansive soils. The first characteristic is associated with significant matric suction variation which occurs within the active zone depth; and the second characteristic is related to the heave which is predominant again in this zone. Other than flow behavior, Estabragh et al. (2013) studies suggest that the swelling behavior of expansive soil is also influenced by the type of wetting fluids: acidic water and saline water reduce the swelling potential of compacted soil while reduction in salt concentration of wetting fluids enhances the swelling potential.

2.3.3 Stress path in the laboratory tests

The laboratory methods used in the measurement of swelling pressure are stress path dependent (Brackley 1975). Soil specimens tested using different methods that follow different stress paths provide different results, in spile infiltration teste of undergoing the same amount of volume change during the testing process. Results that support these conclusions were derived from vertical swelling pressure measurement methods using oedometers by several investigators (Brackley 1975; Basma et al. 1995; Nagaraj et al. 2009). Three methods that have been standardized and widely used (ASTM, D4546) for vertical swelling pressure measurements include the constant volume method, swell and load back method and swell under surcharge method. A typical expansive soil specimen tested in modified odeometer has a stack of lattice layers that are interconnected by up to four layers of crystalline water in a clay particle (2:1 tetrahedral–octahedral–tetrahedral sandwich layer of clay mineral crystals). Then, an assembly of clay particles denoted as the clay aggregate forms the unit of the compacted clay double structure. An assembly of aggregates from the macrostructure, and the voids between the aggregates are denoted as macro voids (Mašín and Khalili 2016). The volume expansion of expansive soil can be attributed to the increasing amount of water intruding into these three level structures; namely, lattice layer, clay particles and clay aggregates. The first level constitutes the crystalline water that exists between lattice layers within the clay particle. The amount of crystalline water present mainly depends on the matric suction forces (Yong 1999) and is sensitive to the pore water chemical properties (Herbert and Moog 2000). The second level is the double-layer water that surrounds individual clay particle in the diffuse double layer. The size (amount) of diffuse double-layer depends on the ion concentration in the equilibrium solution so as to be directly related to osmotic suction (Callaghan and Ottewill 1974; Yong 1999; Pusch 2006). The third level is the macro pore among clay aggregates. The double layer water gradually become equilibrium water as the distance from clay particles increases. The amount of equilibrium water inside the soil specimen is related to matric suction while the volume of macro pores determines the total amount of equilibrium water that can be stored in the test specimen.

In oedometer test, prior to water infiltration [see Figure 2.9(A)], macro pores inside the unsaturated soil specimen are partially filled with water which is under a state of equilibrium condition. Limited amount of double layer water and crystalline water is bound to the cation cloud that forms on the clay particle surface and inside the interlayer space of clay particles, respectively. Upon saturation, the changes within the pore water chemical properties and solution concentration for soil specimens tested using three different methods are almost the same. Due to this reason, the amount of crystalline water and double-layer water gain is almost the same. In other words, clay aggregates inside these specimens undergo similar expansion. However, for soil specimen tested using constant volume condition [see Figure 2.9(B)], during saturation, the volume expansion is restricted by fixed vertical boundary (void ratio *e* is constant). Soil structure changes arise due to enlarged clay aggregates during the swelling process. However, in the swell and load back test [shown in Figure 2.9(C)], significant changes occur in the soil structure that generates more macro pores during saturation of the soil specimen. During the consolidation process, the excess pore water pressure is released and the vertical swelling pressure is expressed as a function of effective stress [see Figure 2.9(D)]. Soil structure changes occur mainly during the consolidation process. In the constant consolidation pressure test, prior to water infiltration, the soil specimen first consolidates under the applied surcharge [as shown in Figure 2.9(E) and (F)]. In other words, soil structure changes occur both in the consolidation and the swelling process. In spile infiltration teste of the final volume of the soil specimen being the same for the different testing methods, the differences in the arrangement and structure of clay aggregates contribute to the differences in the measured values of swelling pressures. Several researchers' investigations suggest that the vertical swelling pressure measurement from constant volume swelling pressure test falls between the swell and load back test (which is typically the largest) and constant consolidation pressure test (which is the lowest) (for example, Sridharan et al. 1986). Modifications were introduced into the traditional oedometers with the objective of measuring the lateral swelling pressure simultaneously along with the vertical swelling pressure measurement. Among the three stress paths introduced above, the swell under surcharge test is the most widely accepted method for the measurement of lateral swelling pressure because it well simulates the scenarios typically encountered in engineering practice. As discussed earlier, in this test, the soil specimen swells under a surcharge load which is representative to over burden pressure associated with unit weight of upper layer soil and/or load from the superstructure.

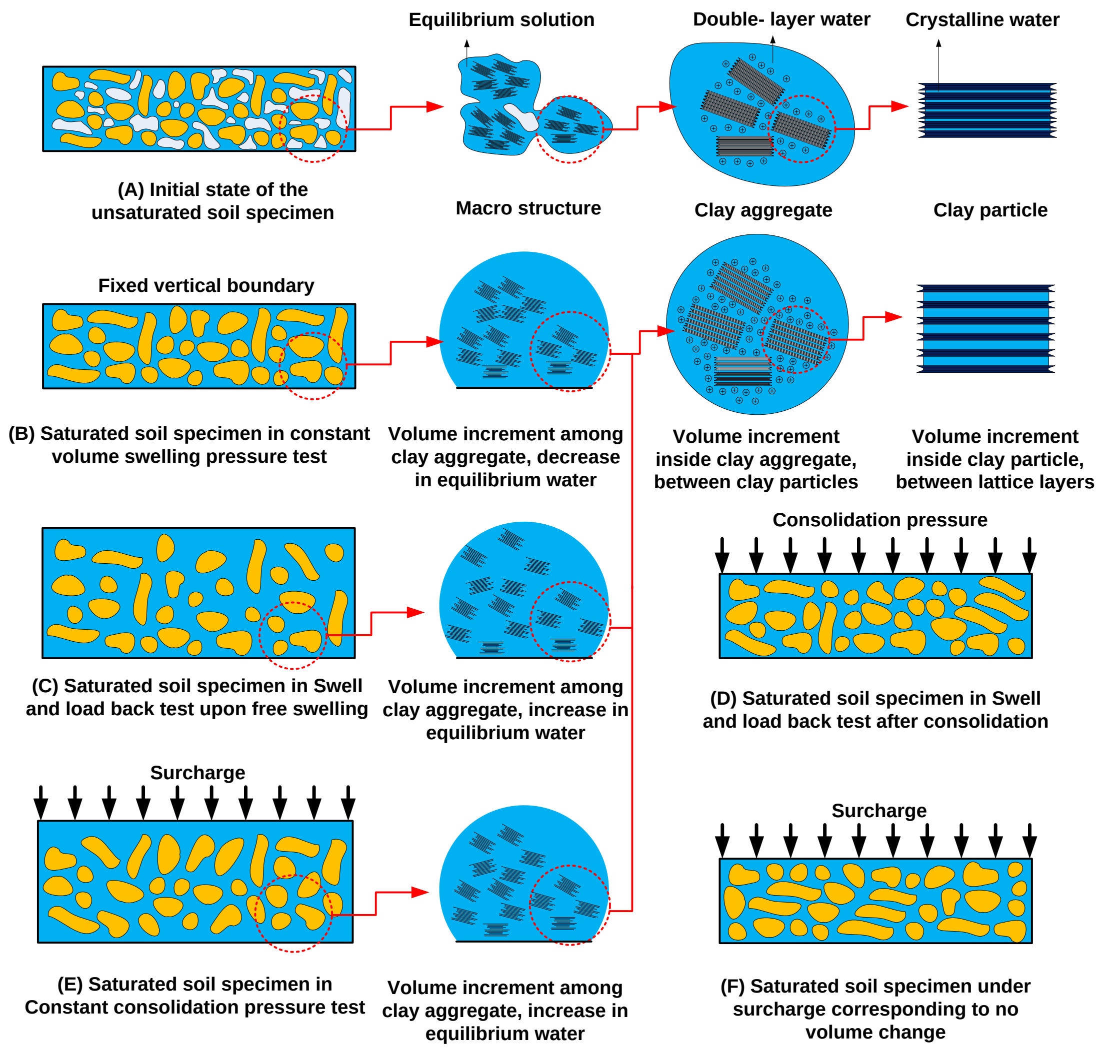

Figure 2.9 Structure changes that arise in the soil specimens upon saturation in different swelling pressure measurement tests

2.3.4 Boundary conditions in engineering practice

In the field, horizontal volume expansion is generally restricted by retaining structures such as the retaining walls and basement walls. Similarly, vertical volume expansion will also be restricted on condition that there is not enough crawl space set between the ground surface and infrastructure to accommodate the ground heave.

There are two key points that deserve due attention in better understanding the influence of boundary conditions on the lateral swelling pressure in expansive soils. The first one is related to the significant reduction in the swelling pressure when a limited strain is allowed in expansive soils (Ofer 1981; Katti et al. 2002; Xie et al. 2007). Geotechnical engineers are aware of this and extend it in engineering practice to reduce the lateral swelling pressure acting on retaining works (Liu et al. 2006; Ikizler et al. 2008; Shelke and Murty 2010). The second point is the mobilization of lateral swelling pressure and the ground heave which are both interrelated (Al-Shamrani and Dhowian 2003). The lateral swelling pressure decreases with an increase in the ground heave. For example, in intact expansive soils, volume strain predominantly occurs in the vertical direction contributing to ground heave. However, if there are significant fissures within the expansive soils, larger portion of volume strain will occur laterally instead of vertical direction; due to this reason there will be limited ground heave (Lytton 1977).

The lateral swelling pressure that mobilizes behind a retaining structure with expansive soil as backfill upon wetting is generally considered as a component in addition to at-rest lateral earth pressure (K_0 condition). Previous sections have presented a detailed discussion on the mobilization of lateral earth pressure considering the lateral swelling pressure behind a rigid retaining wall with matric suction reductions. Focusing on two scenarios that are commonly encountered in engineering practice, the influence of vertical volume expansion restriction on the mobilization of lateral swelling pressure are analyzed.

Figure 2.10(A) shows a fixed retaining wall constructed against expansive soils and Figure 2.10(B) shows a pile which is buried in an expansive soil without crawl space set on the top. For the fixed retaining wall, assuming it is long enough, the strain in *z* direction can be neglected. In other words, focusing on a square soil element inside the cross section as shown in Figure 2.10(A), corresponding analysis can be simplified as a plane strain problem. The soil element has a tendency to expand in both *x* and *y* directions when there is a decrease in matric suction. While expansion in *x* direction is restricted due to the influence of boundary condition; however, in *y* direction expansion is influenced by a vertical stress (i.e. due to soil unit weight and/or surcharge).

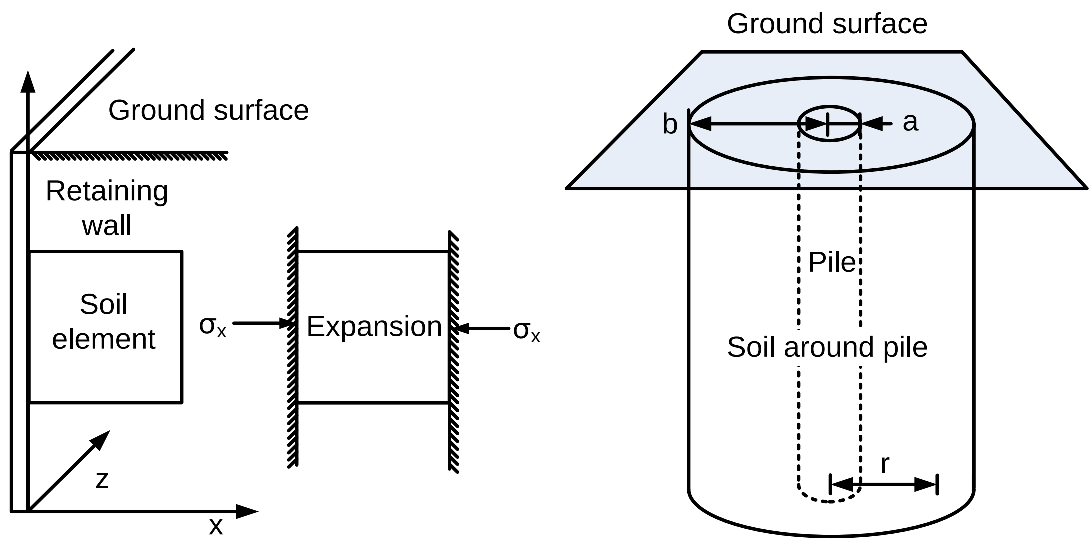

(A) (B)

Figure 2.10 Mobilization of lateral swelling pressure [(A) against retaining wall; (B) around the pile]

Considering matric suction as an independent stress variable in addition to net normal stress, theoretical analysis can be conducted on the lateral earth pressure acting against geotechnical structures considering lateral swelling pressure within elastic range extending soil structure constitutive relationship proposed by Fredlund and Morgenstern 1976 (as shown in Equation 2.7).

$$\begin{cases} \varepsilon_x = \dfrac{(\sigma_x - u_a)}{E} - \dfrac{\upsilon}{E}(\sigma_y + \sigma_z - 2u_a) + \dfrac{(u_a - u_w)}{H} \\ \varepsilon_x = \dfrac{(\sigma_x - u_a)}{E} - \dfrac{\upsilon}{E}(\sigma_y + \sigma_z - 2u_a) + \dfrac{(u_a - u_w)}{H} \\ \varepsilon_y = \dfrac{(\sigma_y - u_a)}{E} - \dfrac{\upsilon}{E}(\sigma_x + \sigma_z - 2u_a) + \dfrac{(u_a - u_w)}{H} \\ \gamma_{xy} = \dfrac{\tau_{xy}}{G} \\ \gamma_{yz} = \dfrac{\tau_{yz}}{G} \\ \gamma_{zx} = \dfrac{\tau_{zx}}{G} \end{cases} \tag{2.7}$$

where $(\sigma_x - u_a)$ = net normal stress in x direction; $(\sigma_y - u_a)$ = net normal stress in y direction; $(\sigma_z - u_a)$ = net normal stress in z direction; $(u_a - u_w)$ = matric suction; E = elastic modulus with respect to net normal stress; τ_{xy} = shear stress on the x-plane in the y-direction (i.e., $\tau_{xy} = \tau_{yx}$); τ_{yz} = shear stress on the y-plane in the z-direction (i.e., $\tau_{yz} = \tau_{zy}$); τ_{zx} = shear stress on the z-plane in the x-direction (i.e., $\tau_{zx} = \tau_{xz}$); H = elastic modulus with respect to matric suction; G = shear modulus; υ = Poisson's ratio.

Focusing on a square soil element inside the cross section as shown in Figure 2.10(A), the constitutive relationship of soil structure can be simplified as plane strain problem as Equation 2.8. With a decrease in matric suction, the soil element has a tendency to expand in both x and y directions. Expansion in x direction is restricted due to the influence of boundary condition and in y direction expansion is influenced by a vertical stress (i.e. due to soil unit weight and/or surcharge). The relationship between the decreased matric suction and developed horizontal stress can be given in Equation 2.9. Then replacing the term $\dfrac{\upsilon}{1-\upsilon}(\sigma_y - u_a)$ in Equation 2.9 which representing the lateral earth pressure due to soil unit weight and/or surcharge, a more rigorous calculation considering both saturated and unsaturated condition appearing in the final phase can be given as Equation 2.10.

$$\begin{cases} \varepsilon_x = \dfrac{(1-\upsilon^2)}{E}[(\sigma_x - u_a) - \dfrac{\upsilon}{1-\upsilon}(\sigma_y - u_a)] + (1+\upsilon)\dfrac{\Delta(u_a - u_w)}{H} \\ \varepsilon_y = \dfrac{(1-\upsilon^2)}{E}[(\sigma_y - u_a) - \dfrac{\upsilon}{1-\upsilon}(\sigma_x - u_a)] + (1+\upsilon)\dfrac{\Delta(u_a - u_w)}{H} \\ \tau_{xy} = \dfrac{E\gamma_{xy}}{2(1+\upsilon)} \end{cases} \tag{2.8}$$

$$\sigma_h = \sigma_x - u_a = \frac{\upsilon}{1-\upsilon}(\sigma_y - u_a) - \frac{\Delta(u_a - u_w)E}{(1-\upsilon)H} \tag{2.9}$$

$$\sigma_h = \begin{cases} \sigma_x - u_a = K_0\sigma_s - \dfrac{\Delta(u_a - u_w)E}{(1-\upsilon)H} & (a) \\ \sigma_x - u_a = K_0\sigma_s' - \dfrac{\Delta(u_a - u_w)E}{(1-\upsilon)H} + u_w & (b) \end{cases} \tag{2.10}$$

where K_0 = coefficient of at rest earth pressure, $K_0 \approx 1 - \sin\phi'$ for normally consolidated soil (Jaky 1944); $K_0 = (1-\sin\phi')OCR^{\sin\phi'}$ for over consolidated soil (Mayne and Kulhawy 1982); ϕ' = the effective internal friction angle of soil; OCR = overconsolidation ratio; σ'_s = effective vertical stress, σ_s = total vertical stress; u_w = pore water pressure; E = elastic modulus with respect to net normal stress; H = elastic modulus with respect to matric suction; $\Delta(u_a - u_w)$ = matric suction variation. (a) is suitable for scenarios in which expansive soil has not been fully saturated after suction variation while (b) is suitable for scenarios in which expansive soil has been fully saturated after suction variation.

For piles placed in expansive soils, the soil around the pile can be assumed as a hollow cylinder with inner diameter *a* and external diameter *b* (*b* is infinite). With a decrease in matric suction, the hollow cylinder tends to expand in both axial and radial directions. However, fixed boundary conditions restrict both the inner and external expansion. Assuming there is no crawl spacing between the ground surface and the foundation to accommodate the possible ground heave, the vertical expansion of the soil element is restricted as well. Due to this reason, this problem can be simplified as a plane strain problem. Neglecting the body force, the equations for equilibrium, geometric and constitutive relationship for soil cylinder are respectively given in Equation 2.11, Equation 2.12 and Equation 2.13.

$$\begin{cases} \dfrac{\partial(\sigma_r - u_a)}{\partial r} + \dfrac{1}{r}\dfrac{\partial \tau_{\varphi r}}{\partial \varphi} + \dfrac{\sigma_r - \sigma_\varphi}{r} = 0 \\ \dfrac{1}{r}\dfrac{\partial(\sigma_\varphi - u_a)}{\partial \varphi} + \dfrac{\partial \tau_{r\varphi}}{\partial r} + \dfrac{2\tau_{r\varphi}}{r} = 0 \end{cases} \tag{2.11}$$

where (σ_r - u_a) = net normal stress in radial direction; (σ_φ - u_a) = net normal stress in circumferential direction; $\tau_{\varphi r}$ = circumferential strain; $\tau_{r\varphi}$ = radial strain; r = the distance from the center of the pile.

$$\begin{cases} \varepsilon_r = \dfrac{\partial u_r}{\partial r} \\ \varepsilon_\varphi = \dfrac{u_r}{r} + \dfrac{1}{r}\dfrac{\partial u_\varphi}{\partial \varphi} \\ \gamma_{r\varphi} = \dfrac{1}{r}\dfrac{\partial u_r}{\partial \varphi} + \dfrac{\partial u_\varphi}{\partial r} - \dfrac{u_\varphi}{r} \end{cases} \tag{2.12}$$

where u_r = radial displacement; u_φ = circumferential displacement.

$$\begin{cases} \varepsilon_r = \dfrac{1-\upsilon^2}{E}[(\sigma_r - u_a) - \dfrac{\upsilon}{1-\upsilon}(\sigma_\varphi - u_a)] + \dfrac{(1+\upsilon)\Delta(u_a - u_w)}{H} \\ \varepsilon_\varphi = \dfrac{1-\upsilon^2}{E}[(\sigma_\varphi - u_a) - \dfrac{\upsilon}{1-\upsilon}(\sigma_r - u_a)] + \dfrac{(1+\upsilon)\Delta(u_a - u_w)}{H} \\ \gamma_{r\varphi} = \dfrac{\tau_{r\varphi}}{G} \end{cases} \tag{2.13}$$

Considering that there is only a change in the matric suction, above three equations can be simplified as Equation 2.14, Equation 2.15 and Equation 2.16, correspondingly.

$$\frac{\partial(\sigma_r - u_a)}{\partial r} + \frac{\sigma_r - \sigma_\varphi}{r} = 0 \tag{2.14}$$

$$\begin{cases} \varepsilon_r = \dfrac{\partial u_r}{\partial r} \\ \varepsilon_\varphi = \dfrac{u_r}{r} \end{cases} \tag{2.15}$$

$$\begin{cases} \varepsilon_r = \dfrac{1-\upsilon^2}{E}[(\sigma_r - u_a) - \dfrac{\upsilon}{1-\upsilon}(\sigma_\varphi - u_a)] + \dfrac{(1+\upsilon)\Delta(u_a - u_w)}{H} \\ \varepsilon_\varphi = \dfrac{1-\upsilon^2}{E}[(\sigma_\varphi - u_a) - \dfrac{\upsilon}{1-\upsilon}(\sigma_r - u_a)] + \dfrac{(1+\upsilon)\Delta(u_a - u_w)}{H} \end{cases} \tag{2.16}$$

Rearranging Equation 2.16, the axial stress and radial stress can be expressed in terms of axial and radial strain as shown in Equation 2.17. Then, by substituting Equation 2.14 and Equation 2.15 into Equation 2.17, Equation 2.18 can be obtained.

$$\begin{cases}(\sigma_r - u_a) = \dfrac{E}{1-\upsilon}\dfrac{1-\upsilon}{1-2\upsilon}(\varepsilon_r + \dfrac{\upsilon}{1-\upsilon}\varepsilon_\varphi) - \dfrac{E}{H}\dfrac{u_a - u_w}{1-2\upsilon} \\ (\sigma_\varphi - u_a) = \dfrac{E}{1-\upsilon}\dfrac{1-\upsilon}{1-2\upsilon}(\varepsilon_\varphi + \dfrac{\upsilon}{1-\upsilon}\varepsilon_r) - \dfrac{E}{H}\dfrac{u_a - u_w}{1-2\upsilon}\end{cases} \tag{2.17}$$

$$\frac{\mathrm{d}^2 u_r}{\mathrm{d}r^2} + \frac{1}{r}\frac{\mathrm{d}u_r}{\mathrm{d}r} - \frac{u_r}{r^2} = \frac{1+\upsilon}{(1-\upsilon)H}\frac{\mathrm{d}\Delta(u_a - u_w)}{\mathrm{d}r} \tag{2.18}$$

The expression for axial displacement can be obtained as summarized in Equation 2.19 by carrying out two integrations on Equation 2.18.

$$u_r = \frac{(1+\upsilon)}{(1-\upsilon)Hr}\int_a^r \Delta(u_a - u_w) r\,\mathrm{d}r + c_1 r + \frac{c_2}{r} \tag{2.19}$$

Using Equation 2.19, a link is built connecting the axial displacement with axial and radial stress, which is given as Equation 2.20.

$$\begin{cases}(\sigma_r - u_a) = -\dfrac{E}{Hr^2(1-\upsilon)}\displaystyle\int_a^r \Delta(u_a - u_w) r\,\mathrm{d}r + \dfrac{E(1-\upsilon)}{(1+\upsilon)(1-2\upsilon)}(\dfrac{c_1}{1-\upsilon} - \dfrac{1-2\upsilon}{1-\upsilon}\dfrac{c_2}{r^2}) \\ (\sigma_\varphi - u_a) = \dfrac{E}{Hr^2(1-\upsilon)}\displaystyle\int_a^r \Delta(u_a - u_w) r\,\mathrm{d}r + \dfrac{E(1-\upsilon)}{(1+\upsilon)(1-2\upsilon)}(\dfrac{c_1}{1-\upsilon} - \dfrac{1-2\upsilon}{1-\upsilon}\dfrac{c_2}{r^2}) - \dfrac{E}{(1-\upsilon)H}\Delta(u_a - u_w)\end{cases} \tag{2.20}$$

In Equation 2.20, c_1 and c_2 are determined from boundary conditions. According to the assumptions that both the inter and external displacement boundary conditions are restricted (Equation 2.21), the values of c_1 and c_2 given in can be acquired by substituting Equation 2.21 to Equation 2.19.

$$\begin{cases} u_{ra} = 0 \\ u_{rb} = 0 \end{cases} \tag{2.21}$$

$$\begin{cases} c_1 = -\dfrac{(1+\upsilon)\Delta(u_a - u_w)}{2H(1-\upsilon)} \\ c_2 = \dfrac{(1+\upsilon)\Delta(u_a - u_w)}{2H(1-\upsilon)} a^2 \end{cases} \tag{2.22}$$

The axial stress acting on the inner diameter can be calculated using Equation 2.23, which is obtained by substituting the value of c_1 and c_2 from Equation 2.22 into Equation 2.20.

$$\sigma_x - u_a = \frac{-\Delta(u_a - u_w)E}{(2\upsilon - 1)H} \tag{2.23}$$

Finally, the total lateral earth pressure acting on the pile can be calculated using Equation 2.24 which includes the lateral earth pressure due to soil unit weight and surcharge (adding the body force which is ignored in the previous analysis by superposition method) to Equation 2.23. Then similar to analysis conducted for lateral earth pressure against retaining walls, theoretical elastic calculation for lateral earth pressure around the pile considering both saturated and unsaturated condition in the final phase can be given as Equation 2.25.

$$\sigma_h = \sigma_x - u_a = -\frac{\Delta(u_a - u_w)E}{(1-2\upsilon)H} \tag{2.24}$$

$$\sigma_h = \begin{cases} \sigma_x - u_a = K_0\sigma_s - \dfrac{\Delta(u_a - u_w)E}{(1-2\upsilon)H} & (a) \\ \sigma_x - u_a = K_0\sigma_s' - \dfrac{\Delta(u_a - u_w)E}{(1-2\upsilon)H} + u_w & (b) \end{cases} \tag{2.25}$$

Equation 2.25(a) is suitable for scenarios in which expansive soil has not been fully saturated after suction variation; however, Equation 2.25(b) is suitable for scenario in which expansive soil is fully saturated (i.e. suction is lost due to wetting associated with infiltration of water).

2.3.5 Time and cyclic wetting and drying effects

The mobilization of lateral swelling pressure also show time effects and fatigue phenomenon. Time effects are well known from both the laboratory studies and in-situ investigations. The swelling pressure increases rapidly due to water infiltration, reaches a peak value and decreases gradually to a stabilized final value (Clayton et al. 1991; Brackley and Sanders 1992; Symons and Clayton 1992; Windal and Shahrour 2002; Xie et al. 2007; Mohamed et al. 2014). Based on experimental data acquired from laboratory and large scale pilot tests, the mobilization of lateral swelling pressure within an expansive backfill can be divided into four stages and arranged in a chronological order: (1) In the first stage, lateral earth pressure initially arises due to the influence soil unit weight over a certain depth after placement or burial; compaction can also contribute to the lateral earth pressure to some extent depending on the compaction energy used. However, the influence is not significant until the compaction pressures reduce the void ratio (e) of the compacted backfill to less than 0.15 (Clayton et al. 1991); (2) In the second stage, soil softening phenomenon leads to a slight decrease in the lateral earth pressure after compaction at constant moisture content; (3) In the third stage, water intrusion induced volume expansion will lead to a further increase in lateral earth pressure to the maximum value under a constant vertical stress; (4) Finally, in the fourth stage, lateral earth pressure reduces gradually with time due to soil softening at saturated water content. The changing pattern of lateral earth pressure after soil volume expansion shows good agreement with the statement made by Joshi and Katti (1980): initial increase occurs quickly to a maximum value and then decreases slightly, and finally remains at an almost constant value. Saba et al. (2014) recently concluded that such a behavior can be attributed to change in the microstructure and collapse of macrostructure.

Meanwhile, cyclic wetting and drying associated with environmental factors can significantly influence the mechanical behavior of expansive soils. The swelling ability of a typical expansive soil starts decreasing after a certain number of wetting and drying cycles (Dif and Bluemel 1991; Estabragh et al. 2015). This behavior is usually defined as fatigue phenomenon. Some investigation studies suggest that predominant swelling or shrinkage occurs during the first wetting and drying cycle (Al-Homoud et al. 1995; Basma et al. 1996). However, volume change behavior significantly reduces after four or five wetting cycles to attain equilibrium conditions. Al-Homoud et al. (1995) monitored the variation in soil structure during wetting and drying cycles with the help of a microscope and found that clay aggregates show weaker orientation in this process due to the integration of soil structure along the bedding. In other words, destruction of large aggregates and disorientation of structural elements continue taking place until a turbulent flocculated soil structure is formed (Basma et al. 1996). Due to this reason, the ability of the expansive soil to imbibe and swell reduces significantly.

2.3.6. Measures available for the reduction of lateral swelling pressure

In most cases, gravel and other materials that are similar to granular materials are recommended for both flexible and rigid retaining walls as backfill, the primary reason for this is a relative simple and clear calculation of lateral earth pressure can be adopted (Coulomb 1776; Rankine 1857). Also, gravel backfills have good drainage conditions and self-settlement characteristics, as well as stable strength parameters which are not time dependent. In general, swelling soil is the least recommended as backfill material against retaining works due to its poor engineering properties (low hydraulic conductivity and time-dependent swelling behavior). However, clay minerals are not always available near the engineering field and continuously extraction of granular materials lead to degeneration of the green belt as well as irritating the emission of carbon dioxide (Sivakumar et al. 2015). Also, in some areas of the world, free draining granular material is scarce and its price can be as high as a constituent of concrete (Clayton et al.1991) so that on site soils are sometimes used as a cost saving measure (Thomas et al. 2009).

All these factors cause the utilization of expansive clay as back fills as an inevitable trend. However, appropriate engineering measures are necessary for the remediation of expansive soils' poor engineering properties. The first issue required to be solved is the considerable lateral swelling pressure generating after water infiltration. Measures can also be taken from three different aspects which cause the generation of lateral swelling pressure as shown in Figure 2.11. To start with, methods focusing on the reduction of swelling potential usually change the chemical composition or structure of soils so as to improve its engineering properties. The second one targets on trigger element, water. Pre-wetting is a simple and economical approach in which the swelling potential of expansive soil has been released in the preparation period. However, a soil allowed to partially shrink to its initial water content shows a reduction in swelling potential during wetting and drying circles while a rise can be observed if the sample is fully shrunk to its shrinkage limit or less (Al-Homoud et al. 1995). Also, during the drying process, cracks developed inside expansive soils may accelerate water infiltration and extend water infiltration into a greater depth upon wetting. Capillary barriers totally prevent the infiltration of water from ground surface while lacking the ability to deal with problems caused by ground water table rise or leakage of underground pipes. All these reasons cause this approach to be less recommended. Thirdly, as mentioned before, even little strain can significantly reduce the lateral swelling pressure (Ofer 1981; Katti et al. 2002; Xie et al. 2007). This thinking has guided the development of engineering techniques for the reduction of lateral swelling pressure. Scholars keep searching for best materials as buffering agent between soil and retaining works to accommodate possible deformation and currently two good choices are presented as geofoam (Ikizler et al. 2008; Shelke and Murty 2010; Lingwall and Bartlett 2014) and soil bags (Reeves and Filz 2000; Liu et al. 2006; Zarnani and Bathurst, 2007, 2008; Trandafir et al. 2010; Ertugrul and Trandafir, 2011).

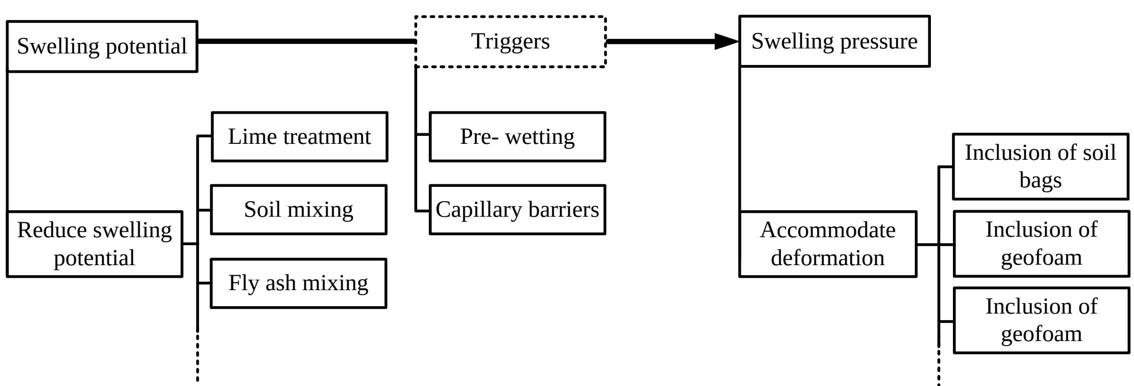

Figure 2.11 Measures for reduction of lateral swelling pressure

2.4 Literature review on unsaturated interface shear strength

The ground water table in expansive soils regions does rise to the natural ground level; for this reason, there is a significant soil layer which is always in a state of unsaturated condition. When structural elements are in contact with unsaturated soil, there is transfer of stress between the two materials through a contact zone referred to herein as an "unsaturated interface." The interaction of unsaturated soils with different structures gives rise to many unsaturated interface problems in civil engineering (such as unsaturated retaining wall backfill, foundations in unsaturated soil) (Hamid and Miller 2009). Several scholars highlighted the important role of the suction played in the mobilization of the interface shear strength (Sharma et al. 2007; Hamid and Miller 2009; Hossain and Yin 2013). However, currently there are limited research available in this filed.

From the available literature, it can be summarized that in order to conduct unsaturated interface direct shear test, typically three different types of apparatus can be used. In the first two types, modifications are introduced to the traditional direct shear apparatus and in the third type the conventional triaxial apparatus is modified to perform the unsaturated interface tests. The first type of modification includes a matric suction control system which enables the interface shear test to proceed under a constant suction. In this kind of tests, axis translation technique was used to control and (or) apply the matric suction in the soil. For example, Hamid and Miller (2009) introduced modifications to a traditional direct shear apparatus which mainly includes the addition of an air-pressure chamber, new testing cells, high air-entry porous disc (HAEPD), and a pore-water pressure control system [as shown in Figure 2.12(A)]. Hamid and Miller (2009) conducted a series of interface shear test between unsaturated Minco silt and stainless steel plates (counterfaces). Three matric suction values used in this test are chosen as 20, 50 and 100kPa. Further, Khoury et al. (2010) used the same apparatus to study the effect of soil matric suction (25, 50 and 100kPa) on the mechanical behavior of unsaturated manufactured silty soil-geotextile interface. Hossain and Yin (2013) performed a series of interface direct shear box tests between a compacted completely decomposed granite soil and cement grout under different matric suctions (50, 100, 200 and 300kPa) and net normal stresses. Borana et al. (2015 and 2016) also used similar apparatus to conduct a series of soil-steel plate interface tests at different shearing planes in the soil. These tests were conducted under a constant net normal stress of 50 kPa and different matric suctions of 0 kPa, 50 kPa and 200 kPa. The second type of modification includes the installation a miniature pore pressure transducer (PPT) to the direct shear apparatus (Fleming et al. 2006), which is shown as Figure 2.12(B). In this way the pore-water pressure changes in the vicinity of structural element–soil interface can be measured during shear. Fleming et al. (2006) and Sharma et al. (2007) monitored changes in the pore water pressure (i.e. matric suction) at geomembrane-soil interfaces during shearing using PPT. Due to the difficulty to keep the ceramic tip of the miniature PPT saturated at a matric suction higher than about 30kPa, a coarse-grained sandy soil was selected instead the fine-grained clayey soil. While in typical waste containment applications, clay is commonly used next to a geomembrane. Hanson et al. (2001) used a modified triaxial apparatus to measure interface shear strength for interfaces with unsaturated geotextiles [as shown in Figure 2.12(C)]. This device mounts inside a triaxial cell and uses triaxial load systems to pressurize and shear the specimen. Similar to the first type of modification, axis translation technique was used to apply matric suction (4.8kPa for this test).

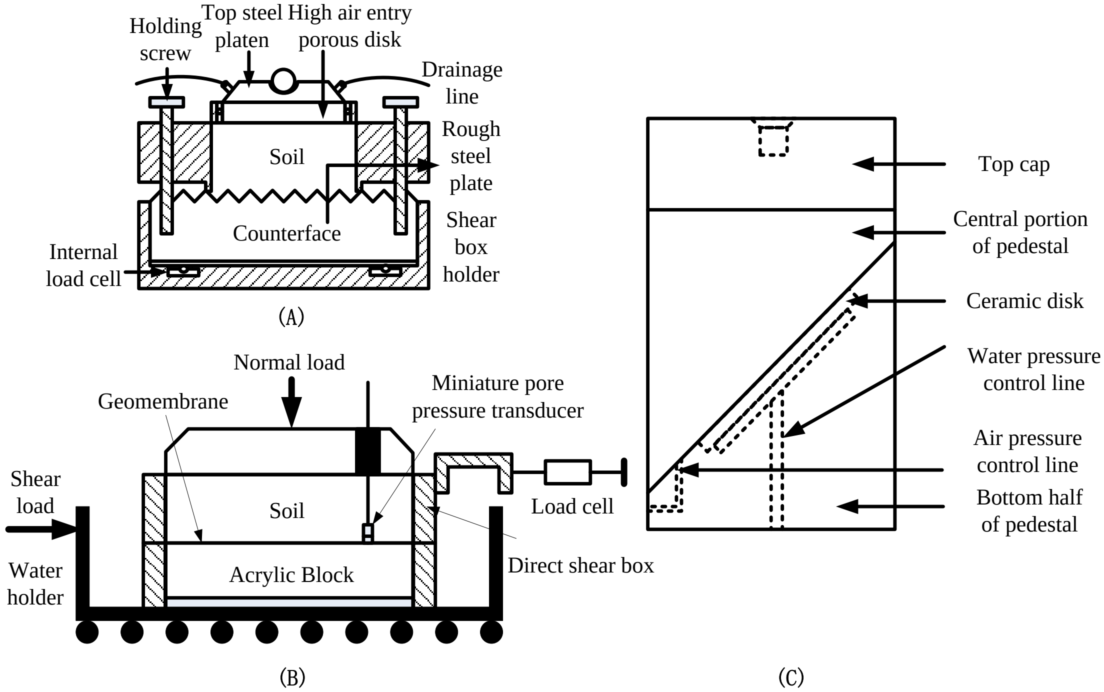

Figure 2.12 Apparatus for the unsaturated interface shear test [(A) is modified after Hamid and Miller 2009; (B) is modified after Fleming et al. 2006; (C) is modified after Hanson et al. 2001]

Vaunat et al. (2006), Vaunat et al. (2007) and Merchán et al. (2008) studied the effect of suction on the residual strength at high suctions (typically higher than 10 MPa). In their tests, vapour equilibrium method were employed to apply suction to the soil sample, which may be extended to high suction unsaturated interface shear test. As shown in Figure 2.13, the entire ring box is put inside a chamber isolated from the relative humidity of the room atmosphere by a vapour-tight rubber membrane. Two small tubes connect the chamber to the atmosphere prevailing above a saline solution in a closed recipient. Different saturated saline solution corresponds to different total suction. A pump connected to one of the tube allows for establishing a forced convection of vapour in the circuit. Eventually the suction inside the soil sample can be applied by the vapour of different relative humidity. A hygrometer equipped with an internal thermometer registers the values of relative humidity and temperature inside the chamber during the test.

Table 2.5 Salt solution and corresponding relative humidity and suction

Salt	RH (%)	Equivalent total suction (MPa)
Lithium Chioride ($LiCl.H_2O$)	11.3	297.6
Magnesium Chloride ($MgCl_2 \cdot 6H_2O$)	32.9	151.7
Magnesium Nitrate ($Mg(NO_3)_2 \cdot 6H_2O$)	53.4	85.6
Sodium Chloride ($NaCl$)	75.7	38.0
Potassium Sulphate (K_2SO_4)	96.8	4.4
Copper Sulphate ($CuSO_4$)	98.6	1.9

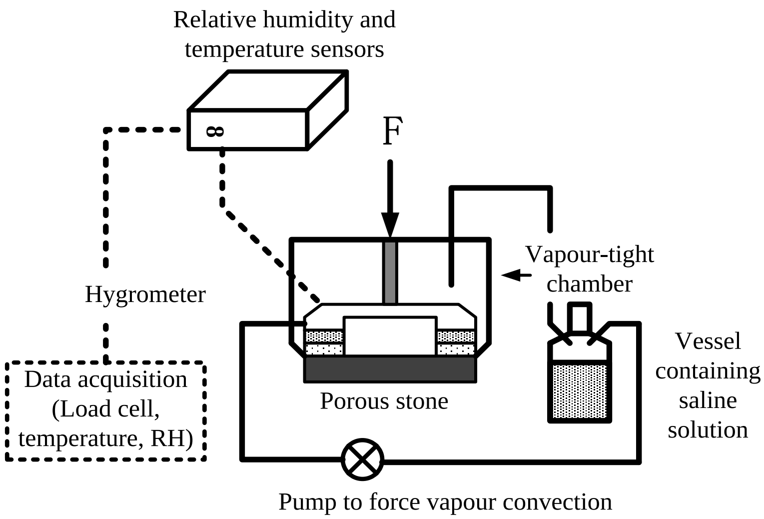

Figure 2.13 Apparatus used by Vaunat et al. (2006) to apply high suction

Apart from controlling or measuring the matric suction during shearing, there are also some scholars choosing to postpone the measurement of the matric suction of the soil after the interface shear test. For example, Hatami and Esmaili (2015) presented the results of small-scale pullout and interface tests on a woven geotextile reinforcement material in different marginal soils in order to quantify the difference in the soil–geotextile interface shear strength as a function of gravimetric water content for practical applications. The suction of the soil after shearing is determined using the water content information from the already measured SWCC. The dew point potentiometer (WP4-T) can also be used for the suction measurement for the shear failed samples to determine the suction at failure point. Chowdhury (2013) used this technique and performed a series of direct shear test to determine influences of suction on the shear strength of unsaturated

Regina clay. In comparison with the axis translation technique, to measure the water content or matric suction of soil sample after the shear test seems to be more fast and convenient. It avoids the long equilibrium time required in the axis translation technique and can be applied to the soil sample in entire suction range (0 to 10^6kPa). However, it is not possible to completely avoid the water loss in the sample collecting process. Further, once the vertical load is removed, volume rebound of the soil can influence the measurement as well.

From experimental studies, some general conclusions regarding the influence of matric suction on the unsaturated interface shear strength can be summarized as following: Suction makes a positive contribution to the peak interface shear strength. However, the contribution of suction to the peak interface shear strength is more significant for soil, followed by rough interface and smooth interface (Hamid and Miller 2009; Khoury et al. 2010; Hossain and Yin 2013; Borana et al. 2015). Also, the most critical interface layer thickness is likely to be zero mm (Borana et al. 2015). As for postpeak (i.e., residual) interface shear strength, is not significantly influence by matric suction at a given net normal stress (Hamid and Miller 2009; Khoury et al. 2010). Hamid and Miller (2009) concluded that reason for the phenomenon that during shearing beyond the peak interface shear stress, the air–water menisci are completely disrupted, resulting in a negligible strength contribution due to matric suction. As for the influence of net normal stress, it not only contributes to the mobilization of interface shear strength, but also changes the interface shear failure mechanism. Fleming et al. (2006) presented that increasing net normal stress could change the interface shear failure mechanism from a sliding mechanism to a combination of sliding and plowing due to embedment of soil particles into the structure interface. This phenomenon is also reported by Fan (2007) in his expansive soil-concrete interface shear test. At sufficiently high normal stresses, in case that soil particles has been completely embedded into the structure surface. The interface shear failure is no longer at the structure surface but within the soil, resulting in the mobilization of particle-to-particle friction (Fleming et al. 2006). There are also some models proposed for the estimation of unsaturated interface shear strength, which are introduced in Table 2.6.

Table 2.6 Approaches for estimating the unsaturated interface shear strength

Reference	Equation/Description	Remarks
Hamid and Miller (2009) and Khoury et al. (2010)	$\tau_{unsat} = c'_a + (\sigma_{nf} - u_{af})\tan\delta' + (u_{af} - u_{wf})\tan\delta^b$ (2.26) $\tau_{unsat} = c'_a + (\sigma_{nf} - u_{af})\tan\delta' + (u_{af} - u_{wf})\tan\delta'(\frac{\theta - \theta_r}{\theta_s - \theta_r})$ (2.27)	Suitable for non-textured geomembrane-soil interfaces.
Fleming et al. (2006)	$\tau_{unsat} = \alpha_{fl} + (\sigma_{nf} - \beta_{fl} u_{wf})\tan\delta'$ (2.28) where $\beta_{fl} = (\tan\delta^b / \tan\delta')$	Suitable for silty sand-geomembrane interface.
Sharma et al. (2007)	$\tau_{unsat} = \alpha_{sh} + [(\sigma_{nf} - u_{af}) + \chi_{sh}(u_{af} - u_{wf})\tan\delta_{sh}$ (2.29)	Suitable for silty sand-geomembrane interface.
Hossain and Yin (2010)	$\tau_{unsat} = c_{aho} + (\sigma_{nf} - u_{af})\tan(\delta' + \psi_{ihy})$ (2.30)	Suitable for granitic soil-cement grout interface.

where (σ_{nf} - u_{af}) = net normal stress at failure; (u_{af} - u_{wf}) = matric suction at failure; δ' = the interface friction angle with respect to net normal stress; δ^b = interface friction angle with respect to matric suction; θ = volumetric water content; θ_s = volumetric water content at a saturation of 100%; θ_r = residual volumetric water content; α_{fl} = the adhesion used in Fleming et al. (2006); σ_{nf} = normal stress at failure; u_{wf} = water pressure at failure; τ_{unsat} = the unsaturated interface shear strength; α_{sh} = the adhesion used in Sharma et al. (2007); δ_{sh} = the angle of shearing resistance at the soil-geomembrane interface; χ_{sh} = a parameter whose value ranges from 0 to 1; c_{aho} = the adhesion intercept, and can be defined as $c_{aho}=c_a'+(u_{af}-u_{wf})tan\delta^b$; ψ_{ihy} = the interface dilation angle; $(\delta'+\psi_i)= \delta_{max}$ = the apparent interface friction angle; c'_a = effective interface cohesion.

2.5 Literature review regarding the load transfer analysis of pile in expansive soil

In this part, literature review was conducted on previous studies on load transfer mechanism of piles in expansive soils main on two aspects, namely experimental studies and methods (including theoretical and numerical methods) available for pile load transfer analysis, thus presenting a brief summary of the previous researches on mechanical behaviors of piles in expansive soils upon infiltration.

2.5.1 Experimental studies on mechanical behaviors of piles in expansive soil

Different from traditional pile tests which mainly focus on determination of the ultimate bearing capacity of piles in certain type of soils, pile tests in expansive soils issue more attention to the variations in mechanical behaviors of pile foundation upon infiltration. In other words, more pile tests were conducted in order to study the influence of water infiltration on the load transfer mechanisms of pile in its service stage. Table 2.7 summarizes representative model and filed tests reported in recent years on piles in expansive soils upon infiltration highlighting their loading conditions, infiltration conditions, measurement conducted on piles and soils and their characteristics. Three different types of loading conditions were applied in these tests, namely zero pile head load, a certain amount of pile head load and displacement fixed pile head. Pile under no head load generally showed more obvious uplift phenomenon in the infiltration process while pile under a certain amount of head load is more approximate to the real scenario encountered in engineering practice. While the purpose of fixed the pile head is to monitor the mobilization of the total uplift force in the infiltration process through a pressure cell. Manual infiltration was generally applied in model pile test to saturate the soil around the pile from initial condition, thus presenting the complete description of pile behaviors from initial condition to most dangerous scenario. As for the pile mechanical behaviors, more attention has been issued to the uplift movement of the pile and/or the uplift force generated in the infiltration process. Further, most tests were conducted under zero pile head load in order to observe a more significant pile uplift displacement. Few tests gave detailed description on the pile load transfer mechanism changes in the infiltration process regarding changes in pile axial force distributions, pile shaft friction distributions and pile base resistance. Although matric suction has been widely accepted as a key stress state variable that affects the mechanical behaviors of piles in unsaturated soils, due to the limitations in testing technique and equipment, in most tests only water content variations of the soil around the pile was measured instead of matric suction. Based on various tests introduced in Table 2.7, Figure 2.14 gives the logic structure of a relative complete pile infiltration test in expansive soil including all the measurements needing to be conducted for analysis of pile mechanical behavior variations.

Table 2.7 Previous experimental studies on piles in expansive soils

Reference	Experiment settings	Boundary conditions (stress and hydraulic)	Measurement conducted	Remarks
Fan (2007); Fan et al. (2007) and Xiao et al. (2011).	Large scale model test (Nanning expansive soil, Guangxi, China): the model pile was 50mm in diameter and 580mm buried in expansive soils.	No load was applied on the pile head; Manual infiltration to saturation.	Pile heave; Pile axial force; Pile base resistance; Ground heave with depth.	Sand drains were adopted to accelerate the infiltration process by manual irrigation.
Soundara and Robinson (2017)	Large scale model test (Siruseri, Tamil Nadu, India): the model pile was made of cement mortar with a mix proportion of one part of cement and two parts of sand with water cement ratio of 0.45. The diameter of the pile is 30mm. The pile penetrates the testing cylindrical mould whose height is 180mm.	The pile head was fixed for the measurement of uplift force; Manual infiltration to saturation.	Uplift force; Ground heave.	Surcharge (from 1 to 140kPa) was applied over the soil sample through the lever arm whose arrangement is similar to conventional consolidation set up.
Mendoza (2013)	Centrifuge test (Tibu expansive soil, Norte de Santander, Colombia): aluminum cubic blocks having a height of 120mm, a width of 70mm and a length of 140mm; Sandpaper was attached to simulate the rough surface; Pressure cells were attached to record the pressure.	No load was applied on the pile head; Manual infiltration to saturation.	Pile heave; Pile axial forces in different depth; Pile base resistance; Lateral pressure with depth; Ground heave with depth; Water content variations with depth.	Centrifuge test conducted to study the variations of shaft friction of piles in expansive soils upon infiltration.

Attwooll et al. (2006) and Overton et al. (2007).	Field investigation (Loveland, Colorado, USA): drilled concrete piles having a diameter of 750mm installed to a depth of 7m.	A dead load of 435kN was applied on the pile head; Natural infiltration.	Pile heave; Ground heave; Water content variations with depth.	Heave of the piles and structural floors of a building constructed in 1991 and 1992 was observed during construction and prior to the occupancy of the building in 1993. Therefore a geotechnical investigation was performed.
Reichler (1997); Durkee (2000); Abshire (2002) and Benvenga (2005).	Field test (Colorado State University Test Site, USA): 350mm diameter concrete piles were installed at the site to a depth of 7.6 m.	No load was applied on the pile head; Natural infiltration.	Pile heave; Pile axial forces with depth; Ground heave with depth; Water content with depth.	Large scale filed tests continuously conducted for several years (from 1997 to 2004), which were subjected to environmental factors changes (natural infiltration and evaporation).
Mohamedzein et al. (1999); Osman and Elsharief (1999); Al-Rawas and Goosen (2006).	Field test (Wad Madani and Elfao, Sudan): piles were 250mm in diameter with lengths ranging from 1 to 4m.	No load was applied on the pile head; Natural infiltration.	Pile heave; Ground heave with depth; Water content with depth.	The test sites were flooded during the rainy season, and the pile and ground heave were measured for a period of 3.5 months. Total suction variations with depth were presented.
Wu et al. (2012)	Field test (Laos): drilled concrete piles having a diameter of 400mm installed to a depth of 2.25m to 5m.	The pile head was fixed for the measurement of uplift force; Manual infiltration for around 10 days.	Uplift force; Ground heave with depth.	Reaction frame was used for the measurement of uplift force upon infiltration.

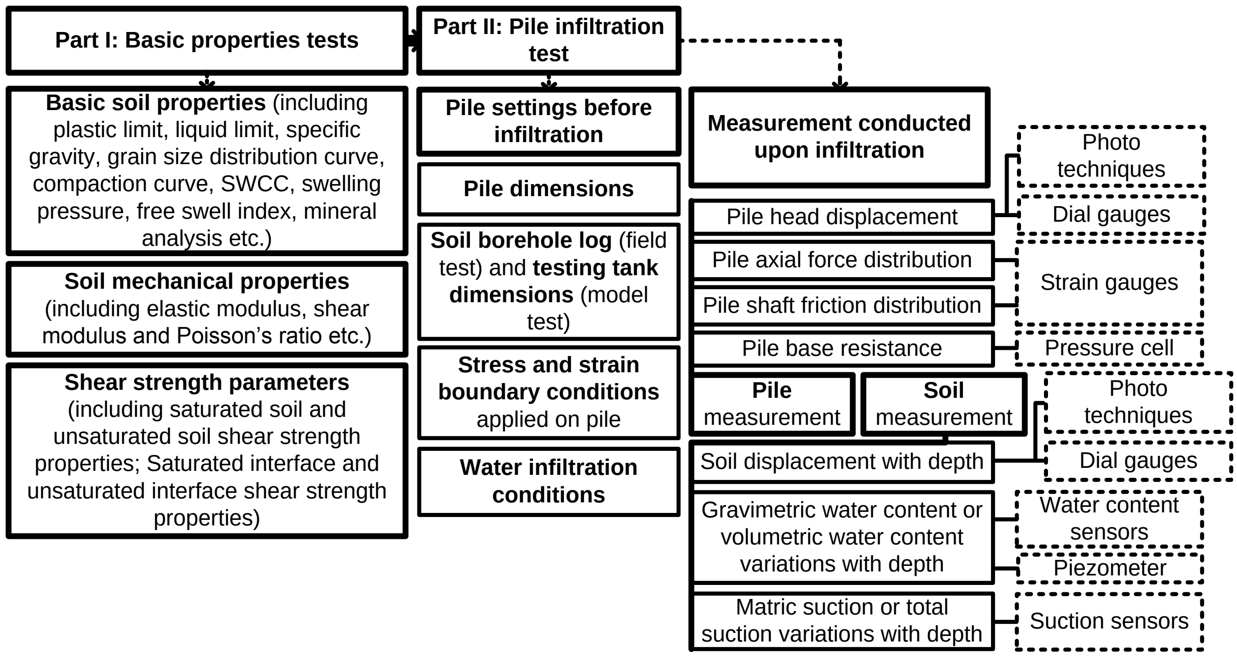

Figure 2.14 Logic structure of a complete pile infiltration test in expansive soil

2.5.2 Available methods for load transfer analysis of pile in expansive soil

Many methods available for the pile load transfer analysis fall into three main categories: (1) Shear displacement method proposed by Cooke in 1974, which assumes that there is no slip in the pile-soil interface and the soil around the pile can be simplified as a series of concentric cylinders. The shear stress is transferred from the pile-soil interface to surrounding soil and cause settlement of soil around the pile. (2) The load –transfer curve method (Coyle and Reese 1966; Kraft et al. 1981; Xiao et al. 2002; Zhang et al. 2010a; Bohn et al. 2016), which use load-transfer function to describe the relationship between the unit skin friction transferred to the surrounding soils and the pile-soil deformation behavior in each soil layer. (3) Numerical method, which includes boundary-element method and finite element method (Mandolini and Viggiani 1997; Mendoça and De paiva 2000; Ai and Han 2009; Sheng et al. 2005; Comodromos et al. 2009; Said et al 2009). By employing various constitutive relationship and numerical models, the soil mass and pile-soil interaction response can be described. Numerical method is one of the most powerful approaches for the analysis of the behavior of single pile or pile groups. However, it is not commonly used in practice because of its high computational requirement (Zhang and Zhang 2012).

Considering the characteristics of expansive soil, several scholars make necessary modifications to common used methods introduced above and proposed suitable methods for the pile load transfer analysis in expansive soils.

Fan (2007) proposed an analytical solution based on the shear displacement method, which achieved relatively good results in monitoring the pile-soil interaction behavior. This method is also available in Fan et al. (2007) and Xiao et al. (2011). This method assumed the soil around the pile to be a serious of concentric cylinders (as shown in Figure 2.15). Based on the traditional shear displacement method proposed by Cooke in 1974, ignoring the body force, the vertical equilibrium equation for a single element is given in Equation 2.31.

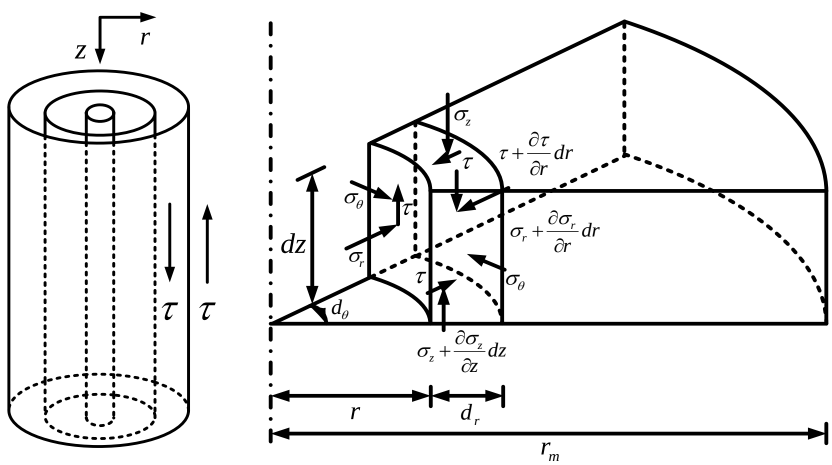

Figure 2.15 Schematic of hollow soil cylinder surrounding the pile and analytical unit

$$\frac{\partial \sigma_z}{\partial z} + \frac{\partial \tau_{rz}}{\partial r} + \frac{\tau_{rz}}{r} = 0 \qquad (2.31)$$

Simplify Equation 2.31 by removing the first item $\partial\sigma_z/\partial z$ because the effect of increase of σ_z is much less than that of τ_{rz}:

$$\frac{\partial \tau_{rz}}{\partial r} + \frac{\tau_{rz}}{r} = 0 \tag{2.32}$$

After integration with the soil-pile interface condition, Equation 2.33 can be acquired.

$$\tau_{rz} = \frac{\tau_0 r_0}{r} \tag{2.33}$$

where τ_0 = shear stress at the interface of soil-pile; r_0 = pile radius.

On the other hand, according to the geometry equation,

$$r = \frac{\partial u}{\partial z} + \frac{\partial w}{\partial r} \tag{2.34}$$

where u and w = radius and vertical displacement, respectively.

Simplifying Equation 2.34 by removing $\partial u/\partial z$ results in

$$r = \frac{\partial w}{\partial r} \tag{2.35}$$

Since

$$r = \frac{\tau_{rz}}{G} \tag{2.36}$$

where G = shear modulus of soil.

With Equation 2.34 to 2.36 obtaining

$$\partial w = \frac{\tau_{rz}}{G}\partial r = \frac{\tau_0 r_0}{G}\frac{\partial r}{r} \tag{2.37}$$

where r_0 = radius of pile; r = distance from pile axis to the calculated position; and τ_0 = shear stress at the pile-soil interface.

After integration of Equation 2.37, the result is

$$\begin{cases} w(z,r) = \int \partial w = \dfrac{\tau_0 r_0}{G}\int_r^{\alpha} \dfrac{\partial r}{r} = \dfrac{\tau_0 r_0}{G}\ln(\dfrac{r_m}{r}) & (r_0 \le r \le r_m) \\ w(z,r) = 0 & (r > r_m) \end{cases} \tag{2.38}$$

where r_m = the distance form pile axis to somewhere that the deformation of soil can be ignored as shown in Figure 2.15, which is dependent on Poisson ratio, υ, and pile length, L (Randolph and Worth 1978):

$$r_m = 2.5L(1-\upsilon) \tag{2.39}$$

Equation 2.38 is the logarithm function proposed by Randolph and Worth (1978) to describe $w(z,r)$. This means that the vertical downward displacement of the soil $w(z,r)$ around the pile relates not only to the soil depth z but also to the distance r from the pile center axis. This is also called shear displacement method.

Equation 2.38 would be the basic formula in deriving the pile-soil interaction in expansive soils. In view of the complication of the pile soil interaction in an expansive soil foundation, some assumptions are required.

Fan (2007) simplify the issue by assuming the pile-soil interaction is the result of two cases: pile into soil under applied loads and soil elevating the pile under the soil's swelling pressure, as illustrated in Figure 2.17(A) and (B). To clarify these two cases in derivation, the subscripts 1 and 2, respectively, are used to denote the two cases.

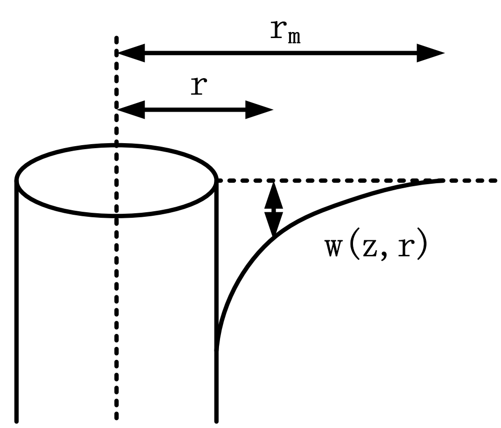

Figure 2.16 Soil deformation assumptions

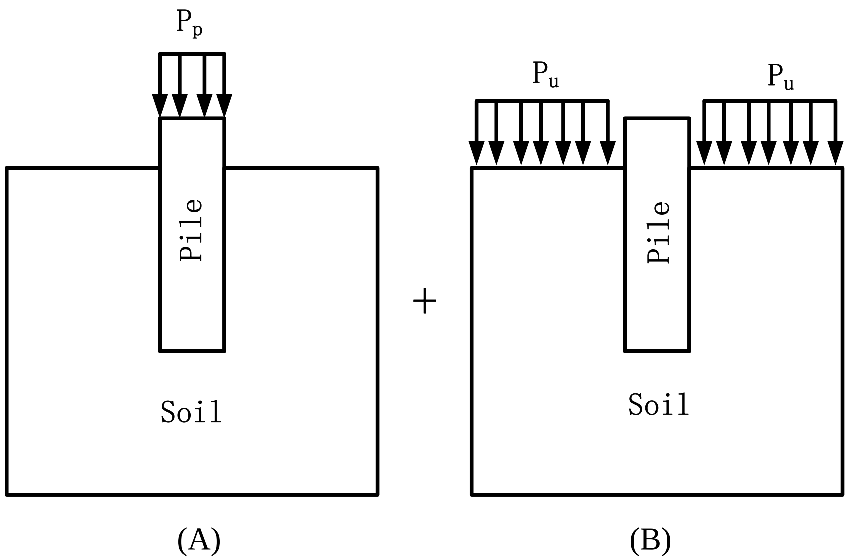

Figure 2.17 Sketch of interaction between pile and soil in expansive soil foundation

In case one, when pile only bears the applied load, the displacement of the pile, $w_{p1}(z)$, pile's skin friction, $\tau_1(z)$, and the axial force of the pile, $P_1(z)$, could be obtained as Equation 2.40 to 2.42.

$$w_{p1}(z) = n_b P_p \frac{\cosh(\beta\theta) + n^{-1}\sinh(\beta\theta)}{\cosh\beta + n\sinh\beta} \tag{2.40}$$

where $\beta=\mu L$; $n=E_pA_p\mu n_b$; θ=1-z/L_0; $\mu=(2/\xi\lambda_p r_0^2)^{0.5}$; $\lambda=E_p/G_s$; $n_b=\eta(1-\upsilon_b)/4r_bG_b$; η= effective parameters of pile-end displacement, generally η=0.5-1.0 (Xiao et al. 2003); υ = Poisson's ratio of the pile-end soil; r_b = radius of the pile end; G_b = shear modulus of the pile-end soil;

$$\tau_1(z) = \frac{G}{r_0\xi} w_{p1}(z) \tag{2.41}$$

where $w_{p1}(z)$ is displacement of pile; ξ is effective parameter of the pile radius ξ is $\ln(r_m/r_0)$, G_s is shear modulus of soil.

$$P_1(z) = P_p \frac{\cosh(\beta\theta) + n\sinh(\beta\theta)}{\cosh\beta + n\sinh\beta} \tag{2.42}$$

In case two, when the pile only bear soil's swelling pressure, the displacement of the pile, $w_{p2}(z)$, pile's skin friction, $\tau_2(z)$, and the axial force of the pile, $P_2(z)$, could be obtained as Equation 2.43 to 2.45.

$$w_{p2}(z)=\begin{cases} w_{p21}(z)=C_3\sinh(\alpha z)+C_4\cosh(\alpha z)-s_0(h_0-z)/h_0 & (0\le z\le h_0) \\ w_{p22}(z)=C_5\sinh(\alpha z)+C_6\cosh(\alpha z) & (h_0\le z\le L) \end{cases} \tag{2.43}$$

where C_3=-s_0/(αh_0); C_5=[C_3+$s_0$cos(αh_0)/(αh_0)]; C_6={-$s_0$cosh(αL)[cosh(αh_0) - 1]}/[αh_0sinh(αL)]; C_4=[C_6-$s_0$sinh(αh_0)]/(αh_0); $\alpha=(2\pi/\lambda_p A_p \xi)^{0.5}$; h_0 = active zone or the maximum depth that the water can be immersed into; and s_0 defines the heave at the expansive soil surface.

$$\tau_2(z)=\frac{G}{r_0\xi}[s(z)+w_{p2}(z)] \tag{2.44}$$

$$P_2(z)=\begin{cases} P_{21}(z)=-E_pA_p(\alpha C_3\cosh(\alpha z)+\alpha C_4\sinh(\alpha z)+s_0/h_0) & (0\le z\le h_0) \\ P_{22}(z)=-E_pA_p(\alpha C_5\cosh(\alpha z)+\alpha C_6\sinh(\alpha z) & (h_0\le z\le L) \end{cases} \tag{2.45}$$

When pile bears both applied load and soil's swelling pressure, which can be referred to as case three. This complex question can be simplified as a linear combination of case 1 and case 2.

$$\begin{cases} w_p(z)=w_{p1}(z)+w_{p2}(z) \\ P(z)=P_1(z)+P_2(z) \\ \tau(z)=\tau_1(z)+\tau_2(z) \end{cases} \tag{2.46}$$

The proposed analysis can be easily used to estimate the pile-soil interaction in an expansive soil foundation. The numerical simulation coincides with the in situ observation and a model pile test. However, the whole deduction process is based on the constitutive relations form elastic mechanics without considering the influence of suction on the volume change and shear strength of the element. So this method has the potential to be further developed by adding matric suction as an independent stress state variable.

Based on the load transfer curve method, Hong (2008) proposed a numerical model for the prediction of the stresses and axial and bending displacements in a drilled pier in expansive soils. With suction variations available, initially the increasing horizontal earth pressures caused by the volume expansion of expansive soil is predicted. Then shear stress induced on the pile shaft can be acquired using the load transfer curve which represents the relationship of the shear stress corresponding to the relative displacement between the soil and the pier shaft. The relative displacement between the soil and the side of pier corresponding to the ultimate shearing resistance adopted by Hong (2008) is 1.2% of the diameter of the pier according to Aurora et al. (1981). The relationship between shear stress and relative displacement is proposed as Equation (2.47).

$$\tau_{sp} = \frac{S_{ult}}{2}\left(\frac{\delta_{relative}}{0.0015 b_{dia}}\right)^{\frac{1}{3}} \tag{2.47}$$

where τ_{sp} = the shear stress between soil and the pier; S_{ult} = the ultimate shearing resistance; $\delta_{relative}$ = the pier soil relative displacement; b_{dia} = the diameter of the pier.

As for the lateral behavior, the load-deflection curves are developed based upon the stress state around the pier and non-linear suction dependent elastic modulus of the unsaturated soils. A numerical model of the bending and stretching of a pier includes a beam column approach and linear distribution of shear stress around the circumference of the pier between the maximum and minimum shear stresses. Case studies of axial and bending of piers are presented with both uniform and non-uniform wetting. A case study is performed in the case of the non-uniform wetting around the pier in moderately expansive soils at a site of National Geotechnical Experimentation Site at the University of Houston, Texas (Kim and O'Neill, 1998). Corresponding to the suction variation and soil profiles, the pier case study for axial behavior shows a good agreement with a heave at ground surface and uplift forces.

Many other research scholars performed the numerical analysis of piles in expansive soils. For example, Ellison et al. (1971) used the finite element method to study the load deformation mechanism of piers in London clay. The axisymmetric stress condition was assumed. The pile was assumed linear elastic and a trilinear elastic stress–strain relationship was assumed for the soil.

Amir and Sokolov (1976) used the finite element method to study the behavior of piers in expansive soils. The conditions of axisymmetric stress for a single pier were assumed and the soil was modeled as linear elastic. Environmental effects were represented by a sinusoidal moisture flux function. A conclusion was given in this study that displacements were smaller for deeper piers and piers with heads laterally fixed. Bells and isolation sleeves showed only a minor effect.

Justo et al. (1984) presented a three-dimensional finite element method to calculate stresses and strains in piles in expansive soils. An outstanding feature of this method is that the stress path during the loading and wetting processes were taken into account. The soil is assumed isotropic, nonlinear, and non-homogeneous. The nonlinearity and non-homogeneity were modeled through the dependence of the initial swelling constraint modulus upon vertical stress. Results show that the stress path had large influences on the calculated heave and tension of the pier.

Mohamedzein et al. (1999) developed a two dimensional axisymmetric finite element based model for analysis of a soil-pile system in expansive soils. The pile is assumed to behave as linearly elastic while the soil is modelled as nonlinear elastic material. Swelling and shrinkage of the soil are related to change in soil suction. The displacement based finite element formulation for soil-structure interaction was implemented in a computer program developed by Mohamedzein (1989). Major changes to the existing code were the addition of new sub-routines for calculation of the displacements in the soil and pile due to an increase or change in soil suction. The proposed model gave reasonable values of vertical upward movement of piles in expansive soil when compared to the results obtained from the field experiments.

Poulos (1993) studied the pile-raft-soil interaction when the soil is subjected to either downward or upward vertical movements as a result of changes in effective stress or suction in the soil. The analysis employed makes use of the simplified boundary element approach, in which the raft is represented as a series of rectangular elements resting on the soil surface, and each of the piles is discretized into a series of shaft and base elements. The general approach to the piled-raft analysis is described by Kuwabara (1989), while the inclusion of external (or free field) vertical soil movements is as described by Kuwabara and Poulos (1989). Recently, a through literature summary can be seen in Al-Rawas and Goosen (2006) on the use of finite-element formulations to analyze pier heave.

2.6 Summary and conclusions

In this chapter, the commonly used types of piles in expansive soils were first introduced. The mechanical behavior variations of piles under traditional loading condition were then discussed extending the mechanics of unsaturated soils taking account of the influence of water infiltration. It can be concluded that the mechanical behaviors of piles in expansive soils is a can be rationally interpreted by coupling the flow behavior, volume change behaviors and interface shear strength properties. Water infiltration gives rise to the ground heave vertically and the mobilization of lateral swelling pressure horizontally. Also, the matric suction variations due to water infiltration also change the pile-soil interface shear strength properties. The shaft friction is combined determined by the increasing lateral earth pressure due to the mobilization of lateral swelling pressure, the changing pile-soil interface shear strength properties and the changing pile-soil relative displacement. Further this shaft friction variation causes the axial stress redistribution and possible movement of the pile.

Focus on these factors, a critical review of various testing methods (laboratory, large scale model and in situ tests) that are used for determination of the lateral swelling pressure are presented and discussed. The various factors that influence the mobilization of lateral swelling pressure are summarized in a flow chart. The influences of several of these factors are not taken into account in the conventional design of geo-infrastructure in expansive soils. Then, some commonly used testing apparatus and technique for the determination of the unsaturated interface shear strength are introduced and discussed. Further, a detailed illustration is issued to various load transfer analysis methods suitable for load transfer analysis of piles in expansive soils including modified shear displacement method, modified load transfer curve method and numerous numerical methods. Following conclusions can be summarized from above literature review:

(1) Several laboratory and in-situ measurement of lateral swelling pressure techniques have been developed during the last 50 years. Lateral swelling pressure measurement based on the laboratory test methods is stress path dependent. Amongst various laboratory measurement techniques that are presently available in the literature, swell under surcharge test is mostly recommended since it can well simulate the scenario that are typically encountered in engineering practice. Compared with laboratory measurement techniques, large scale model and in-situ tests are more comprehensive, time consuming and expensive. However, these tests can provide experimental results that are of significant value for engineering practice applications. Most large scale model and in-situ tests belong to the category of swell under surcharge tests.

(2) Swelling pressure that mobilizes and acts on geotechnical infrastructure can be attributed to water infiltration in expansive soils that triggers swelling potential. Swelling potential is conventionally determined or estimated from derived information of percentage clay, clay minerals or clay structure in expansive soils. Clay particle orientation is a key factor which influences the swelling pressure both in vertical and horizontal directions. Particle orientation is determined by the stress path in natural soils and the compaction method in remoulded soils. In addition, both the time effects and fatigue phenomenon have significant impact on the mobilization of lateral swelling pressure. Such a behavior can be more reliably derived from large scale model and in-situ tests.

(3) Unsaturated interface shear test can be conducted under a certain suction applied by axis translation technique or vapor equilibrium technique, however, generally quite a long time is required for the equilibrium process. It is also available to measure the interface suction during the shearing process or after the shear failure. However, the range for real time measurement of suction is limited by the testing apparatus, while the precision of the suction measurement after the shear failure is influence by various

factors. It is commonly accepted that suction makes a positive contribution to the peak interface shear strength. The contribution of suction to the peak interface shear strength is more significant for soil, followed by rough interface and smooth interface. The residual interface shear strength is not significantly influence by matric suction because during shearing beyond the peak interface shear strength, the air–water menisci are completely disrupted.

CHAPTER THREE

MOBILIZATION OF LATERAL SWELLING PRESSURE ON STRUCTURES IN EXPANSIVE SOILS

Notation

Symbols	
A	Activity of soils
C	Clay content of soils
c'	True cohesion of soil
c_a'	Effective interface cohesion
E_a	Average value of various E_{unsat} calculated using Equation 3.6 over the range of matric suction variation
E_{unsat}	Elastic modulus of unsaturated expansive soil
E_{sat}	Elastic modulus of saturated expansive soil
$E_{(a\text{-}0)}$	Average elastic modulus over the matric suction range from $(u_a - u_w)_a$ to zero
$E_{(a\text{-}b)}$	Average elastic modulus with respect to net normal stress over the matric suction range from $(u_a - u_w)_a$ to $(u_a - u_w)_b$
$E_{(a\text{-}b)}$	Average elastic modulus with respect to net normal stress over the matric suction range from $(u_a - u_w)_a$ to $(u_a - u_w)_b$
$H_{(a\text{-}0)}$	Average elastic modulus over the matric suction range from $(u_a - u_w)_a$ to zero
$H_{(a\text{-}b)}$	Average elastic modulus with respect to matric suction over the matric suction range from $(u_a - u_w)_a$ to $(u_a - u_w)_b$
$H_{(b\text{-}0)}$	Average elastic modulus with respect to matric suction over the matric suction range from $(u_a - u_w)_b$ to zero
h	Thickness of the calculated soil layer
I_P	Index of plasticity
K_0	At rest earth pressure coefficient
OCR	Over consolidation ratio
P_{LS}	Lateral earth pressure considering the contribution of lateral swelling pressure
P_a	Atmospheric pressure
P_s	Vertical swelling pressure acquired from constant volume swelling pressure test
P_{S0}	Intercept on the P_S axis at zero suction value (P_{S0} *is* 55kpa for compacted expansive soils)

$P_{s(a\text{-}0)}$	Constant volume vertical swelling pressure generated from a matric suction reduction from $(u_a - u_w)_a$ to zero
$P_{s(a\text{-}b)}$	Constant volume vertical swelling pressure generated from a matric suction reduction from $(u_a - u_w)_a$ to $(u_a - u_w)_b$
$P_{s(b\text{-}0)}$	Constant volume swell pressure generated from a matric suction reduction from $(u_a - u_w)_b$ to zero
p_0	Pore water pressure
S	Degree of saturation
S_r	Degree of saturation
u_{af}	Pore-air pressure at failure
α_{ad} and β_{ad}	Fitting parameters, Adem (2015) calculated E_{unsat} for five different expansive soils and suggested that β_{ad} is 2 typically and α_{ad} varies from 0.05 to 0.15 for expansive soils
α_T	Modified coefficient for tensile stress in unsaturated soils, within the range of 0.5-0.7 (Baker 1981, Bagge 1985)
β_S	Fitting parameter
Δh	Heave of soil
θ	Current volumetric water content
θ_r	Residual volumetric water content form a SWCC
θ_s	Saturated volumetric water content from a SWCC
σ_c	Lateral earth pressure developed only due to swelling
σ_r	Lateral earth pressure developed only due to soil unit weight and/or surcharge
σ_s	Vertical stress due to soil unit weight and/or surcharge
σ_{nf}	Normal stress at failure
σ_s	Vertical stress due to unit weight of upper soil layers and surcharge
τ_{design}	Design shear strength of soil
ϕ'	Effective internal friction angle of soil
ϕ^b	Angle of friction with respect to matric suction
δ'	Effective interface friction angle
δ^b	Interface friction angle with respect to matric suction
γ	Unit weight of the soil
ψ	Soil suction
$(\sigma_{nf} - u_{af})$	Net normal stress on the failure plane at failure
$(u_{af} - u_{wf})$	Matric suction on the failure plane at failure

The chapter is directed towards analyzing the lateral earth pressure acting on geotechnical infrastructures constructed within expansive soils considering the mobilization of lateral swelling pressure. To facilitate the analyses, a theoretical relationship between the lateral swelling pressure and the vertical swelling pressure measured from constant volume swell test is proposed. This relationship is further developed to estimate the mobilization of lateral earth pressure considering lateral swelling pressure in the infiltration process against a fixed rigid retaining wall. The passive earth pressure as the limiting condition of the mobilization of lateral swelling pressure developed under different situations, are analyzed (i.e. saturated-frictionless interface, saturated-rough interface, unsaturated-frictionless interface, unsaturated-rough interface). Two large scale model retaining wall tests conducted in laboratory environment and two field case studies on retaining walls with in-situ measurements from the published literature are used to illustrate and verify the proposed approach. Good comparison were achieved between experimental data and estimations using the proposed methods. The tools proposed in this paper are simple and can be used by geotechnical engineers in practice for the design of geo-infrastructure placed in both unsaturated and saturated expansive soils, where the lateral swelling pressure is a concern.

3.1 Analytical Method for Estimation of the Lateral Swelling Pressure

3.1.1 Basic assumptions

The following assumptions were used for proposing a simple relationship between the lateral swelling pressure and vertical swelling pressure upon free swelling: (1) both the soil behind the retaining structure and around the pile are considered to be isotropic, homogeneous and elastic in nature without any plastic deformation (such as collapse of soil structures due to over-load) in the swelling process; (2) Strains are relatively small; (3) the pore-air pressure is continuous and is at atmospheric pressure condition; (4) Pore-water is not compressible and both the diffusion of air into the water and the water vapor into the air is negligible.

The soil particle orientation can contribute to different magnitudes of swelling potential in vertical and horizontal directions. The swelling potential is greater when the soil structure is oriented parallel to each other (Gokhale and Jain 1972). Natural expansive soils usually show strong anisotropic behavior. For example, for a flat-lying deposit, the swelling potential in the vertical direction is usually greater than the lateral (horizontal) direction; however, for steeply dipping deposits it is just the opposite (Nelson et al. 2015). The expansive soil backfill behind the retaining structure falls into the category of remoulded soil and the construction or installation of pile typically disturbs the initial soil structure. Also, Gokhale and Jain (1972) studies suggest that variation in swelling trends in vertical and horizontal directions significantly reduces when a non-expansive soil is mixed into expansive soils. Due to these reasons, remoulded expansive soil backfill behind a retaining structure or around the pile can be assumed to be isotropic and homogeneous.

Terzaghi’s (1925, 1926, 1931) pioneering studies suggest that expansive clay swelling and shrinkage are essentially elastic deformations caused by the clay’s affinity for water. From these studies, it can be concluded that the swelling of the soil produced by eliminating the surface tension of the capillary water (suction) is identical with the expansion produced by the removal of the external load. The swelling potential can be considered equivalent to "free energy" generating from the elastic expansion of the solid phase. Previously held under compression by the surface tension of the water, this "free energy" can be totally converted into mechanical force. Terzaghi’s studies were inspiration for providing a theoretical basis in the present study for proposing a relationship between the vertical swelling pressure and the lateral swelling pressure in the elastic range. Adem and Vanapalli (2013) also have extended Terzaghi’s assumptions (1925, 1926, 1931) and proposed modulus of elasticity based method for estimating the 1-D heave of several expansive clays providing reasonable estimations with the measured data.

Figure 3.1 provides a schematic that highlights the stress state of analytical soil elements at different depths behind frictionless retaining structures and around frictionless single pile. In order to simplify the analysis, an analytical element around the pile whose shape is a segment of hollow cylinder is considered as a cubic soil element. Based on this simplification, two different analytical elements under different stress states are shown. The soil element close to ground surface [Figure 3.1(A)] is only subjected to horizontal confinement belongs to the first category. However, soil elements under the influence of surcharge loads and at a greater depth [Figure 3.1(B)] are influenced by a vertical stress as well. They represent the second category of elements. Upon infiltration, the soil element (A) at the surface can swell freely in the vertical direction while the vertical volume expansion of soil element (B) is restricted to a certain extent due to the influence of surcharge. In the horizontal direction, volume expansion of the analytical elements is assumed to be strictly restricted. This assumption is reasonable since horizontal strains can greatly reduce the lateral swelling pressure applied on the retaining wall while a larger lateral swelling pressure estimation can contribute to a more conservative design.

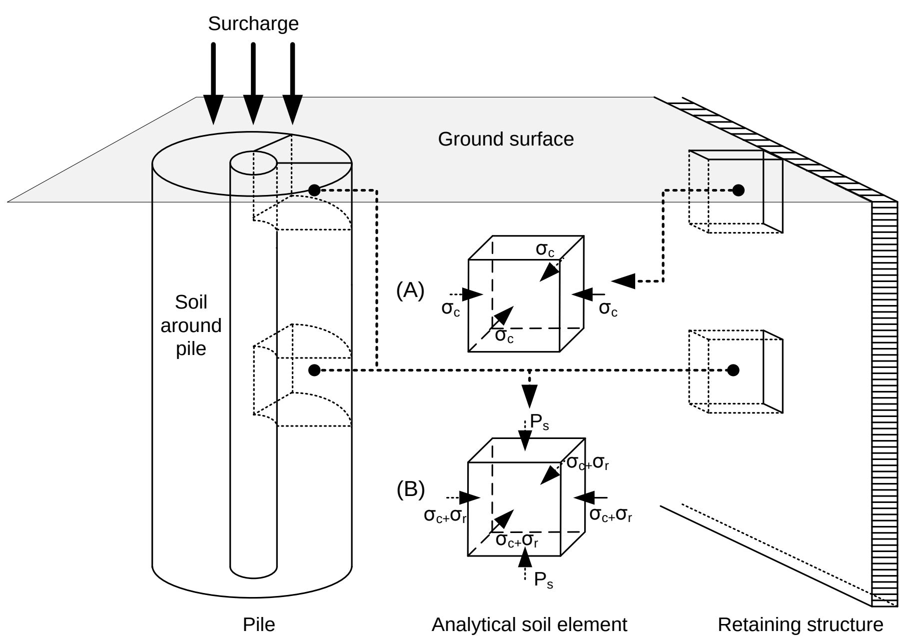

Figure 3.1 Analytical expansive soil element behind frictionless retaining structure and around frictionless pile

3.1.2 Stress state changes in analytical elements upon swelling

Upon water infiltration, the stress state changes that occur in the soil elements shown in Figure 3.1 are illustrated in Figure 3.2. Neglecting the body force, for surface elements (a), the stress state changes arising upon water infiltration are shown in **stage (a).**

Stage (a) shows an analytical element (a) that swells with a reduction in matric suction. In the vertical direction, volume expansion occurs freely such that the vertical side length of the analytical element increases from c to b. However, as the volume deformation is restricted by fixed boundary conditions, the back pressure σ_c produces and acts on the horizontal boundaries.

For analytical element (b), in addition to the reduction in matric suction, there is also surcharge acting on the top of the element. Therefore, superposition method can be extended for analytical element (b) in which a matric suction decrease contributes stress state change as described in **stage (a)**. In addition, the vertical pressure that is imposed on the top of the soil element could be due to surcharge of the superstructure and the overburden pressure. For such a scenario, the soil element will experience a change in stress state as shown in **stage (b)**.

Stage (b) shows that after **stage (a)**, a vertical pressure σ_s is further imposed on the top of the element. Under its influence, the vertical side length decreases from b to d and the horizontal confining pressure that generated in **stage (a)** would further gain an increment σ_r.

Fredlund and Morgenstern (1976) provided constitutive relationship (Equation 2.7) extending continuum mechanics theory for unsaturated soils in terms of two independent stress state variables; namely, net normal stress, $(\sigma - u_a)$ and matric suction, $(u_a - u_w)$. This relationship is employed here to describe the two stress changes: **stage (a), (b)**. Assuming the pore-air pressure is zero, stress state changes in **stage (a)** and **stage (b)** can be described using Equation 3.1 and Equation 3.2 respectively.

$$\begin{cases} \dfrac{b-c}{c} = \dfrac{2\upsilon}{E}\sigma_c - \dfrac{(u_a - u_w)}{H} \\ 0 = \dfrac{\upsilon - 1}{E}\sigma_c - \dfrac{(u_a - u_w)}{H} \end{cases} \tag{3.1}$$

$$\begin{cases} \dfrac{d-b}{b} = \dfrac{2\upsilon}{E}(\sigma_c + \sigma_r) - \dfrac{\sigma_s}{E} \\ 0 = \dfrac{\upsilon}{E}(\sigma_s + \sigma_c + \sigma_r) - \dfrac{(\sigma_c + \sigma_r)}{E} \end{cases} \tag{3.2}$$

Equation 3.3 and Equation 3.4 are expressions that are derived by solving the earlier derived equations for estimating horizontal confining pressure σ_c in **stage (a)** and the horizontal confining pressure increment due to surcharge σ_r in **stage (b)**. The lateral swelling pressure σ_c corresponds to the lateral earth pressure of the soil element associated with swelling, while σ_r corresponds to the lateral earth pressure contribution that arises due to surcharge. By applying superposition method, a general lateral earth pressure estimation model can be proposed which includes both the lateral earth pressure due to swelling and surcharge as shown in Equation 3.5.

$$\sigma_c = \frac{(u_a - u_w)E}{H(\upsilon - 1)} \tag{3.3}$$

$$\sigma_r = \frac{\upsilon}{1-\upsilon}\sigma_s \tag{3.4}$$

$$P_{LS} = \sigma_c + \sigma_r = \frac{(u_a - u_w)E}{H(\upsilon - 1)} + \frac{\upsilon}{1-\upsilon}\sigma_s \tag{3.5}$$

where P_{LS} = the lateral earth pressure considering the contribution of lateral swelling pressure; σ_c = the lateral earth pressure developed only due to swelling; σ_r = the lateral earth pressure developed only due to soil unit weight and/or surcharge; σ_s = the vertical stress due to soil unit weight and/or surcharge.

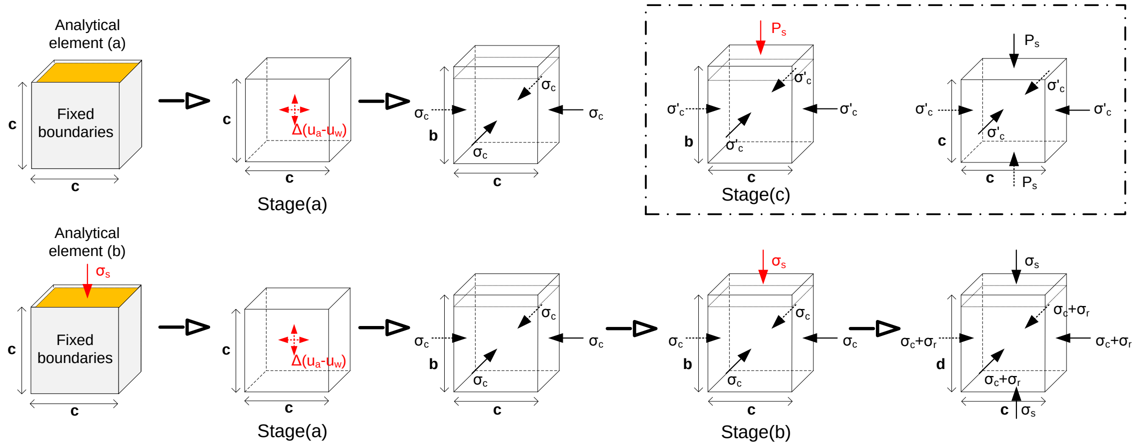

Figure 3.2 Stress states of analytical elements in different stages

Three elastic parameters; namely, modulus of elasticity with respect to net normal stress, modulus of elasticity with respect to matric suction and Poisson's ratio are required for the application of Equation 3.5. Several methods are available for measurement from laboratory and field tests for elastic modulus of saturated soil (E_{sat}) (ASTM D6758-08, D5858-96 and D4015-15). However, the elastic modulus with respect to net normal stress of unsaturated soils (E_{unsat}) is much more complex. The E_{unsat} has been found to be influenced by various parameters, which include (1) the initial level of compaction (dry unit weight or void ratio), (2) the initial state of hydration (water content, degree of saturation or matric suction) and (3) the confinement (deviator stress or lateral stress), (4) soil structure (the size of soil particles), (5) stress path and stress history (Adem and Vanapalli 2014a). Several studies suggested that reasonable estimations of the modulus of elasticity could be achieved taking account of the influence of one or two key parameters. For example, Zhang et al. (2012) and Lu and Kaya (2014) suggested methods linking the elastic modulus with water content. In addition, Rahardjo et al. (2011) proposed a method that links elastic modulus with respect to both mechanical stress and matric suction using multiple regression methods, which is rigorous but time consuming for use in conventional geotechnical practice. Vanapalli and Oh (2010) proposed a semi-empirical model for estimating modulus of elasticity of coarse and fine-grained unsaturated soils. Adem and Vanapalli (2014b) successfully extended this semi-empirical model for estimation of 1-D heave for several expansive soils. In this paper, the model developed by Vanapalli and Oh (2010) (i.e. Equation 3.6) is used for estimation of the modulus of elasticity of unsaturated expansive soils, E_{unsat} in case study **I**. This equation suggests the E_{unsat} decreases with decreasing matric suction (i.e. during the infiltration process). In the calculation of P_{LS} using Equation 3.5, "E" is defined as the average value (E_a) of various E_{unsat} values calculated using Equation 3.6 over the range of matric suction variation along the depth profile. The influence of mechanical stress (confinement) is neglected in this model (Equation 3.6). Such an assumption leads to conservative estimate and can be extended in practice for pavements and lightly loaded residential structures. In these types of structures, typically the soil matric suction changes have a predominant influence on the behavior of unsaturated expansive soils (Adem and Vanapalli 2014b).

$$E_{unsat} = E_{sat}[1+\alpha_{ad}\frac{(u_a-u_w)}{P_a/100}S^{\beta_{ad}}] \tag{3.6}$$

where E_{unsat} = the elastic modulus of unsaturated expansive soil; E_{sat} = elastic modulus of saturated expansive soil; α_{ad} and β_{ad} = fitting parameters, Adem (2015) calculated E_{unsat} for five different expansive soils and suggested that β_{ad} is 2 typically and α_{ad} varies from 0.05 to 0.15 for expansive soils. In this study, an average value, α_{ad} equals to 0.1 is used; P_a = atmospheric pressure, S = degree of saturation.

Due to difficulties in the measurement from experimental studies and long time required for determining the value Poisson's ratio, it is usually assumed in engineering practice applications. A suggested range of values for Poisson's ratios is from 0.2 (dry sand) to 0.5 (saturated clay tested under undrained condition), less common values may be as low as 0.1 for loess deposits (Luna and Jadi 2000). There is no standard on how to measure the Poisson’s ratio for unsaturated soils. In addition, there is no standard on experiments, size of specimens as well as ranges of stress and strain suggested for determining Poisson’s ratio (Sun et al. 2011). Currently, Poisson's ratio is usually tested following two different approaches. In the first approach, static vertical (axial) and lateral (radial) strain are monitored and Poisson's ratio is calculated using its original definition, which is the ratio of lateral strain to vertical strain (Tatsuoka and Shibuya 1992; Lo Presti et al. 1993; Tatsuoka and Kohata 1995). Also, Poisson's ratio can be calculated from the information of surface wave velocity (Brignoli and Stokoe 1996; Suwal and Kuwano 2010). Based on limited studies it was concluded that Poisson's ratio is affected by soil properties such as dry density, water content, grain size distribution, degree of compaction as well as external factors such as the cell pressure or principle pressure ratio (Sun et al. 2011, Suwal and Kuwano 2010, 2012). It is also suggested that elastic modulus and Poisson's ratio can affect each other (Sun et al. 2011, Suwal and Kuwano 2010, 2012). Only limited studies and discussion is available in the literature with respect to the Poisson's ratio in spile infiltration teste of its importance in practice. More studies are required to promote engineers' understanding on this parameter. Currently, a commonly used method is to relate the Poisson’s ratio to the coefficient of earth pressure at rest (K_0) and the over consolidation ratio (OCR) [see Equation 3.7 (Vu and Fredlund 2004, Gu 2005)]. However, it should be noted that from dry condition to wet condition, the Poisson's ratio increases; for this reason geotechnical engineers based on their experience and judgement should make some adjustment with respect to this value.

$$\upsilon = \frac{K_0}{1+K_0} \tag{3.7}$$

$K_0 \approx 1-\sin\phi'$ for normally consolidated soil (Jaky 1944)

$K_0 = (1-\sin\phi')OCR^{\sin\phi'}$ for over consolidated soil (Mayne and Kulhawy 1982),

where K_0 = at rest earth pressure coefficient; ϕ' = effective soil internal friction angle; OCR = over consolidation ratio.

Compared to elastic modulus variation with respect to net normal stress and Poisson's ratio, determination of the elastic modulus with respect to matric suction is much more complex. This parameter is referred to as suction modulus, *H* in the literature. The *H* value can be determined from the void ratio constitutive surface with respect to net normal stress and matric suction. Vu and Fredlund (2004) presented various equations for calculation of the suction modulus, *H* for different loading conditions (i.e. K_0 condition, plane strain condition, or isotropic condition). However, experimental determination of *H* is usually complex and extremely time consuming. To alleviate the difficulties associated with the measurement of sectional modulus, H, a relationship is developed which enables direct prediction of σ_c from constant volume swelling tests without the need of H.

3.1.3 Relationship between the lateral swelling pressure and vertical swelling pressure

A relationship between lateral swelling pressure and vertical swelling pressure is proposed for the analytical element shown in Figure 3.2, which experiences the stress state change described in **stage (a)**. This element is assumed to be subjected to a stress state change as shown in **stage (c)**.

Stage (c) shows that a vertical stress P_s which is applied on top of the soil element compresses back to its original volume. As a consequence, the vertical side length reduces from b to the initial side length c while the horizontal confining pressure increases from σ_c to σ_c'. The mathematical expression for this change is given as Equation 3.8.

$$\begin{cases} \dfrac{c-b}{b} = \dfrac{2\upsilon}{E}\sigma_c' - \dfrac{P_s}{E} \\ 0 = \dfrac{\upsilon}{E}(P_s + \sigma_c') - \dfrac{P_s}{E} \end{cases} \tag{3.8}$$

σ_c can be expressed in terms of P_s and elastic parameters as shown in Equation 3.9 by combining Equation 3.1 and Equation 3.8. In Equation 3.9, P_s is simply the vertical swelling pressure obtained from constant volume swelling test; the applied vertical pressure on the top totally prevents the volume expansion of expansive soil. By substituting Equation 3.9 into Equation 3.5 and using the average elastic modulus (E_a), the lateral earth pressure, P_{LS} can be determined considering the influence of lateral swelling pressure using Equation 3.10 alleviating the need for the suction modulus, H.

$$\sigma_c = \frac{(1-\upsilon-2\upsilon^2)P_s}{1-\upsilon^2 - \dfrac{P_s}{E}(1+\upsilon)(1-\upsilon-2\upsilon^2)} \tag{3.9}$$

$$P_{LS} = \frac{(1-\upsilon-2\upsilon^2)P_s}{1-\upsilon^2-\frac{P_s}{E_a}(1+\upsilon)(1-\upsilon-2\upsilon^2)} + \frac{\upsilon}{1-\upsilon}\sigma_s \qquad (3.10)$$

where P_s = the vertical swelling pressure acquired from constant volume swelling pressure test; E_a = average value of various E_{unsat} calculated using Equation 3.6 over the range of matric suction variation.

Tu and Vanapalli (2016) proposed a semi-empirical equation (Equation 3.11), that can be used in Equation 3.10 for predicting the variation of vertical swelling pressure from initial suction value to fully saturation condition. This equation can alleviate need for the determination of the vertical swelling pressure from laboratory tests.

$$P_S = P_{S0} + \beta_S \cdot \psi \cdot (\frac{S_r}{100})^2 \qquad (3.11)$$

where S_r = the degree of saturation; P_{S0} = the intercept on the P_S axis at zero suction value (P_{S0} *is* 55kPa for compacted expansive soils); β_S = fitting parameter; β_S = $23.05A^{32.315}(0.237I_P - 10.278\rho_{dn}) + 0.164$; A = the activity of soils; $A=I_P/C$, I_P = the index of plasticity; C = the clay content of soils; ψ = the soil suction.

3.1.4 Estimation of lateral earth pressure in expansive soils associated with environmental factors

Equation 3.10 introduced above is capable of estimating lateral earth pressure considering lateral swelling pressure upon free swelling (P_L) according to constant volume vertical swelling pressure (P_s), extending unsaturated soil mechanics. However, simple testing technique or models are not available for the reliable prediction of the constant volume vertical swelling pressure (P_s) from an initial unsaturated state to a subsequent unsaturated state associated with matric suction reduction (Sridharan et al. 1986; Azam and Wilson 2006; Nagaraj et al. 2009; Vanapalli and Lu 2012; Çimen et al. 2012). For this reason, Equation 3.10 can be only applied to the most critical scenario of lateral earth pressure considering lateral swelling pressure arises when the matric suction reduces from a certain initial value to zero (i.e. saturated condition). However, such a scenario is rare as the backfill material is typically in an unsaturated state for most of its design life. For this reason, in the present study, a superposition approach is proposed to estimate the lateral earth pressure considering lateral swelling pressure against fixed rigid retaining structure that arises due to a matric suction reduction while the soil is still in an unsaturated state.

As shown in Figure 3.3, an analytical soil element behind a fixed rigid retaining structure experiences matric suction reduction from $(u_a - u_w)_a$ to $(u_a - u_w)_b$ where $(u_a - u_w)_b$ is an intermediate matric suction value (i.e. not equal to zero) during the infiltration process. As a consequence, lateral swelling pressure mobilizes with a matric suction reduction and adds an additional increment to the lateral earth pressure associated with soil self-weight and surcharge. In order to apply the superposition method, the soil element behind the retaining wall is assumed to experience a series of stress state changes following two different paths. In Path (I), soil element experiences a matric suction reduction directly from $(u_a - u_w)_a$ to zero. However, in Path (II), the soil element initially undergoes a matric suction reduction from $(u_a - u_w)_a$ to $(u_a - u_w)_b$. The matric suction $(u_a - u_w)_b$ subsequently reduces to zero. The stress state changes in the soil element in Path (I) and Path (II) (as shown in Figure 3.4) are illustrated below.

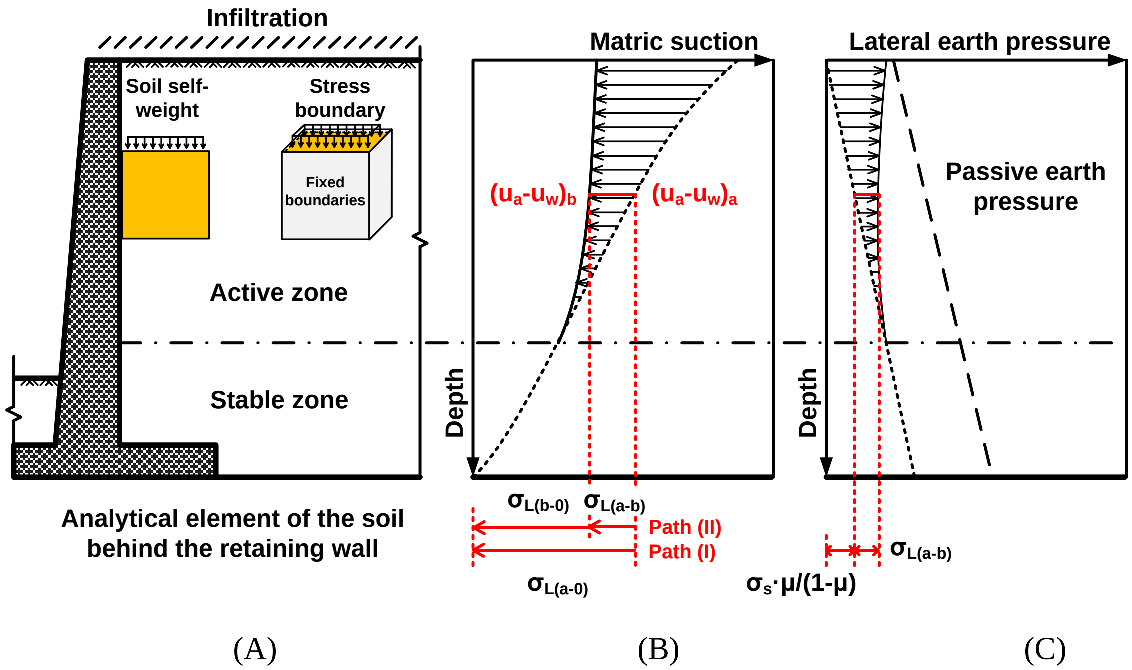

Figure 3.3 Mobilization of lateral swelling pressure behind retaining structure associated with matric suction reduction [(A) Analytical soil element; (B) Matric suction reduction; (C) Lateral earth pressure distribution changes]

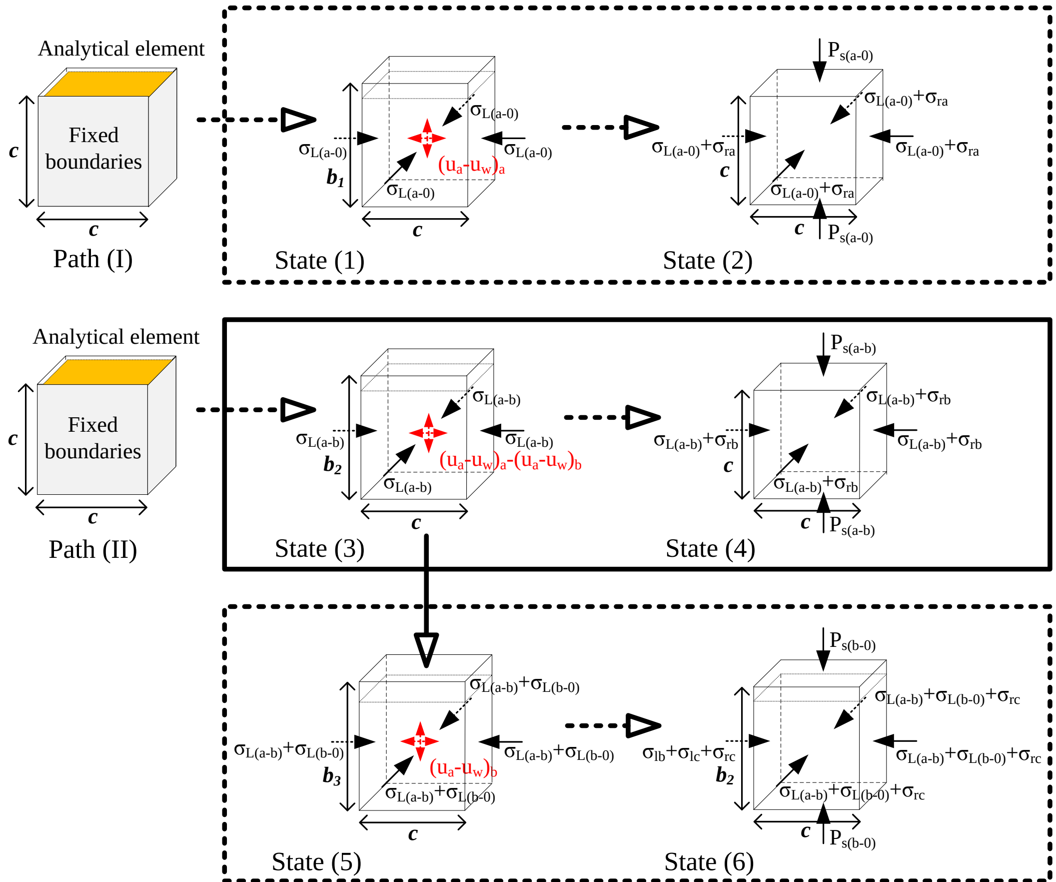

Figure 3.4 Stress states variations of the analytical soil element following different matric suction reduction paths

(i) Following Path (I), from initial state to State (1), there is a lateral pressure increment $\sigma_{L(a\text{-}0)}$ with matric suction reduction from $(u_a - u_w)_a$ to zero in the soil element. In vertical direction, the vertical side length of the soil element increases from initial value c to b_1. From State (1) to State (2), it is assumed that a vertical stress $P_{s(a\text{-}0)}$ compresses the expanding soil element back to its initial volume.

(ii) Following Path (II), from initial state to State (3), the soil element experiences a matric suction reduction $[(u_a - u_w)_a - (u_a - u_w)_b]$. As a consequence, the soil element shown in State (3) gains a stress increment $\sigma_{L(a\text{-}b)}$ in the horizontal direction. In addition, the side length increases from c to b_2 in the vertical direction. From State (3) to State (4), a vertical stress $P_{s(a\text{-}b)}$ compresses the analytical element shown in State (3) back to its initial volume. From State (3) to State (5), after undergoing a matric suction reduction which is equal to [$(u_a - u_w)_a - (u_a - u_w)_b$], the soil element further experiences a matric suction reduction from $(u_a - u_w)_b$ to zero, which means the soil element is fully saturated. For the soil element shown in State (5), in horizontal direction, compared to the element shown in Stage (3), there is a stress increment $\sigma_{L(b-0)}$ that arises due to matric suction reduction, while the vertical side length increases from b_2 to b_3. From State (5) to Stage (6), vertical stress $P_{s(b-0)}$ compresses the volume of the soil element shown in State (6) back to Stage (5). The soil element further gains a stress increment σ_{rc}, in the horizontal direction.

For simplification of analysis, the soil element behind the retaining structure is considered to be isotropic, homogeneous and elastic in nature without any plastic deformation (such as collapse of soil structures due to over-load) in the swelling process (Terzaghi's 1925, 1926, 1931). Also, for extending a conservative approach, horizontal displacement of the soil element is assumed to be strictly restricted. Constitutive relations (Equation 2.7) proposed by Fredlund and Morgenstern (1976) can also be used satisfying the above assumptions for interpreting the stress state variations of the soil element shown in Figure 3.3.

Mathematical expressions corresponding to the stress states shown in Figure 3.4 are summarized as Equation 3.12 for Path (I), initial state to State (1); Equation 3.13 for Path (I), from State (1) to State (2); Equation 3.14 for Path (II), from initial state to Stage (3); Equation 3.15 for Path (II), from State (3) to State (4); Equation 3.16 for Path (II), from State (3) to State (5); Equation 3.17 for Path (II), from State (5) to State (6), respectively. Rearranging above equations, the lateral earth pressures corresponding to different matric suction reductions are given as Equation 3.18.

$$\begin{cases} \dfrac{b_1 - c}{c} = \dfrac{2\upsilon}{E_{(a-0)}}\sigma_{L(a-0)} - \dfrac{(u_a - u_w)_a}{H_{(a-0)}} \\ 0 = \dfrac{\upsilon - 1}{E_{(a-0)}}\sigma_{L(a-0)} - \dfrac{(u_a - u_w)_a}{H_{(a-0)}} \end{cases} \tag{3.12}$$

$$\begin{cases} \dfrac{c-b_1}{b_1} = \dfrac{2\upsilon}{E_{(a-0)}}\sigma_{ra} - \dfrac{P_{s(a-0)}}{E_{(a-0)}} \\ 0 = -\dfrac{\sigma_{ra}}{E_{(a-0)}} + \dfrac{\upsilon}{E_{(a-0)}}[P_{s(a-0)} + \sigma_{ra}] \end{cases} \tag{3.13}$$

where $E_{(a\text{-}0)}$ = the average elastic modulus over the matric suction range from $(u_a - u_w)_a$ to zero; $H_{(a\text{-}0)}$ = the average elastic modulus over the matric suction range from $(u_a - u_w)_a$ to zero; $P_{s(a\text{-}0)}$ = the constant volume vertical swelling pressure generated from a matric suction reduction from $(u_a - u_w)_a$ to zero.

$$\begin{cases} \dfrac{b_2-c}{c} = \dfrac{2\upsilon}{E_{(a-b)}}\sigma_{L(a-b)} - \dfrac{[(u_a-u_w)_a-(u_a-u_w)_b]}{H_{(a-b)}} \\ 0 = \dfrac{\upsilon-1}{E_{(a-b)}}\sigma_{L(a-b)} - \dfrac{[(u_a-u_w)_a-(u_a-u_w)_b]}{H_{(a-b)}} \end{cases} \tag{3.14}$$

$$\begin{cases} \dfrac{c-b_2}{b_2} = \dfrac{2\upsilon}{E_{(a-b)}}\sigma_{rb} - \dfrac{P_{s(a-b)}}{E_{(a-b)}} \\ 0 = -\dfrac{\sigma_{rb}}{E_{(a-b)}} + \dfrac{\upsilon}{E_{(a-b)}}[P_{s(a-b)} + \sigma_{rb}] \end{cases} \tag{3.15}$$

where $E_{(a\text{-}b)}$ = the average elastic modulus with respect to net normal stress over the matric suction range from $(u_a - u_w)_a$ to $(u_a - u_w)_b$; $H_{(a\text{-}b)}$ = the average elastic modulus with respect to matric suction over the matric suction range from $(u_a - u_w)_a$ to $(u_a - u_w)_b$; $P_{s(a\text{-}b)}$ = the constant volume vertical swelling pressure generated from a matric suction reduction from $(u_a - u_w)_a$ to $(u_a - u_w)_b$.

$$\begin{cases} \dfrac{b_3-b_2}{b_2} = \dfrac{2\upsilon}{E_{(b-0)}}\sigma_{L(b-0)} - \dfrac{(u_a-u_w)_b}{H_{(b-0)}} \\ 0 = \dfrac{\upsilon-1}{E_{(b-0)}}\sigma_{L(b-0)} - \dfrac{(u_a-u_w)_b}{H_{(b-0)}} \end{cases} \tag{3.16}$$

$$\begin{cases} \dfrac{b_2-b_3}{b_2} = \dfrac{2\upsilon}{E_{(b-0)}}\sigma_{rc} - \dfrac{P_{s(b-0)}}{E_{(b-0)}} \\ 0 = -\dfrac{\sigma_{rc}}{E_{(b-0)}} + \dfrac{\upsilon}{E_{(b-0)}}[P_{s(b-0)} + \sigma_{rc}] \end{cases} \tag{3.17}$$

where $E_{(b\text{-}0)}$ = the average elastic modulus with respect to net normal stress over the matric suction range from $(u_a - u_w)_b$ to zero; $H_{(b\text{-}0)}$ = the average elastic modulus with respect to matric suction over the matric suction range from $(u_a - u_w)_b$ to zero; $P_{s(b\text{-}0)}$ = the constant volume swell pressure generated from a matric suction reduction from $(u_a - u_w)_b$ to zero.

$$\begin{cases} \sigma_{L(a-0)} = \dfrac{(1-\upsilon-2\upsilon^2)P_{s(a-0)}}{1-\upsilon^2-\dfrac{P_{s(a-0)}}{E_{(a-0)}}(1+\upsilon)(1-\upsilon-2\upsilon^2)} \\ \sigma_{L(a-b)} = \dfrac{(1-\upsilon-2\upsilon^2)P_{s(a-b)}}{1-\upsilon^2-\dfrac{P_{s(a-b)}}{E_{(a-b)}}(1+\upsilon)(1-\upsilon-2\upsilon^2)} \\ \sigma_{L(b-0)} = \dfrac{(1-\upsilon-2\upsilon^2)P_{s(b-0)}}{1-\upsilon^2-\dfrac{P_{s(b-0)}}{E_{(b-0)}}(1+\upsilon)(1-\upsilon-2\upsilon^2)} \end{cases} \tag{3.18}$$

Since the soil elements following Path (I) and Path (II) experience the same matric suction reduction from $(u_a - u_w)_a$ to zero, under the same boundary conditions (fixed boundaries in horizontal direction and free boundary in vertical direction), the lateral swelling pressure in State (1) and State (5) generated due to the matric suction reduction should be the same as well (Equation 3.19). The lateral swelling pressure induced by the matric suction reduction $[(u_a - u_w)_a - (u_a - u_w)_b]$ can be expressed as Equation 3.20. A general equation can be summarized as Equation 3.21 considering the influence of lateral earth pressure due to soil self-weight and surcharge. The $P_{s(a\text{-}0)}$ and $P_{s(b\text{-}0)}$, values in Equation 3.21 represent constant volume vertical swelling pressure generated from initial condition to full saturation, which can be acquired from simple laboratory test according to (ASTM, D4546). If there is no experimental data, a semi-empirical prediction model (Equation 3.11) proposed by Tu and Vanapalli (2016) suitable for compacted expansive soils can be used. This equation can also be extended for expansive soils behind retaining structure as they are disturbed during construction and then compacted to function as backfill material. Employing Equation 3.21 and 3.11, the lateral earth pressure considering lateral swelling pressure behind a fixed rigid retaining structure from an initial unsaturated state to a subsequent unsaturated state can be conveniently predicted based on matric suction profile or water content profile variations using basic soil properties including SWCC; the saturated elastic modulus, E_{sat}; plasticity index, I_p, maximum dry density, $\rho_{d,max}$ and the Poisson ratio, υ.

$$\sigma_{L(a-0)} = \sigma_{L(a-b)} + \sigma_{L(b-0)} \tag{3.19}$$

$$\sigma_{L(a-b)} = \frac{(1-\upsilon-2\upsilon^2)P_{s(a-0)}}{1-\upsilon^2-\frac{P_{s(a-0)}}{E_{(a-0)}}(1+\upsilon)(1-\upsilon-2\upsilon^2)} - \frac{(1-\upsilon-2\upsilon^2)P_{s(b-0)}}{1-\upsilon^2-\frac{P_{s(b-0)}}{E_{(b-0)}}(1+\upsilon)(1-\upsilon-2\upsilon^2)} \tag{3.20}$$

$$\sigma_{L(a-b)} = \frac{(1-\upsilon-2\upsilon^2)P_{s(a-0)}}{1-\upsilon^2-\frac{P_{s(a-0)}}{E_{(a-0)}}(1+\upsilon)(1-\upsilon-2\upsilon^2)} - \frac{(1-\upsilon-2\upsilon^2)P_{s(b-0)}}{1-\upsilon^2-\frac{P_{s(b-0)}}{E_{(b-0)}}(1+\upsilon)(1-\upsilon-2\upsilon^2)} + \frac{\upsilon}{1-\upsilon}\sigma_S \tag{3.21}$$

3.1.5 Proposed model for the prediction of lateral earth pressure in the evaporation process

In engineering practice, the swelling ability of a typical expansive soil starts decreasing after a certain number wetting and drying cycles (Dif and Bluemel 1991). Experimental studies of investigators suggest that predominant swelling or shrinkage occurs during the first wetting and drying cycle (Al-Homoud et al. 1995; Basma et al. 1996). However, generally volume change behavior induced by cyclic wetting and drying significantly reduces after four cycles to attain equilibrium conditions. Beyond the fourth cycle, drying process can be assumed to be following the reverse path of the wetting process (Rosenbalm and Zapata 2016). From this point of view, the lateral earth pressure reduction due to a matric suction increment in the drying process can be calculated using the similar procedure illustrated in the wetting process. As shown in Figure 3.5, in the drying process, the analytical element gains a matric suction increment from $(u_a - u_w)_b$ to $(u_a - u_w)_a$. Adopting the superposition method, the lateral earth pressure reductions due to the shrinkage of the analytical element induced by a matric suction increment $[(u_a - u_w)_b$

to $(u_a - u_w)_a$] can be estimated as the difference between the lateral swelling pressure generated from matric suction reductions from $(u_a - u_w)_a$ to 0 and from $(u_a - u_w)_b$ to 0. Then the decreasing lateral earth pressure after a matric suction increment from $(u_a - u_w)_b$ to $(u_a - u_w)_a$ can be given as Equation 3.22.

$$\sigma_{L(b-a)} = \frac{(1-\upsilon-2\upsilon^2)P_{s(b-0)}}{1-\upsilon^2 - \frac{P_{s(b-0)}}{E_{(b-0)}}(1+\upsilon)(1-\upsilon-2\upsilon^2)} - \frac{(1-\upsilon-2\upsilon^2)P_{s(a-0)}}{1-\upsilon^2 - \frac{P_{s(a-0)}}{E_{(a-0)}}(1+\upsilon)(1-\upsilon-2\upsilon^2)} + \frac{\upsilon}{1-\upsilon}\sigma_S \tag{3.22}$$

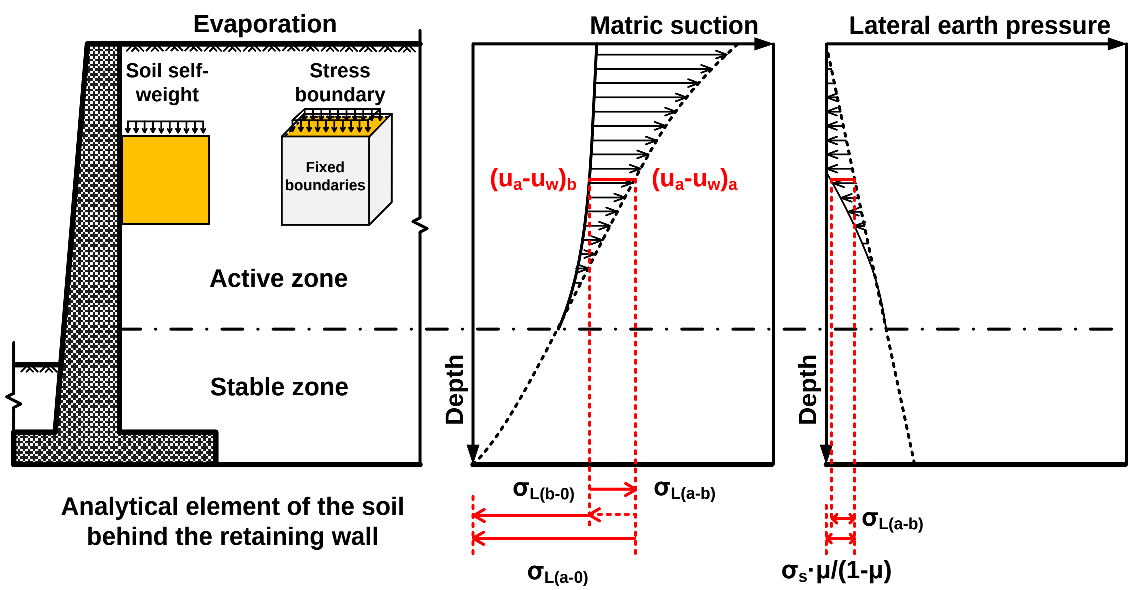

Figure 3.5 Reduction in lateral earth pressure behind retaining structure associated with matric suction increment [(A) Analytical soil element; (B) Matric suction increment; (C) Lateral earth pressure distribution changes]

In the drying process, the calculation of lateral earth pressure of expansive soil has to consider the appearance of cracks. Shrinkage deformation that arises beyond reaching fully mobilized active earth pressure condition can lead to the detachment between expansive soil and retaining structures. The free standing height of the soil is usually referred to as the depth of tensile crack (Das 2015). For saturated soils, the influence of tensile strength of the soil can be neglected. However, for unsaturated expansive soils, suction can act as a withholding force and significantly increase the free standing height of the soil (the depth of tensile crack). There is a certain value of tensile stress for an unsaturated expansive soil, which has a significant influence in the development of tensile cracks. The tensile crack typically arises in an unsaturated expansive soil when its tensile strength is equal to the active earth pressure (Equation 3.23). Similar to passive earth pressure, active earth pressure corresponding to different situations are also presented in Liu and Vanapalli (2018). Active earth pressure can be calculated using Equation 3.24 for unsaturated expansive soil against frictionless surface.

$$\sigma_{ha} = t \tag{3.23}$$

$$\sigma_{ha} = \frac{\sigma_s(1-\sin\phi')}{1+\sin\phi'} - \frac{2[c' + (u_a - u_w)\tan\phi^b]\cos\phi'}{1+\sin\phi'} \tag{3.24}$$

Morris et al. (1992) suggested that the tensile strength of unsaturated soils, σ_t, can be estimated using the equation below, which includes the contribution from suction:

$$\sigma_t = \alpha_T\ [c' +\ (u_a - u_w)\tan\phi^b]\ \cot\phi' \tag{3.25}$$

where α_T = the modified coefficient for tensile stress in unsaturated soils, within the range of 0.5-0.7, ϕ' = the angle of internal friction associated with the net normal stress.

Substituting Equation 3.24 and Equation 3.25 into Equation 3.23 yields Equation 3.26, which can be used for estimating the depth of tensile crack in expansive unsaturated soils in terms of Poisson's ratio, effective internal friction angle and SWCC.

$$\frac{\sigma_s(1-\sin\phi')}{1+\sin\phi'} - \frac{2[c' + (u_a - u_w)\tan\phi^b]\cos\phi'}{1+\sin\phi'} = \alpha_T[c' + (u_a - u_w)\tan\phi^b]\cot\phi' \tag{3.26}$$

If surcharge effects are neglected, the vertical stress can be only attributed to the soil unit weight, which is given as Equation 3.27.

$$\sigma_s = z_c\gamma \tag{3.27}$$

where γ = the unit weight of the soil.

Substituting Equation 3.27 into Equation 3.26 yields Equation 3.28, which can be used to predict the depth of tensile crack in expansive soil.

$$z_c = \frac{[\alpha_T \cot\phi'(1+\sin\phi') + 2\cos\phi'][c' + (u_a - u_w)\tan\phi^b]}{(1-\sin\phi')\gamma} \tag{3.28}$$

If the information of the entire SWCC is available, Equation 3.28 can also be expressed in another form (Equation 3.29).

$$z_c = \frac{[\alpha_T \cot\phi'(1+\sin\phi') + 2\cos\phi'][c' + (u_a - u_w)\tan\phi'(\frac{\theta-\theta_r}{\theta_s-\theta_r})]}{(1-\sin\phi')\gamma} \tag{3.29}$$

3.2 Calculations of active earth pressure and passive earth pressure under different conditions

The development of lateral swelling pressure has a limiting value. As shown in the Mohr-circle below (see Figure 3.6), lateral swelling pressure can be considered as an additional part to the at-rest earth pressure. The diameter of the Mohr’s circle increases upon wetting and decreases upon drying. At a certain limiting condition, the Mohr circle touches the shear strength failure envelop, which can be interpreted extending Rankine's theory. In other words, the total lateral earth pressure acting on retaining works cannot exceed passive earth pressure or will be less than active earth pressure to avoid shear failure. However, traditional Rankine's theory is only suitable for saturated soils against frictionless surface of a structure. In engineering practice, there can be scenarios where the roughness of the structure surface cannot be neglected (e.g. drilled pier). In many scenarios, even after water infiltration, expansive soils may still not attain fully saturated condition. In such situations, both the friction of the soil-structure interface and suction present within the expansive soils can significantly influence the lateral earth pressure that develops. In this section, influence of matric suction and the roughness of soil-structure interface on the passive and active earth pressure are discussed.

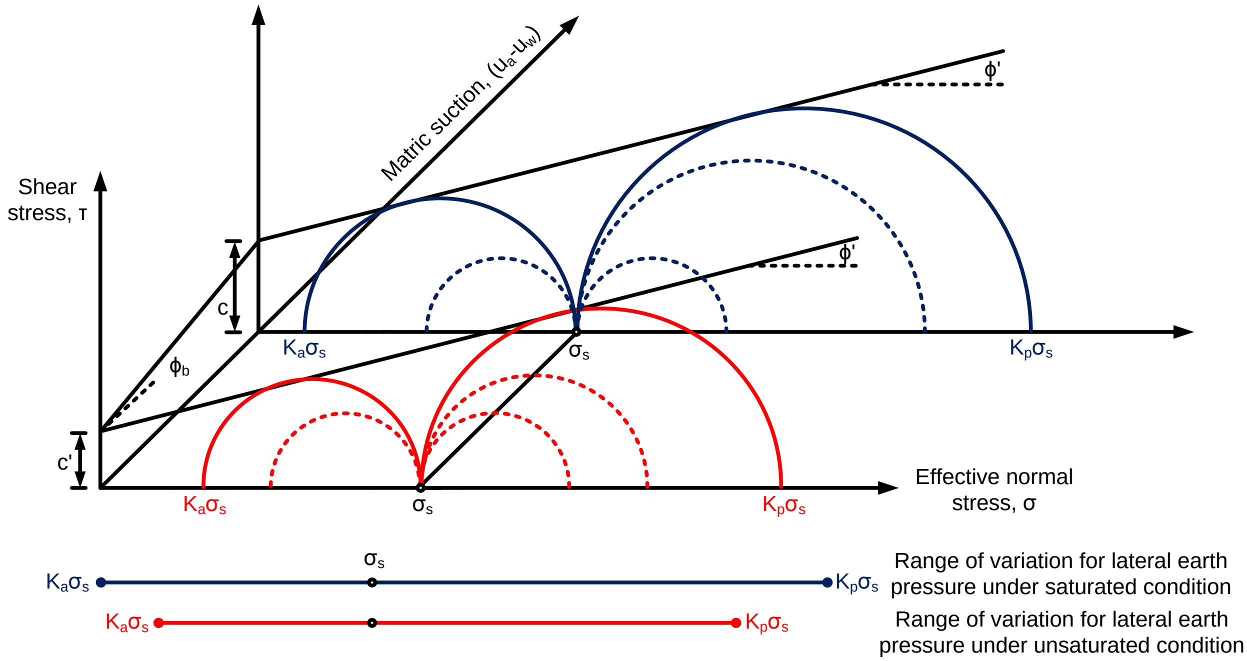

Figure 3.6 Variation lateral earth pressure in expansive soils upon wetting and drying

In the design of conventional retaining structures, Coulomb's theory or extended Coulomb theory are used by taking account of the roughness and slope of the retaining backfill (Terzaghi 1943; Caquot and Kerisel 1948; Janbu 1957; Shields and Tolunay 1973). However, Coulomb's theory facilitates in calculating a resultant force instead of providing stress distribution curve as per Rankine's theory. As a consequence, it cannot satisfactorily address some special problems (e.g., the calculation of pile shaft friction) in which the variation of lateral earth pressure with respect to depth is necessary. Wang et al. (2008b) extended Rankine's earth pressure by taking account of the frictional influence between back-surface of vertical retaining works and soils into consideration. Assuming the shear strength of the soil and the soil-structure interface following Coulomb's law using Equation 3.30 and Equation 3.31, respectively, Rankine's theory was extended for the calculation of passive earth pressure (Equation 3.32) and active earth pressure (Equation 3.33) against rough back-surface of retaining works.

$$\tau_f = \sigma_{nf}\tan\phi' + c' \tag{3.30}$$

$$\tau_a = \sigma_{nf}\tan\delta' + c'_a \tag{3.31}$$

where c' = the true cohesion of soil; c_a' = the effective interface cohesion; σ_{nf} = the normal stress at failure; ϕ' = the effective internal friction angle of soil; δ' = the effective interface friction angle.

$$\sigma_{hp1} = \sigma_s \frac{1+\sin\phi'\cos 2\alpha_p}{1-\sin\phi'\cos 2\alpha_p} + c'\frac{2\cos\phi'\cos 2\alpha_p}{1-\sin\phi'\cos 2\alpha_p} + p_0 \tag{3.32}$$

$$\alpha_p = \frac{1}{2}\arcsin\frac{C}{\sqrt{A^2+B^2}} - \frac{1}{2}\arctan\frac{B}{A}$$

$$\sigma_{ha1} = \sigma_s \frac{1-\sin\phi'\cos 2\alpha_a}{1+\sin\phi'\cos 2\alpha_a} - c'\frac{2\cos\phi'\cos 2\alpha_a}{1+\sin\phi'\cos 2\alpha_a} + p_0 \tag{3.33}$$

$$\alpha_a = \frac{1}{2}\arcsin\frac{C}{\sqrt{A^2+B^2}} + \frac{1}{2}\arctan\frac{B}{A}$$

$$\begin{cases} A = \sigma_s\sin\phi' + c'\cos\phi' \\ B = c'_a\sin\phi' - \sigma_s\sin\phi'\tan\delta' - 2c'\cos\phi'\tan\delta' \\ C = \sigma_s\tan\delta' + c'_a \end{cases}$$

where σ_s = the vertical stress due to unit weight of upper soil layers and surcharge; p_0 = the pore water pressure.

The concept of using two independent stress variables (i.e. net normal stress and matric suction) in the interpretation of the mechanical behavior of unsaturated soils has been widely accepted (Fredlund and Rahardjo 1993). Equation 3.34 proposed by Fredlund et al. (1978) expressed in terms of net normal stress and matric suction is commonly used to model the peak shear strength of unsaturated soils (e.g., Escario and Saez 1986; Gan and Fredlund 1988; Oloo and Fredlund 1996; Vanapalli et al. 1996).

$$\tau_f = c' + (\sigma_{nf} - u_{af})\tan\phi' + (u_{af} - u_{wf})\tan\phi^b \tag{3.34}$$

where u_{af} = the pore-air pressure at failure; ϕ^b = the angle of friction with respect to matric suction; (σ_{nf} - u_{af}) = the net normal stress at failure; and (u_{af}-u_{wf}) = the matric suction at failure.

However, Equation 3.34 does not take into account the nonlinear increase in shear strength as the soil desaturates as a result of an increase in the matric suction. In other words, upon saturation, the friction angle ϕ^b may have a value approximately equal to ϕ'. But once the air-entry value is exceeded, ϕ^b tends to decrease with increasing matric suction. The non-linear behavior of the shear strength of unsaturated soils is strongly related to the wetted contact area among air, water and soil particles. Vanapalli et al. (1996) proposed a semi-empirical equation (Equation 3.35) for predicting the non-linear increase of the shear strength of unsaturated soils with respect to matric suction by deriving the changing trend of the wetted area from the SWCC.

$$\tau_f = c' + (\sigma_{nf} - u_{af})\tan\phi' + (u_{af} - u_{wf})\tan\phi'\left(\frac{\theta - \theta_r}{\theta_s - \theta_r}\right) \qquad (3.35)$$

where θ = the current volumetric water content; θ_r = the residual volumetric water content form a SWCC; and θ_s = the saturated volumetric water content from a SWCC.

Hamid and Miller (2009) suggested that the shear strength of the soil-structure interface, which has different roughness at different degrees of saturation, can be modelled in a similar way as Equation 3.34 and Equation 3.35. Corresponding equations are given as Equation 3.36 and Equation 3.37.

$$\tau_f = c'_a + (\sigma_{nf} - u_{af})\tan\delta' + (u_{af} - u_{wf})\tan\delta^b \qquad (3.36)$$

$$\tau_f = c'_a + (\sigma_{nf} - u_{af})\tan\delta' + (u_{af} - u_{wf})\tan\delta^b\left(\frac{\theta - \theta_r}{\theta_s - \theta_r}\right) \qquad (3.37)$$

where δ' = the interface friction angle with respect to net normal stress; δ^b = the interface friction angle with respect to matric suction.

For simplicity, Equation 3.34 and Equation 3.36 are used for interpreting the soil and soil-structure interface shear failure envelopes for unsaturated conditions, respectively. The modified Rankine's theory proposed by Wang et al. (2008b) is extended to include the influence of the matric suction to the soil shear strength and soil-structure interface shear strength. More discussions are available in Liu and Vanapalli (2017). From Figure 3.7, it can be derived that during the desaturation process, both the passive earth pressure against rough retaining surface and frictionless retaining surface increases. Passive earth pressure against frictionless retaining surface always has a value higher than rough retaining surface. The passive earth pressure for saturated soil against rough surface (σ_{hp1}), saturated soils against frictionless surface (σ_{hp2}), unsaturated soil against rough surface (σ_{hp3}) and unsaturated soils against frictionless surface (σ_{hp4}) are given in Equation 3.32, Equation 3.38, Equation 3.39 and Equation 3.40, respectively.

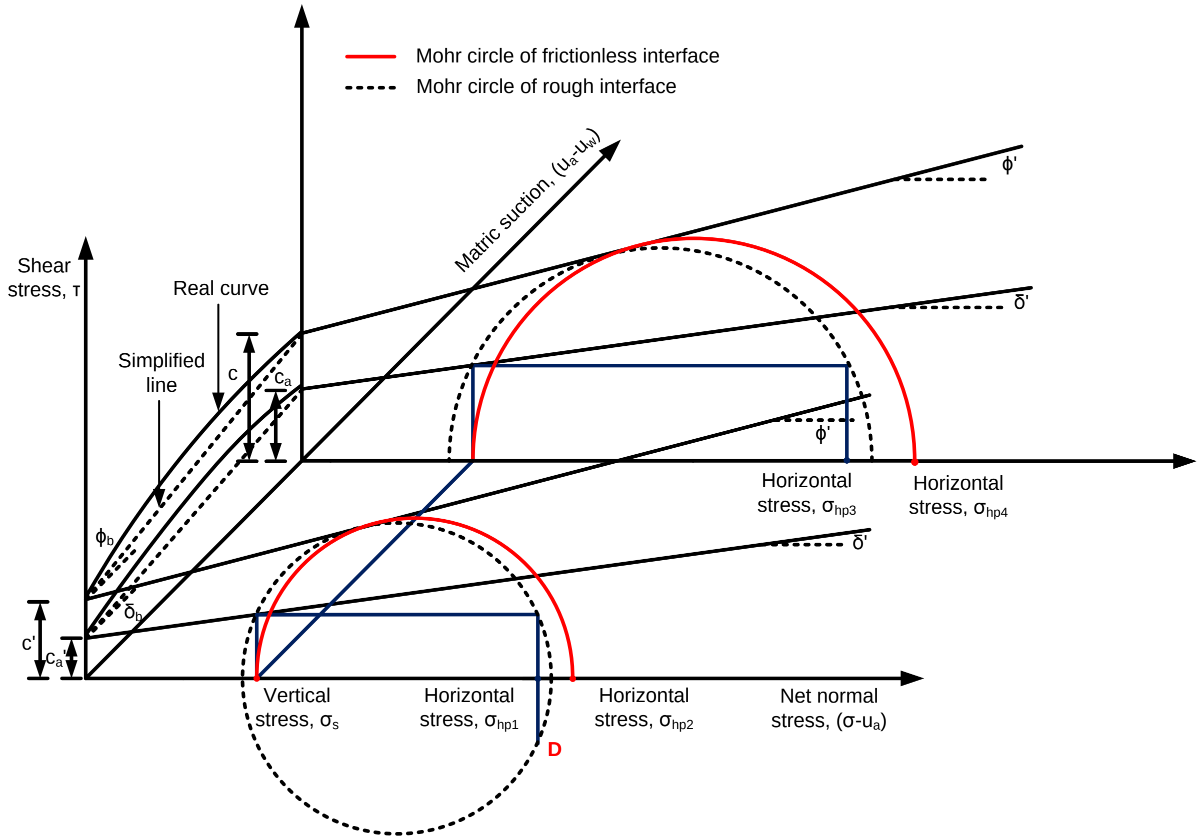

Figure 3.7 Development of Rankine's passive earth pressure in unsaturated soils against frictionless and rough surface

$$\sigma_{hp2} = \frac{\sigma_s(1+\sin\phi')}{1-\sin\phi'} + \frac{2c'\cos\phi'}{1-\sin\phi'} \tag{3.38}$$

$$\sigma_{hp3} = \sigma_s \frac{1+\sin\phi'\cos 2\alpha_p}{1-\sin\phi'\cos 2\alpha_p} + [c' + (u_{af}-u_{wf})\tan\phi^b]\frac{2\cos\phi'\cos 2\alpha_p}{1-\sin\phi'\cos 2\alpha_p} \tag{3.39}$$

$$\alpha_p = \frac{1}{2}\arcsin\frac{C}{\sqrt{A^2+B^2}} - \frac{1}{2}\arctan\frac{B}{A}$$

$$\begin{cases} A = \sigma_s\sin\phi' + [c' + (u_{af}-u_{wf})\tan\phi^b]\cos\phi' \\ B = [c_a' + (u_{af}-u_{wf})\tan\delta^b]\sin\phi' - \sigma_s\sin\phi'\tan\delta' - 2[c' + (u_{af}-u_{wf})\tan\phi^b]\cos\phi'\tan\delta' \\ C = \sigma_s\tan\delta' + [c_a' + (u_{af}-u_{wf})\tan\delta^b] \end{cases}$$

$$\sigma_{hp4} = \frac{\sigma_s(1+\sin\phi')}{1-\sin\phi'} + \frac{2[c' + (u_{af}-u_{wf})\tan\phi^b]\cos\phi'}{1-\sin\phi'} \tag{3.40}$$

Similarly, the development of Rankine's active earth pressure for different values of matric suction against frictionless and rough surface is shown in Figure 3.8. With increases in matric suction, both the active earth pressure against rough retaining surface and frictionless retaining surface decrease. If the vertical stress is assumed to be constant, the active earth pressure against rough retaining surface always has a value higher than frictionless retaining surface neglecting the degree of saturation, which is opposite to that of the passive earth pressure. The active earth pressure for saturated soil against rough retaining surface (σ_{ha1}), saturated soils against frictionless surface (σ_{ha2}), unsaturated soil against rough retaining surface (σ_{ha3}) and unsaturated soils against frictionless surface (σ_{ha4}) are given in Equation 3.33, Equation 3.41, Equation 3.42 and Equation 3.43 respectively.

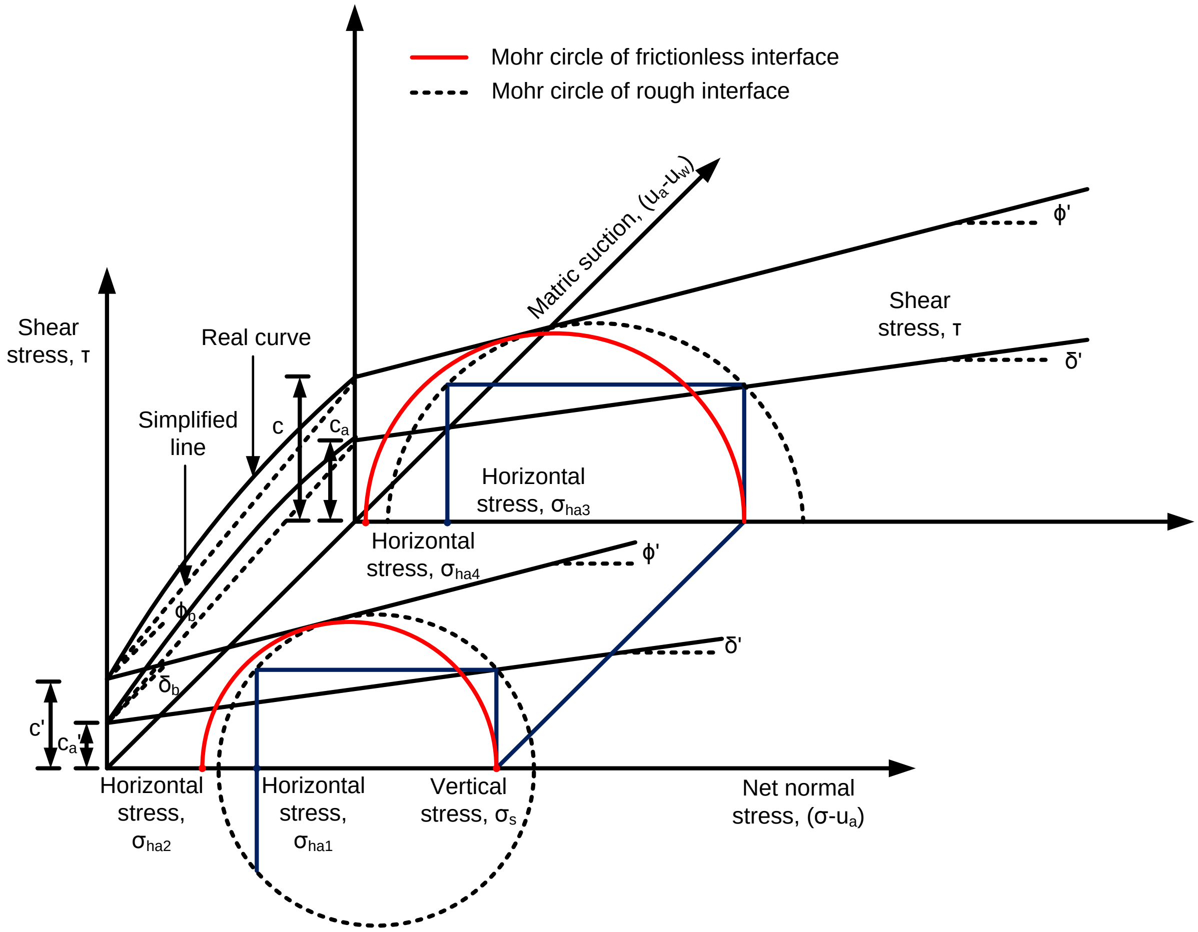

Figure 3.8 Development of Rankine's active earth pressure in unsaturated soils against frictionless and rough surface

$$\sigma_{ha2} = \frac{\sigma_s(1-\sin\phi')}{1+\sin\phi'} - \frac{2c'\cos\phi'}{1+\sin\phi'} \tag{3.41}$$

$$\sigma_{ha3} = \sigma_s \frac{1-\sin\phi'\cos 2\alpha_a}{1+\sin\phi'\cos 2\alpha_a} - [c' + (u_{af} - u_{wf})\tan\phi^b]\frac{2\cos\phi'\cos 2\alpha_a}{1+\sin\phi'\cos 2\alpha_a} \tag{3.42}$$

$$\alpha_a = \frac{1}{2}\arcsin\frac{C}{\sqrt{A^2+B^2}} + \frac{1}{2}\arctan\frac{B}{A}$$

$$\begin{cases} A = \sigma_s \sin\phi' + [c' + (u_{af} - u_{wf})\tan\phi^b]\cos\phi' \\ B = [c'_a + (u_{af} - u_{wf})\tan\delta^b]\sin\phi' - \sigma_s \sin\phi' \tan\delta' - 2[c' + (u_{af} - u_{wf})\tan\phi^b]\cos\phi' \tan\delta' \\ C = \sigma_s \tan\delta' + [c'_a + (u_{af} - u_{wf})\tan\delta^b] \end{cases}$$

$$\sigma_{ha4} = \frac{\sigma_s(1 - \sin\phi')}{1 + \sin\phi'} - \frac{2[c' + (u_{af} - u_{wf})\tan\phi^b]\cos\phi'}{1 + \sin\phi'} \tag{3.43}$$

3.3. Validation of the proposed approach

3.3.1 Large scale model test results by Katti et al. (1983)

Katti et al. (1983) conducted a large scale model test in a laboratory environment to monitor the variation of lateral earth pressure of compacted expansive soil against a fixed model retaining wall [as shown in Figure 3.9(A)]. The expansive soil used in this experiment is collected from Malaprabha Right Bank Canal km No. 76 (MRBC-76) from Karnataka State, India. The properties of MRBC-76 (i.e. expansive clay) are summarized in Table 3.1. Thin coating of grease was applied on the tank walls and covered it with polythene paper to minimize the tank wall friction. In the test, air dried soil was compacted to an average density of 1.32g/cm^3 at a void ratio of 1.0 in the test tank. The compacted expansive soil was then soaked for a period of 70 days to achieve fully saturated condition (Katti et al. 1983). The lateral earth pressure on the rigid wall was measured using reaction jacks and proving rings which were placed at 0.6m depth intervals.

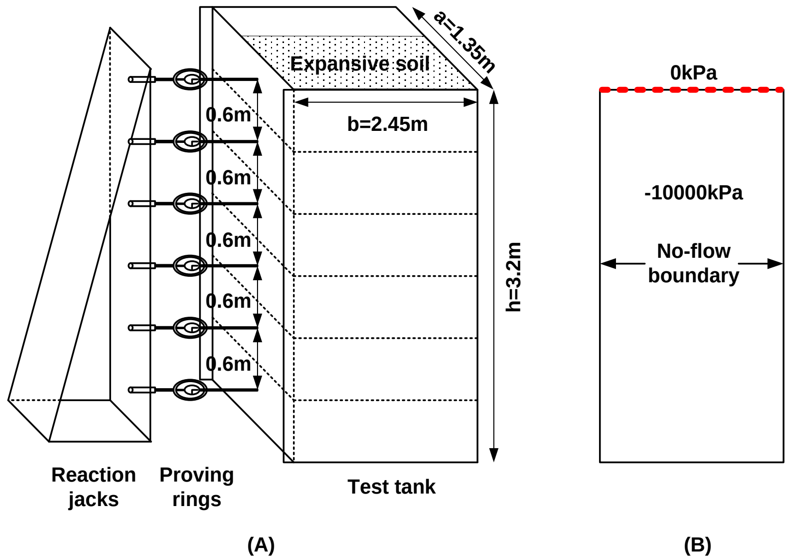

Figure 3.9 (A) Model retaining wall tested by Katti et al. 1983 (modified after Katti et al. 1983); (B) Boundary conditions in numerical simulation

Table 3.1 Properties of expansive soil (MRBC-76) (summarized from Katti et al. 1983)

Physical properties	Expansive soil
Liquid limit, %	71.4
Plastic limit, %	42
Plasticity index	29.4
Shrinkage limit, %	10.4
Specific gravity	2.64
Maximum dry density, g/cm^3	1.46
Optimum moisture content, %	29
Coefficient of permeability, m/sec	1×10^{-9}

The matric suction profile information from the test tank is not available from Katti et al. (1983). For this reason, commercial software SEEP/W from Geo-slope is used to simulate the variation of matric suction profile taking account of environmental factors. Aytekin (1992) proposed a finite element estimation model for prediction of the lateral earth pressure behind retaining wall to simulate the experimental studies of Katti et al. (1983). Aytekin (1992) assumed information of initial suction and SWCC that is required for using finite element model. As good comparisons were achieved between the simulations by Aytekin (1992) and the large scale model experimental results of Katti et al. (1983), key assumptions made by Aytekin (1992) in the simulation were extended in the present study. Reasonable assumptions of 10000 kPa (5pF) for initial suction at air-dried compaction condition and zero soil suction at full saturation in the test tank, respectively by Aytekin (1992) for achieving the simulations. In order to estimate the SWCC, Aytekin (1992) made three assumptions: firstly, the soil suction is around 6.0 pF (100,000kPa) in the driest state (Russam and Coleman, 1961; Vanapalli et al. 1999). Secondly, the soil suction value is around 3.3 pF for the water content value of plastic limit. Furthermore, the soil suction value of 0.1 pF was assumed for the water content value of liquid limit (Croney and Coleman, 1954). The estimated SWCC used in the numerical simulation by Aytekin (1992) based on the three points discussed above failed to describe the widely accepted "S" shape of SWCC. For this reason, in the present study the first two assumptions of Aytekin (1992) were used. The saturated water content of the expansive soil has been estimated to be 0.5 m^3/m^3 (calculated based on the saturated void ratio of *e* is 1.0 from Katti et al. 1983). Based on above information, the SWCC was modified for use in the SEEP/W as an input parameter. Figure 3.10 shows the modified SWCC as well as the position of the SWCC points from the study presented by Aytekin (1992) for comparison purposes. The modified SWCC is more consistent with our present state-of-the-art understanding of the SWCC behavior; however, it is still close to the SWCC used by Aytekin (1992).

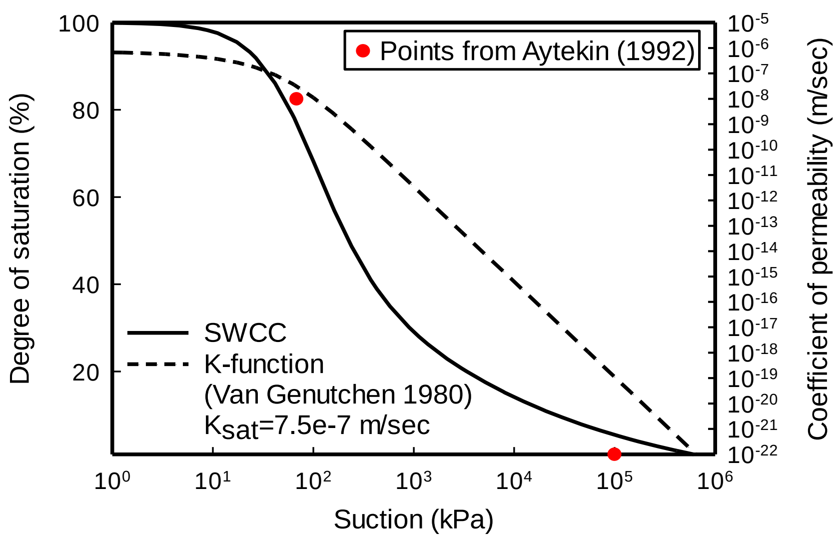

Figure 3.10 Soil water characteristic curve and coefficient of permeability function for the expansive clay in Katti et al. (1983) test

Katti et al. (1983) reported that the soil inside the testing tank was fully saturated in 70 days. However, as per the coefficient of permeability (1×10^{-9} m/sec) information provided by Katti et al. (1983), full saturation condition cannot be achieved from theoretical considerations for the large soil tank used in the study within such a short period of time. It is however postulated, infiltration may have been accelerated in the compacted expansive soil of the test tank due to the likely presence of cracks. In the simulation, in order to fully saturate the expansive soil within the tank within 70 days, a saturated coefficient of permeability value of 7.55×10^{-7}m/sec has been used. This assumption is more realistic and consistent with the coefficient of permeability values of laboratory specimens rather the large scale models and field studies. Several investigators have suggested for in-situ and large size specimens, coefficient of permeability is approximately two orders greater than laboratory specimens (Daniel 1984 and Elsbury et al. 1990). The variation of the coefficient of permeability with respect to suction is illustrated in Figure 3.10. For the hydraulic boundary conditions shown in Figure 3.9(B), the suction profile variations during infiltration simulated using SEEP/W from Geo–Slope is shown in Figure 3.11. It can be seen that because of the initial suction is high (i.e. 10,000kPa), the wetting front advances at a relatively slow rate along the depth.

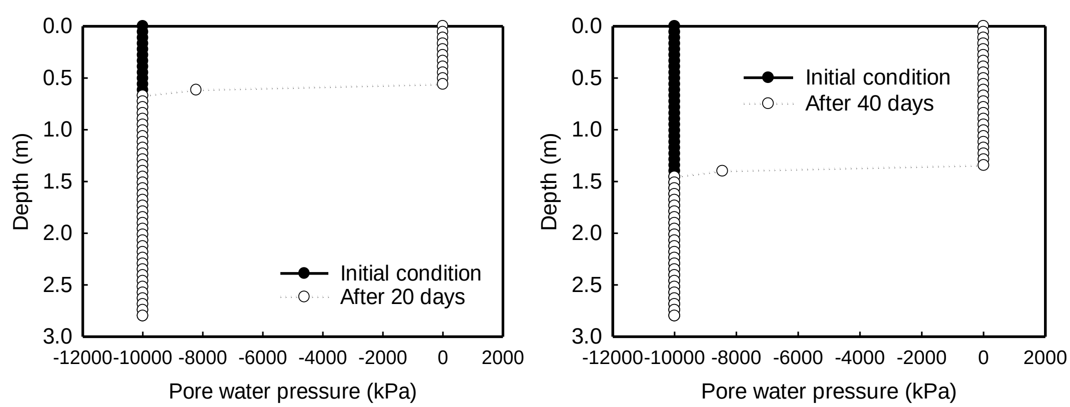

(A) (B)

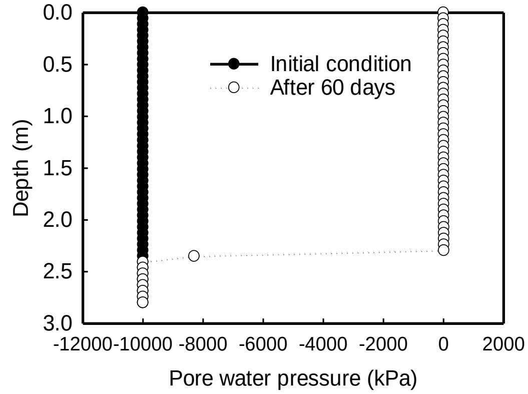

(C)

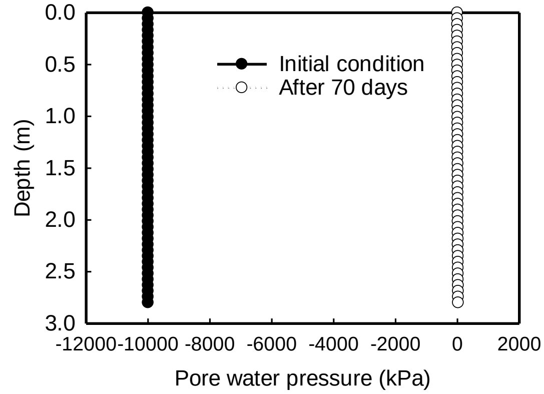

(D)

Figure 3.11 Simulated variations of the suction profiles during the infiltration process in Katti et al. (1983) test

Elastic properties of expansive soil (i.e. saturated elastic modulus E_s, and Poisson ratio, μ) were not available in Katti et al. (1983). For this reason, they were estimated from known soil properties using the relationships proposed by Skempton and Henkel (1957) (Equation 3.44) between shear strength and elastic modulus of London clay which had a plasticity index of around 50 percent (Cooling and Skempton, 1942). This relationship (Equation 3.44) was also employed by Aytekin (1992) to estimate elastic modulus of saturated expansive soil for analyzing Katti et al. (1983) results. In this study, the average saturated modulus of elasticity along the depth is estimated to be 5MPa after calculation. A typical value of Poisson ratio, μ is 0.3 used in Aytekin (1992) numerical simulation has been adopted.

$$E_{sat} = 140 \times \tau_{design} \tag{3.44}$$

where τ_{design} = the design shear strength of soil.

Figure 3.12 shows the comparisons between the estimations using Equation 3.21 and the experimental data. From Figure 3.12(A) to (D), it is clear that estimations well describe the development of lateral swelling pressure associated with a gradual increase in the degree of saturation upon water infiltration. In Figure 3.12(D), after 70 days, the soil within a depth of 2.8m has been fully saturated; due to this reason, the lateral earth pressure profile increases linearly with depth and provides a good comparison with the Katti et al. (1983) experimental data.

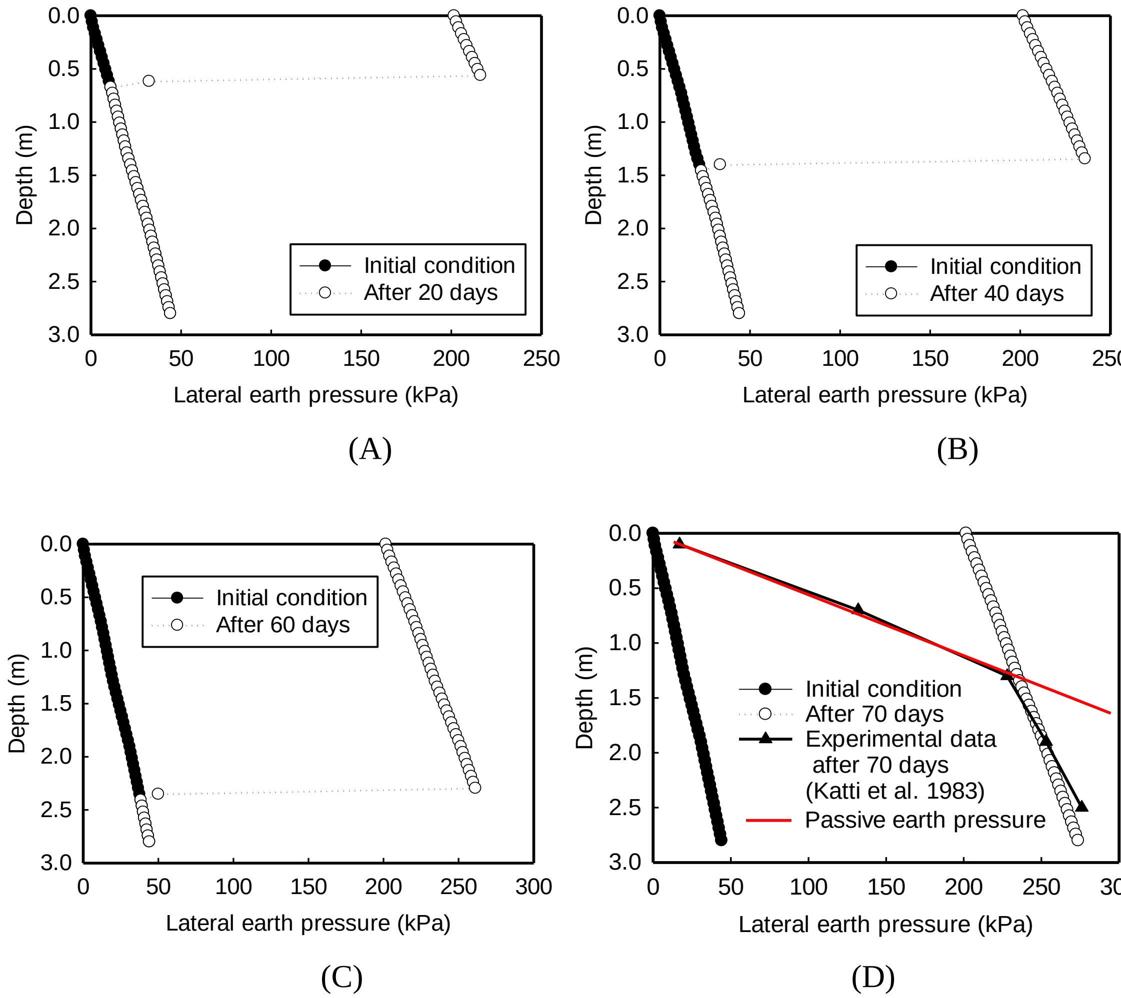

Figure 3.12 Comparison between the estimation and in-situ measurement of the lateral earth pressure in Katti et al. (1983) test

As discussed earlier, passive earth pressure is the upper limit of lateral earth pressure. The passive earth pressure was not measured by Katti et al. (1983); however, this information can be estimated using the lateral earth pressure distribution curve. From the experimental data curve (Katti et al. 1983) in Figure 3.12(D), it can be seen that the measured lateral earth pressure increases linearly with increasing depth due to water infiltration. However, beyond a depth of around 1.4m, this increase slows down. Once the soil achieves saturated condition, both the lateral earth pressure including the lateral swelling pressure and the passive earth pressure should exhibit linear distribution along the depth. However, the measured lateral earth pressure is bi-linear in nature. The bi-linear distribution of lateral earth pressure can be attributed to the mobilization of lateral earth pressure considering the lateral swelling pressure is limited by the passive earth pressure in the shallow depth zone (0 to around 1.4m). However, below 1.4m, the lateral swelling pressure can be fully mobilized without any limitation. These results clearly demonstrate that the passive earth pressure that develops exhibits linear distribution as shown in Figure 3.11.

3.3.2 Centrifuge model test results by Gu (2005)

Gu (2005) performed a series of centrifuge model tests to study the distribution of lateral earth pressure behind a rigid retaining wall filled with expansive soil as backfill material. The test tank was made of transparent polymethyl methacrylate whose original dimensions were 0.685m in length, 0.2m in width and 0.4m in height. A centrifuge in Nanjing Hydraulic Research Institute, China whose maximum centrifugal acceleration can reach 50g was used for conducting this experiment. The dimensions of the test hence can be magnified 50 times due to the application 50g centrifugal acceleration in this experiment. Figure 3.13 provides details of the test tank which are shown with magnified dimensions. Five stainless steel block walls constituted the rigid retaining wall and each blocked wall was connected to a sensor to record the lateral earth pressure. The recorded pressure provided the average pressure imposed on the blocked wall. Also, in order to simulate a frictionless surface, lubricating oil was smeared on the blocked walls. The entire centrifuge testing process was monitored by a closed-circuit television (CCTV) camera. The expansive soil heave was estimated using the deformation mesh marked on the wall of the test tank.

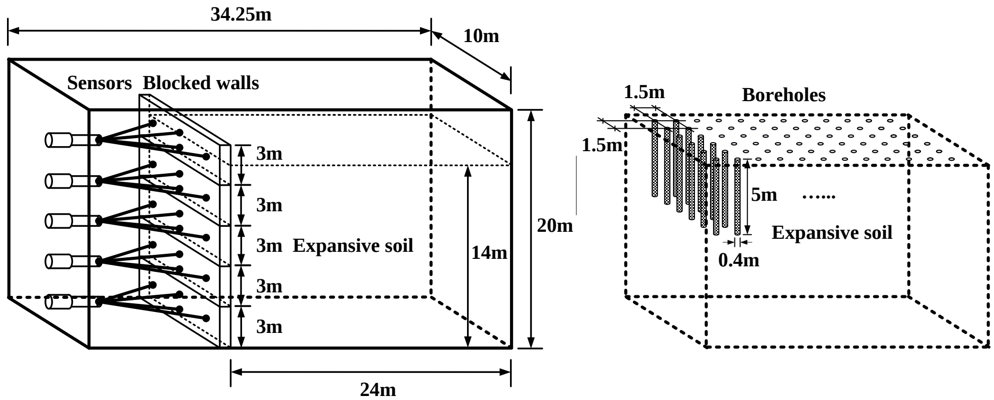

Figure 3.13 Sketch of the test tank in amplified dimensions (modified after Gu 2005)

In this experiment, soil samples were subjected to two different infiltration conditions; namely, surface infiltration and borehole infiltration. The boreholes were assumed to simulate natural cracks in the field as well as to accelerate infiltration and saturate the sample. The technique that was originally introduced by Brackley and Sanders (1992) was followed for conducting this experiment. Boreholes (with sand inside to simulate sand drains) with diameter of 0.4m and depth of 5m (amplified dimensions) were distributed in square shape with a distance of 1.5m between two successive boreholes (as shown in Figure 3.13). The expansive soil used in this experiment was collected from Guangxi province, China whose properties are summarized in Table 3.2. In this test, four soil samples of different initial water contents and dry densities were used (as shown in Table 3.3). The initial suction of each sample was measured using filter paper method while the vertical swelling pressure, P_s was determined from the constant volume swell test.

Table 3.2 Properties of expansive soil (from Gu 2005)

Physical properties	Expansive soil
Liquid Limit, %	72
Plastic Limit, %	28.8
Plastic Index	43.2
Specific Gravity	2.74
Dry density, Mg/m^3	1.77
Optimum Moisture Content, %	14.4

Table 3.3 Properties of prepared soil samples (from Gu 2005)

Soil sample	Initial dry density (Mg/m^3)	Initial water content (%)	Water content at saturation (%)	Initial suction (from filter paper method) (kPa)	Vertical swelling pressure (constant volume swelling tests) (kPa)
1	1.4	20.1	35	1179	94.48
2	1.4	21.1	35	943	93.45
3	1.5	20.1	30.2	892	123.1
4	1.5	21.1	30.2	756	121.72

The water head was kept at 1m higher than the sample surface to simulate rain water ponding for infiltration. The water content variations of the soil samples with respect to depth after infiltration are shown in Figure 3.14. Upon surface infiltration, soil samples with boreholes can be assumed to be fully saturated up to the borehole depth. The water content changes were limited to the borehole depth (i.e. 5m in amplified dimension). There were no significant changes in the water content values below this depth because of low hydraulic conductivity of the expansive soil (Gu 2005).

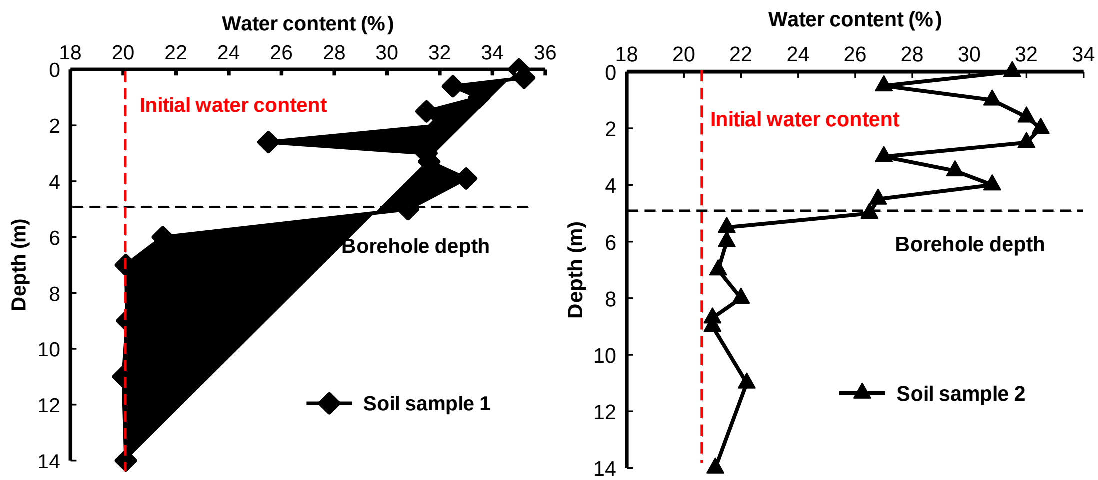

(a) (b)

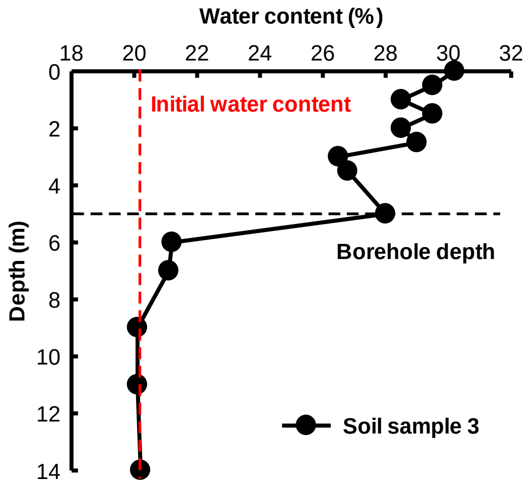

(c)

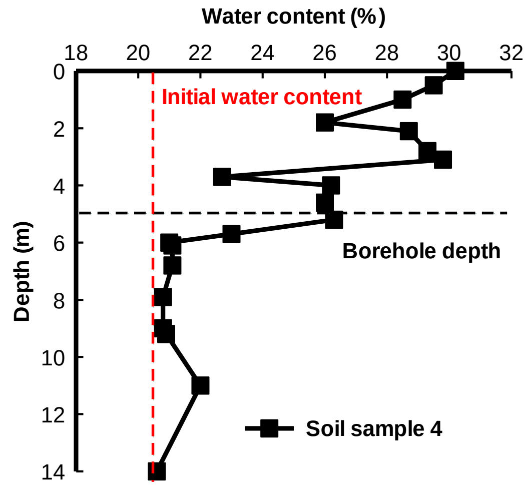

(d)

Figure 3.14 Water content distribution in depth (using amplified dimensions from centrifuge test results) before and after infiltration (modified after Gu 2005)

Both the elastic modulus with respect to net normal stress and the Poisson's ratio values are required for estimation of lateral earth pressure considering the influence of lateral swelling pressure. The heave values of each sample measured by Gu (2005) were used to back calculate modulus of elasticity of unsaturated soil using Equation 3.45 proposed by Adem (2015). The average modulus of elasticity estimated from Equation 3.45 for different soil samples are summarized in Table 3.4.

$$\Delta h = h\left[\frac{(1+\upsilon)(1-2\upsilon)}{E_a(1-\upsilon)}\right]\Delta(u_a - u_w) \tag{3.45}$$

where Δh = heave of soil; h = thickness of the calculated soil layer.

Table 3.4 Summary of back-calculated elastic modulus from ground heave using amplified dimensions from centrifuge test results

Sample group	Measured ground heave (m)	Suction variation (kPa)	Calculated soil layer depth (m)	υ	E_a (MPa)
1	0.07	1179	5	0.41	36.2
2	0.06	934	5	0.41	33.5
3	0.065	892	5	0.44	21.1
4	0.055	756	5	0.44	21.2

Poisson's ratio values for soils used in the experiment at initial matric suction values were back calculated by Gu (2005) using Equation 3.46 which describes the relationship between Poisson's ratio and at rest earth pressure coefficient for unsaturated soils. The calculated average value of 0.384 has been adopted by Gu (2005) in their analysis. However, Poisson's ratio increases when the soil is soaked from unsaturated state to saturation. Typically, Poisson's ratio for saturated clay is in the range from 0.4 to 0.5 (Sharma et al. 1990). As the Poisson's ratio changes during infiltration process, in the present study, in order to achieve reasonable comparisons, a value of 0.41 has been used for soil sample (1), and (2) and a value of 0.44 were used for soil sample (3) and (4).

$$K_0 = \frac{\upsilon}{1-\upsilon} \tag{3.46}$$

Gu (2005) only presented results of the lateral earth pressure due to swelling by reducing the lateral earth pressure due to surcharge from the total lateral earth pressure. The comparison between the measured and estimated lateral earth pressure due to swelling is summarized in Table 3.5. The estimated lateral earth pressure shows a good comparison with the experimental data. As discussed earlier, the maximum lateral earth pressure is limited by the passive earth pressure. It is however necessary to check whether the lateral swelling pressure recorded in the test has reached the passive earth pressure. According to the experimental data by Gu (2005), at a depth of 3.5m, the mobilized lateral earth pressure considering the influence of lateral swelling pressure was still less than the vertical swelling pressure. Since passive earth pressure always has a value higher than vertical stress; due to this reason, it is likely at this depth the lateral swelling pressure has been fully mobilized.

Table 3.5 Comparison between measured and estimated lateral earth pressure due to swelling using amplified dimensions from centrifuge test results (from Gu 2005)

Depth (m)	Lateral earth pressure after infiltration (kPa)			
	Sample 1	Sample 2	Sample 3	Sample 4
1	10.92	12.35	9.96	9.8
3.5	39.08	40.97	38.71	35.66
6.5	12.48	12	13.28	17.51
9.5	12.55	12.1	12.98	10.63
12.5	12.44	12.2	20.75	3.16
Measured lateral earth pressure due to swelling at 3.5m (Gu 2005) (kPa)	26.59	28.87	23.04	25.23
Estimated lateral earth pressure due to swelling at 3.5m (kPa)	31.5	31.2	26.4	26.1

3.3.3 In-situ test results by Mohamed et al. (2014)

Mohamed et al. (2014) measured the lateral swelling pressure development against a retaining wall, which forms one of the Assiut el gadida city projects of Assiut, Egypt. The backfill behind the retaining wall was compacted to achieve a bulk density of 1.43×10^3kg/m^3 in several layers with each layer thickness being equal to 0.25m. Five strain gauges were placed at different positions as shown in Figure 3.15(A) for the measurement of lateral earth pressure. Water was added at the soil surface when the soil shows signs of drying.

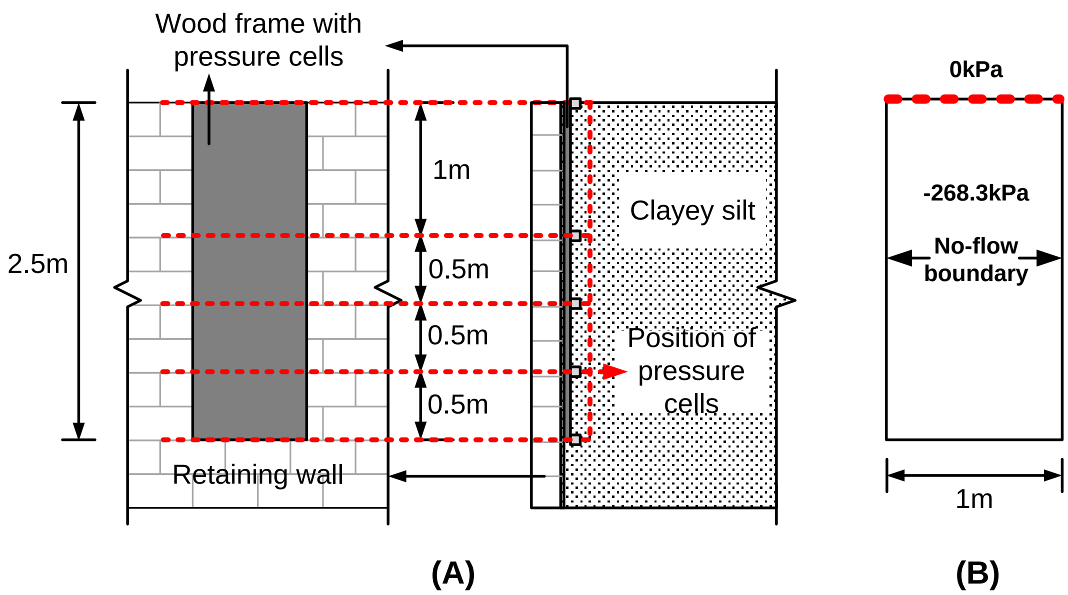

Figure 3.15 (A) Position of pressure cells in the project by Mohamed et al. (2014); (B) Boundary conditions in numerical simulation

The soil used in this investigation study is clayey silt which consists of 9.6 % clay and 84.4 % silt. A maximum lateral swelling pressure of around 173kPa was measured from field investigations. Due to lack of data, Atterberg limits of the soil are estimated based on the soil type and its clay content. This is achieved using the relationship for fine-grained soils provided by Wu and Liu (2008) which only requires the information of the clay content. The liquid limit and plastic limit of the clayey silt are estimated to be 17.8% and 27.2%, respectively. The maximum dry density is estimated as 1.21×10^3kg/m^3 assuming that the soil is compacted at optimum water content.

The suction profile variation in the infiltration process is not available in the study presented by Mohamed et al. (2014). For this reason, similar to the approach used earlier for interpreting Katti et al. (1983)'s case study. Finite element program (SEEP/W from Geo-Slope 2012) is used as a tool to estimate the changes in suction over time. The boundary conditions used in the simulation is shown in Figure 3.15(B). Using SEEP/W, the SWCC (Figure 3.16) is estimated from the grain size distribution data presented by Mohamed et al. (2014). Detailed parameters are listed in Table 3.6. The coefficient of permeability value of 10^{-7}m/sec has been assumed following guidelines for the clayey silt for simulation studies from Sarsby (2000). The simulated suction profile variation is presented in Figure 3.17.

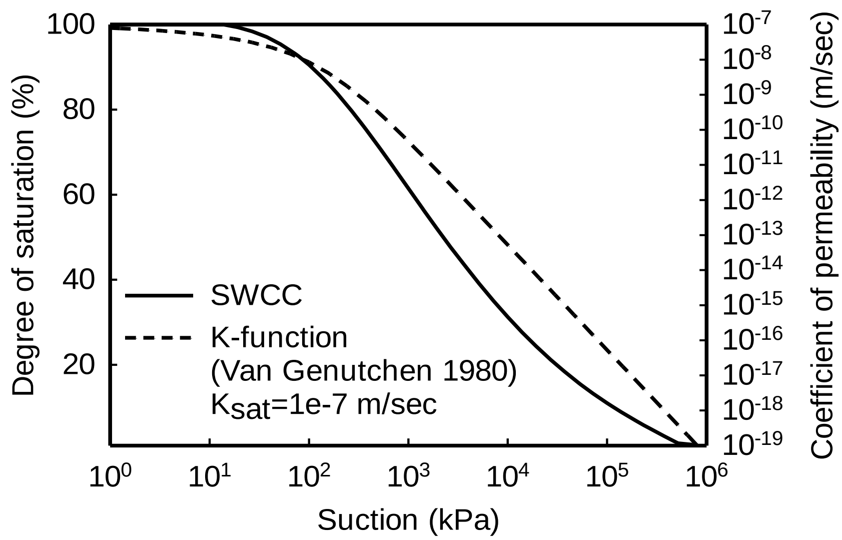

Figure 3.16 Soil water characteristic curve and coefficient of permeability function for clayey silt in Mohamed et al. (2014) project

Table 3.6 Parameters used in the estimation of SWCC

Physical properties	Clayey silt
Liquid Limit, %	27.2
Saturated volumetric water content, m^3/m^3	0.3146
Diameter at 10% passing, mm	0.0025
Diameter at 60% passing, mm	0.013

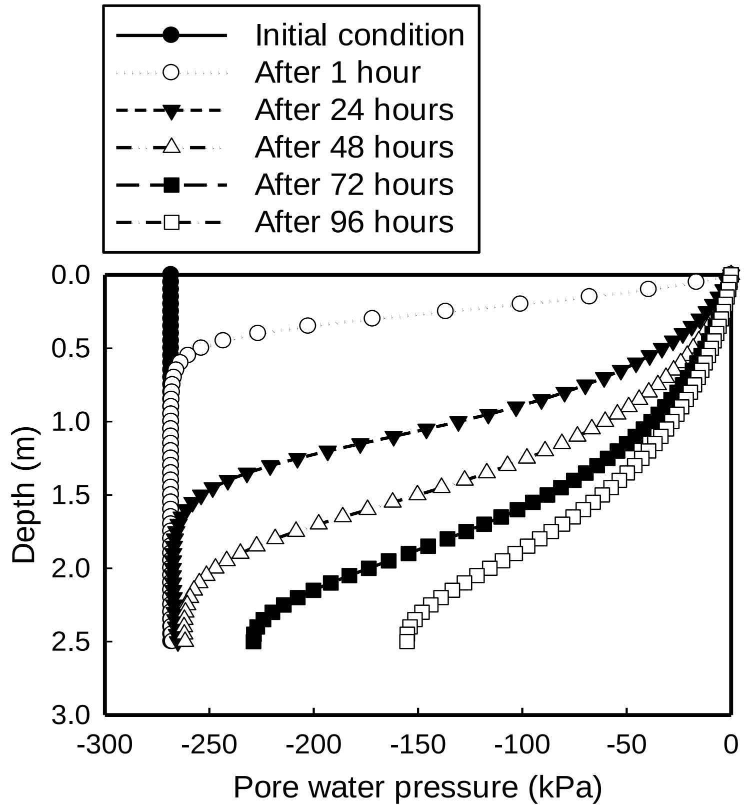

Figure 3.17 Simulated variations of the suction profiles during the infiltration process in Mohamed et al. (2014) project

Mohamed et al. (2014) considered that the soil was initially in an active state and negative values of the active earth pressure were reported. These results suggest that there should be a tension crack between the retaining wall and the soil. Due to this reason, the lateral swelling pressure contribution increased the active earth pressure from negative to a positive value. The maximum value of lateral swelling pressure however was limited by the passive earth pressure. In this study, the passive earth pressure is calculated using the shear strength parameters (ϕ' is 6° and c' is 20kPa) information provided by Mohamed et al. (2014). Since there is no data available in Mohamed et al. (2014), a saturated elastic modulus and Poisson's ratio values for a typical silt of 5MPa and 0.3, respectively were assumed from the studies summarized by Ranjan and Rao (2000) for the calculation of Equation 3.21. Figure 3.18 summarizes the comparisons between the estimated (Equation 3.21) and measured lateral earth pressure at different periods of time. Estimations based on Equation 3.21 well illustrate the development of lateral swelling pressure with the variation of suction [see Figure 3.18(A) thru (D)]. However, there are some differences in the comparisons between the estimated values and the in-situ measurements. For example, in Figure 3.18(D), the calculated passive earth pressure is less than the measured lateral earth pressure. The reasons for these differences can be attributed to following reasons: (i) the idealized boundary conditions described by Mohamed et al. (2014); (ii) assumed coefficient of permeability used for numerical simulations may be different from the actual value; (iii) in-situ infiltration of water into soils can be affected by minor cracks, and the initial natural water content within the soil may be also influenced by in-situ factors; (iv) manual operation such as the installation of the pressure measuring system, and any inclination of the earth pressure cells during installation can considerably influence the lateral earth pressure measurement.

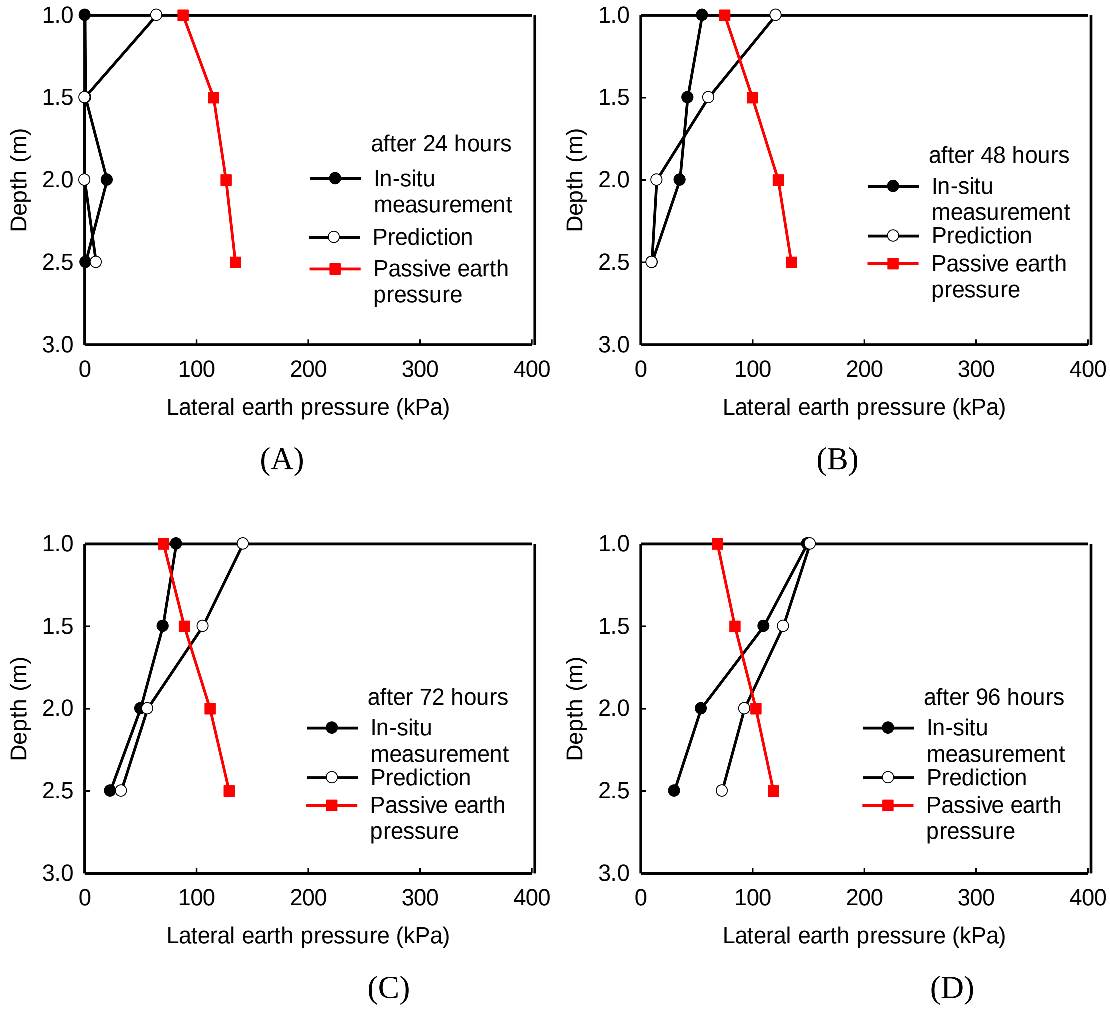

Figure 3.18 Comparison between the estimation and in-situ measurement of the lateral earth pressure in Mohamed et al. (2014) project

3.3.4 In-situ test results by Richards and Kurzeme (1973)

The Gouger Street Mail exchange is a steel-framed building with a reinforced concrete basement structure founded in Hindmarsh clay, which is significantly expansive clay associated with many engineering problems in Adelaide, South Australia (Richards and Kurzeme 1973). The basement construction involved excavation to a depth of around 7.5m so that a reinforced concrete retaining wall was employed to support over most of its depth. The initial lateral earth pressures acting on the retaining wall was low if not zero since the Hindmarsh clay allows a vertical, smooth, free standing face to a depth of 6 to 7 meters. While free water was often encountered during excavation and sampling which triggers the mobilization of lateral swelling pressure, which leads to an increment to the lateral earth pressure. Long-time observations were conducted by Richards and Kurzeme (1973) on the variations of lateral earth pressures as well as soil suctions for evaluating the mechanical behaviors of the retaining wall. The vertical distribution of psychrometers for suction measurement in each borehole was at depths of 2, 4, 6 and 7.5m. Locations of psychrometer installation boreholes are shown in Figure 3.19 as well as the location and distribution of the earth pressure cells.

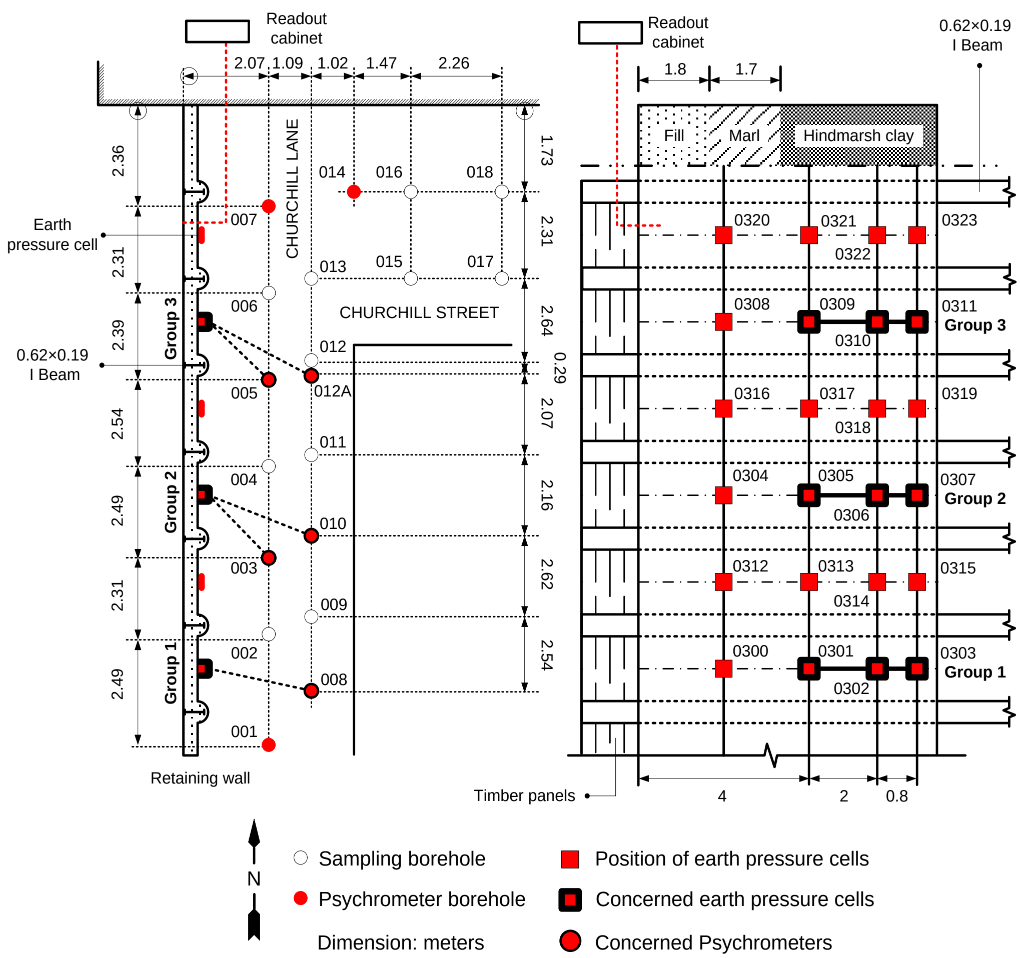

Figure 3.19 Location of earth pressure cells and psychrometers in boreholes at the Adelaide test site (modified after Richards and Kurzeme 1973)

The Hindmarsh clay layer underlies the Adelaide city area and much of the Adelaide metropolitan belongs to a very stiff to hard, high plastic silty clay (USCS symbol CH).

Since detailed soil properties of Hindmarsh clay were not available in Richards and Kurzeme (1973), instead, the soil properties of Hindmarsh clay are estimated based on some other published literatures reporting engineering practice with Hindmarsh clay in Adelaide city area (Jaksa 1995; Cox 1970; Sheard and Bowman 1994). Jaksa (1995) presented the dry density of the Hindmarsh clay at the test site region varies from 1.38×10^3kg/m^3 to 1.82×10^3kg/m^3. In this paper, an average value of 1.6×10^3kg/m^3 is employed for simplicity reasons. Cox (1970) and Sheard and Bowman (1994) reported the Atterberg limit results of Hindmarsh clay from a series of laboratory tests. Sheard and Bowman (1994) reported the average value of liquid limit to be 26.9%, the plastic limit to be 72.4% and the plastic index to be 45.5, which are adopted in this study as well. The SWCC equation proposed by Fredlund and Xing (1994) is used to fit the in-situ measurement database reported by Jaksa (1995). The Fredlund and Xing (1994) model is capable of providing good fit over the entire suction range from 0 to 10^6 kPa. The predicted SWCC curve along with the fitted parameters of the SWCC and the position of in-situ measurements are illustrated in Figure 3.20.

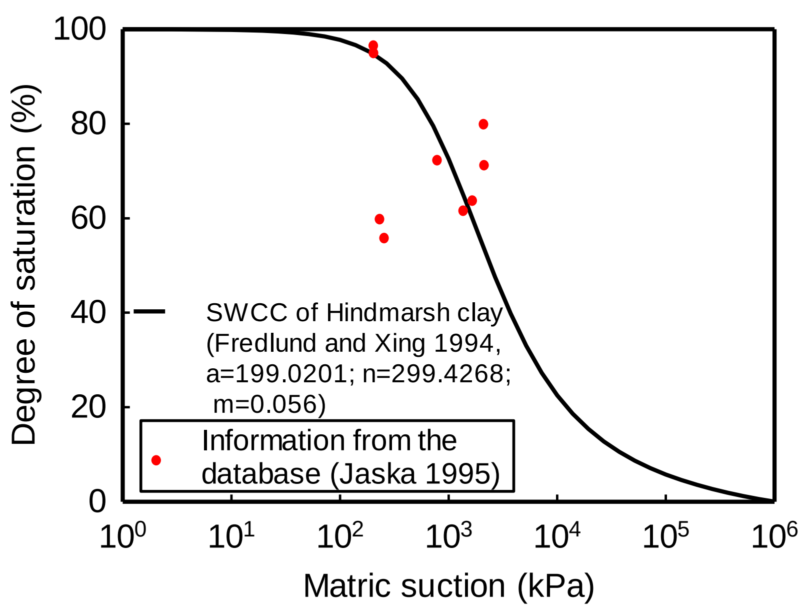

Figure 3.20 Fitting soil water characteristic curve for Hindmarsh clay

Experimental data on vertical earth pressure and lateral earth pressure variations were reported by Richards and Kurzeme (1973) at three locations which are named as earth pressure cell group 1 (including cell 0301, 0302 and 0303), group 2 (including cell 0305, 0306 and 0307) and group 3 (including cell 0309, 0310 and 0311), as shown in Figure 3.19. These earth pressure cells are buried at depth of around 4m, 6m and 6.8m, respectively. The in-situ test conducted by Richards and Kurzeme (1973) lasted from August 1971 to September 1973. The vertical pressure values can change or influenced during this period of measurement due to other construction activities which were in progress within the vicinity during that period. Figure 3.21 summarizes the variation of vertical pressure with respect to depth. As for the suction variations, data recorded by the psychrometer boreholes next to the earth pressure cell groups should be chosen for the validation of the proposed approach. More specifically, earth pressure cell 1 corresponds to psychrometer borehole 008, earth pressure cell 2 corresponds to psychrometer borehole 003 and 010 and earth pressure cell 3 corresponds to psychrometer borehole 005 and 12A. Figure 3.22 summarizes the suction profile variations for each psychrometer boreholes at different depths. However, it should be noted that since the field investigation is influenced by various factors, so that even the neighboring psychrometer boreholes recorded quite different suctions profiles, for example, suction profiles given by psychrometer boreholes 003 and 010, 005 and 012A in Figure 3.22. After comparison, data from psychrometer boreholes 008, 010 and 012A are selected for the computation of lateral swelling pressure in earth pressure cell group 1, 2 and 3 respectively in order to achieve reasonable comparisons.

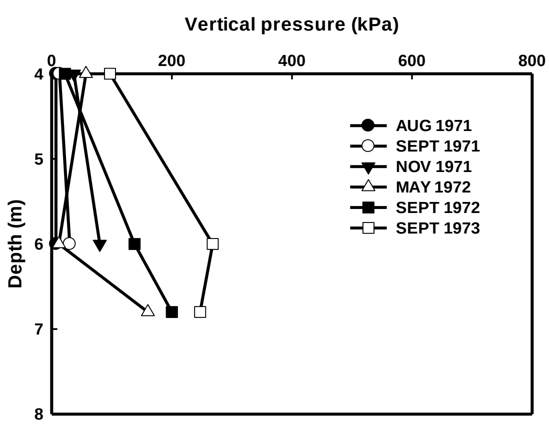

(A)

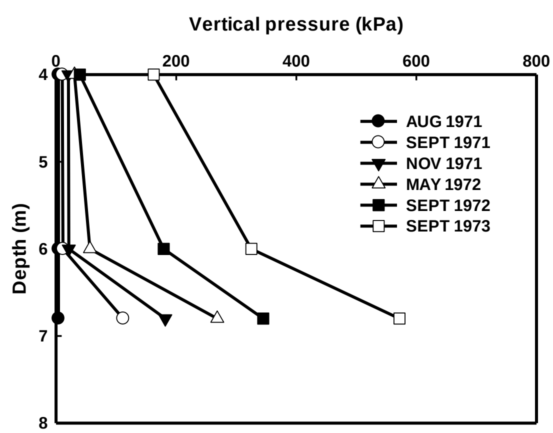

(B)

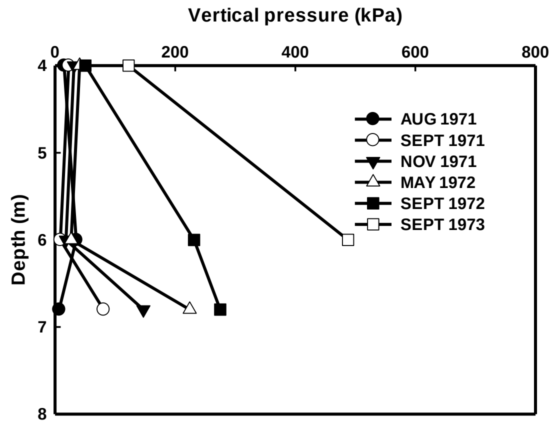

(C)

Figure 3.21 Variation of vertical pressure with time for different earth pressure cell group [(A) for Group 1; (B) for Group 2 and (C) for Group 3] (summarized from Richards and Kurzeme 1973)

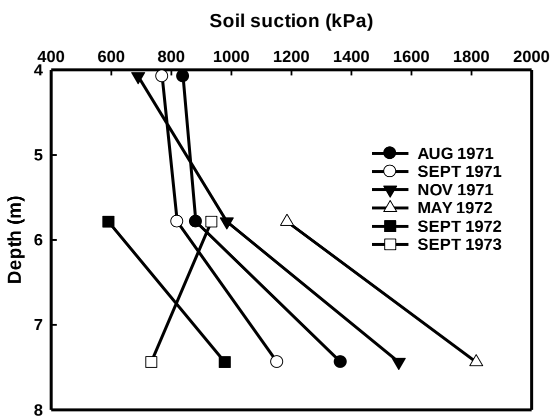

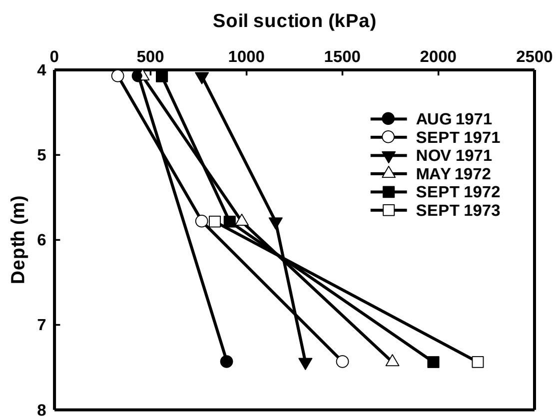

(A) (B)

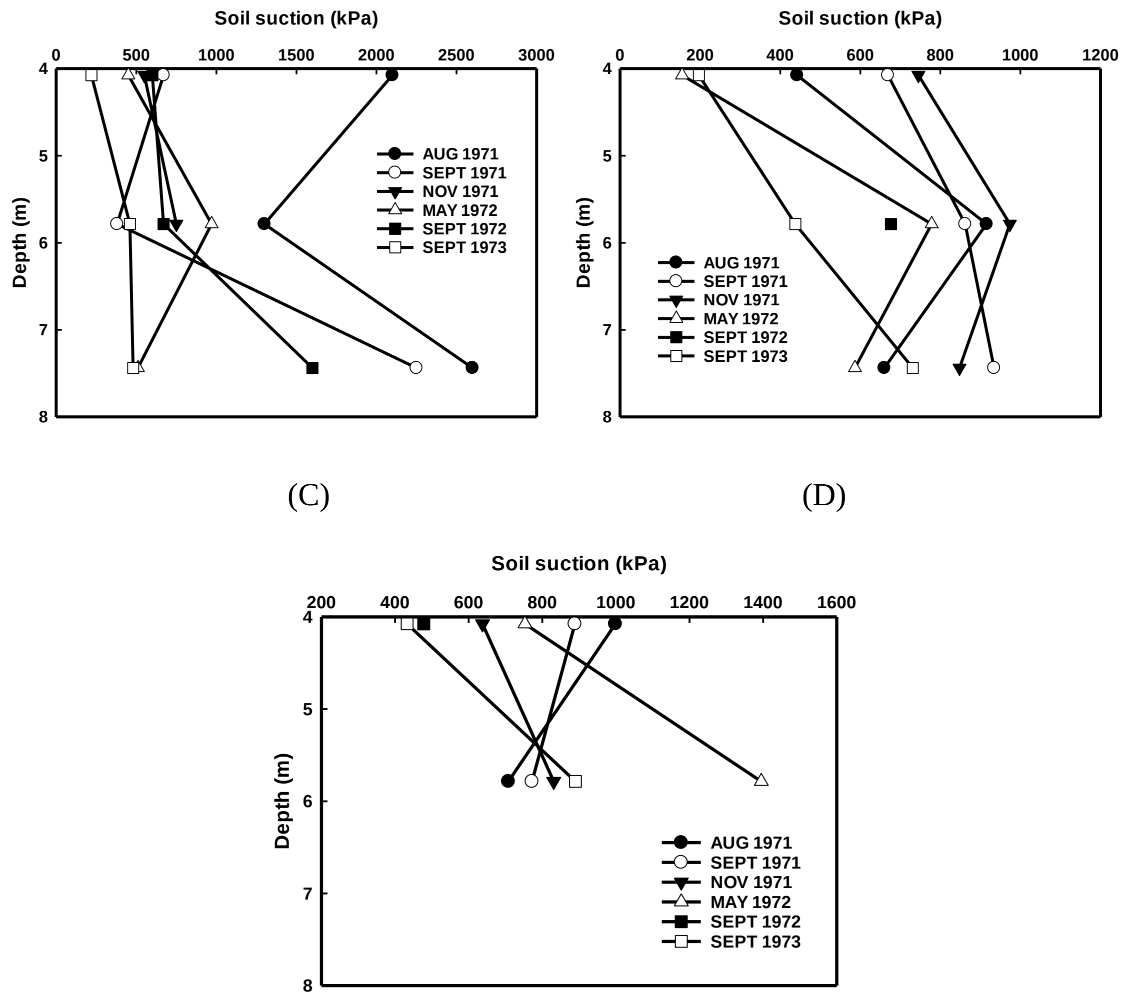

(C) (D)

(E)

Figure 3.22 Variation of soil suctions with time for each psychrometer boreholes [(A) for borehole 008; (B) for borehole 003; (C) for borehole 010; (D) for borehole 005; (E) for borehole 012A] (summarized from Richards and Kurzeme 1973)

For extending the proposed approach [i.e. Equation 3.21 and Equation 3.22] on Hindmarsh clay test site for estimating the lateral swelling pressure, information of the saturated elastic modulus is required. From the database provided by Jaksa (1995), the average water content of the Hindmarsh clay along the depth is around 27% and the water content of the soil at saturated conditons is around 34%). An average modulus of elasticity of 43.1MPa was estimated corresponding to the water content of 27%. Using

Equation 3.6, the saturated elastic modulus was back calculated as 1.36MPa. A typical Poisson's ratio of 0.3 is assumed in the calculation.

Figure. 3.23 shows the comparisons between the estimation using proposed approach [i.e. Equation 3.21 and Equation 3.22] and the in-situ measurement data. Reasonably good comparisons can be obtained. The undrained shear strength parameters from field test were presented by Richards and Kurzeme (1973) and Jaksa (1995); however, effective shear strength parameters information was not available. For this reason, the variations of PEP cannot be summarized for this example. Also, it should be noted that the suction values reported by psychrometers belong to total suction, which can be directly introduced in Equation 3.11 for the calculation of constant volume vertical swelling pressure. While for the calculation of unsaturated elastic modulus in Equation 3.21 and Equation 3.22 using Equation 3.6, matric suction values are necessary. At high suctions (i.e., greater than about 1500 kPa), matric suction and total suction can generally be assumed to be equivalent (Fredlund and Xing 1994). While at low suction ranges (i.e., lower than 1500kPa), corresponding calculations using total suction instead of matric suctions may cause errors to a certain extent.

Figure 3.23 shows the comparisons between the estimation using proposed approach [i.e. Equation 3.21 and Equation 3.22] and the in-situ measurement data. Reasonably good comparisons can be observed between the estimation and in-situ measurements in earth pressure cell group 1 and 2. While in group 3, good comparisons can only be obtained at a certain date such as August 1971, September 1971 and May 1973. The reason can be attributed to the difference in the suction profile recorded by the psychrometers in borehole 012A and the real suction distribution next to the earth pressure cell group 3, where there is an around 3m distance. The undrained shear strength parameters from field test were presented by Richards and Kurzeme (1973) and Jaksa (1995); however, effective shear strength parameters information was not available. For this reason, the variations of passive earth pressure cannot be summarized for this example. Also, it should be noted that the suction values reported by psychrometers belong to total suction, which can be directly introduced in Equation 3.11 for the calculation of constant volume vertical swelling pressure. While for the calculation of unsaturated elastic modulus in Equation 3.21 and Equation 3.22 using Equation 3.6, matric suction values are necessary. At high suctions (i.e., greater than about 1500 kPa), matric suction and total suction can generally be assumed to be equivalent (Fredlund and Xing 1994). While at low suction ranges (i.e., lower than 1500kPa), corresponding calculations using total suction instead of matric suctions may cause errors to a certain extent.

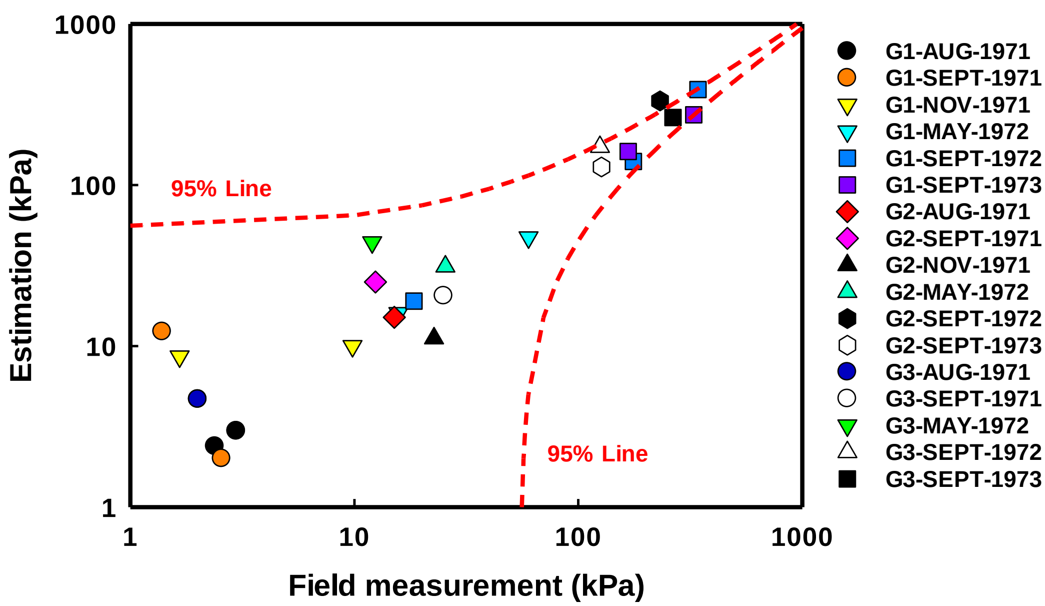

Figure 3.23 Comparison between the estimated LEP using the proposed method and the in-situ measurement at the Adelaide site (G1-Group 1; G2-Group 2; G3-Group 3)

3.4 Summary and conclusions

Lateral swelling pressure mobilization due to water infiltration within expansive soils can pose significant threats to the safety and stability of the geo-infrastructure. In this chapter, the development of lateral earth pressure against fixed rigid retaining structures is analyzed. The total lateral earth pressure can be calculated by superposition method taking account of the influence of lateral swelling pressure in addition to the lateral earth pressure due to soil unit weight and surcharge. However, the total lateral earth pressure is limited to a maximum value of passive earth pressure (i.e. the total lateral earth pressure cannot exceed passive earth pressure). In this chapter, a model is proposed to predict the lateral earth pressure considering lateral swelling pressure against fixed rigid retaining structure taking account of variation of matric suction associated with water infiltration, extending mechanics of unsaturated soils. The superposition method can be further extended for the estimation of lateral earth pressure of expansive backfill behind rigid retaining structures in the drying process considering volume shrinkage. Models for estimations the active and passive earth pressures under different degree of saturation and interface roughness are also presented as the limiting states of lateral earth pressures variations.

The proposed model is verified using the experimental data from a large scale model retaining wall test by Katti et al. (1983) and Gu (2005) along with the in-situ measurements by Mohamed et al. (2014) and Richards and Kurzeme (1973) on retaining structures. The model proposed is capable of reasonably predicting lateral swelling pressure mobilization from an initial unsaturated state to subsequent unsaturated state during the infiltration process employing only limited number of soil properties, which include SWCC, the saturated elastic modulus, E_{sat}, Plasticity index, I_p, maximum dry density, $\rho_{d,max}$ and the Poisson ratio, μ. The proposed simple model is valuable in geotechnical engineering practice for assisting geotechnical engineers to quickly estimate the increasing lateral earth pressure due to lateral swelling pressure mobilization behind retaining structures during the infiltration process, thus contributing to the rational design or construction decisions.

CHAPTER FOUR

PREDICTION OF MECHANICAL BEHAVIORS OF SINGLE PILE IN EXPANSIVE SOIL UPON INFILTRATION

Notation

Symbols	
A_p	Cross sectional area of the pile
A_3	Area of segment 3
c'_{ar}	Residual effective cohesion
E_p	Elastic modulus of the pile
f_{sBE}	Average ultimate shaft friction
G_s	Shear modulus of soil around the pile
G_{sb}	Shear modulus of the soil below the pile base
L	Pile length
L_3	Length of segment 3
k_t	Ratio of the load increment to the settlement increment at the pile head, $k_t = \Delta P_t/\Delta w_t$
P_3	Average perimeter of segment 3
r_0	Radius of pile
r	Horizontal distance between the calculated point and the pile axis
r_m	Maximum influencing radius of pile on the soil, generally r_m can be estimated using Equation 2.39 (Xiao et al. 2011)
$S_{\%}$	Percentage of expansive soil swell in oedometer test
$S_s(z)$	Pile soil relative displacement at a given depth
S_{su}	Pile soil relative displacement corresponding to peak interface shear strength
w	Vertical settlement of soil around the pile
x_{swell}	Constant volume vertical swelling pressure whose unit is psf
y_{swell}	Volumetric water content
α_{BE}	Empirical adhesion coefficient
ΔP_t	Increased load at the pile head when the settlement at the pile base is larger than the limiting pile base settlement of the first stage of the τ_b versus w_b curve
Δw_t	Increased settlement at the pile head induced by ΔP_t
θ	Current volumetric water content

θ_r	Residual volumetric water content
θ_s	Volumetric water content at a saturation of 100%
σ'_{cs}	Vertical swelling pressure acquired from consolidation-swell oedometer test
σ'_i	Confining pressure in oedometer test
$\tau_s(z)$	Interface shear stress (shaft friction) at a given depth
τ_{su}	Peak interface shear strength
τ_{sr}	Residual interface shear strength
δ_r	Residual interface friction angle
υ_b	Poisson's ratio of the soil below the pile base

In this chapter, considering the ground heave and variations of soil properties with respect to matric suction, two methods are proposed for the load transfer analysis of a single pile in expansive soil upon infiltration using unsaturated soil mechanics. First, the traditional shear displacement method which is based on saturated soil mechanics principles, is modified for the analysis of the load-displacement response of a single pile in expansive soil upon infiltration. Then, universal load transfer curve model is modified considering the influence of matric suction on the pile-soil interface shear strength. Based on this model, the traditional load transfer curve method is modified for the load settlement analysis of single piles in expansive soils, taking account of the influence of water infiltration. Both methods are verified using a large scale model pile test performed in the geotechnical laboratory of the University of Ottawa and a field case study collected from the published literature. Good comparisons were observed between the estimation and the experiment results. The proposed methods are useful for the practicing engineers such that they can quickly and reasonably evaluate the mechanical behaviors of a single pile in unsaturated expansive soils taking account of the influence of water infiltration.

4.1 Modified shear displacement method

4.1.1 Theoretical analysis and derivation

The models (Equation 2.26 and 2.27) proposed by Hamid and Miller (2009) illustrate the influence of matric suction on the influence of structure-unsaturated soil interface shear strength. Also, no empirical parameters are included in this model. Due to this reason, this model has received wide acceptance since it was proposed. This study extended the application of this model to calculate the interface shear strength between structure and expansive soil (Equation 4.1) by adding the contribution of increasing normal stress (mobilization of lateral swelling pressure).

$$f = c'_a + \tan\delta'[\frac{(1-\upsilon-2\upsilon^2)P_s}{1-\upsilon^2-\frac{P_s}{E_a}(1+\upsilon)(1-\upsilon-2\upsilon^2)} + \frac{\upsilon}{1-\upsilon}\sigma_s + (u_a-u_w)_r\frac{(\theta-\theta_r)}{(\theta_s-\theta_r)}] \tag{4.1}$$

where θ = the current volumetric water content; θ_r = the residual volumetric water content; θ_s = the volumetric water content at a saturation of 100%.

Equation 4.1 is capable to estimate the ultimate uplift friction (interface shear strength) considering both increasing normal stress (mobilization of lateral swelling pressure) and matric suction. However, besides the normal stress and matric suction, the mobilization of pile shaft friction is also a function of the pile-soil relative displacement. The softening behaviors have been reported by numerous scholars working on the unsaturated soil-structure interface (Fan 2007; Hamid and Miller 2009; Khoury et al. 2010; Hossain and Yin 2013; Borana et al. 2015).

Through a series of interface direct shear test between unsaturated expansive soils and concrete, Fan (2007) simplified the softening relationship between interface shear stress and displacement as following: at the beginning of the shearing, shear stress (τ_s) increase linearly with shear displacement (w), while after reaching the peak value (τ_{su}), it experiences a sudden decrease and finally stabilizes at a post peak value (τ_{sp}). However, in the theoretical method by Fan et al. (2007) to analyze the mechanical behaviors of piles in expansive soils considering environmental factors changes (wetting and drying), shear modulus of expansive soil around the pile (G_s) is assumed as a constant value. A constant shear modulus typically defines a linear relationship between the pile-unsaturated soil interface shear stress and displacement, while in fact softening behaviors have been observed by various scholars including Fan (2007). Also, the shear modulus of unsaturated soil (G_s) definitely changes with matric suction changes (Oh and Vanapalli

2013). Further, theoretical method presented by Fan (2007) did not highlight the influences of matric suction or matric suction variations on the mechanical behaviors variations of piles during wetting and drying. Key parameters such as the shear modulus and ground heave need to be determined through laboratory tests or regression equations for the soil under investigation. Such studies are need trained professionals and are time confusing because of the low hydraulic conductivity of expansive soils. To alleviate these problems, another version of modified shear displacement method is proposed in this thesis. Both the mobilization of interface shear strength (shaft friction) and changes of ground displacement are directly linked to matric suction and/or matric suction variations.

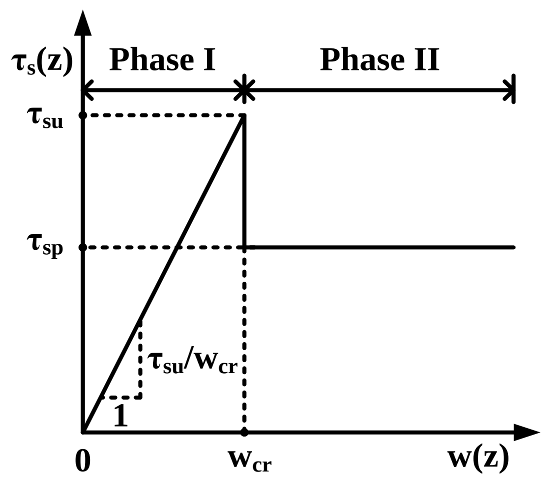

Figure 4.1 Relationship between the interface shear stress and displacement

The basic assumptions used in the traditional shear displacement method are also extended for the modified shear displacement method, which are summarized below:

(I) Expansive soil around the pile is assumed to be homogeneous, isotropic and linear elastic;

(II) The cross section is constant along the pile, without considering the non-linear compressive behavior, and the pile can assumed to sustain both compressive and tensile stress.

Based on the traditional shear deformation method proposed by Cooke in 1974, the soil around the pile can be assumed to be a series of concentric cylinders (as shown in Figure 4.2). The vertical settlement of soil around the pile at a certain depth z can be given as Equation 4.2.

$$w(z,r) = \frac{\tau_0 r_0}{G_s}\int_{r_0}^{\infty}\frac{\partial r}{r} = \frac{\tau_0 r_0}{G_s}\ln(\frac{r_m}{r}) \tag{4.2}$$

where w = the vertical settlement of soil around the pile, G_s = the shear modulus of soil around the pile, r_0 = the radius of pile, r = the horizontal distance between the calculated point and the pile axis, r_m = the maximum influencing radius of pile on the soil, generally r_m can be estimated using Equation 2.39 (Xiao et al. 2011).

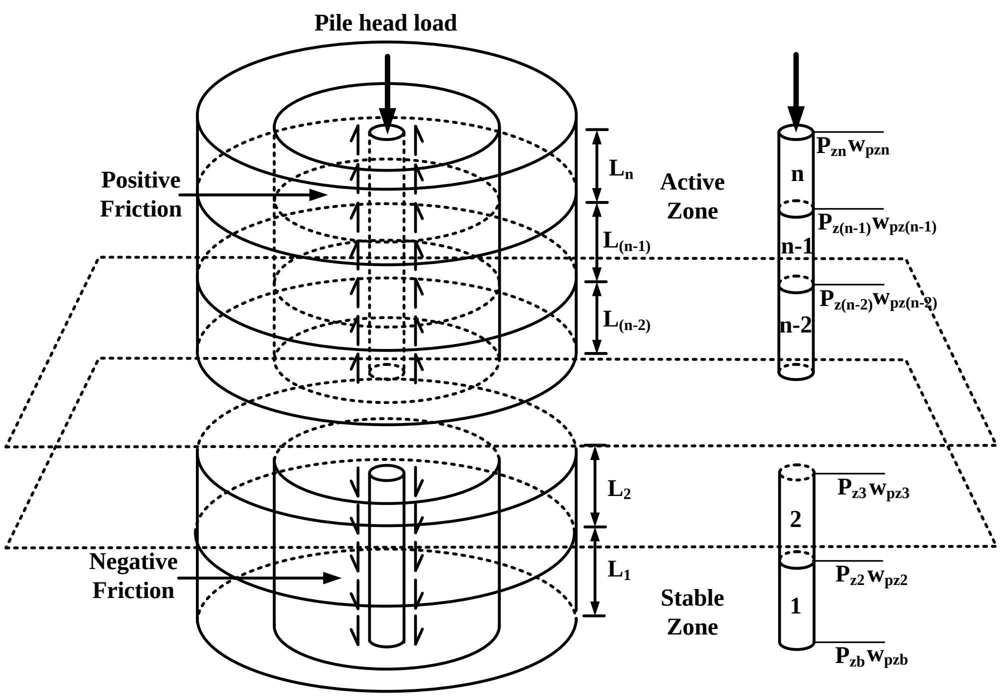

Figure 4.2 Analytical model of pile and soil around the pile

The relationship between axial force of pile and the shaft friction around the pile is given as Equation 4.3. The relationship between the axial force of pile and the pile displacement is given as Equation 4.4.

$$\frac{\partial P_z}{\partial z} = 2\pi r_0 \tau_0 \tag{4.3}$$

$$\frac{\partial w_{pz}}{\partial z} = \frac{P_z}{E_p A_p} \tag{4.4}$$

Equation 4.5 can be acquired by combining Equation 4.2, Equation 4.3 and Equation 4.4.

$$\frac{\partial^2 w_{pz}}{\partial z^2} - \frac{k}{A_p E_p} w_{pz} = 0 \tag{4.5}$$

Solving Equation 4.5, the pile displacement is given as Equation 4.6.

$$w_{pz} = Ae^{r_1 z} + Be^{r_2 z} \tag{4.6}$$

$$k = 2\pi G_s / \ln(\frac{r_m}{r_0})\ ;\ r_1 = \sqrt{\frac{k}{A_p E_p}}\ ;\ r_2 = -\sqrt{\frac{k}{A_p E_p}}$$

However, Equation 4.6 is only suitable for certain simple scenarios in which ground heave is not considered. For expansive soil, possible ground displacement in the active zone should also be taken into account as well. The heave prediction equation in the elastic range presented by Adem and Vanapalli (2016) (Equation 3.45) is employed in this paper. Since the soil is assumed to be elastic, this equation can be also used to estimate the ground settlement during the drying process. For soil layers at different depth, the matric suction variations can be different. Also, the soil displacement in vertical direction is cumulative from bottom to the top soil layer of the active zone. As a consequence, the vertical displacement calculated using Equation 3.45 for different soil layers is different. In this paper, within a certain soil layer, the development of the vertical displacement is simplified as a linear distribution (Equation 4.7) as shown in Figure 4.3.

$$\Delta h = Hz + a \tag{4.7}$$

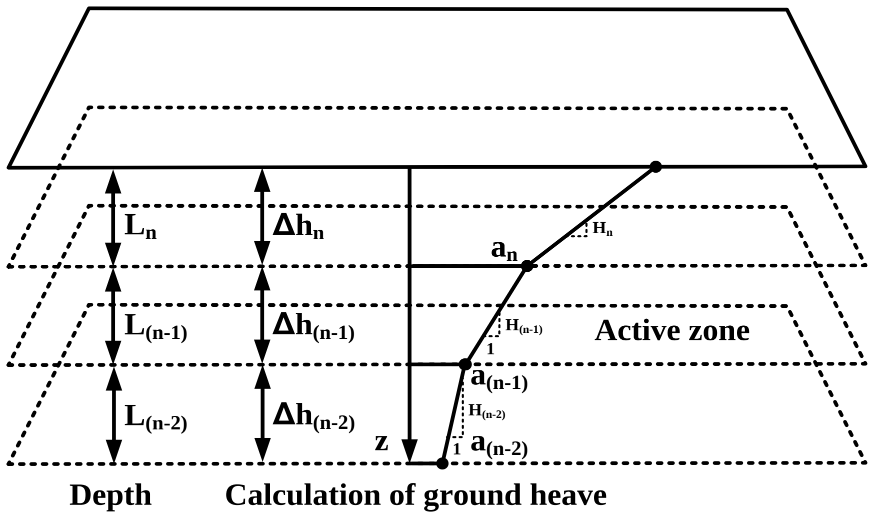

Figure 4.3 Simplification of the ground heave calculation model

Considering the ground heave, the pile displacement is given as Equation 4.8. Combining with Equation 4.2, the pile axial force is given as Equation 4.9. Equation 4.10 can be acquired by expressing Equation 4.8 and Equation 4.9 in a matrix form. Equation 4.10 can be simplified as Equation 4.11.

$$w_{pz} + (Hz + a) = Ae^{rz} + Be^{-rz} \tag{4.8}$$

$$P_z = -A_p E_p \frac{\partial w_{pz}}{\partial z} = A_p E_p [-Are^{rz} + Bre^{-rz} + H] \tag{4.9}$$

$$\begin{Bmatrix} w_{pz} \\ P_z \end{Bmatrix} = \begin{Bmatrix} e^{rz} & e^{-rz} \\ -A_p E_p re^{rz} & A_p E_p re^{-rz} \end{Bmatrix} \begin{Bmatrix} A \\ B \end{Bmatrix} + \begin{Bmatrix} -Hz - a \\ A_p E_p H \end{Bmatrix} \tag{4.10}$$

$$\begin{Bmatrix} w_{pz} \\ P_z \end{Bmatrix} = [T(z)] \begin{Bmatrix} A \\ B \end{Bmatrix} + \begin{Bmatrix} -Hz - a \\ A_p E_p H \end{Bmatrix} \tag{4.11}$$

As at different depth, the soil properties can experience significant variations, in this paper both the pile and soil are divided into several segments as shown in Figure 4.2. For a typical pile segment which is given as segment *n* in Figure 4.2, the pile axial force and displacement equation at the top and bottom of the segment are given as Equation 4.12 and Equation 4.13, respectively.

$$\begin{Bmatrix} w_{pzn} \\ P_{zn} \end{Bmatrix} = [T(z)_{(n)bot}] \begin{Bmatrix} A \\ B \end{Bmatrix}_{(n)bot} + \begin{Bmatrix} -H_n z_n - a_n \\ A_p E_p H_n \end{Bmatrix} \tag{4.12}$$

$$\begin{Bmatrix} w_{pz(n-1)} \\ P_{z(n-1)} \end{Bmatrix} = [T(z)_{(n-1)top}] \begin{Bmatrix} A \\ B \end{Bmatrix}_{(n-1)top} + \begin{Bmatrix} -H_n z_{(n-1)} - a_n \\ A_p E_p H_n \end{Bmatrix} \tag{4.13}$$

For the same pile segment n, Equation 4.14 is valid. Thus Equation 4.15 can be deduced.

$$\begin{Bmatrix} A \\ B \end{Bmatrix}_{(n)bot} = \begin{Bmatrix} A \\ B \end{Bmatrix}_{(n-1)top} \tag{4.14}$$

$$\begin{Bmatrix} w_{pzn} \\ P_{zn} \end{Bmatrix} = [T(z)_{(n)bot}][T(z)_{(n-1)top}]^{-1} \begin{Bmatrix} w_{pz(n-1)} \\ P_{z(n-1)} \end{Bmatrix} + [T(z)_{(n)bot}][T(z)_{(n-1)top}]^{-1} \begin{Bmatrix} H_n z_{(n-1)} + a_n \\ -A_p E_p H_n \end{Bmatrix} - \begin{Bmatrix} H_n z_n + a_n \\ -A_p E_p H_n \end{Bmatrix} \tag{4.15}$$

According to Equation 4.15, the pile axial force and displacement at the top of segment n can be calculated based on the pile axial force and displacement at the base of the segment. Also, through Equation 4.7 to 4.9, the influence of ground displacement induced by matric suction variations has been taken into account. However, as discussed earlier, the shear modulus of unsaturated soil keeps changing with matric suction variations. However, in Equation 4.6 a constant G_s is used for the calculations of pile displacement. In order to consider the softening relationship between the interface shear stress and displacement, the simplified relationship used by Fan (2007) is used in this thesis. As shown in Figure 4.1, the interface shearing is divided into two phases using three key parameters, namely the peak interface shear strength (τ_{su}), the post peak interface shear strength (τ_{sr}) and the critical shear displacement corresponding to the peak interface shear strength (w_{cr}). Phase *I* shows the interface shear stress increases linearly with the interface shear displacement so that a constant shear modulus is indicated. As shown in Equation 4.16, the magnitude of the shear modulus in phase *I* is determined by the slope of τ_{su} over w_{cr}. Then $T_{(z1)}$ and $T_{(z2b)}$ in Equation 4.12 and Equation 4.13 can be calculated using Equation 4.17 and Equation 4.18, respectively. Substituting Equation 4.17 and 4.18 into Equation 4.15, the displacement at the top of segment n (w_{pz2}) can be calculated. Then a comparison is made between the calculated displacement (w_{pz2}) and the critical displacement (w_{cr}). A calculated displacement (w_{pz2}) higher than critical displacement indicates that shear softening has occurred. The interface shear strength has dropped from the peak value to a post peak value. For this scenario, the pile axial force and displacement should be calculated using Equation 4.19 instead of 4.15.

$$k = 2\pi G_s / \ln(\frac{r_m}{r_0}) = 2\pi r_0 (\frac{\tau_{su}}{w_{cr}}) \tag{4.16}$$

$$T(z)_{(n)bot} = \begin{Bmatrix} e^{r_n z_n} & e^{-r_n z_n} \\ -A_p E_p r_n e^{r_n z_n} & A_p E_p r_n e^{-r_n z_n} \end{Bmatrix} \tag{4.17}$$

$$T(z)_{(n-1)top} = \begin{Bmatrix} e^{r_n z_{(n-1)}} & e^{-r_n z_{(n-1)}} \\ -A_p E_p r_n e^{r_n z_{(n-1)}} & A_p E_p r_n e^{-r_n z_{(n-1)}} \end{Bmatrix} \tag{4.18}$$

$$r_n = \sqrt{\frac{k_n}{A_p E_p}}\ ;\ k_n = \frac{2\pi \tau_{su(n)} r_0}{w_{cr}}$$

$$\begin{Bmatrix} w_{pzn} \\ P_{zn} \end{Bmatrix} = \begin{Bmatrix} w_{pz(n-1)} \\ P_{z(n-1)} \end{Bmatrix} + \begin{Bmatrix} (\frac{2P_{z(n-1)} + \tau_{sp(n)} L \pi d}{2})(\frac{L}{A_p E_p}) \\ \tau_{sp(n)} L \pi d \end{Bmatrix} \tag{4.19}$$

Equation 4.12 to 4.19 presents an example illustrating detailed calculations of the head force and displacement according to base force and displacement for a typical pile segment. Following this procedure, similar calculations can be conducted from the bottom segment to the top segment. For a certain matric suction profile, by assuming a series of pile base movement, the pile head load displacement response can be obtained.

In most cases, the pile base is located in the stable zone, thus the pile base resistance can be directly calculated using Equation 4.20 proposed by Randolph and Wroth (1978). However, if the positive friction (uplift friction) increases significantly during the infiltration process and exceeds the withholding force (pile head load and negative friction), pile moves upwards. In other words, under such a scenario, it is possible for the pile base to detach from the soil so that the pile base settlement (w_b) may have negative value. Considering this possibility, Equation 4.21 is proposed for the calculation of the pile base resistance considering the possible detachment of the pile base and soil upon infiltration.

$$P_{zb} = \frac{4G_{sb}r_0}{1-\upsilon_b} w_b \tag{4.20}$$

$$P_{zb} = \begin{cases} 0 & w_b < 0 \\ \dfrac{4G_{sb}r_0}{1-\upsilon_b} w_b & w_b \geq 0 \end{cases} \tag{4.21}$$

Since the softening relationship (Figure 4.1) between the shear stress and shear displacement plays a key role in the modified shear displacement method introduced above. Detailed discussions are issued to the determination of the three key parameters determining the shape of the curve, namely the peak interface shear strength (τ_{su}), the post peak interface shear strength (τ_{sr}) and the critical shear displacement corresponding to the peak interface shear strength (w_{cr}). Introducing Equation 3.21 and Equation 3.22 into Equation 4.1, Equation 4.22 and Equation 4.23 can be obtained for the calculations of peak interface shear strength in wetting and drying process, respectively. From limited data collected from literatures regarding the interface direct shear test with matric suction control or measurement, the mobilization of peak interface shear strength (τ_{su}), post peak interface shear strength (τ_{sr}) and the critical interface shear displacement (w_{cr}) with net normal stress and matric suction variations are summarized as Figure 4.4, Figure 4.5 and Figure 4.6, respectively. Through comparison between Figure 4.4 and Figure 4.5, the post peak interface shear strength seems to be less affected by the matric suction compared to the peak interface shear strength. Hamid and Miller (2009) concluded that the possible reason for this behavior was the disruption of air-water menisci along the failure surface during continued shearing after achieving the peak interface shear strength. For this reason, the residual interface shear strength can be estimated only by considering the contribution of net normal stress as shown in Equation 4.24. In Equation 4.24, both the residual effective cohesion (c'_{ar}) and the residual interface friction angle (δ'_r) should be determined from experimental studies for specific structure surface and soil. If there is no experimental data available on the residual interface shear strength, the value of residual interface shear strength can be assumed as 0.83 to 0.97 times the value of peak interface shear strength based on a series of field tests on bored piles under compression loading according to the experimental studies from Zhang et al. (2010a, 2011b).

Similar to the post peak interface shear strength, Figure 4.6 illustrated that the matric suction also pose minor influences on the critical interface shear displacement. The reason can also be given as the disruption of air-water menisci along the failure surface. While except for matric suction, the critical interface shear displacement (w_{cr}) is influenced by various other factors like the soil type, structure surface type, stratigraphy, loading procedure and environmental factors. Because of the complexities associated in understanding the independent contribution of each of these factors, generally w_{cr} is suggested to be determined experimentally or back-analysis from field test. There are also several scholars presenting suggested values for different scenarios, although most of them are explicit and completely defined by the authors for direct use. For example, API (1993) suggested the value of w_{cr} to be 2 percent of the pile diameter for piles in clay. Vijayvergiya (1997) suggested a fixed value of 7.5mm for piles in sand while Krasiński (2012) suggested a fixed value of 15mm for piles in sand. From a series of field tests (Zhao et al. 2009; Zhang et al. 2010b; Zhang et al. 2011b; Zhang and Zhang 2012) for bored piles (diameter from 0.7-1.1m) in different kinds of soils (e.g., mud, clay, sandy silt, silty clay), Zhang and Zhang (2012) summarized that the value of S_{su} varies within a range from 5 to 25mm.

$$f = c'_a + \tan\delta'\{\frac{(1-\upsilon-2\upsilon^2)P_{s(\psi mi-0)}}{1-\upsilon^2-\dfrac{P_{s(\psi mi-0)}}{E_{a(\psi mi-0)}}(1+\upsilon)(1-\upsilon-2\upsilon^2)} - \frac{(1-\upsilon-2\upsilon^2)P_{s(\psi mw-0)}}{1-\upsilon^2-\dfrac{P_{s(\psi mw-0)}}{E_{a(\psi mw-0)}}(1+\upsilon)(1-\upsilon-2\upsilon^2)} + \frac{\upsilon}{1-\upsilon}\sigma_S + (u_{ar}-u_{wr})\frac{\theta-\theta_r}{\theta_s-\theta_r}\} \tag{4.22}$$

$$f = c'_a + \tan\delta'\{\frac{(1-\upsilon-2\upsilon^2)P_{s(\psi mi-0)}}{1-\upsilon^2-\dfrac{P_{s(\psi mi-0)}}{E_{a(\psi mi-0)}}(1+\upsilon)(1-\upsilon-2\upsilon^2)} - \frac{(1-\upsilon-2\upsilon^2)P_{s(\psi md-0)}}{1-\upsilon^2-\dfrac{P_{s(\psi md-0)}}{E_{a(\psi md-0)}}(1+\upsilon)(1-\upsilon-2\upsilon^2)} + \frac{\upsilon}{1-\upsilon}\sigma_S + (u_{ar}-u_{wr})\frac{\theta-\theta_r}{\theta_s-\theta_r}\} \tag{4.23}$$

$$\tau_{sr} = c'_{ar} + (\sigma_{nf} - u_{af})\tan\delta'_r \tag{4.24}$$

where c'_{ar} = the residual effective cohesion; δ'_r = the residual interface friction angle.

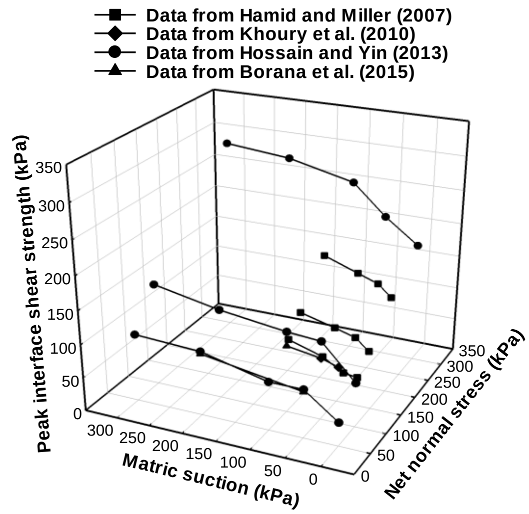

Figure 4.4 Mobilization of peak interface shear strength with net normal stress and matric suction

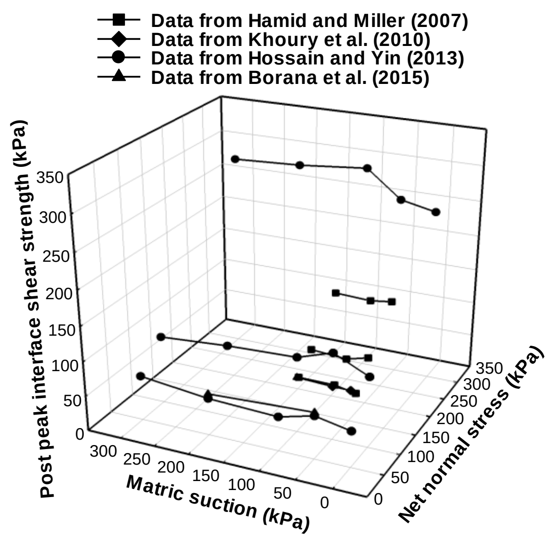

Figure 4.5 Mobilization of post peak interface shear strength with net normal stress and matric suction

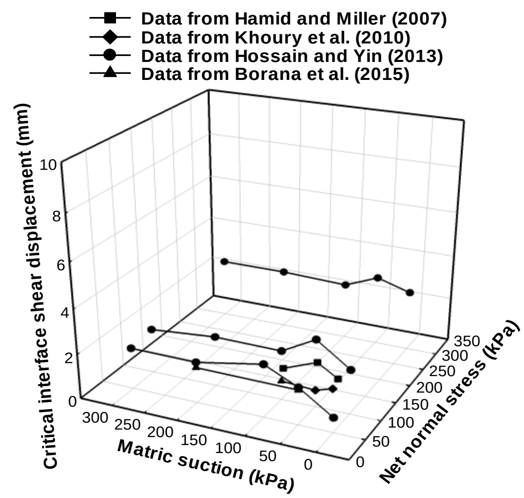

Figure 4.6 Variations of critical interface shear displacement with net normal stress and matric suction

4.1.2 Validation of proposed modified shear displacement method

4.1.2.1 Model pile test presented by Fan (2007)

Fan (2007) conducted a large scale model test to investigate the mechanical behaviors of a single pile in expansive soil upon water infiltration, which are illustrated for verification of the modified shear displacement method proposed in this study. The schematic of the pile test is given as Figure 4.7. The circular testing tank was filled with 0.1m gravel, 0.16m medium sand and 0.58m expansive soil from bottom to the top. The model pile was made of PVC pipe with fly-ash filled in side. A series of strain gauges were installed at different depths for the measurement of axial strain of the model pile during the testing process.

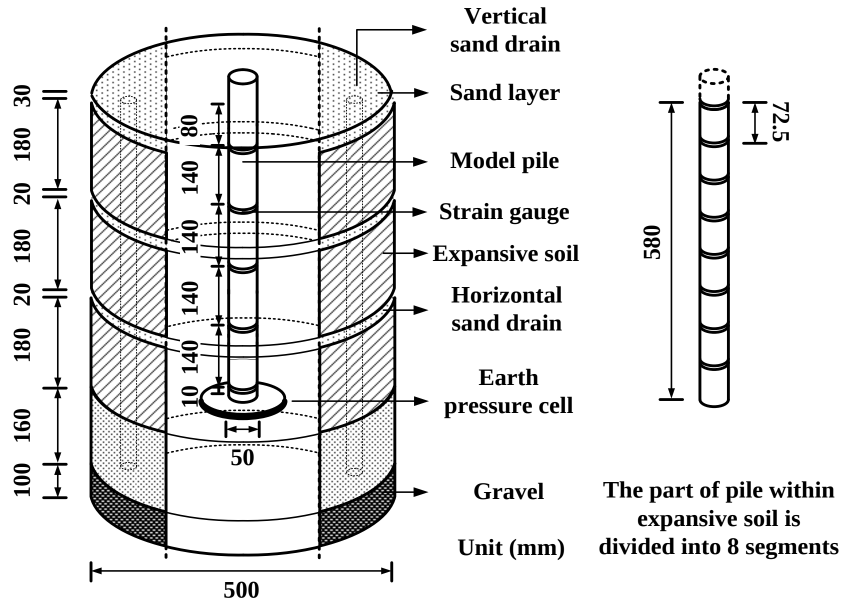

Figure 4.7 Sketch of the model pile and test tank used in Fan (2007)

The expansive soil filled in the testing tank was collected from Nanning, Guangxi province in China, whose properties are given in Table 4.1. The expansive clay filled in the testing tank has a degree of compaction higher than 90%. The soil in the test tank was subjected to manual irrigation from surface for a period of 230 hours until both the ground heave and the pile head displacement had stabilized, which means the soil is close to saturated condition. A ground heave of 41.2mm and the pile head upward displacement of 3.59mm were recorded. A series of constant volume swelling pressure tests were conducted by Fan (2007) conducted for the determination of volume swelling pressure. The testing results indicated that a volume swelling pressure of 400kPa was mobilized when a compacted specimen was saturated from initial water content of 15.8% to approximately 26% (which is the saturated water content). Besides the basic soil properties as given in Table 4.1, other properties necessary for the verification of the modified shear displacement method are acquired from the finite element program developed by Fan (2007), as given in Table 4.2. By modifying the Barcelona Basic Method (Alonso et al. 1990), Fan (2007) well estimated the soil heave as 39.53mm and the upward movement of the pile as 5.71mm, which is in good agreement with the model pile test results (41.2mm and 3.59mm respectively).

Table 4.1 Properties of expansive soil in the test (Modified after Fan 2007)

Property	Nanning soil
Liquid limit, %	48.1
Plastic limit, %	21.2
Plastic index	26.9
Specific Gravity	2.74
Maximum dry density (Mg/m^3)	1.89
Optimum water content (%)	15.8
Saturated unit weight (kN/m^3)	20

Table 4.2 Parameters of expansive soil used in the simulation (Modified after Fan 2007)

Property	Nanning soil
Average elastic modulus, E_a (MPa)	5.94
Elastic modulus of the pile, E_p (MPa)	1820
Poisson ratio, υ	0.3
Effective interface friction angle, δ' (°)	35.4
Effective interface cohesion, c'_a (kPa)	46.7
Residual interface friction angle, δ_r' (°)	27.1
Residual interface cohesion, c'_{ar} (kPa)	7.5

Since the real time suction measurement was not conducted by Fan (2007), only the pile mechanical behaviors in the final phase (almost saturated state) can be estimated using the proposed modified shear displacement. The peak and residual interface shear strength in the final phase (almost saturated state) are calculated using Equation 4.25 and Equation 4.26 proposed by Fan (2007) in the numerical simulations, respectively. Since there is no load applied on the pile head, the pile base experienced upward movement upon infiltration, which has resulted in the detachment of the pile base and the soil. For this reason, there is no pile base resistance contribution from the pile base. The vertical swelling pressure and the ground heave are set as 400kPa and 41.2mm, which are derived from the results of experimental investigations. According to the numerical simulation conducted by Fan (2007), ground heave develops linearly from the depth of 0.3m to the ground surface. The pile is divided into eight segments. The pile-soil relative displacement corresponding to the peak interface shear strength (S_{su}) is set as 0.01m (which is a reasonable assumption and is within the range of 5 to 25mm suggested by Zhang and Zhang (2012) in order to achieve good comparisons.

$$\tau_{su} = c'_a + (\sigma_{nf} - u_{af})\tan\delta' \tag{4.25}$$

$$\tau_{sr} = c'_{ar} + (\sigma_{nf} - u_{af})\tan\delta'_r \tag{4.26}$$

Based on the modified shear displacement method, in the final phase, the pile head upward movement of 5.51mm is estimated, which shows good comparisons with the model test of 3.59mm and the numerical simulation of 5.71mm. Good comparisons can also be achieved between the pile axial stress distribution and pile shaft friction distribution curves obtained from the experiment results and numerical simulations performed by Fan (2007) and the calculation using the method proposed in this paper from Figure 4.8 and Figure 4.9, respectively. Since several key parameters inside the modified shear displacement method and the ground heave development are derived from the finite element program proposed by Fan (2007), both the estimated pile axial stress distribution and pile shaft friction distribution are closer to the numerical simulation rather than the numerical simulation.

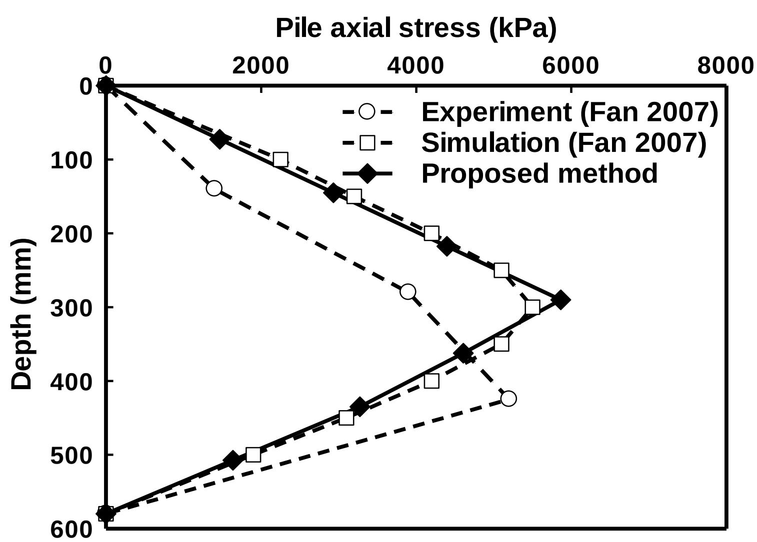

Figure 4.8 Comparison of the pile axial stress in model pile by Fan (2007)

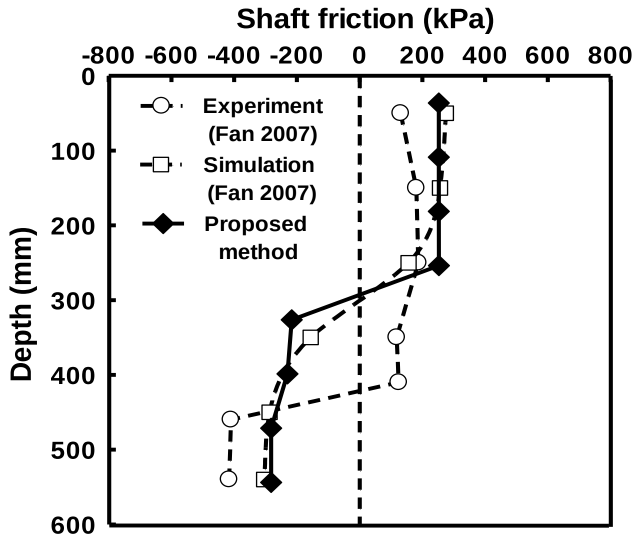

Figure 4.9 Comparison of the pile shaft friction distribution in model pile by Fan (2007)

4.1.2.2 Field investigation case study presented by Benvenga (2005)

The Colorado State University (CSU) expansive soils test site located in an area of the Pierre Shale formation has been widely documented by many investigations (Porter 1977; Goode 1982; Chapel 1998; Durkee 2000; Abshire 2002; Benvenga 2005 and Nelson et al. 2011). The pile test involved four reinforced concrete piles installed at this site. Figure 4.10 shows the schematic of the piles and positions of various measurement accessories. In the testing process, experimental data including pile axial strains, water content, free ground heave around the pile and pile heave were recorded from September 1995 to April 2004 (Benvenga 2005), which are shown in Table 4.3 (Nelson et al. 2011). Since four piles showed similar behaviors, one pile numbered as D1.130 was selected as a validation of the modified shear displacement method (Nelson et al. 2011). The measured and predicted ground displacements during the testing process were presented by Benvenga (2005), which is given as Figure 4.11. According to Figure 4.11, from February 1997 to August 1997, the soil experienced ground heave up to 64mm, while in October 2002, the soil showed a settlement of around 2mm below the zero point. From then on, the soil swelled a little and kept to be around 6mm higher than the zero point. In this paper, the mechanical behaviors of the pile at two representing time points (i.e., August 1997 and

September 2003) were discussed for the validation of the modified shear displacement method.

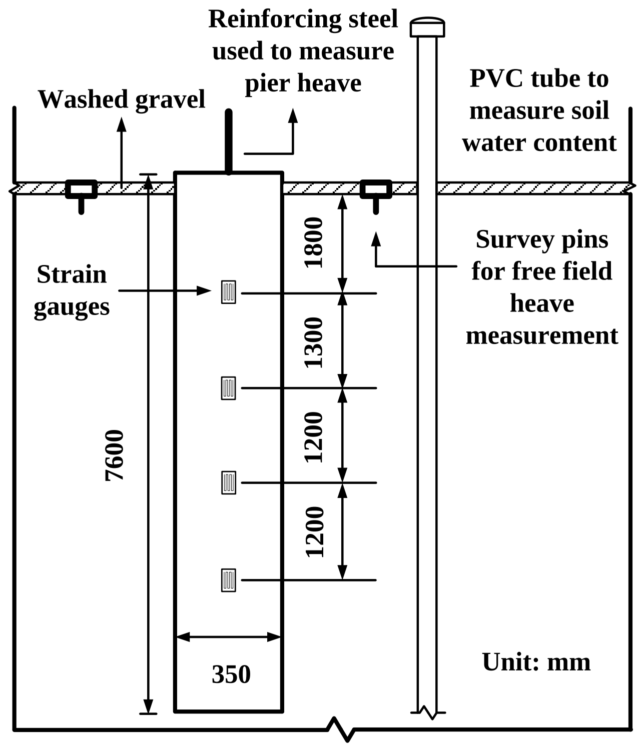

Figure 4.10 Diagram of the drilled reinforced concrete pier at CSU expansive soil test site (Modified after Benvenga 2005)

Table 4.3 Geotechnical Properties for CSU expansive soil test site (Modified after Nelson et al. 2011)

Depth	Material	Water content (%)	Dry Density (kN/m^3)	$S_{\%}$(%)	σ'_{cs}(kPa)	σ'_i(kPa)
0-1.5	Clay	14	17.3	1	39.9	23.9
1.5-1.8	Clay	13.9	17.7	2.9	205.9	47.9
1.8-2.4	Weathered claystone	15.6	17.4	2.5	215.5	47.9
2.4-3.2	Weathered claystone	20.6	18.1	0.9	124.5	47.9
3.2-4.3	Weathered claystone	10.4	17.6	3.8	430.9	29.7
4.3-4.7	Weathered claystone	11.5	17.9	1.9	210.7	29.7
4.7-7	Weathered claystone	11.5	17.9	3.8	287.3	29.7

where $S_{\%}$ = the percentage of expansive soil swell in oedometer test; σ'_{cs} = vertical swelling pressure acquired from consolidation-swell oedometer test; σ'_i = the confining pressure in oedometer test.

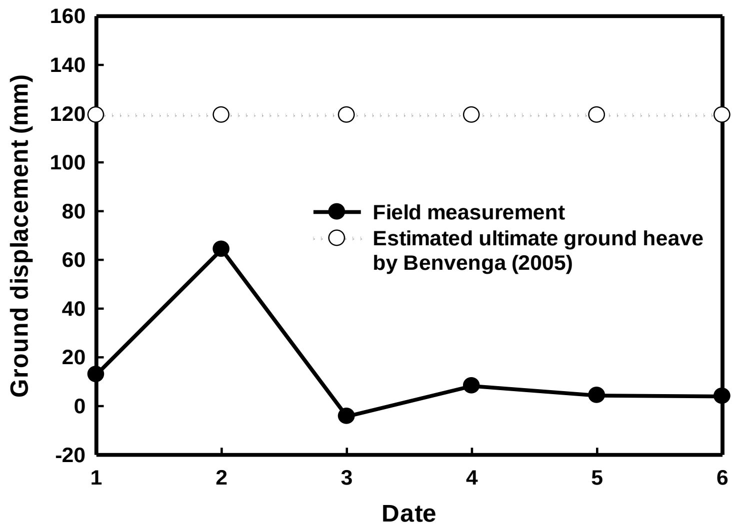

Figure 4.11 Ground displacement measurement and estimation by Benvenga (2005) [1-February 1997; 2- August 1997; 3-October 2002;4- June 2003; 5-September 2003; 6-April 2004] (Modified after Benvenga 2005)

In order to simplify the calculation, the soil properties of soil layers at different depth were averaged and a relationship between constant vertical swelling pressure and volumetric water content of the soil was proposed by Benvenga (2005) (Equation 4.27). According to the water content measurement shown in Figure 4.12(A), employing Equation 4.27, Benvenga (2005) calculated the constant volume vertical swelling pressure of expansive soil as shown in Figure 4.12(B).

$$y_{swell} = 12.949 \ln(x_{swell}) - 69.45 \tag{4.27}$$

where x_{swell} = constant volume vertical swelling pressure whose unit is psf; y_{swell} = the volumetric water content.

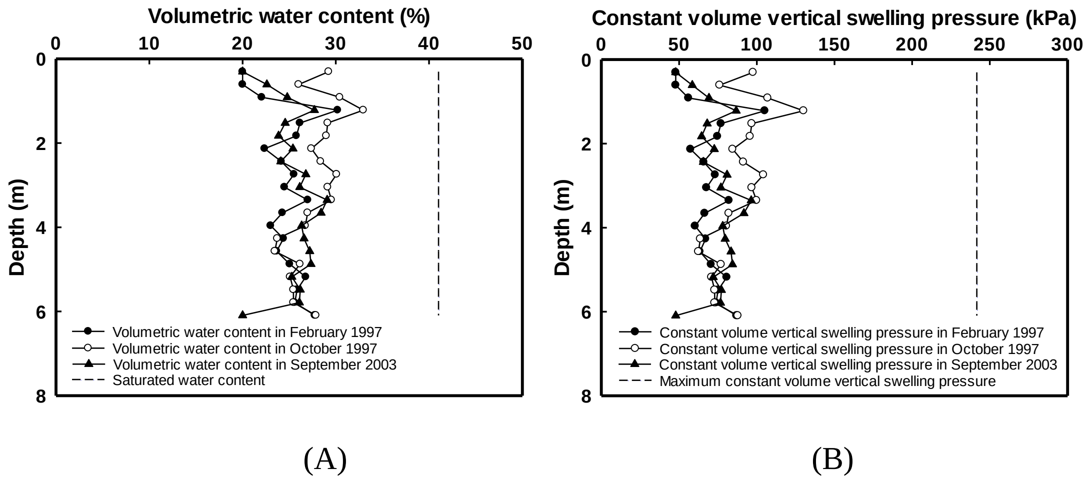

Figure 4.12 (A) Volumetric water content in February 1997 and October 1997; (B) Constant volume vertical swelling pressure in February 1997 and October 1997 (Modified after Benvenga 2005)

Based on the information shown in Figure 4.12, using Equation 3.11, the SWCC and matric suction variation of the expansive soil around the pile can be estimated as shown in Figure 4.13 and Figure 4.14. In order to apply Equation 3.11, plasticity index, I_p and maximum dry density ($\rho_{d,max}$) are necessary. Benvenga (2005) used the average soil properties for calculation of the vertical swelling pressure. An average value of maximum dry density of 17.7kN/m^3 was used. However, plasticity index information for different soil layers along the depth of the pile was not available in Benvenga (2005). Nelson et al. (2015) summarized that the expansive soils in the Front Range area of Colorado typically have a liquid limit ranging from 35 to 75 percent and a plasticity index ranging from 15 to 50 percent. For this reason, an average plasticity index of 30 was used for different soil layers for this case study. This value falls in the range of medium swelling potential (25 to 35) according to the expansive soil classification system proposed by O’Neill and Poormoayed (1980).

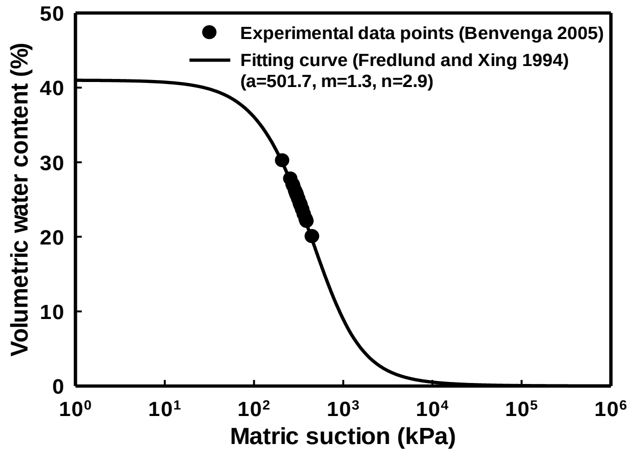

Figure 4.13 Estimated SWCC using model proposed by Fredlund and Xing (1994)

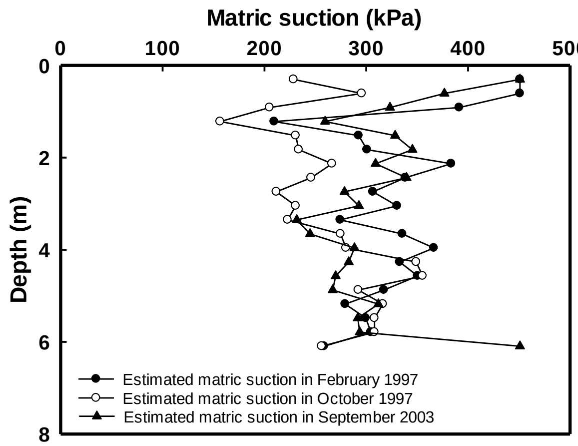

Figure 4.14 Matric suction variations in February 1997, October 1997 and September 2003

Benvenga (2005) estimated the average ultimate shaft friction between the pile and soil using Equation 4.28 and suggested the range of α varies 0.6 to 1.0 in October 1997. Using the matric suction profiles and SWCC shown in Figure 4.13, it is possible to use Equation 4.1 to back calculate the average shear strength properties of the pile-soil interface.

$$f_{sBE} = \alpha_{BE} \sigma'_{cv} \tag{4.28}$$

where f_{sBE} = the average ultimate shaft friction; α_{BE} = the empirical adhesion coefficient.

Employing Equation 4.1, the effective pile-soil interface cohesion, c_a and the effective pile-soil interface friction angle δ' are estimated as 15kPa and 25°, respectively. Comparisons among back calculated results and the estimations made by Benvenga (2005) using different α values regarding shaft friction distribution are shown in Figure 4.15. Also, β_s and S_u are set as 0.85 and 0.01m, respectively, which are both in the suggested range as per (Zhang and Zhang 2012).

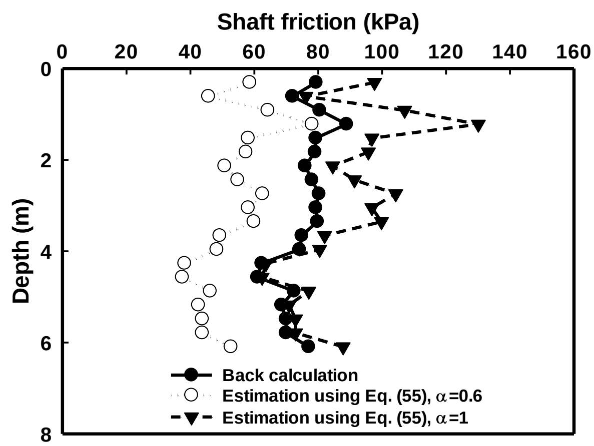

Figure 4.15 Comparison of pile shaft friction distribution in case study by Benvenga (2005)

Using the information introduced above, the mechanical behaviors of pile in October 1997 and September 2003 are analyzed employing the modified shear displacement method. Comparison of the pile head displacement is given in Figure 4.16, more reasonable can be achieved using modified proposed method compared to the estimations conducted by Benvenga (2005). Figure 4.17(A) and (B) give the comparisons of the pile axial force distribution in October 1997 and September 2003. Nelson et al. (2015) proposed a finite element program and also analyzed the mechanical behaviors of the pile in October 1997 as a case study. Through Figure 4.17, it can be seen that the proposed modified shear displacement method well estimate the mechanical behaviors of the piles during environmental factors changes extending unsaturated soil mechanics. The proposed approach is simple and can facilitate practicing engineers to make quick and reasonable estimations of the mechanical behaviors of single pile in expansive soils.

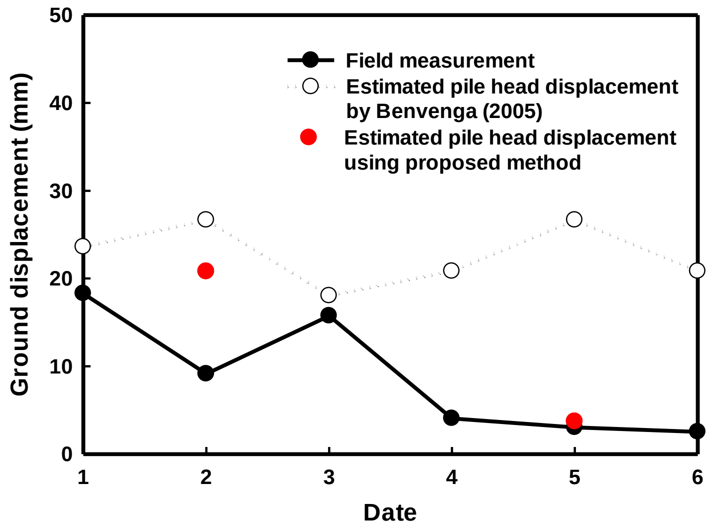

Figure 4.16 Comparison of pile head displacement [1-February 1997; 2- August 1997; 3-October 2002; 4- June 2003; 5-September 2003; 6-April 2004]

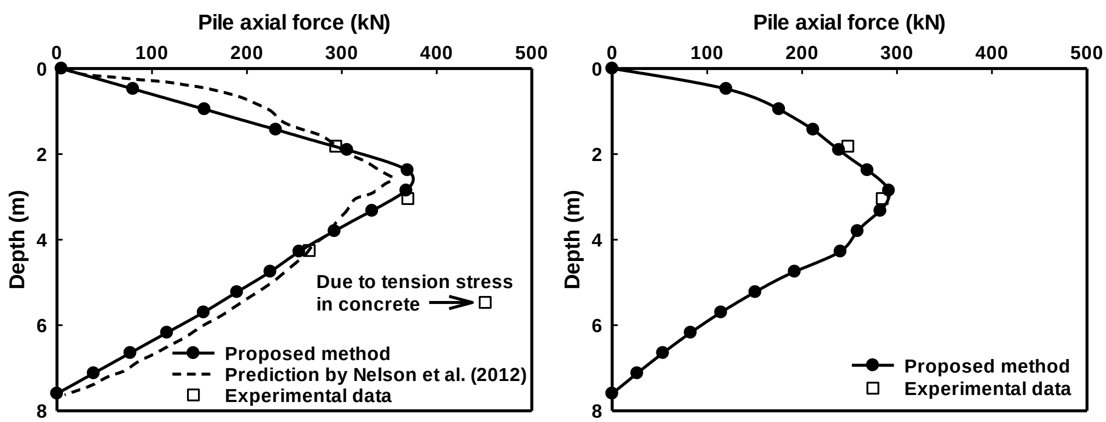

(A) (B)

Figure 4.17 Comparison of pile axial force distribution (A) October 1997; (B) September 2003

4.2 Modified load transfer curve method

4.2.1 Theoretical analysis and derivation

The load transfer curve method for the analysis of single pile settlement was originally proposed by Coyle and Reese (1966). Using the curve relating the interface shear strength (shaft friction) to the pile displacement in different soil layers (pile soil relative displacement), the pile head load and settlement can be calculated according to pile base resistance and settlement. Through decades of application studies, it has gained wide acceptance in practice applications (Poulos and Davis 1980). The key factor in this method is the curve relating the interface shear strength to the pile soil relative displacement, which is referred to as transfer curve model in this paper. Such transfer curve models were developed by Seed and Reese (1957), Gambin (1963) and Cambefort (1964). Several other investigators have also undertaken research studies in this area for the past half a century (Coyle and Reese 1966; Poulos and Davis 1980; Zhu and Chang 2002; Liu et al. 2004 and Chen et al. 2007; Nanda and Patra 2013; Bohn et al. 2016). For example, Coyle and Reese (1966) and Coyle and Sulaiman (1967) presented the transfer curve models suitable for different situations based on either laboratory tests and/or field measurements. Several research scholars have kept improving transfer curves by taking account of the influence of several factors such as the modulus degradation, negative fiction and have also extended it for layered soils (Zhu and Chang 2002; Liu et al. 2004 and Chen et al. 2007). A detailed summary on various transfer curve models is available in Bohn et al. (2016).

The pile soil interface shear strength degradation (softening phenomenon) has been investigated from field tests by some investigators during the last few years (Zhao et al. 2009; Zhang et al. 2010b, 2011a, 2011b). Extending this point of view, Zhang and Zhang (2012) proposed a simplified approach for the nonlinear analysis of the load displacement response of a single pile considering both shaft friction degradation and base resistance hardening. This approach is based on two models; namely, the softening nonlinear transfer curve model relating the pile-soil interface shear strength to the pile displacement relative to soil in different soil layers and the bi-linear model relating the pile base resistance to the pile base settlement.

The shape of the softening nonlinear transfer curve model proposed by Zhang and Zhang (2012) is shown in Figure 4.18(A). The pile unit shaft friction shows a nonlinear increase with increasing pile head load. When the pile soil relative displacement reaches S_{su}, the unit shaft friction achieves the peak value τ_{su}. The unit shaft friction then starts decreasing with a further increase in the pile soil relative displacement. The mathematical expression for the curve shown in Figure 4.18(A) is given as Equation 4.29.

$$\tau_s(z) = \frac{S_s(z)[a + cS_s(z)]}{[a + bS_s(z)]^2} \tag{4.29}$$

$$\begin{cases} a = \dfrac{\beta_s - 1 + \sqrt{1-\beta_s}}{2\beta_s}\dfrac{S_{su}}{\tau_{su}} \\ b = \dfrac{1-\sqrt{1-\beta_s}}{2\beta_s}\dfrac{1}{\tau_{su}} \\ c = \dfrac{2-\beta_s - 2\sqrt{1-\beta_s}}{4\beta_s}\dfrac{1}{\tau_{su}} \end{cases}$$

$$\beta_s = \frac{\tau_{sr}}{\tau_{su}} \tag{4.30}$$

where $\tau_s(z)$ = the interface shear stress (shaft friction) at a given depth, z; $S_s(z)$ = the pile soil relative displacement at a given depth, z; S_{su} = pile soil relative displacement corresponding to peak interface shear strength; τ_{su} = the peak interface shear strength; τ_{sr} = the residual interface shear strength; A series of field tests on bored piles under compression loading (Zhang et al. 2010b, 2011a, 2011b) demonstrated that the value of β_s to be within the range of 0.83-0.97.

The shape of the bi-linear model relating the pile base resistance to the pile base settlement is shown in Figure 4.18(B) and the mathematical relationship for this model is given as Equation 4.31.

$$\tau_b = \begin{cases} k_{b1}w_b & w_b < S_{bu} \\ k_{b1}S_{bu} + k_{b2}(w_b - S_{bu}) & w_b \geq S_{bu} \end{cases} \tag{4.31}$$

Randolph and Wroth (1978) proposed a model for the determination of k_{b1} shown as Equation 4.32.

$$k_{b1} = \frac{4G_{sb}}{\pi r_0(1-\upsilon_b)} \tag{4.32}$$

where G_{sb} and υ_b are the shear modulus and Poisson's ratio of the soil below the pile base, respectively.

The value of k_{b2} can be approximately calculated using the Equation 4.33 proposed by Zhang et al. 2010a.

$$k_{b2} = \frac{\Delta P_t}{\Delta w_t - (\Delta P_t L / E_p A_p)} = \frac{k_t}{1 - (k_t L / E_p A_p)} \tag{4.33}$$

where ΔP_t = the increased load at the pile head when the settlement at the pile base is larger than the limiting pile base settlement of the first stage of the τ_b versus w_b curve; Δw_t = the increased settlement at the pile head induced by ΔP_t; L = the pile length; E_p = the pile elastic modulus; A_p = the cross sectional area of the pile; and k_t = the ratio of the load increment to the settlement increment at the pile head, $k_t = \Delta P_t/\Delta w_t$.

Results of the field tests on seven single piles in different soils (mud, sandy silt and clays) presented by Zhang et al. (2010b and 2011a) are used to validate the reliability of the softening nonlinear transfer curve model relating the interface shear strength to the pile settlement. Similarly, the capacity of the proposed bi-linear model relating the pile base resistance to the pile base settlement is verified by comparing the calculated pile base resistance settlement curve with measured results from experimental studies (Zhang et al. 2010b and 2011b). Since the softening nonlinear transfer curve model Equation 4.29 and bi-linear model Equation 4.31 are efficient, relatively simple. In this study, these two models are extended for analysis of mechanical behaviors of a single pile in expansive soil introducing the necessary modifications extending the principles of unsaturated soil mechanics.

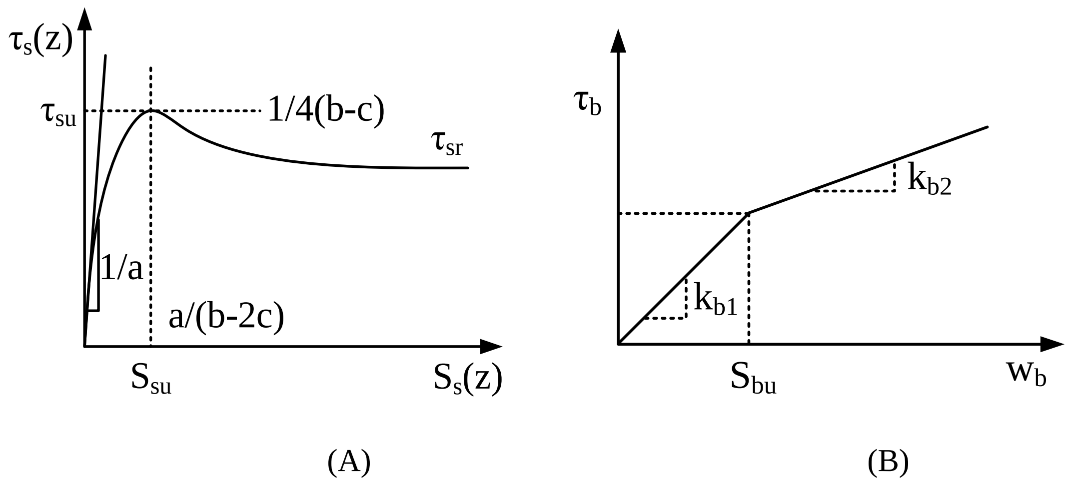

Figure 4.18 (A) Relationship between skin friction and relative shaft displacement at the pile-soil interface; (B) Relationship between base resistance and pile-base settlement (Modified after Zhang and Zhang 2012)

4.2.2 Modification of the model relating the interface shear strength to the pile-soil relative displacement

The softening nonlinear transfer curve model (Equation 4.29) can be extended to characterize the transfer curves in different soil layers with totally different soil properties (Zhang and Zhang 2012). This transfer curve model contains three key parameters; namely the peak interface shear strength (τ_{su}), the residual interface shear strength (τ_{sr}) and the pile soil relative displacement corresponding to the peak interface shear strength (S_{su}). For pile in expansive soil, the transfer curves for the part of pile in the stable zone keep constant during the infiltration process. For the portion of pile embedded in the active zone, both the peak (τ_{su}) and residual interface shear strength (τ_{sr}) can be significantly influenced by the matric suction changes in the infiltration process. As discussed in proceeding sections, the peak interface shear strength (τ_{su}) can be reasonably estimated using Equation 4.22 and 4.23 and the residual interface shear strength can be estimated using Equation 4.24. Detailed discussions are also available for the determination of pile soil relative displacement corresponding to the peak interface shear strength (S_{su}).

4.2.3 Modification of the model relating the pile base resistance and pile base settlement

In most cases, the pile base is located in the stable zone, thus the pile base resistance can be directly calculated using Equation 4.31 proposed by Zhang and Zhang (2012). However, in case that the positive friction (uplift friction) increases significantly in the infiltration process and exceeds the withholding force (pile head load and negative friction), the pile will move upward. In other words, under such a scenario, it is possible for the pile base to detach from the soil so that the pile base movement (ρ_t) can have negative value. Considering this possibility, Equation 4.31 proposed by Zhang and Zhang (2012) is modified as Equation 4.34 for the calculation of the pile base resistance considering the possible detachment of the pile base and soil upon infiltration.

$$\tau_b = \begin{cases} 0 & w_b < 0 \\ k_{b1} w_b & 0 < w_b < S_{bu} \\ k_{b1} S_{bu} + k_{b2}(w_b - S_{bu}) & w_b \geq S_{bu} \end{cases} \tag{4.34}$$

4.2.4 Modification on the traditional load transfer curve method

The load transfer curve method proposed by Coyle and Reese (1966) is widely utilized to predict the load settlement behavior of a single pile subjected to axial load. This method has a relatively simple analytical procedure and can be applied to any complex composition of soil layers with a nonlinear stress-strain relationship for a nonhomogeneous medium or any other variation in the section along a pile (Poulos and Davis 1980). This method is modified following the summarized procedures below in this study to estimate the load displacement response of a single pile in unsaturated expansive soils upon infiltration：

1. The pile as shown in Figure 4.19(A) is divided into a number of segments as illustrated in Figure 4.19(B).

2. Assume a small base movement, ρ_t and calculate corresponding pile base resistance according to Equation 4.34.

3. A pile soil relative displacement, ρ_3, may be assumed at mid-height of the bottom segment as shown in Figure 4.19(B) (for the first trial, it is suggested to use a value of ρ_3 is ρ_t).

4. The matric suction profile keeps changing during the infiltration process [as shown in Figure 4.19(C)]. The different transfer curve models [as shown in Figure 4.19(D)] at different depths for a certain matric suction profile can be estimated using the method proposed in this paper.

5. From the estimated transfer curve model, the interface shear strength corresponding to pile-soil relative displacement ρ_3 can be obtained as τ_3. It should be noted that for the pile soil relative displacement in the active zone, the ground heave should be taken into account. The ground heave within a certain soil layer can be estimated using Equation 3.45 proposed by Adem and Vanapalli (2016).

6. The load Q_3 on the top of segment 3 can then be calculated as

$$Q_3 = P_t + \tau_3 L_3 P_3 \quad (4.35)$$

where L_3 = length of segment 3; P_3 = average perimeter of segment 3.

7. The elastic deformation at the midpoint of the pile segment (assuming a linear variation of load in the segment) is calculated as

$$\Delta'\rho_3 = (\frac{Q_m + P_t}{2})(\frac{L_3}{2A_3E_p}) \quad (4.36)$$

where $Q_m = \frac{Q_3 + P_t}{2}$; A_3 = area of segment 3; E_p = elastic modulus of the pile.

8. The new pile-soil relative displacement at the middle point of the segment 3 is then given as

$$\rho_3' = \rho_t + \Delta\rho_3' \quad (4.37)$$

9. The calculated ρ'_3 is compared with the estimated value of ρ_3 from step (3).

10. If the computed movement ρ'_3 does not agree with ρ_3 within a specified tolerance (in this study, 10^{-11}m is used), step (2) to step (10) are repeated and a new midpoint pile soil relative displacement is calculated.

11. When the tolerant convergence is achieved, the next segment up is considered (for example, from segment 3 to segment 1 in Figure 4.19). This iteration technique is continued until the value of pile head load (Q_1) and pile head displacement (ρ_0) are obtained.

12. Following the laid out procedure detailed through step (1) to step (11), the pile axial force is calculated from the bottom segment to the top segment, for a certain matric suction profile, by assuming a series of pile base movement, the pile head load displacement response can be obtained.

A series of curves reflecting the pile head load displacement response for different matric suction profile can be obtained during the infiltration process. Through these curves, for a certain pile head load (Q_1), the pile head displacement (ρ_0) variations in the infiltration process can be estimated.

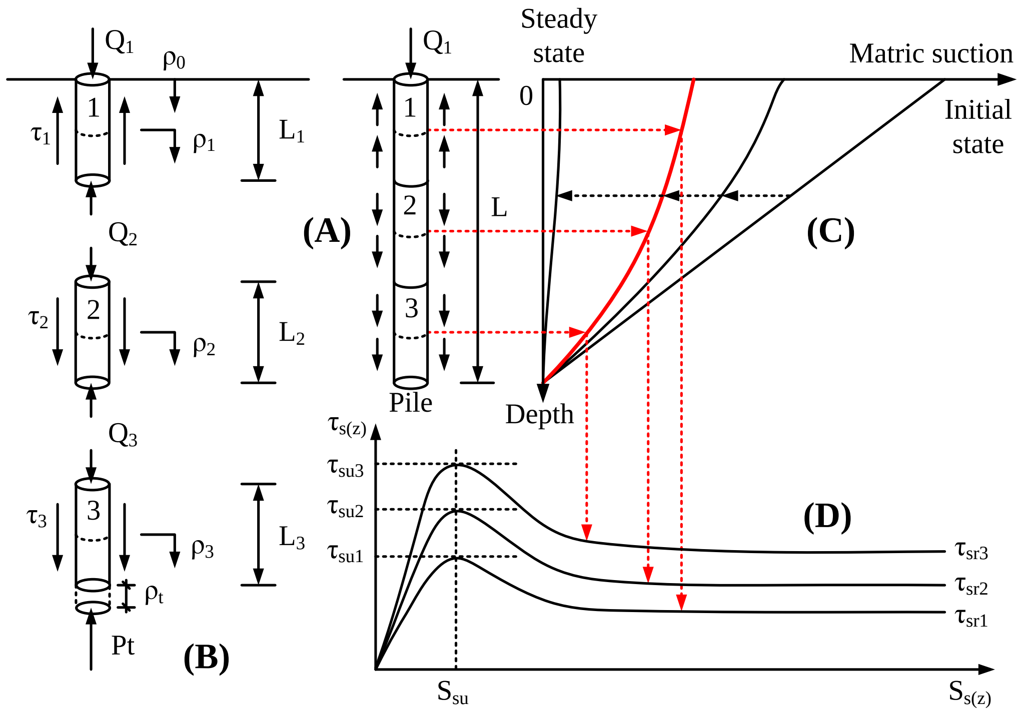

Figure 4.19 Load transfer analysis for pile in expansive soil upon infiltration

4.2.5 Example Problem of the modified load transfer curve method

An example problem is presented in this section to illustrate the proposed method in this study. It is assumed that a single pile is constructed in Regina clay, which is a typical expansive soil from Canada as shown in Figure 4.20. The load displacement response and the mechanical behavior of the pile due to the influence of infiltration are analyzed using the proposed method.

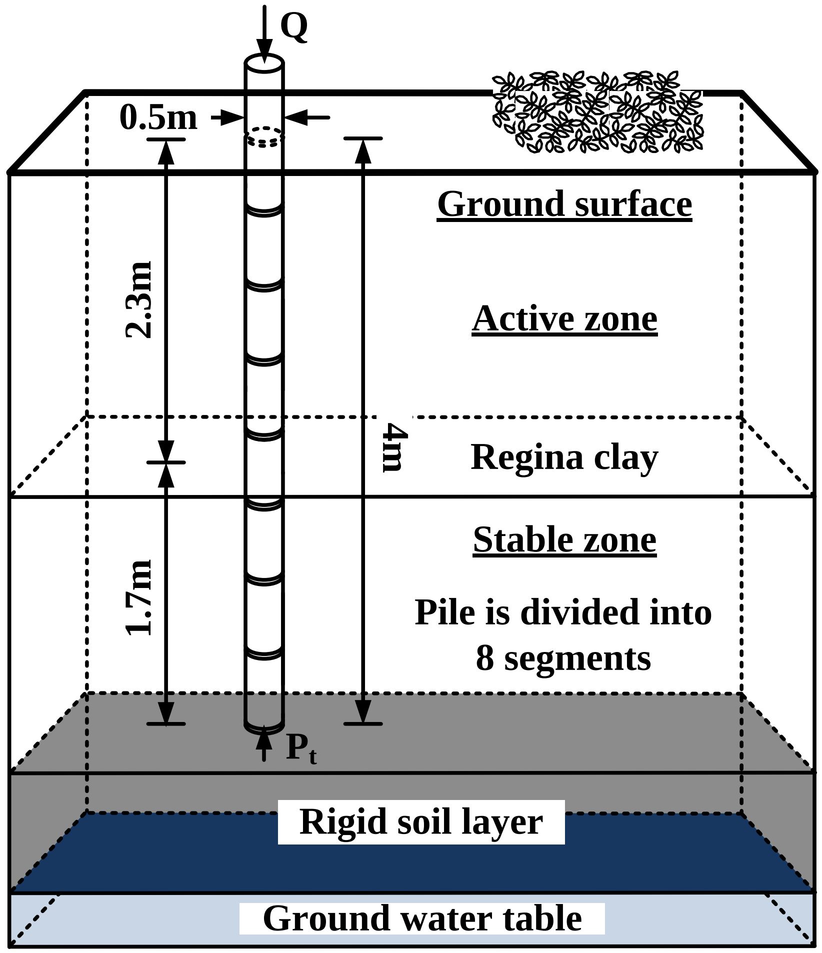

Figure 4.20 Details of single pile used in the example problem along with soil profile

Basic properties of Regina clay are summarized by Vu and Fredlund (2004) for analyzing a case study related to ground heave are presented in Table 4.4. Adem and Vanapalli (2016) also used this case study to validate the ground heave prediction model (Equation 3.45). Figure 4.21 presents the SWCC and the variation of the coefficient of permeability with respect to matric suction (Vu and Fredlund 2004). The shear strength properties are derived from the tests conducted by Chowdhury (2013) on Regina clay. Following assumptions are made regarding the interface shear strength properties: the interface friction angle with respect to net normal stress (δ') and interface cohesion (c_a') is 60% of the internal friction angle of soil with respect to net normal stress (ϕ') and soil cohesion (c') respectively. The assumed shear strength properties are summarized in Table 4.5.

Table 4.4 Basic properties of Regina clay (from Vu and Fredlund 2004)

Liquid limit, LL (%)	77
Plastic limit, PL (%)	33
Plastic index, PI	44
Specific gravity, G	2.82
Unit weight, γ (kN/m^3)	18.8
Initial void ratio, e_0	0.962
Swelling index, C_s	0.09
Saturated coefficient of permeability, k_{sat} (m/s)	7.9×10^{-10}
Saturated volumetric water content, θ_s	0.493
Natural water content	0.29

Table 4.5 Strength parameters of soil and interface

Effective internal friction angle of soil with respect to net normal stress, ϕ' (°)	27.9
Effective interface friction angle with respect to net normal stress, δ' (°)	16.7
Effective soil cohesion, c' (kPa)	16.3
Effective interface cohesion, c_a' (kPa)	9.8

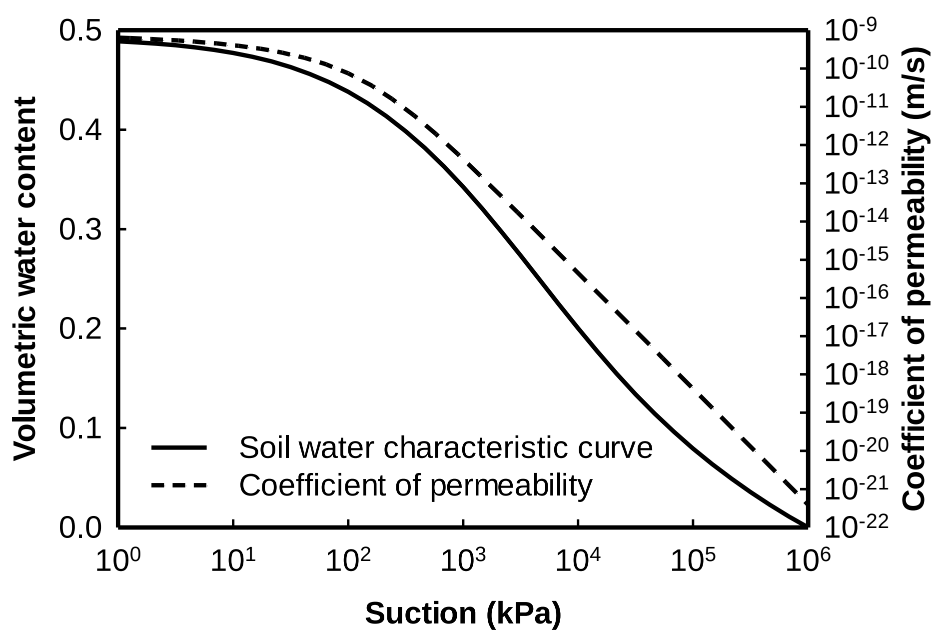

Figure 4.21 Soil water characteristic curve and coefficient of permeability of Regina clay used in the example problem

The pile is divided into eight segments for the calculation of the pile head load displacement response using proposed method. Four of these segments are in the active zone (from 0 to 2m) and the remainder four segments are in the stable zone (from 2 to 4m). The elastic modulus of the pile is set as 5000MPa, the residual interface shear strength (τ_{su}) is set as 83% of the peak interface shear strength (τ_{sr}) based on the past studies (Zhang et al. 2010b, 2011a, 2011b) and the pile soil relative displacement for the fully mobilization of the peak interface shear strength (S_{su}) is set as 0.01m (Zhang and Zhang 2012). The saturated elastic modulus of Regina clay and Poisson's ratio are set as 550kPa and 0.4, respectively (Adem and Vanapalli 2016). It is assumed that the pile base is located in a rigid soil layer whose elastic modulus is 10 times higher than the Regina clay. In this study, in order to simplify the example problem, it is assumed that the pile end settlement is always less than S_{bu}. Upon infiltration, the matric suction variations in the active zone are shown in Figure 4.22 (Vu and Fredlund 2004), while the soil in the stable zone is always in a saturated state.

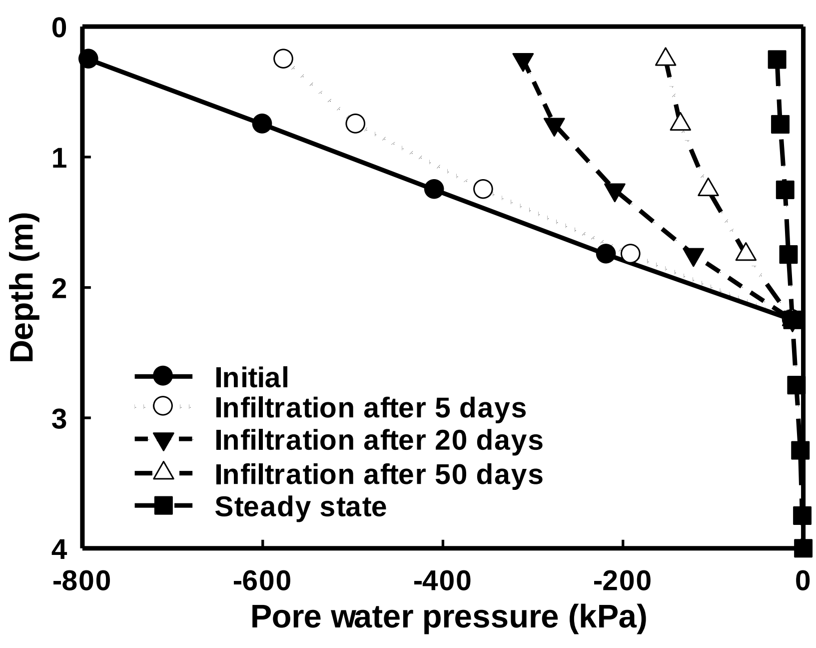

Figure 4.22 Matric suction variations in the active zone (Modified after Vu and Fredlund 2004)

Figure 4.23 shows the variation of the lateral earth pressure considering the mobilization of the lateral swelling pressure and the passive earth pressure which limits the mobilization of the lateral swelling pressure during the infiltration process. In the active zone, the lateral earth pressure keeps increasing during the infiltration process (due to the mobilization of lateral swelling pressure) with matric suction reduction while the passive earth pressure keeps decreasing. As a consequence, after infiltration for 50 days, at shallow depth the mobilization of lateral earth pressure is limited by the passive earth pressure.

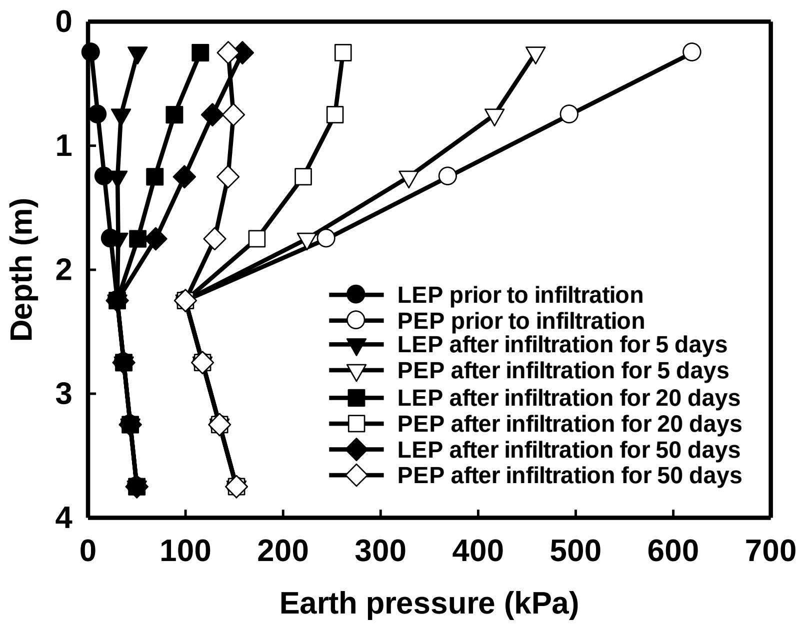

Figure 4.23 Variation of lateral earth pressure and passive earth pressure during the infiltration process (LEP is lateral earth pressure, PEP is passive earth pressure)

Figure 4.24 shows the variations of transfer curve models at different depths in the infiltration process. The pile soil relative displacement corresponding to the peak interface shear strength (S_{su}) is set as 0.01m and the residual interface shear strength is set as a proportion of the peak interface shear strength (i.e. 83%). Therefore, discussion in this section focuses only on the influence of peak interface shear strength on the shape of transfer curve models. Initially, at a certain depth in the active zone, the peak interface shear strength keeps decreasing during the infiltration process. This is because matric suction reduction transfers into normal stress increment, while the peak interface shear strength reduction induced by matric suction reduction outweighs the peak interface shear strength increase due to the normal stress increase in the infiltration process. Secondly, the peak interface shear strength in the active zone always has a value higher than the stable zone. The reason can be attributed to the contribution of matric suction to the peak interface shear strength in the active zone. Also, in the active zone, large matric suction reduction can lead to more significant peak interface shear strength variations. This phenomenon can also be explained as the reduction in the peak interface shear strength caused by matric suction reduction is more significant in comparison to the contribution caused by normal stress increment.

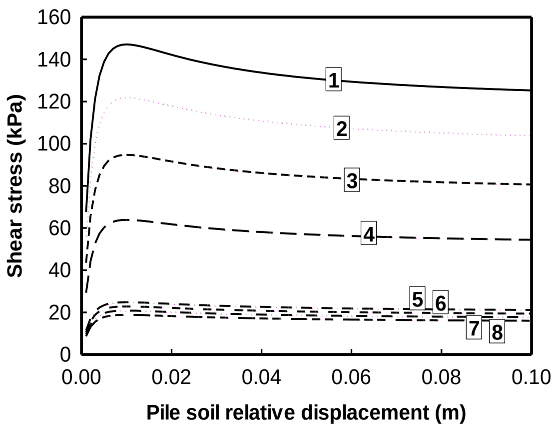

(A)

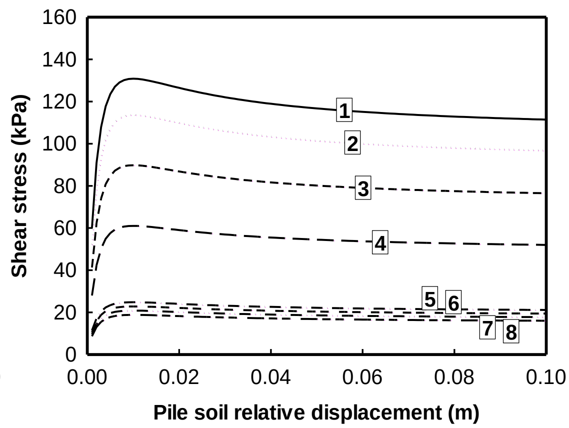

(B)

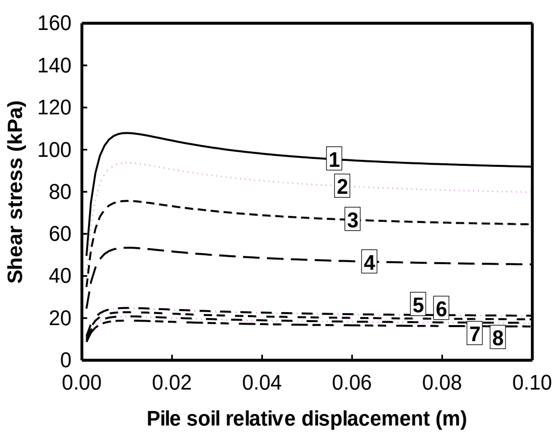

(C)

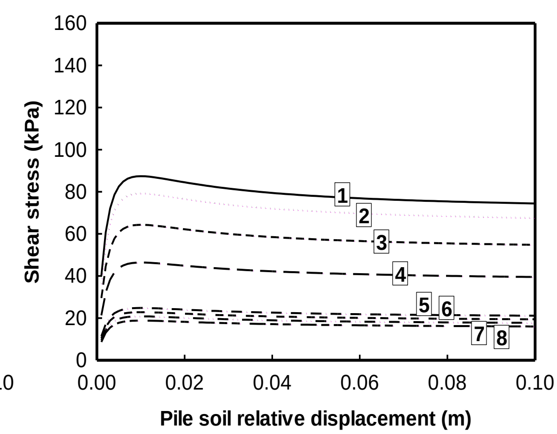

(D)

Figure 4.24 Transfer curve variations in the infiltration process [(1)0.25m; (2)0.75m; (3)1.25m; (4)1.75m; (5)2.25m; (6)2.75m; (7)3.25m; (8)3.75m] [(A) prior to infiltration; (B) after infiltration for 5 days; (C) after infiltration for 20 days; (D) after infiltration for 50 days]

Figure 4.25 shows the pile head load displacement response at different stages during the infiltration process. When the pile head load is low (which corresponds to the lightly loaded structure), the pile typically shows an upward movement upon water infiltration. However, when the pile head load is high (which corresponds to the heavily loaded structure), the pile has a possibility to experience a further settlement instead; which is due to reduction in the bearing capacity of the pile. There are two reasons responsible for this phenomenon. The first reason is associated with the shape variations of the transfer curve models with respect to peak interface shear strength changes due to matric suction variations (as shown in Figure 4.24). The second reason can be attributed to the increment in pile soil relative displacement due to the development of ground heave.

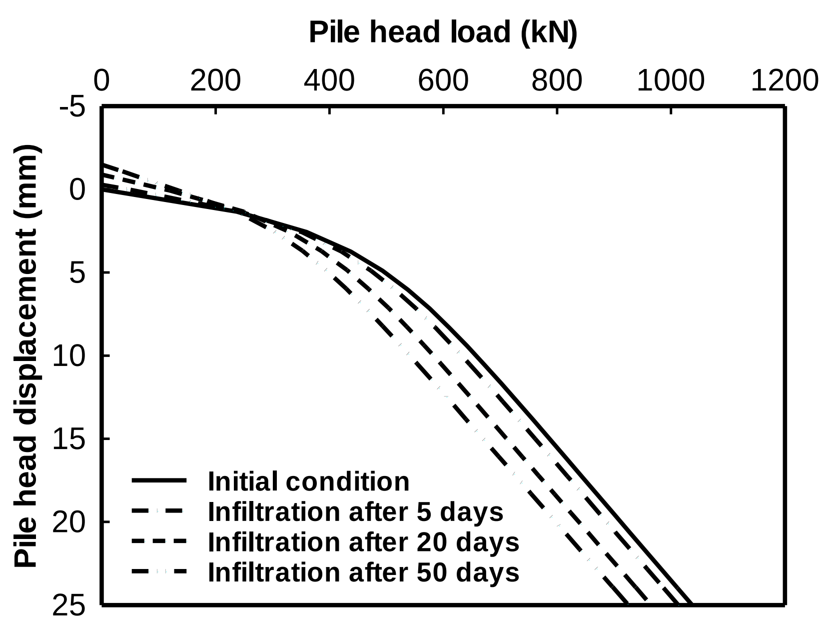

Figure 4.25 Variations of pile head load displacement response in the infiltration process

The mechanical behavior changes of the pile under light and heavy load during the infiltration process are illustrated assuming a load of 100kN and a load of 300kN applied on the pile head, respectively. The variation of pile axial force and pile shaft friction with the infiltration process under a light load of 100kN are shown in Figure 4.26(A) and Figure 4.26(B), respectively. According to Figure 4.25, the pile shows an uplift displacement during the infiltration process; due to this reason, there is no pile base resistance. As shown in Figure 4.26(A), the pile head load is mainly carried by the shaft friction in the active zone in the infiltration process. As shown in Figure 4.26(B), during the infiltration process, the uplift friction in the active zone keeps increasing while negative friction gradually increases in the stable zone. This is mainly because that the ground heave causes an increment in the pile soil relative displacement and contributes to an increase in the interface shear strength from a small value towards the peak value.

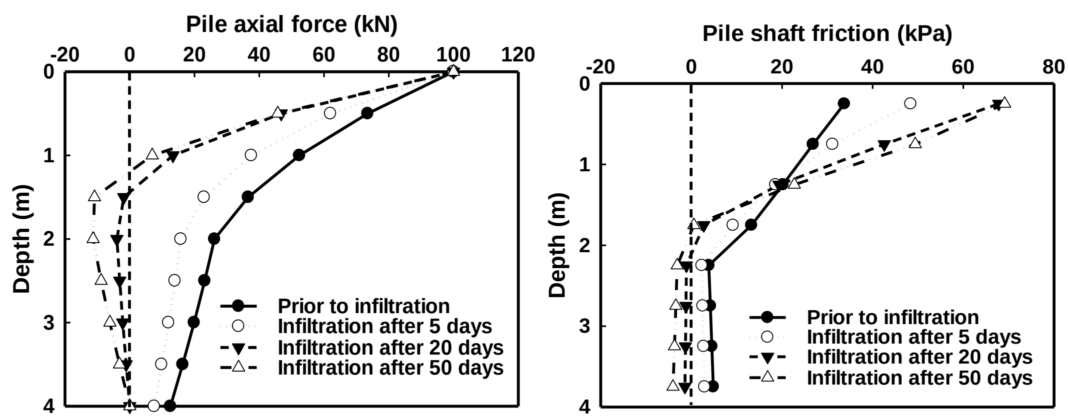

(A) (B)

Figure 4.26 Variations of mechanical behaviors of pile upon infiltration under a pile head load of 100kN (a) Axial force (b) Shaft friction

The variation of pile axial force and pile shaft friction with the infiltration process under a heavy load of 300kN are shown in Figure 4.27(A) and Figure 4.27(B), respectively. According to Figure 4.25, the pile suffers a further settlement during the infiltration process. As shown in Figure 4.27(A), the pile base resistance increases as the pile suffers a further settlement in the infiltration process. From Figure 4.27(B), it can be seen that as the infiltration continues, the shaft friction in the active zone decreases and the shaft friction in the stable zone begins to carry more pile head load. These mechanical behavior changes can be attributed to two reasons. The first reason can be attributed the reduction in peak interface shear strength along with infiltration process as discussed above. The second reason is that for pile under heavy load, initially the pile soil relative displacement is relative high, which means most part of the pile has reached or almost reached the peak shear strength. During the infiltration process, ground heave further increases the pile soil relative displacement, which can cause the interface shear strength decrease from peak to residual value in the active zone.

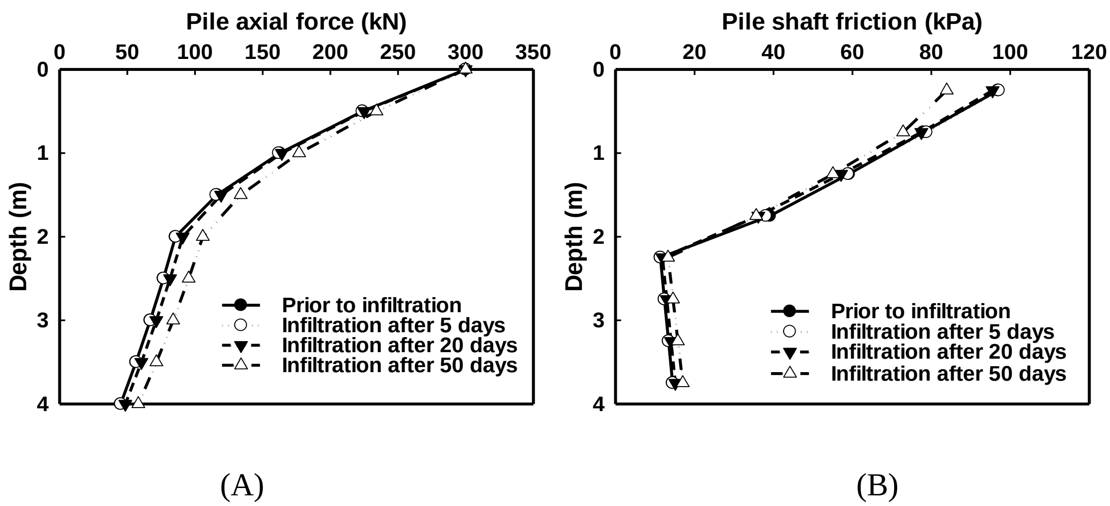

Figure 4.27 Variations of mechanical behaviors of pile upon infiltration under a pile head load of 300kN (A) Axial force (B) Shaft friction

4.2.6 Parametric Analysis

In order to better understand the proposed modified load transfer curve method, a further study is presented regarding the influence of pile soil relative displacement corresponding to the peak shear strength (S_{su}) on the pile head load displacement response. As shown in Figure 4.28, the pile head settlement increases with increasing S_{su} from zero pile head load to the bearing capacity during different stages of infiltration process. This is because when S_{su} is low, the interface shear strength can reach a higher value even for small pile-soil relative displacement. After the interface shear strength has reached the peak value, the interface shear strength decreases with increasing pile soil relative displacement. Due to this reason, the S_{su} has a minor influence on the pile head load displacement response curve after reaching the maximum bearing capacity of the pile. Similar conclusion was derived by Zhang and Zhang (2012) in the parametric analysis with respect to the influence of S_{su} on the pile head load displacement response.

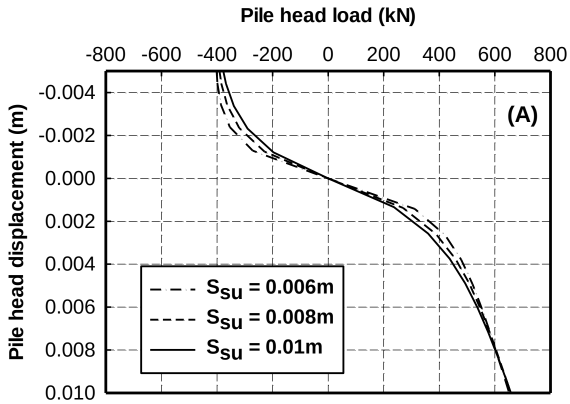

(A)

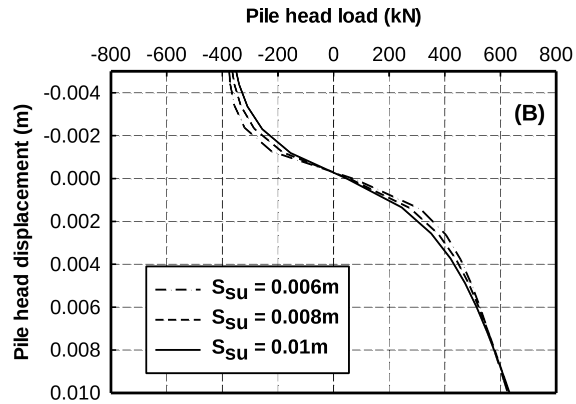

(B)

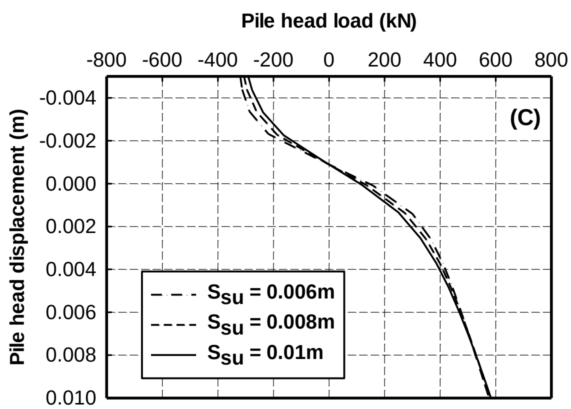

(C)

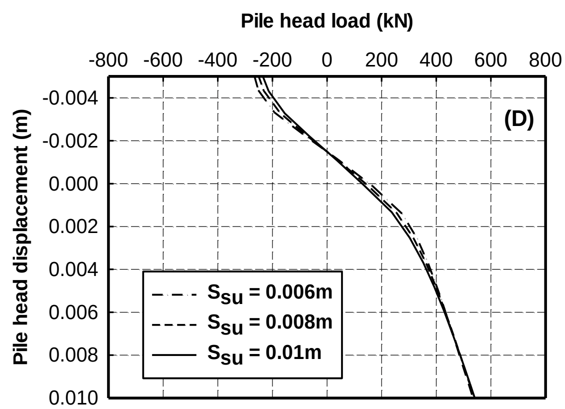

(D)

Figure 4.28 Influence of S_{su} on the load displacement response of a single pile [(A): Prior to infiltration; (B): after infiltration for 5 days; (B): after infiltration for 20 days; (D): after infiltration for 50 days)]

4.2.7 Validity of the Proposed Modified Load Transfer Curve Method

4.2.7.1 Model pile test presented by Fan (2007)

For the same case study illustrated in section 4.1.2.1, employing the proposed modified load transfer curve method, the pile head upward movement is estimated to be 4.2mm, which is in good agreement with the model test of 3.59mm and the numerical simulation of 5.71mm. Reasonably good comparisons can also be observed among the pile shaft friction distribution and pile axial stress distribution curves obtained from the experiment results, numerical simulations performed by Fan (2007) and the calculation using the proposed load transfer curve method (see Figure 4.29 and Figure 4.30, respectively). From the results summarized above, it can be seen the proposed program well simulates the uplift movement of the pile and the generation of the uplift friction along the upper part of the pile in the active zone. The main advantage of proposed modified load transfer curve method in the present study compared to Fan (2007) is related to its simplicity and ability to compute the interface shear strength for different matric suction profile using the SWCC and saturated interface shear strength properties. This approach alleviates the need for conducting cumbersome interface shear tests on soil samples with different matric suction values under several normal stress values. In addition, the input parameters required for using modified load transfer curve method can be obtained from conventional tests in comparison to implementing Fan (2007) finite element program. Finally, the proposed approach provides relatively better comparisons with the measured results.

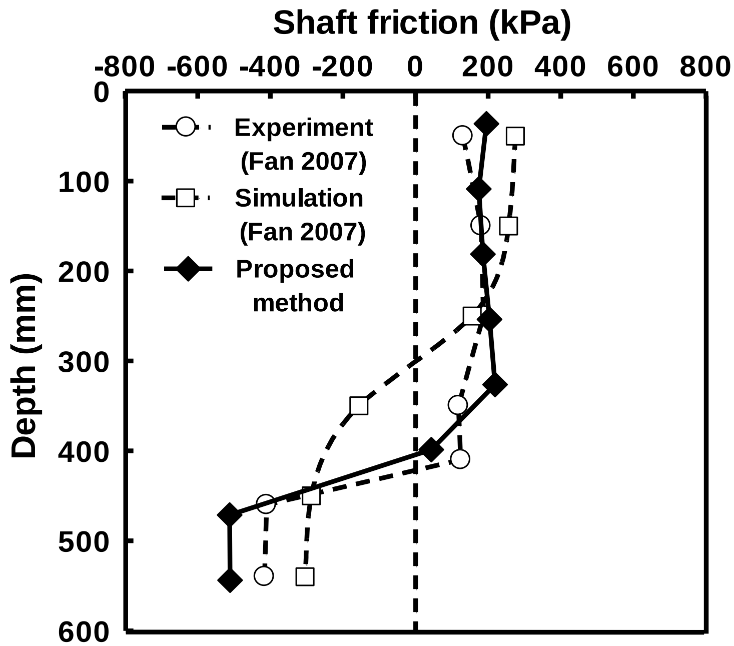

Figure 4.29 Comparison of the pile shaft friction distribution in model pile by Fan (2007)

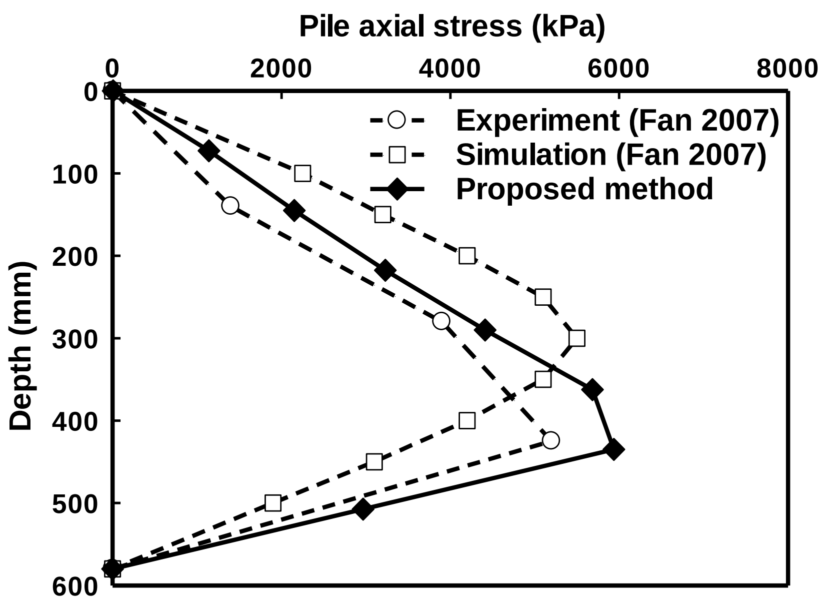

Figure 4.30 Comparison of the pile axial stress in model pile by Fan (2007)

4.2.7.2 Field investigation case study presented by Benvenga (2005)

As for the field case study presented by Benvenga (2005), in order to use the modified load transfer curve method, β_s and S_u are set as 0.85 and 0.01m, respectively. They are both in the suggested range as per Zhang and Zhang (2012). The pile uplift displacement in October 1997 and September 2003 are estimated to be 9.5mm and 8mm, utilizing the proposed load transfer curve method, which are comparable to the measured value of 9mm and 3mm. The estimated pile axial force distribution is shown in Figure 4.31. From Figure 4.31, the whole pile is under tension. The estimated axial force distribution agrees well with the experimental data and the predictions using the finite element method developed by Nelson et al. (2011), which provides validation of the modified load transfer curve method proposed in this study. In October 1997, comparison is also made with the numerical simulation presented by Nelson et al. (2011). The finite element program developed by Nelson et al. (2011) is robust and versatile. However, to use this program, several parameters for different layers in the entire soil profile are required. These parameters include elastic modulus (E), Poisson's ratio (υ), peak and residual angle of internal friction (ϕ_p and ϕ_r), cohesion (c), coefficient of lateral stress (K_o), effective overburden stress (σ'_{vo}), and coefficient of friction between the pile and the soil (α). Nelson et al. (2011) presented a detailed discussion regarding the influence of water content on the determination of above factors. Compared with program by Nelson et al. (2011), the proposed modified load transfer curve method directly computes elastic modulus of unsaturated expansive soil, mobilization of lateral swelling pressure, development of ground heave and mobilization of interface shear strength within the program. The required information includes only the matric suction profile, SWCC and limited number of soil properties (saturated elastic modulus, saturated interface shear strength properties, Poisson's ratio, plasticity index and maximum dry density of expansive soil). The proposed approach is simple and can facilitate practicing engineers to make quick and reasonable estimations of the load displacement response of a single pile in expansive soils upon water infiltration.

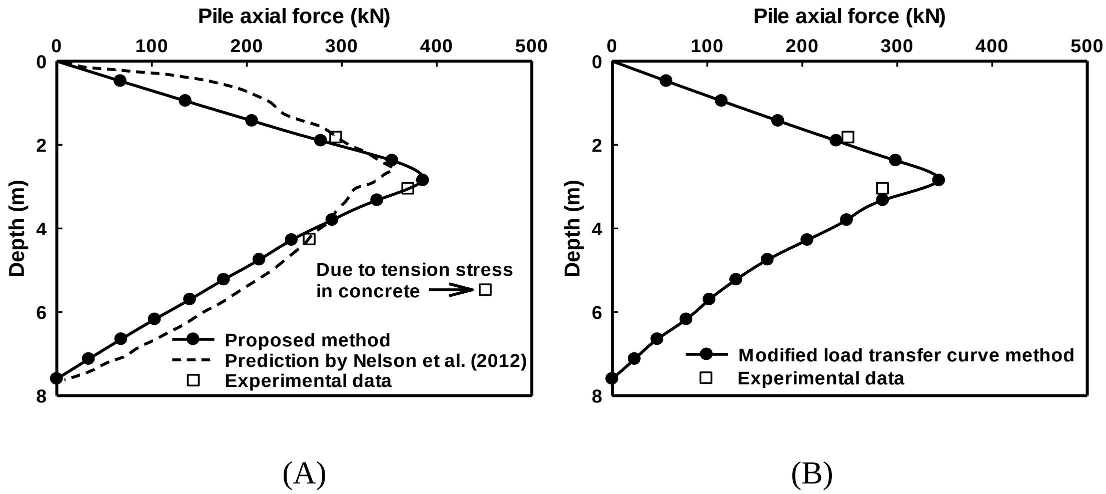

Figure 4.31 Comparison of pile axial force distribution (A) October 1997; (B) September 2003

4.3 Summary and conclusions

For piles constructed in expansive soil area, upon infiltration, the mechanical behaviors of pile can experience significant changes. In this Chapter, two theoretical methods are proposed for the load transfer analysis of a single pile in expansive soil upon infiltration. The first one is a modified shear displacement method proposed for the estimation of the pile head load-settlement response in expansive soil. The second one modifies the load transfer curve model proposed by Zhang and Zhang (2012) considering influencing factors including ground heave, mobilization of lateral swelling pressure and changes in interface shear strength parameters. Further, the traditional load transfer curve method proposed by Poulos and Davis (1980) is modified for the prediction of the pile head load-settlement relationship with respect to matric suction variations. The outstanding advantage of the modified shear displacement method is that calculations using this method can be completed in a high speed since no iterations was including in the calculations. While the inclusion of the softening model describing the development of the pile-soil interface shear stress with pile-soil relative displacement enables the load transfer curve method to give a better prediction.

For the second method, an example problem is given assuming a single pile constructed in Regina clay, upon water infiltration, the influences of matric suction variations on the pile head load-settlement relationship variations and the mechanical behaviors of the pile are analyzed in detail. Matric suction variation can pose significant influences on the mechanical behaviors of the pile in expansive soils. Upon water infiltration, light structures may suffer ground heave problem. However, for structure under great load, ground heave may lead to a shaft friction reduction which cause more serious settlement problem. There are two reasons responsible for this behavior. The first reason can be attributed to the changes in the interface shear strength regarding the mobilization of the lateral swelling pressure and the reduction of the interface shear strength properties. The second one is that ground heaves lead to an increment of the pile soil relative displacement, which causes an interface shear strength decrease from peak value to residual value. Parametric analysis was conducted regarding the influence of pile-soil relative displacement corresponding to the peak interface shear strength (S_{su}) is conducted. The results indicated that S_{su} is not a key factor to be considered in the presented softening load transfer curve model.

Both the modified shear displacement method and the modified load transfer curve method were verified using the experimental results from Fan (2007) and Benvenga (2005). Good comparisons were observed between the predictions using proposed method and the experimental data. The modified shear displacement and load transfer curve method proposed in this study is valuable for practicing engineers to make a quick and reasonable estimation on the mechanical behavior variations of piles in expansive soils upon infiltration.

CHAPTER FIVE

EXPERIMENTAL STUDY ON A SINGLE MODEL PILE IN EXPANSIVE SOIL UPON INFILTRATION

Notation

Symbols	
A_p	Pile base area
l_i	Layer thickness of the soil layer i
Q_{uk}	Ultimate single pile bearing capacity
Q_{us}	Ultimate pile shaft resistance
Q_{pk}	Ultimate pile base resistance
q_{sik}	Standard pile shaft friction within soil layer i
q_{pk}	Standard pile base stress
u_{peri}	Perimeter of the model pile

Mechanical behavior of piles in expansive soil are significantly influenced by suction variations. However, till now few tests on pile in expansive soils are available in literature with suction measurement. Such a phenomenon can be attributed to two main reasons: initially due emphasis was not issued to the impact of suction on the mechanical behaviors of piles in expansive soils. Also, due to technical limitations, relevant suction measurement apparatus might be not available in previous experimental studies. In order to illustrate the influence of suction and suction variations on the mechanical behaviors of piles in expansive soils in a more clear and practical way, a large scale model pile test was conducted in the geotechnical engineering lab in the University of Ottawa. The whole test can be divided into three parts; namely, index properties test, soil and interface shear strength test and pile infiltration test.

5.1 Soil properties of Regina clay

Various soil properties required for interpreting the pile infiltration test were measured through laboratory tests.

5.1.1 Physical soil properties tests

The expansive soil used in this test was collected from a construction site in Regina, Saskatchewan, Canada. The soil was air-dried for more than two weeks in a lab environment and was then pulverized using a grinding mill. The soil that passed thru No. 10 sieve (< 2mm) was used for measuring the basic soil properties tests. The hygroscopic water content of the soil was 2.5%.

The X-ray fluorescence (XRF) tests and X-ray diffraction (XRD) tests were performed to determine the chemical and mineralogical composition of the Regina clay. Figure 5.1 shows the measured XRD results of Regina clay. Table 5.1 summarizes the major oxides and the minerals present in Regina clay. The presence of the highly hydrophilic Montmorillonite ($(Na,Ca)_{0.33}(Al,Mg)_2(Si_4O_{10})(OH)_2 \cdot nH_2O$) in the clay has a predominant influence in the mobilization of swelling pressure.

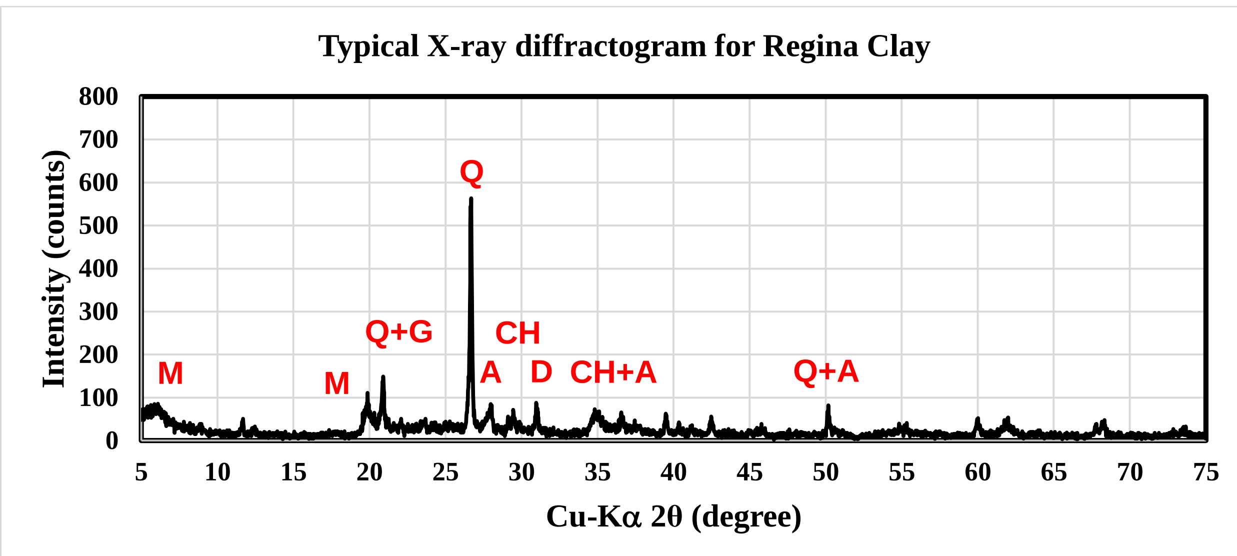

Figure 5.1 XRD test results for Regina clay

Table 5.1 Chemical and mineralogical composition of Regina clay

Chemical composition	Na_2O	MgO	Al_2O_3	SiO_2	P_2O_5	K_2O	CaO	TiO_2	MnO	Fe_2O_3
Mass%	0.872	3.015	14.658	54.059	0.078	2.219	4.153	0.611	0.1	5.713
Mineralogical composition	Quartz(SiO_2); Montmorillonite-15A($Na_{0.3}(Al,Mg)_2(Si_4O_{10})(OH)_2\cdot 4H_2O$); Dolomite($CaMg(CO_3)_2$); Albite (low)($NaAlSi_3O_8$); Calcium iron catena-silicate, Hedenbergite high($CaFeSi_2O_6$); Gypsum($CaSO_4\cdot 2H_2O$).									

The soil gradation curve of the Regina clay performed following ASTM D422- 63 (drying method) is summarized in Figure 5.2. Table 5.2 summarizes the other soil properties of Regina clay determined following different ASTM standards. The tested clay is a highly expansive soil because of its high plasticity index, vertical swelling pressure and free swell index values. The vertical swelling pressure was determined using soil that was compacted at a gravimetric water content of 27% and a dry density of 1367 kg/m^3 from the compaction curve. The chosen water content corresponds to dry side of the optimum moisture content, which is 29%, in order to achieve a greater swelling pressure. The SWCC measurement and the pile infiltration test were also conducted at the same dry density and the initial water content to achieve “identical” conditions with respect to the soil structure.

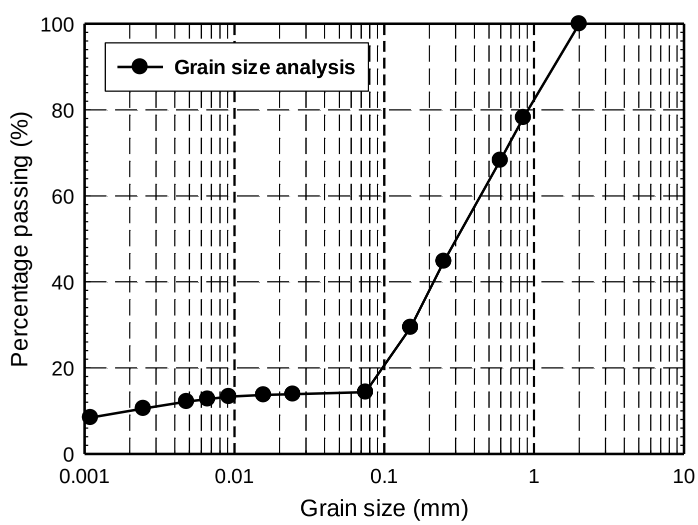

Figure 5.2 Soil gradation curve for Regina clay

Table 5.2 Various properties of Regina clay

Atterberg limits test (ASTM D4318-10$^{\varepsilon1}$)	Liquid limit, LL (%)	89
	Plastic limit, PL (%)	32
	Plastic index, PI	57
Specific gravity test (ASTM D854-14)	Specific gravity, *G*	2.85
Compaction curve (ASTM, 12400 ft-lbf/ft^3 (600 kN-m/m^3) (ASTM D698-12$^{\varepsilon2}$)	Maximum dry unit weight, $\gamma_{d,max}$ (kN/m^3)	13.82
	Optimum water content, w (%)	29
Constant volume swelling pressure test (ASTM, D4546)	Vertical swelling pressure under constant volume condition (from gravimetric water content of 27% to fully saturation), (kPa)	136
Free swell index (IS 2720)	Free swell index=[(V_d -V_k) / V_k] ×100% where V_d =volume of soil specimen read from the graduated cylinder containing distilled water; V_k =volume of soil specimen read from the graduated cylinder containing kerosene.	100.6

5.1.2 Measurement of SWCC incorporating image technique

Four methods were combined employed for the measurement of the entire SWCC (i.e., in the suction range of 0 to 10^6 kPa) namely, chilled mirror hygrometer (WP4) method (ASTM 6836-16), pressure plate method (ASTM 6836-16), filter paper method (ASTM D5298-10) and desiccator method. Image technique was applied on three testing methods (i.e. pressure plate, filter paper and desiccator methods) to monitor the volume changes of test specimen while simultaneously measuring the SWCC.

The WP4 apparatus measures water potential (total suction) by determining the relative humidity of the air above a test specimen in a closed chamber (ASTM 6836-16). For WP4 tests conducted on Regina clay, soils were mixed with distilled water to prepare a series of powder-state specimens of different initial water contents. The prepared soil specimens were stored in a humidity-controlled chamber for a period of 24 hours to achieve equilibrium conditions with respect to different water content. These soil specimens were then placed in the chamber of WP4 for total suction measurement.

Image technique was used to monitor the test specimen’s volume changes during the measurement of SWCC in the pressure plate, filter paper and desiccator methods. The volume was estimated following a three-step-procedure, which is described below.

The first step involves taking photographs of the soil specimen and using the "Autodesk 123D Catch" software to construct the 3D model. Figure 5.3(A) shows photographs that were continuously taken along the cycle type tracks at two fixed elevations. The "Autodesk 123D Catch" software creates the 3D scene by automatically finding and matching the common features from different photographs. This is achieved by gathering high quality photographs, using the “matching process” feature to construct a high quality 3D model. One of key requirements is that all the features of the soil specimen should be visible in more than three photographs from different angles in order to construct the 3D model. A 20^{o} interval is used to cover all the features on the top surface of the test specimen at each elevation; in other words, for each elevation, at least 18 photographs should be taken. In addition, in order to obtain high quality 3D models, it is suggested that all the photographs should be shot at the same brightness. The image technique employed in present study has two distinct advantages. The first advantage is that the refraction correction is not required if all the photographs are directly shot at the same brightness on the test specimen. Secondly, the completely different textures from point to point from different photos [as shown in Figure 5.3(A)] facilitate the software to capture the features and construct a reliable 3D model.

The second step is to define the reference distance. A fixed size label that was placed on the top of the soil sample facilitated to define the reference distance on the digital 3D model [as shown in Figure 5.3(B)].

The third step is to repair the model and read the volume. It is important to note that no photographs of the bottom of the test specimen were collected. In other words, the data collected of the 3D model is more like the shape of a bottle cap [Figure 5.3(C) and (D)]. Due to this reason, a hole appears at the bottom of the 3D model of the test specimen. The "Autodesk netfabb studio" software is only capable of measuring the volume of the closed 3D models. To alleviate this limitation, the meshes should be repaired or corrected to seal the open bottom [Figure 5.3(E)]. The employed software "Autodesk netfabb studio", has this correction function. A series of tests conducted on prefabricated black plastic cylinders of two different dimensions (one is 30mm in diameter and 20mm in height and another one is 50mm in diameter and 20mm in height) suggest that the error associated with the volume measurement using image technique is less than 1%.

In pressure plate and desiccator methods, saturated soil specimens with a diameter of 50mm and a thickness of 20mm were prepared in oedometer. The preparation technique of soil specimen is consistent with procedure followed in the constant volume swelling pressure test (ASTM, D4546). Filter paper method was employed following ASTM D5298-10. A series of soil specimens of the same dry density (13.67g/cm^3) but different water content (namely, 24%, 27% and 30%) were prepared and used for both matric suction and total suction measurement.

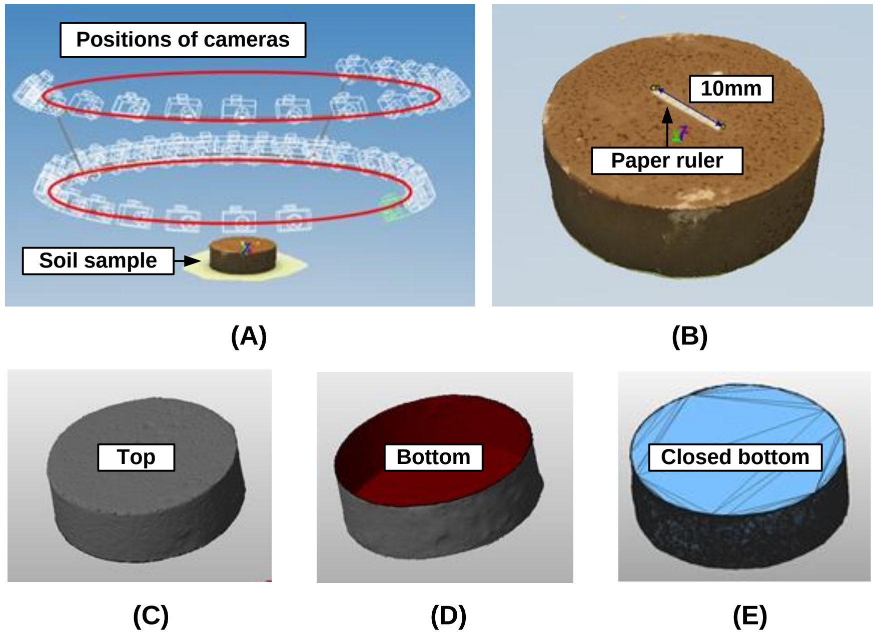

Figure 5.3 Soil sample volume measurement using image technique

The pressure plate method was conducted for measuring the SWCC following ASTM D6836-16. As shown in Figure 5.4(A), each time mass measurements of the test specimen were read, image technique was used to monitor the volume changes of soil samples. For the desiccator method, different salt solutions (as summarized in Table 5.3) were used to fill the base of the desiccators. The vapor evaporated from the salt solution gradually changes the water content within the test specimen. At equilibrium condition, the test specimen would have a relative humidity (i.e. equivalent total suction) which is the same as the vapor evaporated from the salt solution. The volume of the saturated soil specimens were measured using the image technique before the test. The specimens after measuring their initial volumes were put into the desiccator for relative humidity equalization [as shown in Figure 5.4(B)]. A period of 6 months was required for achieving equilibrium conditions, which was ascertained by constant mass of the test specimen in the desiccator. After reaching equilibrium, image technique was extended again to calculate the volume of the test specimen. For the filter paper method, volume measurement was conducted immediately after the soil specimens of different wet densities were prepared. The soil specimen’s volume was also measured after they have been totally oven-dried.

Table 5.3 Saturated salt solutions and corresponding relative humidity and suction

Salt	RH (%)	Equivalent total suction (MPa)
Lithium Chioride ($LiCl{\cdot}H_2O$)	11.3	297.6
Magnesium Chloride ($MgCl2{\cdot}6H_2O$)	32.9	151.7
Magnesium Nitrate ($Mg(NO_3)_2{\cdot}6H_2O$)	53.4	85.6
Sodium Chloride (NaCl)	75.7	38
Potassium Sulphate (K_2SO_4)	96.8	4.4
Copper Sulphate ($CuSO_4$)	98.6	1.9

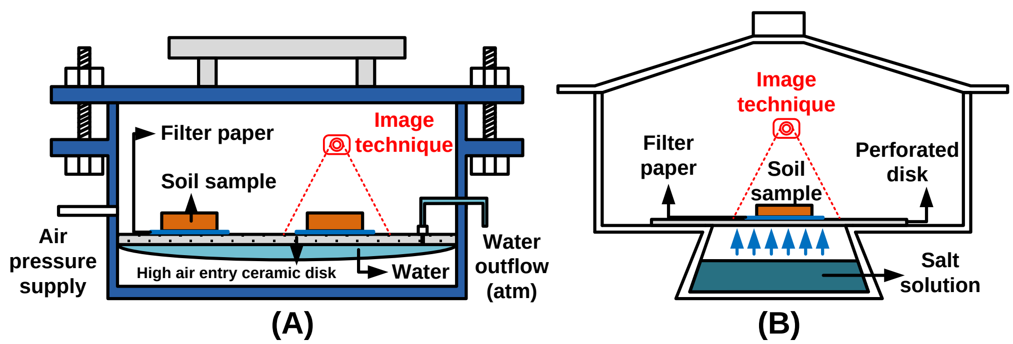

Figure 5.4 Applications of image technique for the volume measurement in different methods

The variation of gravimetric water content with respect to soil suction is presented in Figure 5.5(A) from a series of test results. The variation of void ratio with respect to the gravimetric water content taking account of volume changes extending image technique is shown in Figure 5.5(B). The SWCC data in Figure 5.5(A) and (B) is presented in Figure 5.5(C) and (D), respectively as variation of volumetric water content and degree of saturation with respect to soil suction. The SWCC shown in Figure 5.5(C) and (D) were fit using the Fredlund and Xing (1994) equation. The test results suggest that in high suction range (usually higher than 1500kPa), for the same water content, the difference between the matric suction and total suction is negligible. These results are consistent with the conclusions presented by Fredlund and Xing (1994).

It is important to understand the differences in the water retention behavior of in-situ soil and in the soil specimen tested in the laboratory. The in-situ soil element near the ground surface and at greater depth experience significantly different volume changes during the soaking process under different vertical stress boundary conditions. For this reason, SWCC measured from in-situ soil samples collected from different depths can be different. However, in the present study, only the SWCC under zero stress boundary condition was measured and used in the analysis of the model PIT. This is reasonable since in the PIT, the thickness of the expansive soil layer around the model pile is only 0.4m; due to this reason, the influence of vertical stress on the soil volume change can be assumed negligible. This assumption was also extended because of the difficulties associated with the volume measurements of the SWCC of soil specimens under a surcharge in the laboratory environment.

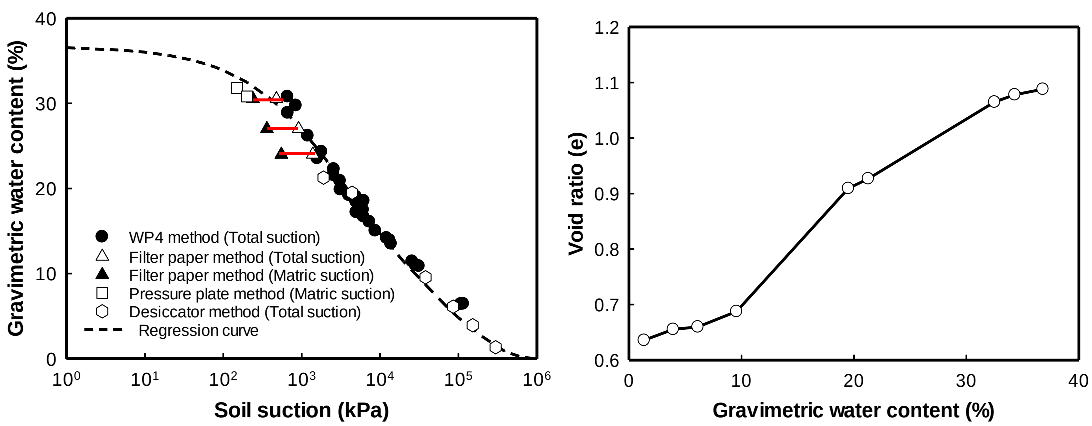

(A) (B)

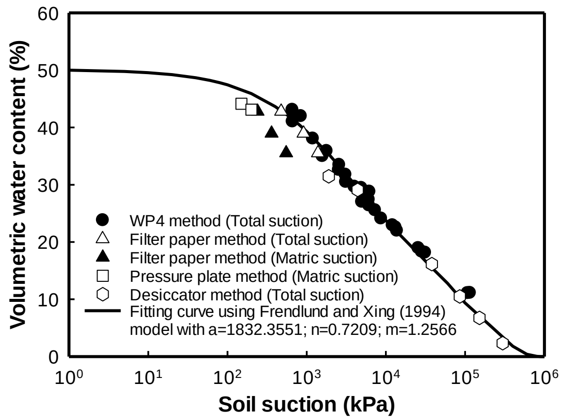

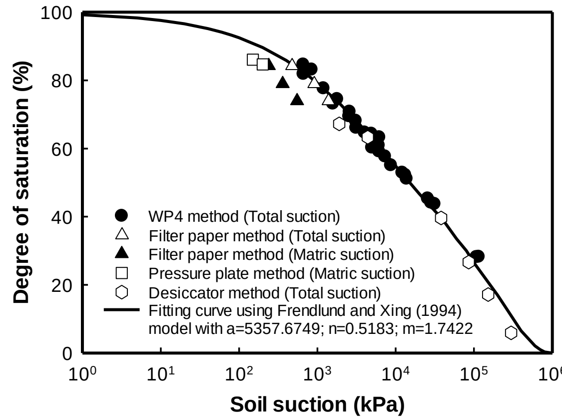

(C) (D)

Figure 5.5 SWCC of Regina clay measured over the entire suction range using multiple methods

Furthermore, the SWCC behavior is essentially hysteretic; due to this reason, for a certain suction value, the water content associated with wetting path is less than that for a drying path (Pham et al. 2005). Klausner (1991) summarized four key factors that are responsible for the hysteresis nature of SWCCs. These factors include: (i) the irregularities in the cross-sections of the voids passages; (ii) the contact angle being greater in an advancing meniscus than in a receding meniscus; (iii) the differences in the entrapped air volume between the suction increasing and decreasing processes; and, (iv) aging effects associated with the prolonged wetting and drying history of the soil. Several laboratory and field methods are available for measuring the SWCC following the wetting or the drying path. For example, column infiltration/drainage methods can be used for measuring the wetting path of the SWCC. The axis translation method is widely used for measuring the SWCC following the drying-path. The SWCC following the drying path is commonly used in practice since they are less demanding in terms of complexity and time (Lu and Likos 2004; Fredlund et al. 2012 and Likos et al. 2013). Besides direct measurements, there are several models developed and presented by various scholars in last half a century for predicting the SWCC (for example, Mualem 1977; Hogarth et al. 1988; Pham et al. 2003; Huang et al. 2005; Mady and Shein 2018). However, most models for predicting wetting SWCC from drying curve require information of several points in the wetting curve (Pham et al. 2005). The measurement of a complete set of hysteretic SWCCs is extremely time-consuming and costly. In addition, it is difficult to represent these curves in a simple mathematical form for use in routine engineering practice (Fredlund 2018). For these reasons, the SWCCs are assumed non-hysteretic in nature for simplicity purposes (Pham et al. 2005).

5.2 Direct shear tests on soil and pile-soil interface

A series of direct shear tests on compacted unsaturated soil specimens and unsaturated pile-soil interface were conducted using a direct shear apparatus to study the soil and pile-soil interface shear strength properties. The shear strength behavior was measured on compacted soil specimens prepared at the same dry density but with different "initial" water content values of 24%, 27% and 30%. Table 5.4 summarizes the stress conditions and shearing rates used for performing different soil and interface shear tests.

Table 5.4 Applied normal stress and gravimetric water content of soil samples in the shear tests

Gravimetric water content	Unsaturated soil samples			Saturated soil samples
	24%	27%	30%	(consolidation and saturation last for 30 days)
Dry density (g/cm^3)	1.37	1.37	1.37	1.37
Normal stress (kPa)	50	50	50	50
	100	100	100	100
	150	150	150	150
Shearing rate (mm/min)	1	1	1	0.005

The area of the shear chamber in the direct shear test box is 60mm × 60mm. Direct shear tests were conducted on saturated soil specimens following ASTM D3080/D3080M-11 under consolidated drained condition. The setting of the shear chamber for direct shear test on saturated soil and unsaturated soil specimens are shown in Figure 5.6(B) and (C), respectively. For unsaturated soil shear test, during the shearing process all the openings or gaps in the shear chamber were covered using wet cotton to alleviate moisture losses associated with water evaporation.

For the interface shear test, a prefabricated aluminum block with a rough counterface [as shown in Figure 5.6(A)] was placed at the bottom of the direct shear chamber. The rough surface was achieved by pasting a thin layer of epoxy on the steel surface and then pouring sand (the average size of the sand particle is 1mm). This technique was useful in achieving a thin sand layer surface with a uniform roughness. Prior to subjecting the specimen to shearing, the holding screws that facilitate holding upper and bottom shearing chamber were gently separated to form a gap of around 1mm [as shown in Figure 5.6(D) and (E)]. The gap facilitates the shearing process to proceed along the soil-rough counterface of the aluminum block. In other words, the teeth of the rough counterface would not be blocked by the upper part of the direct shear chamber during the shearing process.

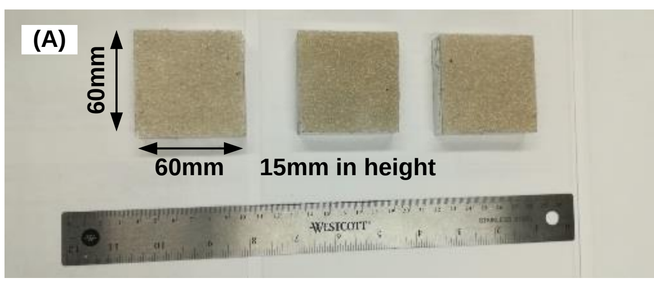

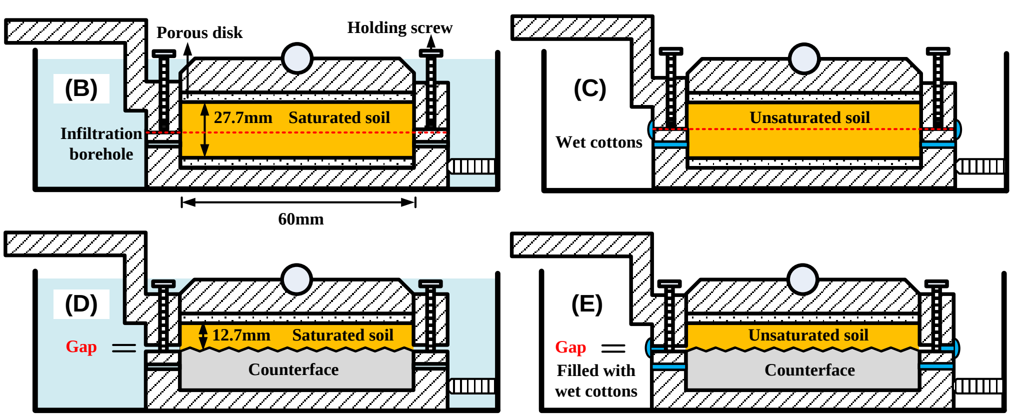

Figure 5.6 Settings of soil and interface shear tests (A) Steel block with rough surface; (B) Shear chamber for saturated soil shear test; (C) Shear chamber for unsaturated soil shear test; (D) Shear chamber for saturated interface shear test; (E) Shear chamber for unsaturated interface shear test

Figure 5.7 summarizes the contributions of net normal stress and matric suction to the soil and interface shear strength under both saturated and unsaturated conditions. Both the peak shear strength of saturated soil and saturated interface can be described by Mohr-Coulomb failure criteria, which are given as Equation 5.1 and 5.2, respectively. For soil and interface shear tests conducted under unsaturated conditions [as shown in Figure 5.7(B) and (D)], the peak strength envelope was approximately linear with both net normal stress and matric suction. Equation 3.34 proposed by Fredlund et al. (1978) expressed in terms of net normal stress and matric suction is commonly used to model the peak shear strength of unsaturated soil (e.g., Escario and Saez 1986; Gan and Fredlund 1988; Oloo and Fredlund 1996; Vanapalli et al. 1996). Hamid and Miller (2009) suggested that the shear strength of the soil-structure interface can be interpreted using Equation 3.36 which is similar to Equation 3.34.

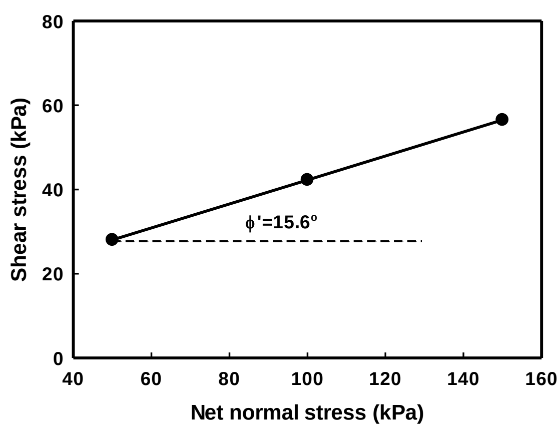

(A)

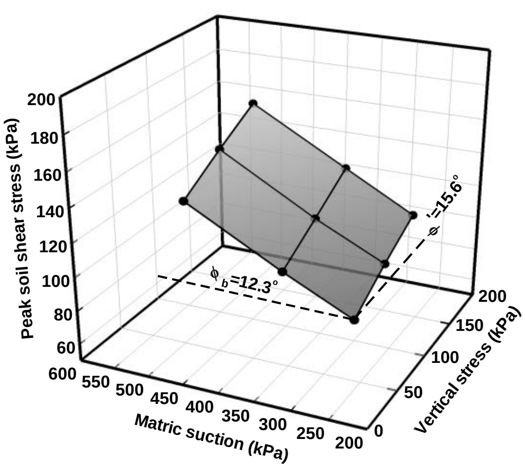

(B)

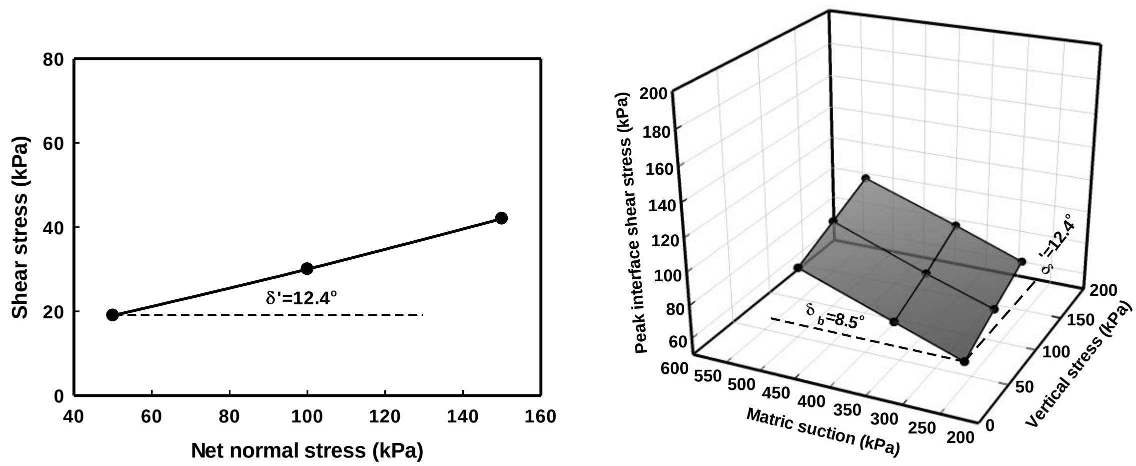

(C) (D)

Figure 5.7 Direct shear test results of (A) Saturated soil; (B) Unsaturated soil; (C) Saturated interface; (D) Unsaturated interface.

$$\tau_{ss} = c' + (\sigma_{nf} - u_{af})\tan\phi' \tag{5.1}$$

$$\tau_{si} = c'_a + (\sigma_{nf} - u_{af})\tan\delta' \tag{5.2}$$

The soil and interface shear strength parameters determined from the above tests conducted using a direct shear apparatus are summarized in Table 5.5.

Table 5.5 Summary of soil and interface shear strength parameters of Regina clay

Effective internal friction angle with respect to net normal stress (ϕ')	15.6°
Effective internal friction angle with respect to matric suction (ϕ_b)	12.3°
Effective interface friction angle with respect to net normal stress (δ')	12.4°
Effective interface friction angle with respect to matric suction (δ_b)	8.5°
Effective cohesion (c')	14kPa
Effective interface cohesion (c'_a)	8kPa

5.3 Pile infiltration test

The large-scale model pile infiltration test performed in Regina clay in this study has three key characteristics. Firstly, the pile infiltration test well simulates the commonly encountered in-situ scenario in which infiltration happens in the service stage of the pile. Secondly, all measurements required for the rational interpretation of the hydro-mechanical behavior were collected for understanding pile load transfer mechanism. Thirdly, influence of the stress state variable, matric suction and its variation are highlighted in the interpretation of the load transfer mechanism. The pile infiltration test conducted is summarized in three sections; namely, the experiment preparation, testing procedure and experiment results analysis.

5.3.1 Experiment preparation

The pile infiltration test was conducted in a cylindrical aluminum tank with an internal diameter of 300mm and a height of 700mm (Figure 5.8). Boreholes were drilled on the tank wall to lead cables of the GS-3 water content sensors, MPS-6 dielectric water potential sensors buried at different depth and the load cell located at the bottom of the pile out of the testing tank. Table 5.6 summarizes the key details of various sensors used for collecting data during the pile infiltration test.

Table 5.6 Device parameters of various sensors set inside expansive soil

Sensor	Manufacturer	Range	Resolution	Accuracy
GS-3 water content sensor	Decagon Devices, Inc.	Apparent dielectric permittivity: 1 (air) to 80 (water)	(0.2% VWC) from 0 to 40% VWC; (0.1% VWC) > 40% VWC.	±3% VWC
MPS-6 dielectric water potential sensor	Decagon Devices, Inc.	-9 to -100000kPa	0.1kPa	± (10% of reading + 2kPa)
Load cell	Honeywell international Inc.	0 to 3000lbs.	infinite	±0.1% full scale

where: VWC is the volumetric water content.

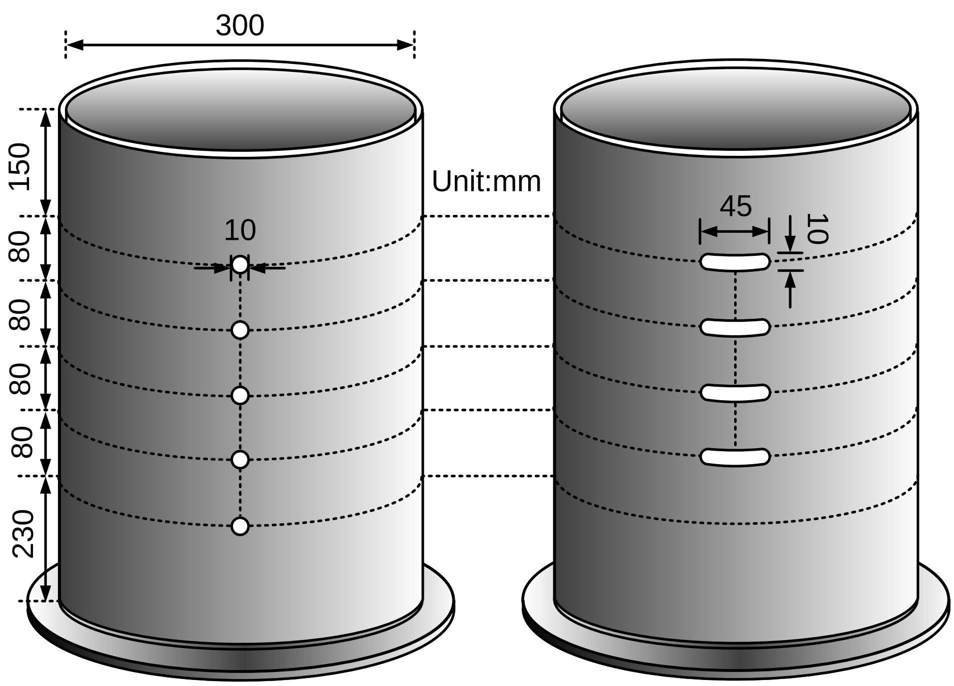

Figure 5.8 Schematic of the cylindrical aluminum tank

The model pile used in the pile infiltration test was fabricated following a three-step-procedure as shown in Figure 5.9. In the first step, four different components, highlighted in the Figure 5.9 were prepared for the fabrication of the aluminum model pile. Component one and two were made by cutting aluminum pipes with an outer diameter of 25.4mm, a wall thickness of 3mm and a height of 600mm. The ratio of the diameter of testing tank to the diameter of the model pile was designed to be around 12. This ratio is considered satisfactory to alleviate the influence of boundary conditions on the pile load test results based on the recent pile tests results in unsaturated soils (Fan 2007 and Han et al. 2016). Five strain gauges were pasted inside component one. The strain gauges (gauge type: FLG-02-23) produced by Tokyo Sokki Kenkyujo Co., Ltd. that have a length of 3.5mm, a width of 2.5mm and a resistance of 120Ω were used. Component three and four were aluminum columns used to block the hollow model at the pile top and bottom. A bolt hole was drilled at the top of component three to connect the load tank. In the second step, four components fabricated in step one were assembled, a borehole having a diameter of 10mm was drilled in order to lead the cable of the strain gauges out. In the third step, a thin layer of sand was pasted on the pile surface using epoxy to form the rough surface. This procedure is similar to preparing aluminum block with rough surface in the interface direct shear test, which was detailed earlier.

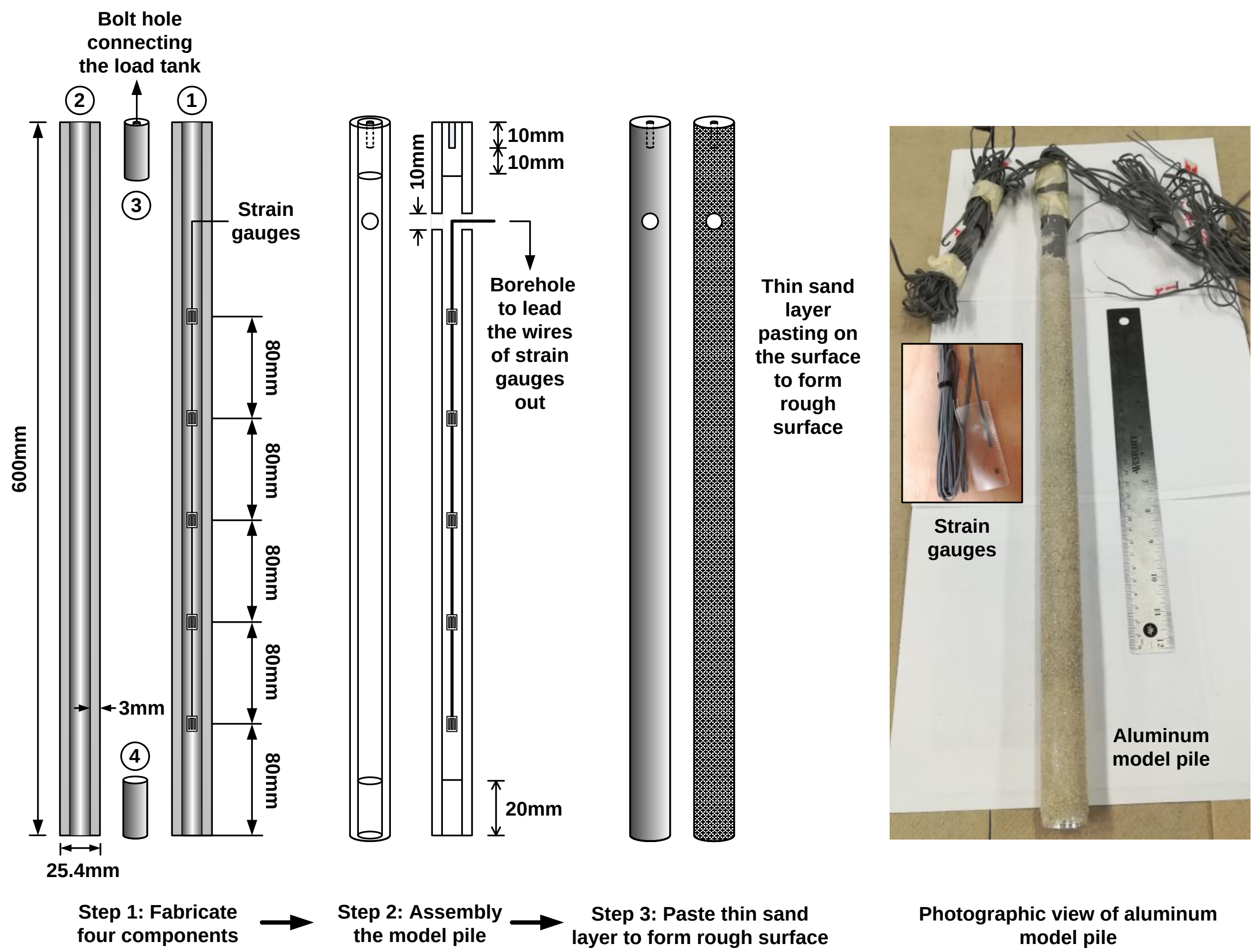

Figure 5.9 Schematic of the model pile

The compaction tank and compaction hammer (as shown in Figure 5.10) were designed and fabricated for compacting expansive soil. The bottom plate of the compaction tank [as shown in Figure 5.10(B)] was designed to compact half of soil in the test tank at a time. By rotating the compaction tank by 45^{o} after each compaction, soil can be uniformly compacted to the specified wet density. A semicircular borehole was reserved at the bottom plate to alleviate any contact with the pile fixed on the loading frame during the compaction process. The load tank was specially fabricated and used to apply the required pile head load as shown in Figure 5.11. Lead balls were filled in the load tank to act as the pile head load during the pile infiltration test.

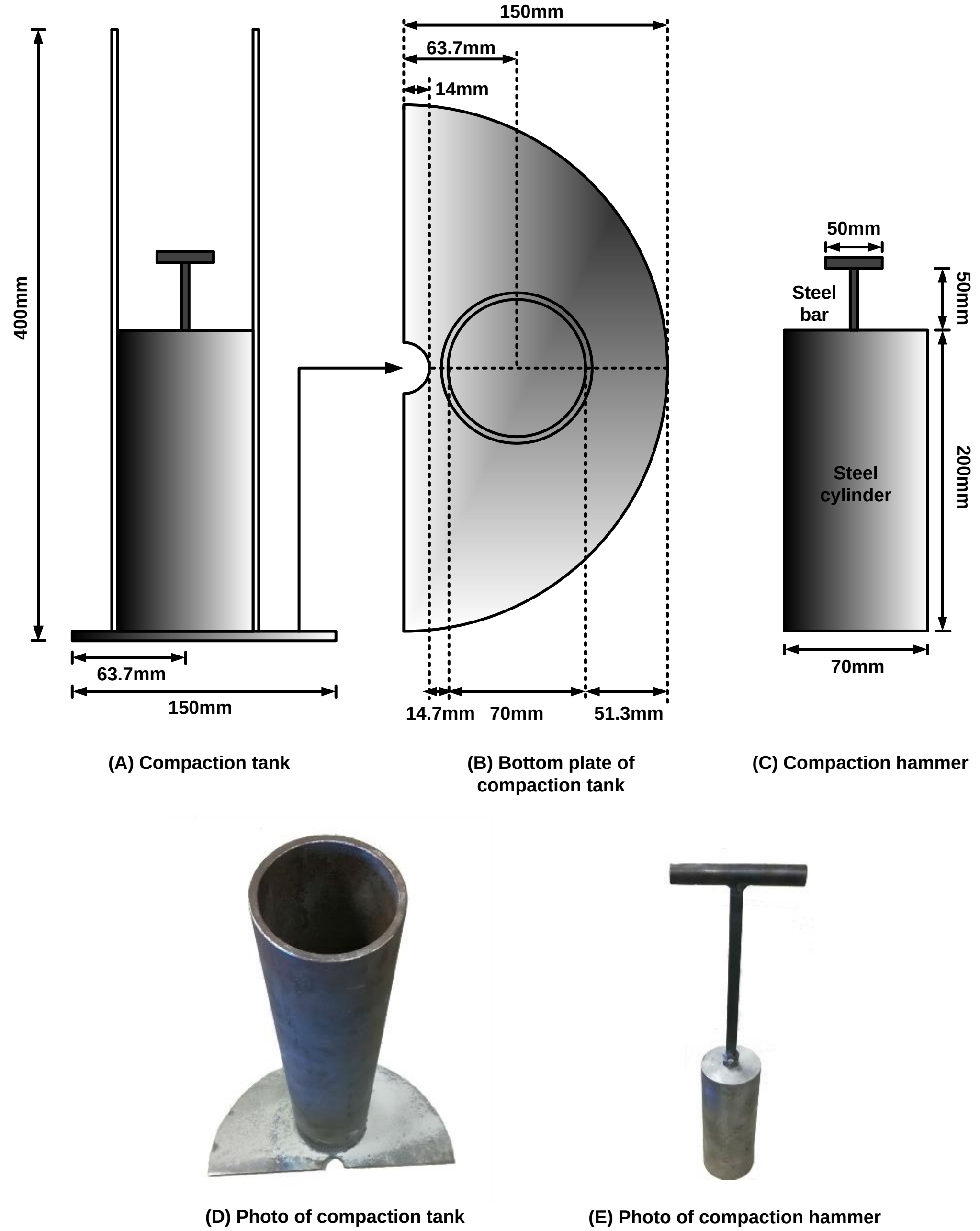

Figure 5.10 Schematic of the compaction tank

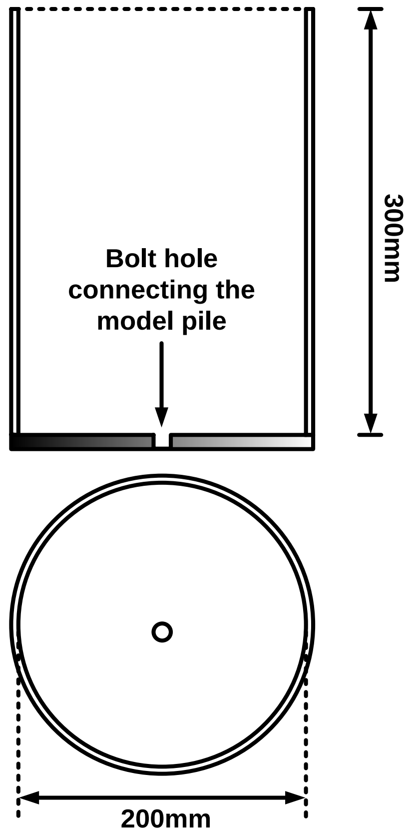

(A) Load tank

(B) Photo of load tank

Figure 5.11 Schematic of the load tank

5.3.2 Testing procedure

The pile infiltration test was conducted following a four-step-procedure as described in Figure 5.12. In the first step [Figure 5.12(A)], the model pile was fixed to the loading machine using a bolt to keep its position fixed during the compaction process. A waterproof ruler was pasted on the inner wall of the testing tank in order to measure the height of the soil during compaction, loading and infiltration process.

In the second step [Figure 5.12(B)], fine sand, which was used to achieve rough surface on aluminum pile was poured into the testing tank until a height of 150mm was reached. A load cell was placed at the bottom of the model pile. The cable connecting the load cell was taken out from the testing tank through a pre-drilled borehole. The cable of the load cell was covered with a PVC plastic pipe to separate it from the surrounding soil to alleviate friction between the load cell cable and the soil. After following these initial precautions, the soil that was already mixed with a water content of 27% was compacted in 20 equal layers (each layer with a thickness of 20mm) to achieve a wet density of 17.36×10^3kg/m^3 (i.e., dry density of 13.67×10^3kg/m^3). After each soil layer was compacted, the surface was scarified using a spatula to achieve a corrugated surface and facilitate in achieving a close contact between adjacent compacted soil layers. During the compaction process of various soil layers, GS-3 and MPS-6 sensors were set at various positions as shown in Figure 5.12(B).

In the third step [as shown in Figure 5.12(C)], the loading machine used to fix the pile was removed and the load tank was connected to the pile head. Two dial gauges were set at the top of the load tank to record the pile displacement during the loading and infiltration process. The ultimate bearing capacity of the model pile was estimated to be 1000N using Equation 5.3 from Chinese Technical Code for Building Pile Foundations (JGJ 94-2008). Using a factor of safety value of two, an allowable load of 500N was applied on the pile head prior to water infiltration. Manual irrigation was performed and soil deformation was measured with aid of a scale that was pasted on the testing tank. Once the soil deformation stabilized, manual irrigation was stopped.

$$Q_{uk} = Q_{us} + Q_{pk} = u\sum q_{sik} l_i + q_{pk} A_p \tag{5.3}$$

where Q_{uk} is the ultimate single pile bearing capacity; Q_{us} is the ultimate pile shaft resistance; Q_{pk} is the ultimate pile base resistance; u is the perimeter of the model pile; q_{sik} is the standard pile shaft friction within soil layer i, for pre-cast concrete pile with pile shaft in contact with high plasticity index clay, q_{sik} is estimated as 24kPa; l_i is the layer thickness of the soil layer i; q_{pk} is the standard pile base stress, for pre-cast concrete pile with pile base on loose fine sand, the q_{pk} is estimated as 500kPa; A_p is the pile base area.

Pile head load of 500N was applied in three steps (150N, 150N and 200N). Initially, a load of 150N was applied on the pile head by adding lead balls inside the load tank. Pile displacement was measured at hourly intervals. The next level of load was applied after the pile head displacement was observed to be constant for 24 hours. A total load of

500N was applied on the pile head and a stable pile settlement of around 3mm was recorded. During this process, the ground surface was covered with plastic wrap to minimize evaporation losses. A cable system as shown in Figure 5.12(C) was set and a spirit level was used to assure that there is no eccentricity in the applied load. In other words, it was assured that only axial load was acting on the pile in vertical direction.

In the fourth step [Figure 5.12(D)], water was added manually as required to assure the ground water table was always higher than the ground surface. Pile mechanical behavior information, which include the axial force distribution, pile base resistance, pile head displacement and the soil behaviors including the soil displacement, soil volumetric water content variations and suction variations were monitored during the infiltration process. Experiment was terminated when the pile head displacement stabilized and all the GS-3 and MPS-6 sensors indicated that the soil has been fully saturated. Figure 5.13 provides a photographic view of experimental settings during the infiltration stage.

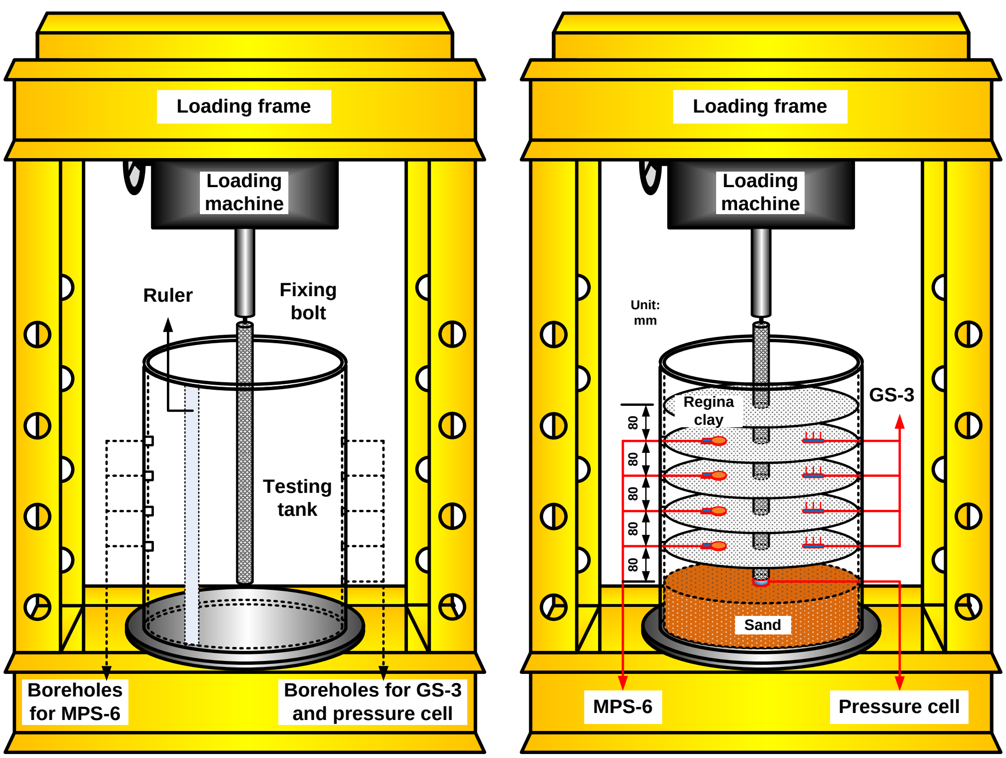

(A) (B)

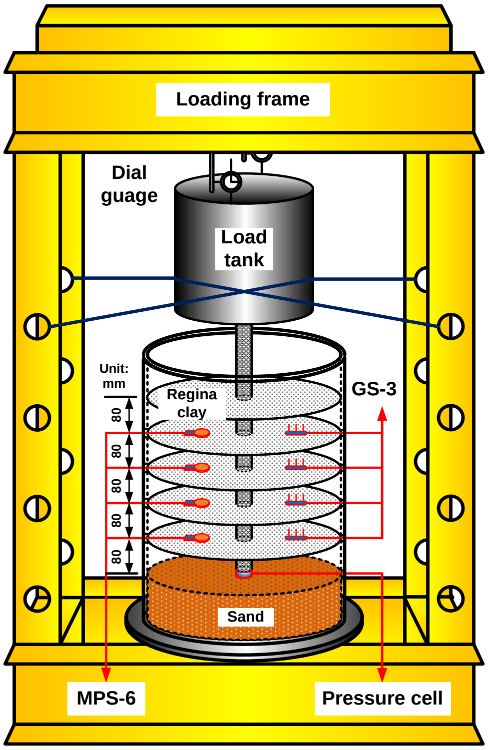

(C)

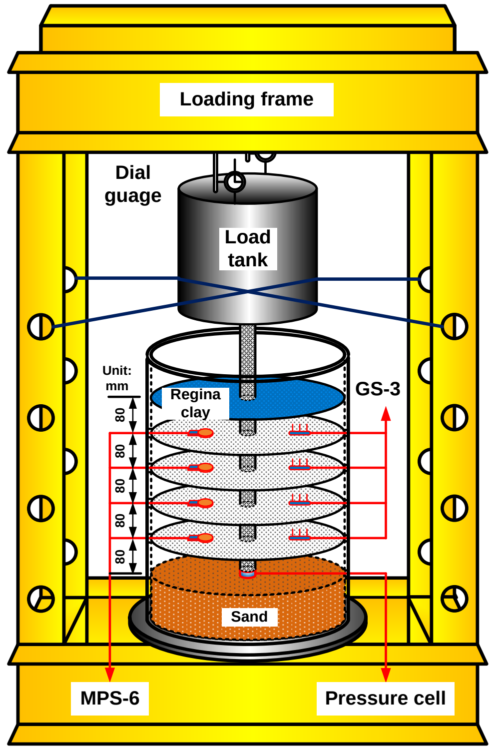

(D)

Figure 5.12 Four steps to conduct the pile infiltration test in expansive soils

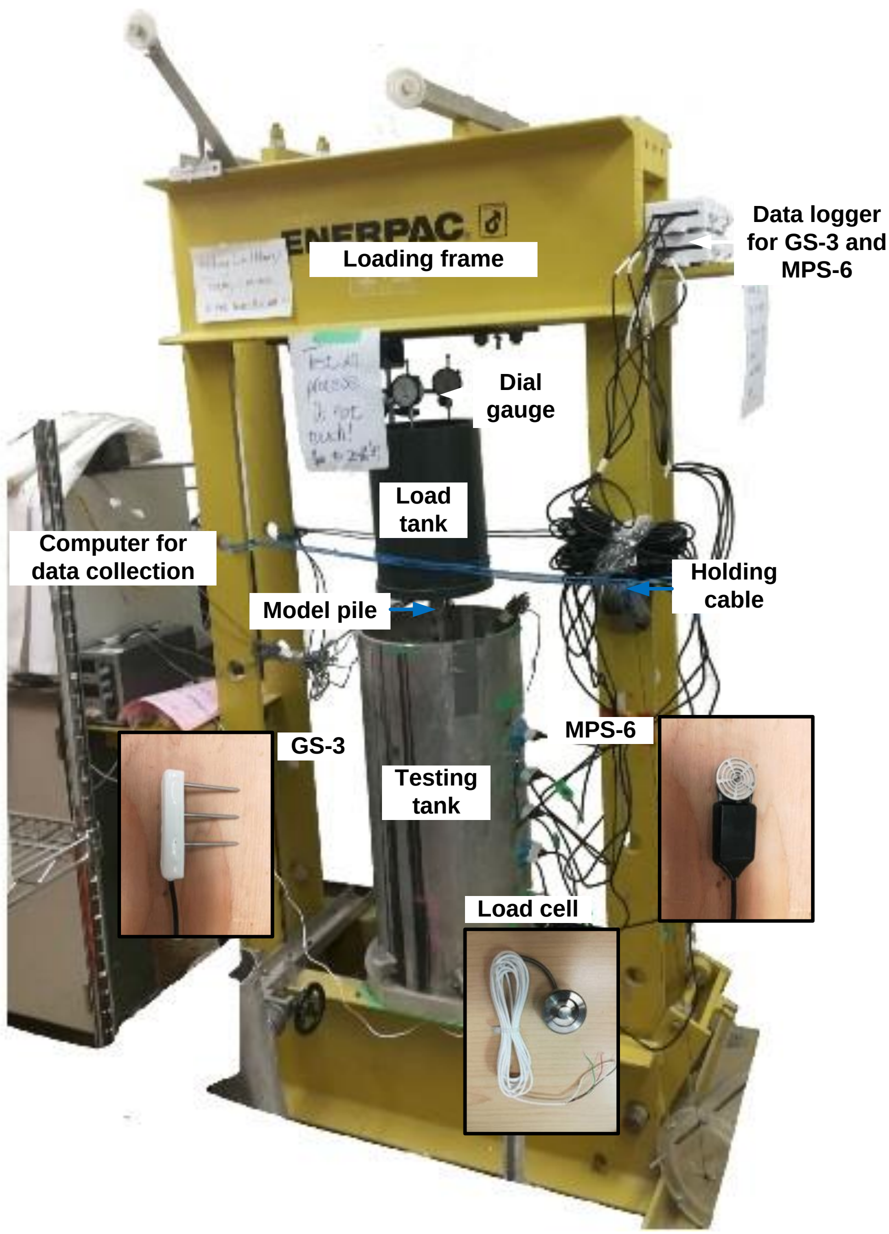

Figure 5.13 Photographic view of pile infiltration test experimental settings

5.3.3 Experiment result analysis

From the application of the first level load (150N) until the soil around the pile was fully saturated, the pile infiltration test was conducted for 400 hours. More specifically, the static loading process took around 160 hours and the infiltration process took the rest 240 hours. Figure 5.14 shows the variations of the soil and pile head displacement during the pile infiltration test. In the static loading process, pile experienced a settlement of around

3mm under the applied load of 500N while no noticeable soil settlement was detected in this process. After water was added by manual irrigation, expansive soil around the pile showed a strong volume expansion in the vertical direction which behaved as ground heave and ground heave development did not terminate until around 200 hours. Eventually a ground heave of 25mm was detected. However, the pile head settlement increased from around 3mm to around 7mm due to the influence of matric suction. Since the water content of the sand fill at the bottom of the pile was not influenced by water infiltration at the beginning, the greater pile head settlement can be only attributed to the loss of pile shaft friction.

Volumetric water content and the suction changes happening in the testing process were revealed in Figure 5.15 and Figure 5.16, respectively. From the beginning of manual irrigation, only around 40 hours was necessary for water to fully saturate the expansive soil layer with a thickness of 400mm. This is because the volume expansion of the expansive soil greatly increases the void ratio of the expansive soil. After the infiltration test, the expansive soil collected from the ground surface has totally become slurry. A clear correlation can be observed between the volumetric water content or suction changes and the development of the ground heave.

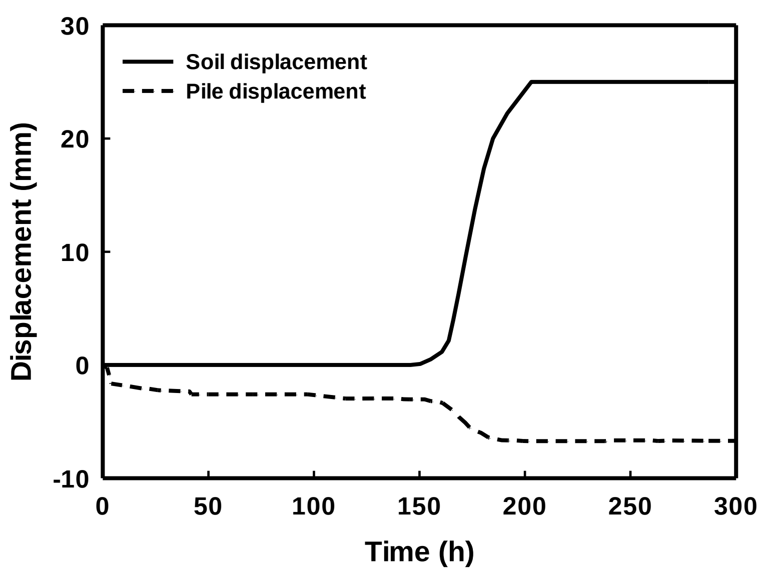

Figure 5.14 Variations of soil and pile head displacement with time

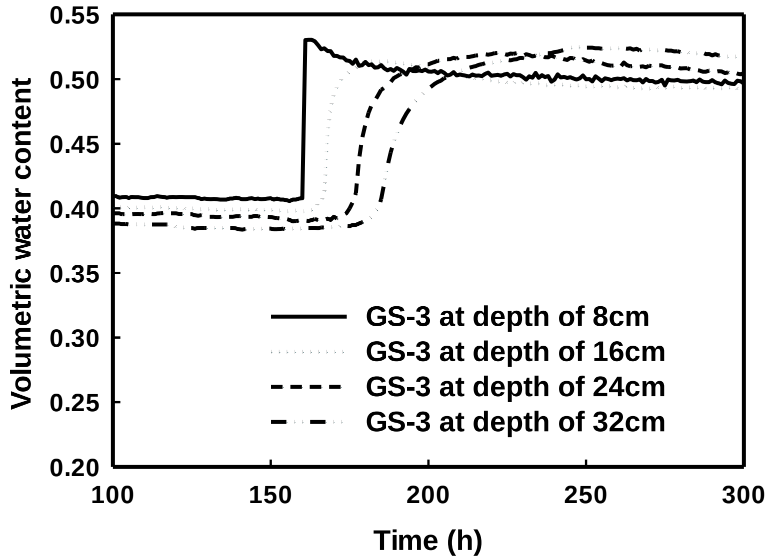

Figure 5.15 Variations of volumetric water content distribution with time

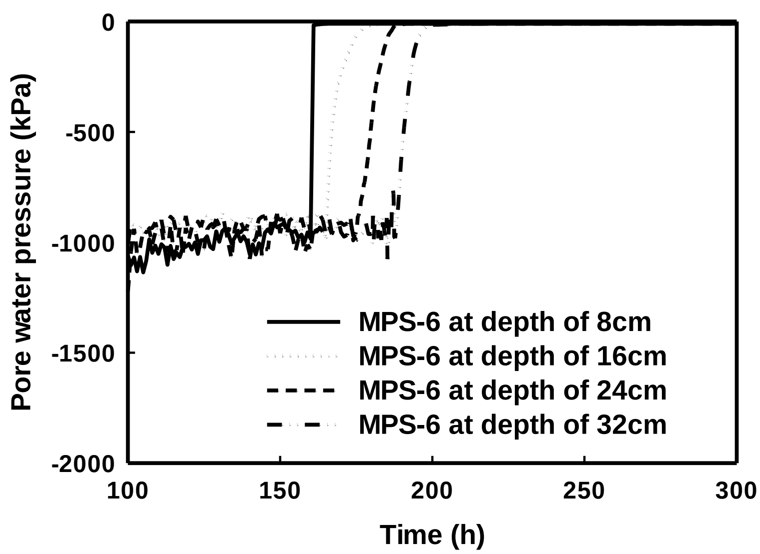

Figure 5.16 Variations of water potential (suction) distribution with time

Figure 5.17 shows the pile axial force variations recorded by strain gauges installed at different depth of the model pile. A clear trend was demonstrated by Figure 5.17 that the pile axial force kept increasing in the infiltration process and such pile axial force increment became more significant at greater depth. Figure 5.18 shows the variations of the pile base resistance in the testing process. In the static loading process, the pile base resistance gradually stabilized at a value of 34N, while in the infiltration process, the pile base resistance grew rapidly to a value of around 183N within only 40hours. Such a pile base resistance increment reflects the pile shaft friction loss in the infiltration process. After the expansive soil had been fully saturated, the slight increment in the pile base resistance can be explained by the soil stress relaxation effect. In order to reveal the pile load transfer mechanism changes in a more detailed and clear way, pile axial force distribution and pile shaft friction distribution at four specific time points (160h, 170h, 180h and 200h) were shown in Figure 5.19 and 5.20, respectively. These four time points were selected since they gave different volumetric water content or suction profiles according to Figure 5.15 and Figure 5.17. Figure 5.19 reveals that in the infiltration process, more pile head load was gradually transferred to greater depth of the pile and was finally born by the pile base. The reason for such pile load transfer mechanism changes could be explained by Figure 5.20. From 160hours to 180hours, pile shaft friction within the already saturated zone kept decreasing while the pile shaft friction in the unsaturated zone kept increasing. Using unsaturated soil mechanics (Equation 4.22 and Equation 4.34), such behaviours can be explained as following: suction reduction induced by water infiltration reduced the contribution of matric suction to the pile shaft friction. Although lateral swelling pressure was mobilized due to the suction reduction and added an additional part to the normal stress acting on the pile-soil interface, apparently the reduction in pile shaft friction caused by suction reduction was more significant. As a consequence, loss of the pile shaft friction in the saturated zone resulted in more load born by the pile in the unsaturated zone and pile base. Further, loss of pile shaft friction also generated a greater pile settlement, and this settlement increased the pile-soil relative displacement. Considering that prior to water infiltration, pile-soil relative displacement due to static loading was lower than the critical value corresponding to the peak interface shear strength. The pile-soil relative displacement increment just increases the pile-soil interface shear strength (shaft friction) towards the peak value. This can be a dominant cause for the increase in pile shaft friction in unsaturated zone at 170hours and 180hours. However, as the entire expansive soil layer had been fully saturated at 200hours. The contribution of suction to the pile shaft friction completely vanished so that the peak interface shear strength along the whole pile decreased and the far greater pile settlement was observed. Apart from the reduction in peak interface shear strength, a further increase in pile head settlement may cause the pile-soil interface shear strength to reduce from the peak value to post peak value. Therefore the lowest pile shaft friction distribution was observed under fully saturated condition.

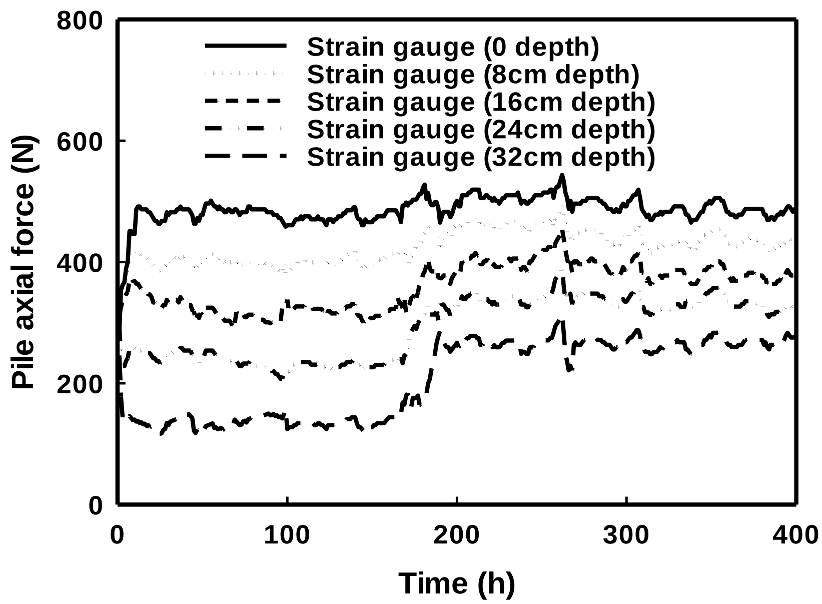

Figure 5.17 Variations of pile axial force distribution with time

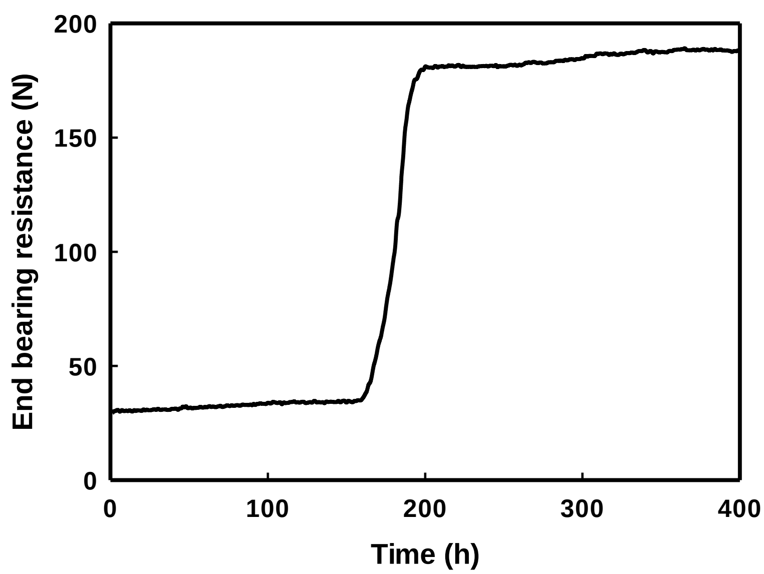

Figure 5.18 Variations of pile base resistance with time

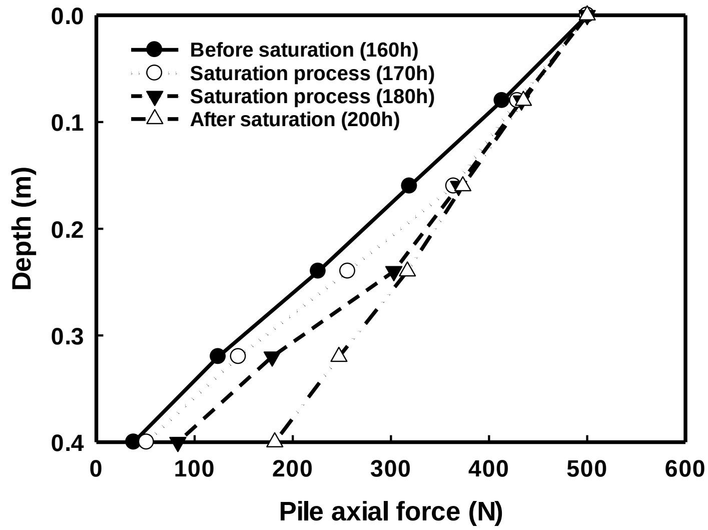

Figure 5.19 Variations of pile axial force distribution

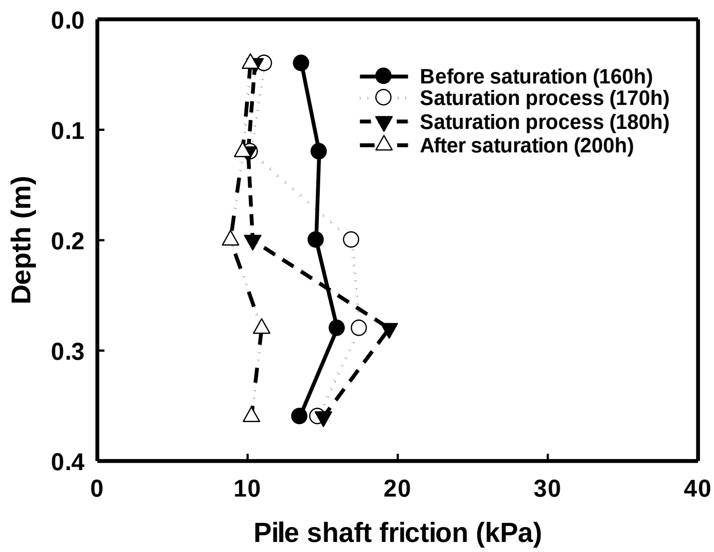

Figure 5.20 Variations of pile shaft friction distribution

5.3.4 Comparisons between the experimental data and predictions made using modified shear displacement method and modified load transfer curve method

Employing the basic soil properties listed in Table 5.3 and soil and interface shear strength parameters listed in Table 5.5. The modified shear displacement method and modified load transfer method proposed in this study can be used for the prediction of the mechanical behaviors of the pile in the conducted infiltration test. The elastic modulus of the aluminum model pile is set as 70Gpa and a Poisson's ratio of 0.3 is set for the expansive clay. Since sand was poured into the testing tank and no compaction was applied, the soil at the bottom of the pile was in a relative loose state. In order to achieve reasonable comparisons between the predictions and experimental results, an elastic modulus of 1000kPa for the sand located at the bottom of the pile was used in the calculation of the modified shear displacement method and modified load transfer curve method. Similar to the experiment results analysis, mechanical behaviors including pile head displacement and pile axial force distribution (pile shaft friction distribution) at four time points (160h, 170h, 180h and 200h) were predicted and analyzed. The pile-soil relative displacement corresponding to the peak interface shear strength was set a 0.01m. As discussed earlier, during the shear test for the determination of the unsaturated soil and unsaturated interface shear strength parameters, the shear chamber was sealed to prevent the possible water content loss. As a consequence, along with the volume changes (dilation or contraction) happening in the shearing process, the volumetric content and suction in the shearing plane keep changing. For peak soil and interface shear strength, the soil water menisci formed in the compaction process is still in a relative intact state and contributes to the peak shear strength. Relative intact soil water menisci indicate that no significant variations happening to the matric suction in the shearing plane. However, for the post-peak interface shear strength, the rapture of the soil menisci results in considerable changes in matric suction (Hamid and Miller 2009 and Khoury et al. 2010) and such matric suction changes keep happening as the shearing continues. As a consequence, post-peak interface shear strength parameters cannot be obtained from the interface direct shear test conducted. Instead, the post-peak interface shear strength was set as 0.85 of the peak interface shear strength based on the empirical relationship presented by Zhang et al. (2010a, 2011b).

5.3.4.1 Prediction made using modified shear displacement method

Figure 5.21 shows the predicted pile axial force and pile shaft friction distributions at four different time points using modified shear displacement method. In general they show similar variation trend as the experimental data. Figure 5.22 presents the comparisons of the pile axial force distribution between the experimental data and the prediction made using modified shear displacement method. At all four time points, the estimated pile axial forces at different depth were higher than the experimental data. This is because for the modified shear displacement method, the interface shear strength directly drops from the peak value to the post peak value after the critical pile-soil relative displacement. Since a maximum ground heave of 25mm was recorded in the pile infiltration test and was introduced in the calculation of the modified shear displacement method. For a considerable part of pile, the pile-soil relative displacement has exceeded the critical value, thus resulting in the mobilization of the post-peak interface shear strength. A sudden reduction in pile shaft friction from the peak value to post peak value in the modified shear displacement method causes more pile head load was transferred to the pile base instead of bearing by the shaft friction.

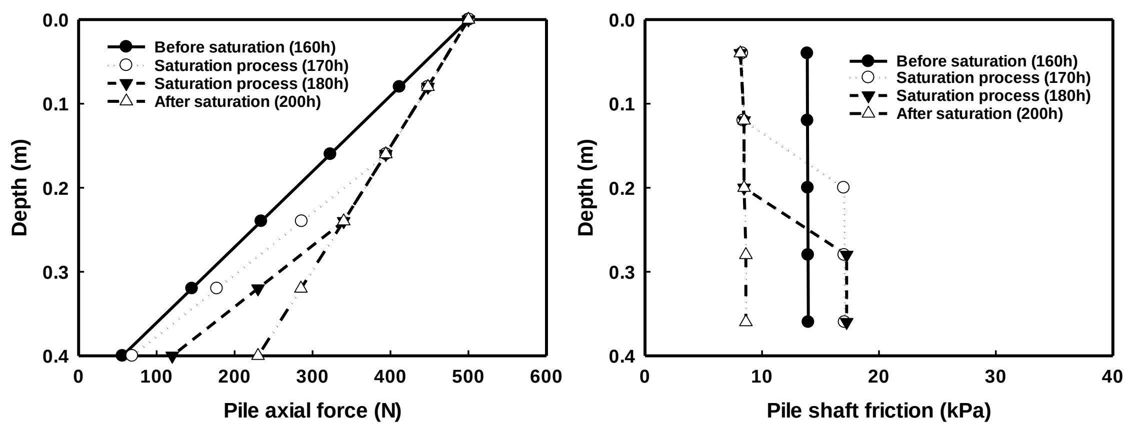

(A) (B)

Figure 5.21 Predictions made using the modified shear displacement method (A) Pile axial force distribution; (B) Pile shaft friction distribution

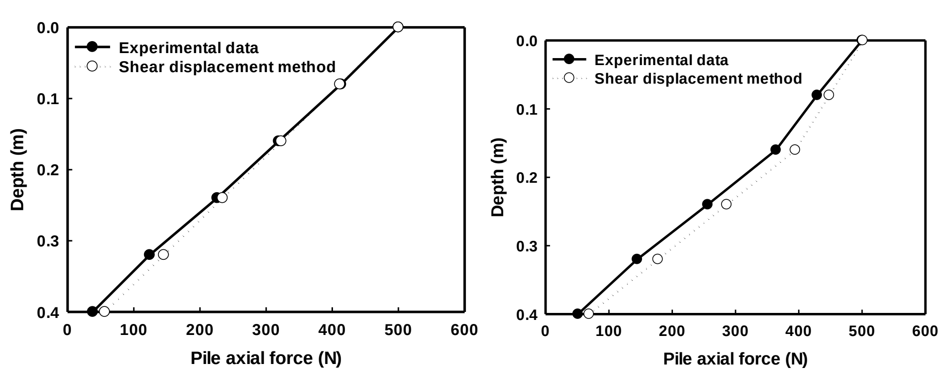

(A) (B)

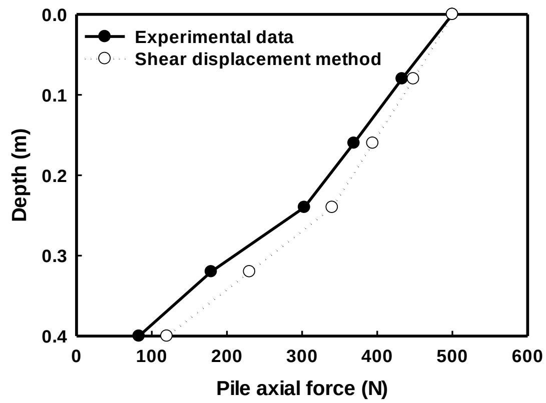

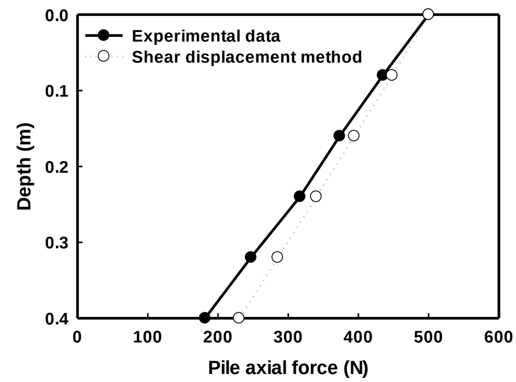

(C) (D)

Figure 5.22 Comparisons of the pile axial force distribution using modified shear displacement method (A) 160h; (B) 170h; (C) 180h; (D) 200h

5.3.4.2 Prediction made using modified load transfer method

Figure 5.21 shows the predicted pile axial force and pile shaft friction distributions at different time points using modified load transfer curve method. Similarly, they show similar variation trend as the experimental data. Figure 5.22 presents the comparisons of the pile axial force distribution between the experimental data and the prediction made using modified load transfer curve method. Better comparisons can be achieved compared to the predictions made using modified shear displacement method. This is because the load transfer curve model used in the modified load transfer curve method allows the pile-soil interface shear strength gradually falls from the peak to the post peak value.

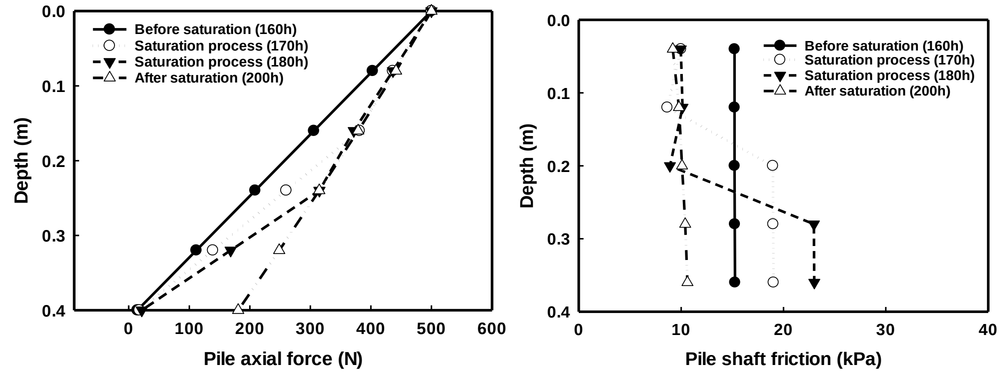

(A) (B)

Figure 5.23 Predictions made using the modified load transfer curve method (A) Pile axial force distribution; (B) Pile shaft friction distribution

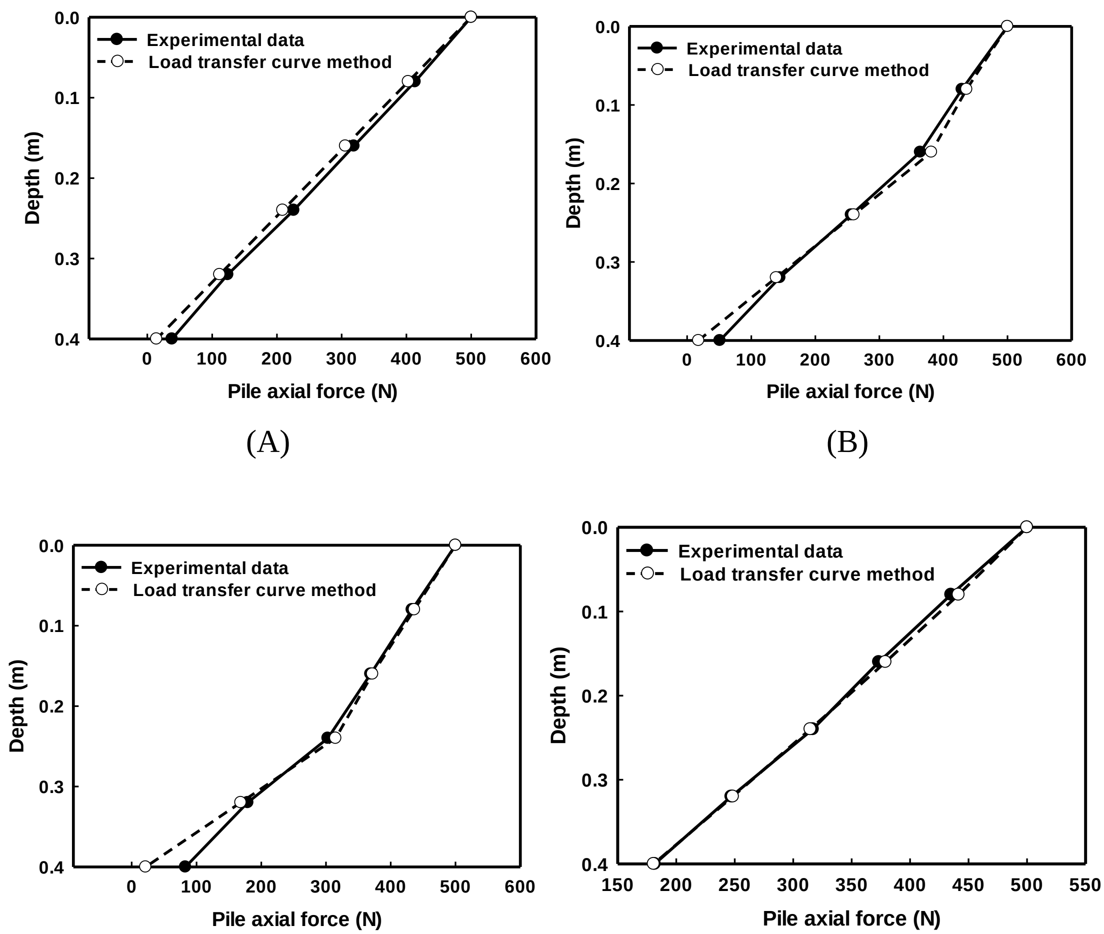

(C) (D)

Figure 5.24 Comparisons of the pile axial force distribution using modified load transfer curve method (A) 160h; (B) 170h; (C) 180h; (D) 200h

Figure 5.25 shows the comparisons of the pile head displacement predictions using modified shear displacement method and modified load transfer curve method with experimental data. Both predictions made using modified shear displacement method and modified load transfer method reasonably predict the variation trend of the pile head displacement. Since in modified shear displacement method, more pile head load was transferred to the pile base so that higher pile base resistance was predicted compared to the modified load transfer curve method.

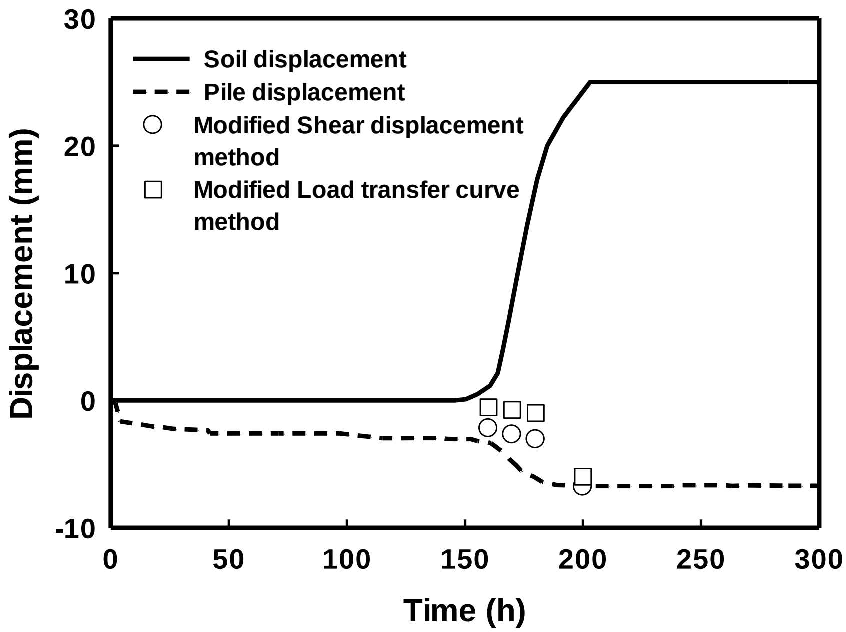

Figure 5.25 Comparisons of the pile head displacement using modified shear displacement method and modified load transfer curve method

5.4 Summary and conclusions

The mechanical behaviors of pile foundation constructed in expansive soil regions can experience significant changes upon water infiltration, which further threat the safety and stability of superstructures. In this chapter, pile infiltration test in unsaturated expansive soil was conducted to study the mechanical behaviors changes of piles in expansive soils upon infiltration from three innovative aspects: initially the pile test simulate the most commonly encountered scenarios in engineering practice that water infiltration happens in the service stage of the pile. Secondly, measurements were conducted for comprehensive understanding of the pile behaviors prior to the pile infiltration tests and during the pile infiltration tests. Thirdly, the functions of matric suction and matric suction variations were highlighted. Through this study, following conclusions can be summarized:

Image technique using commercial software can be easily and conveniently integrated with various lab testing techniques for the measurement of SWCC (including pressure plate method, desiccator method and filter method) considering the volume changes. Two reasons can be given as following: initially photos are directly taken on the soil samples, so that the refraction correction is not required. Further, the cylinder soil sample shows completely different textures from point to point which facilitate the software to catch the features from different photos to construct the 3D model.

The soil and pile-soil interface direct shear test results show that both development of the soil and pile-soil interface shear strength with shear displacement show softening characteristics. Both net normal stress and matric suction (through soil-water menisci) contribute to the peak soil-pile interface shear strength. The development of the interface shear strength with net normal stress and matric suction can be well described by the model proposed by Hamid and Miller (2009).

For a pile in expansive soil under a service load, water infiltration causes a reduction in the pile shaft friction. As a consequence, more pile head load is transferred to the pile at greater depth, resulting in the development of the pile head settlement and pile base resistance. One reason for such behaviors is that suction reduction induced by water infiltration reduces the contribution of matric suction to the pile shaft friction. Although lateral swelling pressure is mobilized due to the suction reduction and added an additional part to the normal stress acting on the pile-soil interface, apparently the reduction in pile shaft friction caused by suction reduction is dominant. Meanwhile, during the infiltration process, the pile-soil relative displacement kept increasing due to the development of ground heave and pile settlement. The pile-soil relative displacement increment increases the pile-soil interface shear strength (shaft friction) at greater depth towards the peak value in the beginning of the infiltration process. However, as the entire expansive soil layer had been fully saturated, increase in pile head settlement may cause the pile-soil interface shear strength to reduce from the peak value to post peak value. Therefore the lowest pile shaft friction is observed under fully saturated condition.

Comparisons were made between the experimental data and the predictions made using the modified shear displacement method and modified load transfer curve method. Relative good comparisons can be achieved using both methods in pile head displacement and pile axial force (shaft friction) distributions. Since the modified load transfer curve model uses a softening model which allows the pile soil interface shear strength gradually drops from peak to post peak values, it provided relative better predictions.

CHAPTER SIX

CONCLUSIONS AND SUGGESTIONS FOR FUTURE RESEARCH

6.1 Summary

Pile foundations have been widely used in various regions of the world with expansive soil deposits to alleviate stability and settlement problems and ensure safety of both the sub- and superstructures. These types of foundations are designed extending saturated soil mechanics principles assuming drained conditions (effective stress). However, the soil surrounding the pile is typically in a state of unsaturated condition and the mechanical behavior of the soil and soil-pile interface is significantly influenced by matric suction changes associated with infiltration. After undertaking a comprehensive literature review on various factors influencing the mechanical behaviors of piles in expansive soils, two theoretical methods are proposed in present study for rationally interpretation and estimation of the load transfer mechanism variations. Employing the modified shear displacement method, the pile head load-displacement relationship can be achieved. The modified load transfer curve method is more comprehensive which has the ability to show changes in the pile shaft friction distribution, pile end bearing capacity, pile head and end movement in the infiltration process. The proposed methods are simple in formulation and require only limited parameters to be determined through experiment.

6.2 Major conclusions

6.2.1 Literature review

(I) Lateral swelling pressure measurement based on the laboratory test methods is stress path dependent. Amongst various laboratory measurement techniques available, swell under surcharge test is mostly recommended since it can well simulate the scenario that are typically encountered in engineering practice. Compared with laboratory measurement techniques, large scale model and in-situ tests are more comprehensive, time consuming and expensive. However, these tests can provide experimental results that are of significant value for engineering practice applications. Most large scale model and in-situ tests belong to the category of swell under surcharge tests.

(II) Swelling pressure that mobilizes and acts on geotechnical infrastructure can be attributed to water infiltration in expansive soils that triggers swelling potential. Swelling potential is conventionally determined or estimated from derived information of percentage clay, clay minerals or clay structure in expansive soils. Clay particle orientation is a key factor which influences the swelling pressure both in vertical and horizontal directions. Particle orientation is determined by the stress path in natural soils and the compaction method in remoulded soils. In addition, both the time effects and fatigue phenomenon have significant impact on the mobilization of lateral swelling pressure.

(III) It is commonly accepted that suction makes a positive contribution to the peak interface shear strength. The contribution of suction to the peak interface shear strength is more significant for soil, followed by rough interface and smooth interface. The residual interface shear strength is not significantly influenced by matric suction because during shearing beyond the peak interface shear strength, the air-water menisci are completely disrupted.

6.2.2 Mobilization of lateral swelling pressure on structures in expansive soils

The total lateral earth pressure can be calculated by superposition method taking account of the influence of lateral swelling pressure in addition to the lateral earth pressure due to soil unit weight and surcharge. However, the total lateral earth pressure is limited to a maximum value of passive earth pressure (i.e. the total lateral earth pressure cannot exceed passive earth pressure). A model is proposed in this study to predict the lateral earth pressure considering lateral swelling pressure against fixed rigid retaining structure taking account of variation of matric suction associated with water infiltration, extending mechanics of unsaturated soils. The superposition method can be further extended for the estimation of lateral earth pressure of expansive backfill behind rigid retaining structures in the drying process considering volume shrinkage. Models for estimations the active and passive earth pressures under different degree of saturation and interface roughness are also presented as the limiting states of lateral earth pressures variations.

The proposed model is verified using the experimental data from a large scale model retaining wall test by Katti et al. (1983) and Gu (2005) along with the in-situ measurements by Mohamed et al. (2014) and Richards and Kurzeme (1973) on retaining structures. The model proposed is capable of reasonably predicting lateral swelling pressure mobilization from an initial unsaturated state to subsequent unsaturated state during the infiltration process employing only limited number of soil properties, which include SWCC, the saturated elastic modulus, E_{sat}, Plasticity index, I_p, maximum dry density, $\rho_{d,max}$ and the Poisson ratio, μ. The proposed simple model is valuable in geotechnical engineering practice for assisting geotechnical engineers to quickly estimate the increasing lateral earth pressure due to lateral swelling pressure mobilization behind retaining structures during the infiltration process, thus contributing to the rational design or construction decisions.

6.2.3 Prediction of mechanical behaviors of single pile in expansive soil upon infiltration

Two theoretical methods are proposed for the load transfer analysis of a single pile in expansive soil upon infiltration. The first one is modified shear displacement method and the second one is the modified the load transfer curve method. The outstanding advantage of the modified shear displacement method is that calculations using this method can be completed rapidly since no iterations are required in the calculations. While the inclusion of the softening model describing the development of the pile-soil interface shear stress with pile-soil relative displacement enables the load transfer curve method to give a better prediction. Example problem analysis using modified load transfer curve method indicates that matric suction variation can pose significant influence on the mechanical behaviors of the pile in expansive soils. Upon water infiltration, light structures may suffer ground heave problem. However, for structure under great load, ground heave may lead to a shaft friction reduction which cause more serious settlement problem. There are two reasons responsible for this behavior. The first reason can be attributed to the changes in the interface shear strength regarding the mobilization of the lateral swelling pressure and the reduction of the interface shear strength properties. The second one is that ground heaves lead to an increment of the pile soil relative displacement, which causes an interface shear strength decrease from peak value to residual value.

Both the modified shear displacement method and the modified load transfer curve method were verified using the experimental results from Fan (2007) and Benvenga (2005). Good results can be achieved by comparing the predictions using proposed method with the experimental data. The modified shear displacement and load transfer curve method proposed in this study can well help practicing engineers to make a quick and reasonable estimation on the mechanical behavior variations of piles in expansive soils upon infiltration.

6.2.4 Experimental study on a single model pile in expansive soil upon infiltration

(I) Image technique using commercial software can be easily and conveniently integrated with various lab testing techniques for the measurement of SWCC (including pressure plate method, desiccator method and filter method) considering the volume changes. Two reasons can be given as following: initially photos are directly taken on the soil samples, so that the refraction correction is not required. Further, the cylinder soil sample shows completely different textures from point to point which facilitate the software to catch the features from different photos to construct the 3D model.

(II) The soil and pile-soil interface direct shear test results show that both development of the soil and pile-soil interface shear strength with shear displacement show softening characteristics. Both net normal stress and matric suction (through soil-water menisci) contribute to the peak soil-pile interface shear strength. The development of the interface shear strength with net normal stress and matric suction can be well described by the model proposed by Hamid and Miller (2009).

(III) For pile in expansive soil under a service load, water infiltration causes a reduction in the pile shaft friction. As a consequence, more pile head load is transferred to the pile at greater depth, resulting in the development of the pile head settlement and pile base resistance. One reason for such behaviors is that suction reduction induced by water infiltration reduces the contribution of matric suction to the pile shaft friction. Although lateral swelling pressure is mobilized due to the suction reduction and added an additional part to the normal stress acting on the pile-soil interface, apparently the reduction in pile shaft friction caused by suction reduction is predominant. Meanwhile, during the water infiltration process, the pile-soil relative displacement kept increasing due to the development of ground heave and pile settlement. The pile-soil relative displacement increment increases the pile-soil interface shear strength (shaft friction) at greater depth towards the peak value in the beginning of the infiltration process. However, as the entire expansive soil layer had been fully saturated, increase in pile head settlement may cause the pile-soil interface shear strength to reduce from the peak value to post peak value. Therefore the lowest pile shaft friction is observed under fully saturated condition. Relative good comparisons can be achieved between predictions using both methods and experiment results for pile head displacement and pile axial force (shaft friction) distribution predictions. Since the modified load transfer curve model uses a softening model which allows the pile soil interface shear strength gradually drops from peak to post peak values, it provided relative better predictions.

6.3 Recommendations and Suggestions for Future Research Studies

Due to time limitation, only infiltration test was conducted on the pile in expansive soils, however, the proposed modified shear displacement and modified load transfer curve method can be extended for the analysis of pile mechanical behaviors both in wetting process (infiltration) and drying process (evaporation). So in the future, it is suggested a series tests including both the wetting and drying process should be conducted to acquire a complete data log for the mechanical behaviors of pile under environmental factor changes. Also, currently analysis and experiment were only focused on a single pile, but in engineering practice it is group pile foundations that are widely used. Future studies should be directed from single pile to group pile foundations to extend the application of the modified shear displacement method and the modified load transfer curve method.

Further, a robust and universal model for the estimation of the post-peak pile-soil interface shear strength give adequate considerations to the matric suction reserved in the pile-soil interface is also an important research direction.

REFERENCES

ASTM (American Society for Testing and Materials). (2008). “Standard Test Method for Measuring Stiffness and Apparent Modulus of Soil and Soil-Aggregate In-Place by Electro-Mechanical Method.” ASTM D6758-08, ASTM international, West Conshohocken, Pa.

ASTM (American Society for Testing and Materials). (2012). “Standard Test Methods for Laboratory Compaction Characteristics of Soil Using Standard Effort (12 400 ft-lbf/ft3 (600 kN-m/m3)).” D698-12$^{\varepsilon 2}$, ASTM international, West Conshohocken, Pa.

ASTM (American Society for Testing and Materials). (2014). “Standard Test Methods for One-Dimensional Swell or Collapse of Soils.” ASTM D4546-14, ASTM international, West Conshohocken, Pa.

ASTM (American Society for Testing and Materials). (2015). “Standard Guide for Calculating In Situ Equivalent Elastic Moduli of Pavement Materials Using Layered Elastic Theory.” ASTM D5858-96, ASTM international, West Conshohocken, Pa.

ASTM (American Society for Testing and Materials). (2015). “Standard Test Methods for Modulus and Damping of Soils by Fixed-Base Resonant Column Devices.” ASTM D4015-15, ASTM international, West Conshohocken, Pa.

ASTM (American Society for Testing and Materials). (2012). “Direct Shear Test of Soils Under Consolidated Drained Conditions.” ASTM D3080/D3080M-11, ASTM international, West Conshohocken, Pa.

ASTM (American Society for Testing and Materials). (2010). “Standard Test Method for Measurement of Soil Potential (Suction) Using Filter Paper.” ASTM D5298-10, ASTM international, West Conshohocken, Pa.

ASTM (American Society for Testing and Materials). (2010). “Standard Test Methods for Liquid Limit, Plastic Limit, and Plasticity Index of Soils.” ASTM D4318-10ε1, ASTM international, West Conshohocken, Pa.

ASTM (American Society for Testing and Materials). (2007). “Standard Test Method for Particle-Size Analysis of Soils.” ASTM D422-63, ASTM international, West Conshohocken, Pa.

ASTM (American Society for Testing and Materials). (2014). “Standard Test Methods for Specific Gravity of Soil Solids by Water Pycnometer.” ASTM D854-14, ASTM international, West Conshohocken, Pa.

ASTM (American Society for Testing and Materials). (2016). “Standard Test Methods for Determination of the Soil Water Characteristic Curve for Desorption Using Hanging Column, Pressure Extractor, Chilled Mirror Hygrometer, or Centrifuge.” ASTM D6836-16, ASTM international, West Conshohocken, Pa.

Alonso, E.E., Gens, A., and Josa, A.A. (1990). “A constitutive method for partially saturated soils.” *Géotechnique*, 40(3): 405-430.

Adem, H.H., and Vanapalli, S.K. (2013). “Constitutive modeling approach for estimating the 1-D heave with respect to time for expansive soils.” *International Journal of Geotechnical Engineering*, 7(2): 199-204.

Attwooll, B., Reins, J., and Lykosh, P. (2006). “Heave at manufacturing facility: Observations and response.” Proceeding of 4th International Conference on Unsaturated Soils, ASCE, Reston, VA, 147(1): 323-346.

Abshire, M. S. (2002). “Differential moisture migration and heave beneath slabs over dipping expansive shale.” M.S. thesis, Colorado State Univ., Fort Collins, CO.

Adem, H.H., and Vanapalli, S.K. (2014a). “Elasticity moduli of expansive soils from dimensional analysis.” *Geotechnical Research*, 1(2): 60-72.

Adem, H.H., and Vanapalli, S.K. (2014b). “A simple method for prediction of the modulus of elasticity of unsaturated expansive soils.” *UNSAT2014 Conference Unsaturated Soils, Research and Application*, Sydney, Australia.

Adem, H.H. (2015). “Modulus of elasticity based method for estimating the vertical movement of natural unsaturated expansive soils.” Ph.D thesis, University of Ottawa, Ottawa, Canada.

Adem, H.H., and Vanapalli, S.K. (2016). “Heave prediction in a natural unsaturated expansive soil deposit under a lightly loaded structure.” *Geotechnical and Geological Engineering*, 34(4): 1181-1192.

API (American Petroleum Institute). (1993). Recommended practice for planning, designing and constructing fixed offshore platforms–Working stress design, 20th Ed., Washington, DC.

Ai, Z. Y., and Han, J. (2009). "Boundary element analysis of axially loaded piles embedded in a multi-layered soil." *Computers and Geotechnics*, 36(3): 427-434.

Azam, S., and Wilson, G. W. (2006). "Volume change behavior of a fissured expansive clay containing anhydrous calcium sulfate." *Unsaturated Soils 2006*, 906-915, ASCE.

Agus, S. S., and Schanz, T. (2008). "A method for predicting swelling pressure of compacted bentonites." *Acta Geotechnica*, 3(2): 125-137.

Aurora, R.P., Peterson, E.H., and O'Neill, M.W. (1981). "Model Studies of Long Piles in Clays." *Proceedings 13th Offshore Technology Conference*: 331-338.

Amir, J.M., and Sokolov, M. (1976). "Finite element analysis of piles in expansive soils." *Journal of Soil Mechanics and Foundations, ASCE*, 102: 701-20.

Al-Shamrani, M. (2004). "Influence of lateral restraint on the swelling behavior of expansive soils." *Geotechnical Engineering*, 35(3): 101-112.

Al-Rawas, A. A., and Qamaruddin, M. (1998). "Construction problems of engineering structures founded on expansive soils and rocks in northern Oman." *Building and Environment*, 33: 159-171.

Al-Rawas, A. A., and Goosen, M. F. A. (2006). Expansive soils, Recent advances in characterization and treatment, Taylor and Francis, London.

Al-Shamrani, M. A., and Dhowian, A. W. (2003). "Experimental study of lateral restraint effects on the potential heave of expansive soils." *Engineering Geology*, 69(1): 63-81.

Al-Homoud, S., Basma, A., Malkawi, H., and Bashabsheh, A. (1995). "Cyclic swelling behaviour of clays." *Journal of Geotechnical Engineering (ASCE)*, 121(7): 562-565.

Aytekin, M. (1992). "Finite element modeling of lateral swelling pressure distributions behind earth retaining structures." Ph.D thesis, Texas Tech University, Lubbock, TX, USA.

Abbas, M. F., Elkady, T. Y., and Al-Shamrani, M. A. (2015). "Evaluation of strain and stress states of a compacted highly expansive soil using a thin-walled odometer." *Engineering Geology*, 193: 132-145.

Benvenga, M. M. (2005). “Pier-soil adhesion factor for drilled shaft piers in expansive soil.” Master’s thesis, Colorado State Univ., Fort Collins, CO.

Brignoli, E. G. M., and Stokoe, K. H., II, (1996), “Measurement of shear waves in laboratory specimens by means of piezoelectric transducers.” *Geotechnical Testing Journal*, 19(4): 384-397.

Bohn, C., Lopes dos Santos, A., and Frank, R. (2016). “Development of axial pile load transfer curves based on instrumented load tests.” *Journal of Geotechnical and Geoenvironmental Engineering*, 143(1): 04016081.

Borana, L., Yin, J. H., Singh, D. N., and Shukla, S. K. (2015). “A modified suction-controlled direct shear device for testing unsaturated soil and steel plate interface.” *Marine Georesources and Geotechnology*, *33*(4): 289-298.

Borana, L., Yin, J. H., Singh, D. N., and Shukla, S. K. (2016). “Interface behavior from suction controlled direct shear test on completely decomposed granitic soil and steel surfaces.” *International Journal of Geomechanics*, *16*(6): D4016008.

Brackley, I.J.A. (1975). “Swell under load.” Proceeding of 6th Regular Conference for Africa, Durban, 1975.

Basma, A. A., Al-Homoud, A. S., and Husein, A. (1995). “Laboratory assessment of swelling pressure of expansive soils.” *Applied Clay Science*, 9(5): 355-368.

Brackley, I.J.A., and Sanders, P.J. (1992). “In-situ measurement of total natural horizontal stresses in an expansive clay.” *Géotechnique*, 42(2): 443-451.

Basma, A.A., Al-Homould, A.S., Husein, M., and Ai-Bashabsheh, M.A. (1996). “Swelling-shrinkage behavior of natural expansive clays.” *Applied Clay science*, 11(2-4): 211-277.

Cooling, L.F., and Skempton, A.W. (1942). “A laboratory study of London clay.” *Journal of Institution of Civil Engineers*. 17: 251-276.

Cox, J.B. (1970). “A review of the geotechnical characteristics of the soils in the Adelaide city area.” Symp. On Soil and Earth Structures in Arid Climates, Inst. Eng., Aust. And Aust. Geomech. Soc., Adelaide: 72-86.

Coyle, H.M., and Sulaiman, I.H. (1967). “Skin friction for steel pile in sand.” *Journal of the Soil Mechanics and Foundations Division*, 93(SM6): 261-278.

Chapel, T. A. (1998). “Field investigation of helical and concrete piers in expansive soils.” M.S. thesis, Colorado State Univ., Fort Collins, CO.

Cambefort, H. (1964). "Essai sur le comportement en terrain homogène des pieux isolés et des groupes de pieux." *Annales de l'lnstitut Technique du Bâtiment et des Travaux Publics*, Paris, France: 1479-1518.

Chen, F.H. (1988). Foundations on Expansive Soils. ELSEVIER, Denver, Colorado, USA.

Chen, R.P., Zhou, W.H., Cao, W.P., and Chen, Y.M. (2007). "Improved hyperbolic model of load-transfer for pile-soil interface and its application in study of negative friction of single piles considering time effect." *Yantu Gongcheng Xuebao* (*Chinese Journal of Geotechnical Engineering*), 29(6): 824-830.

Callaghan, I.C., and Ottewill, R.H. (1974). "Interparticle forces in montmorillonite gels." *Faraday Discussions of the Chemical Society*, 57: 110-118.

Croney, D., and Coleman, J. D. (1954), "Soil structure in relation to soil suction (pF)." *Journal of Soil Science*. 5 (1): 75-84.

Clayton, C. R. I., Symons, I. F., and Hiedra-Cobo, J. C. (1991). "The pressure of clay backfill against retaining structures." *Canadian Geotechnical Journal*, 28: 282-297.

Comodromos, E. M., Papadopoulou, M. C., and Rentzeperis, I. K. (2009). "Pile foundation analysis and design using experimental data and 3-D numerical analysis." *Computers and Geotechnics*, 36(5): 819-836.

Coulomb, C.A. (1776). "Essai sur une application des regles de maximis et minimis a quelques problemes de statique, relatifs a l'architecture." *Memories de Mathematique dt de Physique presents a l'Acedemie Royale des Sciences*, Paris 1773(7): 343-382.

Chowdhury, M., and Hoque, R. (2013). "Shear strength properties of compacted expansive soils." Ph.D thesis, Faculty of Graduate Studies and Research, University of Regina.

Çimen, Ő., Keskin, S. N., and Yıldırım, H. (2012). "Prediction of swelling potential and pressure in compacted clay." *Arabian Journal of Science and Engineering*, 37(6): 1535-1546.

Coyle, H. M., and Reese, L. C. (1966). "Load transfer for axially loaded piles in clay." Journal of the Soil Mechanics and Foundations Division, 92(2): 1-26.

Caquot, A., and Kerisel, J. (1948). Tables for the calculation of passive pressure, active pressure and bearing capacity of foundations. Gauthier-Villars, Paris.

Cooke, R.W. 1974. "The settlement of friction pile foundations." *Proceeding of Conference on Tall Buildings*, Kuala Lumpur, Malaysia.

Das, B. M. 2015. Principles of foundation engineering. Cengage learning.

Durkee, D. B. (2000). “Active zone depth and edge moisture variation distance in expansive soils.” Ph.D thesis, Colorado State Univ., Fort Collins, CO.

Dif, A. E., and Bluemel, W. F. (1991). “Expansive soils under cyclic drying and wetting.” *Geotechnical Testing Journal*, *Technical Note*, 14 (1): 96-102.

Daniel, D.E. (1984). “Predicting hydraulic conductivity of clay liners.” *Journal of Geotechnical Engineering*, ASCE, 110(2): 285-300.

Ertugrul, O. L., and Trandafir, A. C. (2011). “Reduction of lateral earth forces acting on rigid nonyielding retaining walls by EPS geofoam inclusions.” *Journal of Materials in Civil Engineering*, 23 (12): 1711-1718.

Ellison, R.D., D'Appolnia, E., and Thiers, G.R. (1971). “Load deformation mechanism for bored piles.” *Journal of Soil Mechanics and Foundations*, 97: 589-733.

Ertekin, Y. (1991). “Measurement of lateral swell pressure with thin wall odometer technique.” M.S thesis, in Civil Engineering, Middle East Technical University, Ankara, Turkey.

Estabragh, A. R., Moghadas, M., and Javadi, A. A. (2013). “Effect of different types of wetting fluids on the behaviour of expansive soil during wetting and drying.” *Soils and Foundations*, 53(5): 617-627.

Estabragh, A. R., Parsaei, B., and Javadi, A. A. (2015). “Laboratory investigation of the effect of cyclic wetting and drying on the behaviour of an expansive soil.” *Soils and Foundations*, 55(2): 304-314.

Elsbury , B.R., Daniel, D.E., Sraders, G.A., and Anderson, D.C. (1990). “Lessons learned from a compacted clay liner.” *Journal of Geotechnical Engineering*, ASCE, 111 (4): 465-478.

Ekshtein, L. I. (1978). “Investigation of the uplift of pile groups in swelling soils.” *Soil Mechanics and Foundation Engineering*, 15(3): 170-171.

Escario, V., and Saez, J. (1986). “The Shear Strength of Partly Saturated Soils." *Géotechnique*, 36(3): 453-456.

Edil, T. B., and Alanazy, A. S. (1992). “Lateral Swelling Pressures.” *Proceedings of 7th International Conference on Expansive Soils*, Dallas, Texas: 227-232.

Fleming, I. R., Sharma, J. S., and Jogi, M. B. (2006). “Shear strength of geomembrane–soil interface under unsaturated conditions.” *Geotextiles and Geomembranes*, *24*(5): 274-284.

Fredlund, D.G., and Morgenstern, N.R. (1976). “Constitutive relations for volume change in unsaturated soils.” *Canadian Geotechnical Journal*, 13(3): 261-276.

Fourie, A.B. (1988). “Laboratory evaluating of lateral swelling pressure.” *Journal of Geotechnical Engineering*, 115(10): 1481-1485.

Fan, Z. H., Wang, Y. H., Xiao, H. B., and Zhang, C. S. (2007). “Analytical method of load-transfer of single pile under expansive soil swelling.” *Journal of Central South University of Technology*, *14*(4): 575-579.

Fan, Z.H. (2007). “Research on swelling-shrinkage characteristic and pile-soil interaction of expansive soil foundation.” Ph.D thesis, Central South University, Changsha, China. (In Chinese)

Fredlund, D.G., and Rahardjo, H. (1993). “Soil mechanics for unsaturated soils.” John Wiley and Sons, New York.

Fredlund, D.G., Morgenstern, N.R., and Widger, R.A. (1978). “The shear strength of unsaturated soils.” *Canadian Geotechnical Journal*, 15: 313-321.

Fredlund, D. G., and Xing, A. (1994). “Equations for the soil-water characteristic curve.” *Canadian geotechnical Journal*, 31(4): 521-532.

Fredlund, D. G., Rahardjo, H., and Fredlund, M. D. (2012). Unsaturated soil mechanics in engineering practice, Wiley, Hoboken, NJ.

Fredlund, D. G. (2018). “State of Practice for use of the Soil-Water Characteristic Curve in Geotechnical Engineering.” *Canadian Geotechnical Journal*, (ja).

Gan, J. K. M., Fredlund, D. G., and Rahardjo, H. (1988). “Determination of the shear strength parameters of an unsaturated soil using the direct shear test.” *Canadian Geotechnical Journal*, 25(3): 500-510.

Gambin, M. (1963). “Calcul du tassement d’une fondation profonde en fonction des résultats pressiométriques.” *Sol-Soils*, 7: 11-28.

Goode, J. C. (1982). “Heave prediction and moisture migration beneath slabs on expansive soils.” M.S. thesis, Colorado State Univ., Gu, X.W. (2005). “Study on the interaction between unsaturated expansive soils and structure.” M.S thesis, Nanjing Hydraulic Research Institute, Nanjing, China (In Chinese).

Gourley, C.S., Newill, D., and Schreiner, H.D. (1993). “Expansive soils, TRL's research strategy.” *Proceeding of 1st International Symposium, Engineering Characteristics of Arid Soils*.

Gokhale, K. V. G. K., and Jain, K. K. (1972). “Anisotropic Swelling in Black Cotton Soil.” *Bulletin of the International Association of Engineering Geology*, Paris, 5: 63-72.

Huang, H. C., Tan, Y. C., Liu, C. W., and Chen, C. H. (2005). “A novel hysteresis model in unsaturated soil.” *Hydrological Processes: An International Journal*, 19(8): 1653-1665.

Hogarth, W. L., Hopmans, J., Parlange, J. Y., and Haverkamp, R. (1988). “Application of a simple soil-water hysteresis model.” *Journal of Hydrology*, 98(1-2): 21-29.

Hong, G. T. (2008). “Earth Pressures and Deformations in Civil Infrastructure in Expansive Soils.” Ph.D Dissertation, Texas A & M University, College Station, Texas, USA.

Herbert, H.-J., and Moog, H.C. (2000). “Modelling of saturation and swelling effects in clays under different saline conditions.” *In Eurosafe Forum 2000*, Seminar 4, Waste management.

Han, Z., Vanapalli, S. K. and Kutlu, Z. N. (2016). “Modeling behavior of friction pile in compacted glacial till.” *International Journal of Geomechanics*, 16(6), D4016009.

Hanson, J.L., Gilbert, R.B., Wright, S.G., and Thiel, R.S. (2001). “Unsaturated Interface Shear Strength Properties for Nonwoven Geotxtiles.” *Proceedings of Geosynthetics conference*, Portland, Oregon USA: 135-148.

Hamid, T. B., and Miller, G. A. (2009). “Shear strength of unsaturated soil interfaces.” *Canadian Geotechnical Journal*, *46*(5): 595-606.

Hossain, M. A., and Yin, J. H. (2010). “Behavior of a compacted completely decomposed granite soil from suction controlled direct shear tests.” *Journal of Geotechnical and Geoenvironmental Engineering*, ASCE, 136(1): 189-198.

Hossain, M. A., and Yin, J. H. (2013). “Unsaturated soil-cement interface behaviour in direct shear tests.” *Australian Geomechanics Journal*, 48(3): 141-154.

Hatami, K., and Esmaili, D. (2015). “Unsaturated soil–woven geotextile interface strength properties from small-scale pullout and interface tests.” *Geosynthetics International*, *22*(2): 161-172.

Ikizler, S.B., Aytekin, M., and Nas, E. (2008). “Laboratory study of expanded polystyrene (EPS) geofoam used with expansive soils.” *Geotextiles and Geomembranes,* 26 (2): 189-195.

Ikizler, S. B., Vekli, M., Dogan, E., Aytekin, M., and Kocabas, F. (2012). “Prediction of swelling pressures of expansive soils using soft computing methods.” *Neural Computing and Applications*, 24(2): 1-13.

Jaky, J. (1944). “The coefficient of earth pressure at rest.” *Journal of the Society of Hungarian Architects and Engineers*, 78(22): 355-358.

Janbu, N. (1957). “Earth pressure and bearing capacity calculations by generalized procedure of slices.” *In Proceedings of the 4th International Conference on Soil Mechanics and Foundation Engineering*, London, 2: 207-212.

Justo, J.L., Rodriguez, J.E., Delgado, A. and Jaramillo, A. (1984). “A finite element method to design and calculate pier foundations in expansive soils.” *Proceedings of 5th International Conference on Expansive Soils,* Adelaide, Australia: 119-123.

Jaksa, M. B. (1995). “The influence of spatial variability on the geotechnical design properties of a stiff, overconsolidated clay.” Ph.D thesis. University of Adelaide, Australia.

Jaremski, J. (2012). “Application of the joining pile for foundations on expansive clays and rocks.” *American International Journal of Contemporary Research*, 2(10): 53-58.

Jiang, Z.X., and Qin, X.L. (1991). “A new method for calculating lateral swell pressure in expansive soil.” *Proceeding of 7th International Conference on Expansive Soils*, Dallas, Texas, 1: 233-238.

Joshi R. P., and Katti, R. K. (1980). “Lateral pressure development under surcharges.” *Proceeding of 4th International Conference on expansive soils*, Denver, CO: 227-241.

Krasiński, A. (2012). “Proposal for calculating the bearing capacity of screw displacement piles.” *Studia Geotechnica et Mechanica*, 34(4): 41-51.

Kuwabara, F. (1989). “An elastic analysis for piled raft foundations in a homogeneous soil.” *Soils and Foundations*, 29(1): 82-92.

Kuwabara, F., and Poulos, H. G. (1989). “Downdrag forces in group of piles.” *Journal of Geotechnical Engineering*, ASCE, 115(6): 806-818.

Khoury, C. N., Miller, G. A., and Hatami, K. (2010). “Shear strength of unsaturated soil-geotextile interfaces.” In *GeoFlorida 2010, Advances in Analysis, Modeling and Design*: 307-316.

Komornik, A., and Zeitlen, J.G. (1965). “An apparatus for measuring lateral soil swelling pressure in the laboratory.” *Proceeding of the 6th International Conference on Soil Mechanics and Foundation Engineering*, Canada, 1: 278-281.

Katti, R.K., Katti, D.R., and Katti, A.R. (2002). “Behavior of saturated expansive soil and control methods.” revised and enlarged edition, The Netherlands, Balkema.

Katti, R. K., Bhangle, E. S., and Moza, K. K. (1983), “Lateral earth pressure of expansive soil with and without a cohesive non-swelling soil layer- Applications to earth pressures of cross drainage structures of canals and key walls of dams (studies of K_0 condition).” *Central Board of Irrigation and Power. Technical Report No. 32*, New Delhi, India.

Komornik, A., and Livneh, M. (1968). “The effect of anisotropy on swelling of a compacted clay.” *Proceeding 3rd Asian Regional Conference on Soil Mechanics and Foundation Engineering*, 2: 181-185.

Kassiff, G., and Zeitlen, J.G. (1962). “Behaviors of Pipes Buried in Expansive Clays.” *Proceeding of ASCE*, *Journal of Soil Mechanics and Foundation Engineering*, SM 2, No. 3103.

Kraft Jr, L. M., Ray, R. P., and Kagawa, T. (1981). “Theoretical t-z curves.” *Journal of Geotechnical and Geoenvironmental Engineering*, 107(ASCE 16653).

Klausner, Y. 1991. Fundamentals of continuum mechanics of soils. Springer-Verlag, New York.

Kim, M.H., and O’Neill, M.W. (1998). “Side Shear Induced in Drilled Shaft by Suction Change.” *Journal of Geotechnical and Geoenvironmental Engineering*, ASCE, 124(8): 771-780.

Lu, N., and Likos, W.J. (2004). Unsaturated soil mechanics, Wiley Hoboken, NJ.

Likos, W. J., Lu, N., and Godt, J. W. (2013). “Hysteresis and uncertainty in soil water-retention curve parameters.” *Journal of Geotechnical and Geoenvironmental Engineering*, 140(4), 04013050.

Luna, R., and Jadi, H. (2000). “Determination of dynamic soil properties using geophysical methods.” *Proceeding of the First International Conference on the Application of Geophysical and NDT Methodologies to Transportation Facilities and Infrastructure,* St. Louis, MO.

Lu, N., and Kaya, M. (2014). “Power law for elastic moduli of unsaturated soil.” *Journal of Geotechnical and Geoenvironmental Engineering*, 140(1): 46-56.

Lo Presti, D., Pallara, O., Lancelotta, R., Amandi, M., and Maniscalco, R. (1993). “Monotonic and cyclic loading behavior of two sands at small strains.” *Geotechnical Testing Journal*, 16(4): 409-424.

Liu, Y., and Vanapalli, S.K. (2018). “Mechanical behaviors of geotechnical infrastructures in expansive soils under the influence of environmental factors.” Submitted to *Canadian Geotechnical Journal*.

Lambe, T.W. (1958). “The Structure of Compacted Clay.” *Journal of the Soil Mechanical and Foundation Division* (*ASCE),* 84: 1-35.

Liu, J., Xiao, H. B., Tang, J., and Li, Q.S. (2004). “Analysis of load-transfer of single pile in layered soil.” *Computers and Geotechnics*, 31(2): 127-135.

Liu, H.L., Deng, A., and Chu, J. (2006). “Effect of different mixing ratios of polystyrene prepuff beads and cement on themechanical behavior of lightweight fill.” *Geotextiles and Geomembranes*, 24 (6): 331-338.

Liu, Y., and Vanapalli, S. K. (2017). “Influence of Lateral Swelling Pressure on the Geotechnical Infrastructure in Expansive Soils.” *Journal of Geotechnical and Geoenvironmental Engineering*, 143(6), 04017006.

Lytton, R.L. (1977). “Foundations in expansive soils.” *Numerical methods in geotechnical engineering*. C.S. Desai and J.T. Christan, (Eds.), McGraw Hill Book Company.

Lingwall, B., and Bartlett, S. (2014). “Full-scale testing of an EPS geofoam cover system to protect pipelines at locations of lateral soil displacement.” *Pipelines*: 605-615.

Mualem, Y. (1977). “Extension of the similarity hypothesis used for modeling the soil water characteristics.” *Water Resources Research*, 13(4): 773-780.

Mady, A. Y., and Shein, E. (2018). “Modelling and validation hysteresis in soil water retention curve using tomography of pore structure.” *International Journal of Water*. 12(4): 370-381.

Mohamed, O.Z., Taha, Y.K., and El-Aziz, E.M. (2013). “Field study of the distribution of lateral swelling pressure of expansive soil on the retaining structure.” *Journal of Engineering Sciences*, Assiut University, Faculty of Engineering, 42(2): 289-302.

Mayne, P.W., and Kulhawy, F.H. (1982). “K_0–OCR relationships in soil.” *Journal of the Geotechnical Engineering Division (ASCE),* 108(GT6): 851–872.

Moza, K.K., Katti, R.K., and Katti, D.R. (1987). “Active pressure studies in saturated expansive soil.” *Proceedings of the Eighth Asian Regional Conference on Soil Mechanics and Foundation Engineering*, Kyoto, Japan: 189-192.

Mendonça, A. V., and De Paiva, J. B. (2000). “A boundary element method for the static analysis of raft foundations on piles.” *Engineering Analysis with Boundary Elements*, 24(3): 237-247.

Ministry of Housing and Urban-Rural Development of the People's Republic of China (MOHURD). (2013). Technical code for building in expansive regions, China Architecture and Building Press, Beijing.

Mašín, D., and Khalili N. (2016). “Swelling phenomena and effective stress in compacted expansive clays.” *Canadian Geotechnical Journal*, 53(1): 134-147.

Mohamed, O.Z., Taha, Y.K., and El-Aziz, E.M. (2014). “Field study of the distribution of lateral swelling pressure of expansive soil on retaining structure.” *Journal of Engineering Sciences*, 42(2): 289-302.

Mohamedzein, Y.E.A., Mohamed, M.G., and El Sharief, A.M. (1999). “Finite-element analysis of short piles in expansive soils.” *Computer and Geotechnics*, 24(3): 231-243.

Mohamedzein, YE-A. (1989). “Non-linear Finite element analysis of soil culvert interaction.” Ph.D. thesis, School of Civil Engineering, Purdue University, West Lafayette, IN.

Mandolini, A., and Viggiani, C. (1997). “Settlement of piled foundations.” *Géotechnique*, 47(4): 791-816.

Merchán, V., Vaunat, J., Romero, E., and Meca, T. (2008). “Experimental study of the influence of suction on the residual friction angle of clays.” CRC Press: 423-428.

Morris, P.H., Graham, J., and Williams, D.J. (1992). “Cracking in drying soils.” *Canadian Geotechnical Journal*. 29: 263-277.

Mendoza, C. (2013). “Measurement of friction on piles over neutral plane in expansive soils.” Advances in unsaturated soils-Caicedo et al. (eds). Taylor & Francis Group, London, ISBN 978-0-415-62095-6.

Nanda, S., and Patra, N.R. (2013). “Theoretical load-transfer curves along piles considering soil nonlinearity.” *Journal of Geotechnical and Geoenvironmental Engineering*, 140(1): 91-101.

Nusier, O. K., and Alawneh, A. S. (2004). “Micropile technique to control upward movement of lightweight structures over expansive soils.” *Geotechnical and geological engineering*, *22*(1): 89-104.

Nusier, O.K., Alawneh, A.S., and Rabadi, R.(2007). “Micropiles reinforcement for expansive soils, large-scale experimental investigation.” *Ground Improvement*, 11(2): 55–60.

Nelson, J.D., Chao, K.C., Overton, D.D., and Nelson, E.J. (2015). “Foundation Engineering for Expansive Soils.” John Wiley and Sons, Hoboken, New Jersey, USA.

Nelson, J.D., and Miller, D.J. (1992). “Expansive soils, problems and practice in foundation and pavement engineering.” New York, John Wiley and Sons: 117-144.

Nagaraj, H., Munnas, M., and Sridharan, A. (2010). “Swelling behavior of expansive soils.” *International Journal of Geotechnical Engineering*, 4(1): 99-110.

Nelson, J.D., Overton, D.D., and Durkee, D.B. (2001). “Depth of wetting and the active zone.” *Expansive clay soils and vegetative influence on shallow foundations*, ASCE Geotechnical special publications, 116: 95-109.

Nelson, J. D., Thompson, E. G., Schaut, R. W., Chao, K. C., Overton, D. D., and Dunham-Friel, J. S. (2011). “Design procedure and considerations for piers in expansive soils.” *Journal of Geotechnical and Geoenvironmental Engineering*, 138(8): 945-956.

Nagaraj, H. B., Munnas, M., and Sriharan, A. (2009). “Critical evaluation of determining swelling pressure by swell-load method and constant volume method.” *Geotechnical Testing Journal*, ASTM, 32(4): 1-10.

O'Neill, M.W. (1988). “Adaptive model for drilled shafts in expansive clay.” *Proceeding of Geotechnical and Eng*ineering *Division*, National Convention, ASCE, New York: 1-22.

Ofer, Z. (1980). “Instruments for laboratory and in-situ measurements of lateral swelling pressure of expansive clays.” *Proceeding of 4th International Conference on Expansive Soils*, ASCE and International Society for Soil Mechanics and Foundation Engineering, Denver: 45-53.

Ofer, Z. (1981). “Laboratory Instrument for Measuring Lateral Soil Pressure and Swelling Pressure.” *Geotechnical Testing Journal*, 4(4): 177-182.

Oh, W. T., and Vanapalli, S. K. (2013). “Scale effect of plate load tests in unsaturated soils.” *International Journal of Geomate*, 4(2): 585-594.

Oloo, S. Y., and Fredlund, D. G. (1996). “Scale effect of plate load tests in unsaturated soils A method for determination of φ_b for statically compacted soils.” *Canadian Geotechnical Journal*, 33(2): 272-280.

O’neill, M. W. and Poormoayed, N. (1980). “Methodology for foundations on expansive clays.” *Journal of the Geotechnical Engineering Division*, 106 (GT12): 1345 -1367.

Overton, D. D., Chao, K. C., and Nelson, J. D. (2007). “Heave distress of a manufacturing building.” Proceeding of Geo-Denver 2007: Contemporary Issues in Deep Foundations, ASCE, Reston, VA.

Osman, M., and Elsharief, A. M. (1999). “Field experiments on piles in the expansive soils of central Sudan.” *Journal of Building and Road Research*, 2: 17–26.

Pham, H. Q., Fredlund, D. G., and Barbour, S. L. (2005). “A study of hysteresis models for soil-water characteristic curves.” *Canadian Geotechnical Journal*, 42(6): 1548-1568.

Pham, H. Q., Fredlund, D. G., and Barbour, S. L. (2003). “A practical hysteresis model for the soil-water characteristic curve for soils with negligible volume change.” *Géotechnique*, 53(2): 293-298.

Pusch, R. (2006). “Mechanical properties of clays and clay minerals.” *Developments in clay science*, 1: 247-260.

Poulos, H. G., and Davis, E. H. (1980). Pile foundation analysis and design, Wiley, New York.

Poulos, H. G. (1993). “Piled rafts in swelling or consolidating soils.” *Journal of Geotechnical Engineering*, 119: 374-380.

Puppala, A.J., and Cerato, A. (2009). “Heave distress problems in chemically-treated sulfate-laden materials.” *Geo-Strata*, 10(2): 28-30, 32.

Puppala, A. J., Wattanasanticharoen, E., Dronamraju, V. S. and Hoyos, L. R. (2007). “Ettringite Induced Heaving and Shrinking in Kaolinite Clay.” *In Problematic Soils and Rocks and In Situ Characterization*: 1-10.

Puppala, A. J., Pedarla, A., Hoyos, L. R., Zapata, C. and Bheemasetti, T. V. (2016). “A semi-empirical swell prediction model formulated from clay mineralogy and unsaturated soil properties.” *Engineering Geology*, 200: 114-121.

People's Republic of China Ministry of Construction. (2008). Technical Code for Building Pile Foundations (JGJ 94- 2008), China Architecture & Building Press, Beijing, China.

Porter, A. A. (1977). “The mechanics of swelling in expansive clays.” M.S. thesis, Colorado State Univ., Fort Collins, CO.

Reeves, J.N., and Filz, G.M. (2000). “Earth Force Reduction by a Synthetic Compressible Inclusion.” Report of Research Conducted under the Sponsorship of Geo-Tech Systems Corporation and Virginia' S Center for Innovative Technology. Dept. of Civil Engineering, Virginia Tech., Blacksburg, VA.

Rahardjo, H., Melinda, F., Leong, E.C., and Rezaur, R.B. (2011). “Stiffness of a compacted residual soil.” *Engineering Geology*, 120(1-4): 60-67.

Richards, B.G., and Kurzeme, M. (1973). “Observations of Earth Pressures on a Retaining Wall at Gouger Street Mail exchange, Adelaide.” *Australian Geomechanics Journal*, G3 (1): 21-26.

Robertson, A.M.G., and Wangener, F.V.M. (1975). “Lateral swelling pressure in active clay.” *6th Conference for Africa on Soil Mechanics and Foundation Engineering, Durban*, South Africa: 107-114.

Ranjan, G., and Rao, A.S.R. (2000). “Basic and applied soil mechanics (second edition).” New Age International (P) Ltd, New Delhi, India.

Rao, S. M., Reddy, B. V. V., and Muttharam, M. (2001). “The impact of cyclic wetting and drying on the swelling behavior of stabilized expansive soils.” *Engineering Geology*, 60: 223-233.

Rankine, W.M. (1857). “On the stability of loose earth.” *Philosophical Transactions of the Royal Society of London*, 147: 9-27.

Rosenbalm, D., and Zapata, C. E. (2016). “Effect of wetting and drying cycles on the behavior of compacted expansive soils.” *Journal of Materials in Civil Engineering*, 29(1), 04016191.

Russam, K., and Coleman, J. D. (1961). “The effect of climatic factors on subgrade moisture conditions.” *Géotechnique,* 11(1): 22-28.

Randolph, M.F., and Wroth, C.P. (1978). “Analysis of deformation of vertically loaded piles.” *Journal of the Geotechnical Engineering Division*, ASCE, 104(12): 1465-1488.

Reichler, D. K. (1997). “Investigation of variation in swelling pressure values for an expansive soil.” M.S. thesis, Colorado State Univ., Fort Collins, CO.

Sarsby, R. (2000). Environmental Geotechnics. Thomas Telford Publishing, Thomas Telford Ltd, 1 Heron Quay, London, England.

Shelke A.P., and Murty D.S. (2010). “Reduction of swelling pressure of expansive soils using EPS Geofoam.” *Indian Geotechnical conference, IIT Mumbai,* (II): 495-498.

Saba, S., Barnichon, J. D., Cui, Y. J., Tang, A. M., and Delage, P. (2014). “Microstructure and anisotropic swelling behaviour of compacted bentonite/sand mixture.” *Journal of Rock Mechanics and Geotechnical Engineering*, 6(2): 126-132.

Sapaz, B. (2004). “Lateral versus vertical swell pressures in expansive soils.” M.S thesis, Middle East Technical University, Ankara, Turkey.

Seed, H.B., and Reese, L.C. (1957). “The action of soft clay along friction piles.” *Transactions of the American Society of Civil Engineers*, 122: 731-754.

Sharma, H. D., Dukes, M. T., and Olsen, D. M. (1990). “Field measurement of dynamic moduli and Poisson’s ratios of refuse and underlying soils at a landfill site.” *Geotechnics of waste landfills: Theory and practice, A. Landva and G. D. Knowles, eds., ASTM, West Conshohocken, PA,* 57-70.

Shields, D.H., and Tolunay, A.Z. (1973). “Passive pressure coefficients by method of slices.” *Journal of the Soil Mechanics and Foundations Division, ASCE*, 99 (12): 1043-1053.

Sun, Y., Shao, L., and Fan, Z. (2011). “Experimental research on Poisson's ratio of sandy soil.” *Geomechanics and Geotechnics, From Micro to Macro – Jiang et al. (eds).* Taylor and Francis Group, London: 433-438.

Skempton, A. W., and Henkel, D. J. (1957). “Tests on London clay from deep borings at Paddington, Victoria and South Bank.” *Proceeding of the 4th International Conference on Soil Mechanics and Foundation Engineering*, London: 100-106.

Said, I. D., De Gennaro, V., and Frank, R. (2009). “Axisymmetric finite element analysis of pile loading tests.” *Computers and Geotechnics*, 36(1): 6-19.

Sahin, H. (2011). “Characterization of expansive soil for retaining wall design.” M.S thesis, Texas A and M University, Texas, USA.

Soundara, B., and Robinson, R. G. (2017). “Hyperbolic model to evaluate uplift force on pile in expansive soils.” *KSCE Journal of Civil Engineering*, 21(3): 746-751.

Symons, I.F., and Clayton, C.R.I. (1992). “Earth pressures on backfilled retaining walls.” *Ground Engineering*: 26-34.

Seed, H.B., Woodward, Jr., and Lundgren, R. (1962). “Prediction of swelling potential for compacted clays.” *Journal of the Soil Mechanics and Foundations Division*, 88(3): 53-88.

Skempton, A.W. (1961). “Horizontal stresses in an over consolidated Eocene clay.” *Proceeding of 5th International Conference on Soil Mechanics and Foundation Engineering*, Paris, 1: 351-357.

Schanz, T., and Al-Badran, Y. (2014). “Swelling pressure characteristics of compacted Chinese Gaomiaozi bentonite GMZ01.” *Soils and Foundations*, 54(4): 748-759.

Sridharan, A., Rao, A. S., and Sivapullaiah, P. V. (1986). “Swelling pressure of clays.” *Geotechnical Testing Journal*, 9 (1): 24-33.

Symons, I. F., Clayton, C. R. I., and Darley, P. (1989). “Earth pressures against an experimental retaining wall backfilled with heavy clays.” *Transport and Road Research Lab. Research Report No. 192*, Crowthome, Berkshine.

Sharma, J. S., Fleming, I. R., and Jogi, M. B. (2007). “Measurement of unsaturated soil–geomembrane interface shear-strength parameters.” *Canadian Geotechnical Journal*, 44(1): 78-88.

Sheng, D., Eigenbrod, K. D., and Wriggers, P. (2005). “Finite element analysis of pile installation using large-slip frictional contact.” *Computers and Geotechnics*, 32(1): 17-26.

Suwal, L. P., and Kuwano, R. (2010). “Development of disc shaped pieze-ceramic plate transducer for elastic wave measurements in laboratory specimens.” *Seisan-Kenkyu*, *Bimonthly Journal of Institute of Industrial Science, The University of Tokyo*, 61(6): 123-128.

Suwal. L.P., and Kuwano, R. (2012). “Poisson's ratio evaluation on silty and clayed sands on laboratory specimens by flat disk shaped piezo-ceramic transducer.” *Bulletin of ERS, Institute of Industrial Science*, *The University of Tokyo*, 45: 141-158.

Sheard, M.J., and Bowman, G.M. (1994). “Soils, Stratigraphy and Engineering Geology of Near Surface Materials of Adelaide Plains.” S.A. Dept. Mines and Energy Report Book, 94/9, Adelaide.

Sivakumar, V., Zaini, J., Gallipoli, D., and Solan, B. (2015). “Wetting of compacted clays under laterally restrained conditions, initial state, overburden pressure and mineralogy.” *Géotechnique*, 65(2): 111-125.

Sudhindra, C., and Moza, K. K. (1987). “An approach for lateral pressure assessment in expansive soils.” *Proceeding of 6th International Conference of Expansive Soils*, Central Board of Irrigation and Power, New Delhi, India: 67-70.

Terzaghi, K. (1925). “Principles of soil mechanics, I-Phenomena of cohesion of clays.” *Engineering News-Record*, 95(19): 742-746.

Terzaghi, K. (1926). “The mechanics of adsorption and swelling of gels.” 4th Colloid Symposium Monograph, Chem. Catal. Co., New York: 58-78.

Terzaghi, K. (1931). “The influence of elasticity and permeability on the swelling of two-phase systems.” Colloid Chemistry, J. Alexander, ed., 3, New York, Chem. Catal. Co., 65-88.

Terzaghi, K. (1943). Theoretical soil mechanics. John Wiley and Sons, New York.

Trandafir, A.C., Bartlett, S.F., and Lingwall, B.N. (2010). “Behavior of EPS geofoam in stress controlled cyclic uniaxial tests.” *Geotextiles and Geomembranes*, 28 (6): 514-524.

Tatsuoka, F., and Shibuya, S. (1992). “Deformation Characteristics of Soils and Rocks from Field and Laboratory Tests.” *Proceeding of 9th Asian Regional Conf. of SMFE*, Bangkok, 2: 101-170.

Tatsuoka, F. and Kohata, Y. (1995). “Stiffness of hard soils and soft rocks in engineering applications.” Keynote Lecture, *Proceeding of International Symposium Pre-failure Deformation of Geomaterials (Shibuya et al., eds)*, Balkema, 2: 947-1063.

Tu, H., and Vanapalli, S. K. (2016). "Prediction of the variation of swelling pressure and one-dimensional heave of expansive soils with respect to suction using the soil-water retention curve as a tool." *Canadian Geotechnical Journal*, 53(8): 1213-1234.

Thomas, M. G., Puppala, A. J., Hoyos, L. R. (2009). "Influence of Swell Pressure from Expansive Fill on Retaining Wall Stability." *American Society of Civil Engineers Conference Proceedings*. 337 (75): 590-597.

Vu, H. Q., and Fredlund, D. G. 2004. "*The prediction of one, two- and three dimensional heave in expansive soils*." *Canadian Geotechnical Journal*, 4: 1-25.

Vaunat, J., Amador, C., Romero, E., and Djeran-Maigre, I. (2006). "Residual strength of a low plasticity clay at high suctions." *In Unsaturated Soils 2006*: 1279-1289.

Vaunat, J., Merchán, V., Romero, E., and Pineda, J. (2007). "Residual strength of clays at high suctions." *Theoretical and Numerical Unsaturated Soil Mechanics*: 151-163.

Vijayvergiya, V.N. (1977). "Load-movement characteristics of piles." *Ports '77, 4th Annual Symp. of the Waterway, Port, Coastal, and Ocean Division*, ASCE, Los Angeles: 269-284.

Vanapalli, S.K., Fredlund, D.G., Pufahl, D.E., and Clifton, A.W. (1996). "Method for the prediction of shear strength with respect to soil suction." *Canadian Geotechnical Journal*, 33(3): 379-392.

Vanapalli S.K., and Oh W.T. (2010). "A method for predicting the modulus of elasticity of unsaturated soils using the soil-water characteristic curve." *International Journal of Geotechnical Engineering*, 4(4): 425-433.

Vanapalli, S.K., Fredlund, D.G. and Pufahl, D.E. (1999). "The influence of soil structure and stress history on the soil-water characteristic curve of a compacted till." *Géotechnique*, 49: 143-159.

Vanapalli, S., and Lu, L. (2012). "A state-of-the art review of 1-D heave prediction methods for expansive soils." *International Journal of Geotechnical Engineering*, 6(1): 15-41.

Windal, T. and Shahrour, I. (2002). "Study of the swelling behavior of a compacted soil using flexible odometer." *Mechanics Research Communications*, 29: 375-382

Wang, N. X., Zhang, W., Gu, X.W. and Zeng, Y.J. (2008a). "Lateral swelling pressure of expansive soil acting on retaining wall due to inundation." *Journal of Hydraulic Engineering*, 39(5): 580-587. (In Chinese)

Wang, C.H., Liu, Q.C. and Li, B. (2008b). “Rankine's earth pressure theory considering roughness of wall back surface.” *Chinese Journal of Geotechnical Engineering*, 30(supp): 129-133.

Wu, Z. W., Song, H. Z., Wang, H. Y., Liu, C. J., and Jiang, Y. (2012). “Prototype experimental study of expansive force of pile embedded in expansive soil.” Rock and Soil Mechanics, 33(S2): 173-177.

Wu, H and Liu, Y.B. (2008). “The relationship between the plastic index and clay content in the soil classification.” *China municipal engineering*, 131: 62-63, 67 (in Chinese).

Xie, Y., Chen, Z.H., Sun, S.G., Li, G., and Fang, X.W. (2007). “Test research on three-dimensional swelling pressure of remolded expansive clay.” *Rock and Soil Mechanics*, 28(8): 1636-1642. (In Chinese)

Xiao, H. B., Zhong, H. H., and Wan, Y. H. (2003). “Analysis of pile’s load transfer in layered soils.” *Journal of Central South University Technology.*, 34(6): 687-690 (in Chinese).

Xiao, H. B., Luo, Q. Z., Tang, J., and Li, Q. S. (2002). “Prediction of load–settlement relationship for large- diameter piles.” *The Structural Design of Tall and Special Building*s, 11(4): 285-293.

Xiao, H. B., Zhang, C. S., Wang, Y. H., and Fan, Z. H. (2011). “Pile-soil interaction in expansive soil foundation, Analytical solution and numerical simulation.” *International journal of geomechanics*, 11(3): 159-166.

Yong, R.N. (1999). “Soil suction and soil-water potentials in swelling clays in engineered clay barriers.” *Engineering Geology*, 54: 3-13.

Yang, G.L., Teng, K., and Qin, C.H. (2014). “An in-situ experimental research of lateral swelling pressure on expansive soils.” *Journal of Central South University (Science and Technology)*, 45(7): 2326-2332.

Yeşil, M. M., Paşamehmetoğlu, A. G., and Bozdağ, T. (1993). “A triaxial swelling test apparatus.” *In International journal of rock mechanics and mining sciences and geomechanics abstracts*, 30(4): 443-450.

Zhang, D., Liu, S., and Zhang, T. (2012). “Water content and modulus relationship of a compacted unsaturated soil.” *Journal of Southeast University (English Edition)*, 28(2): 209-214.

Zhu, H., and Chang, M. F. (2002). “Load transfer curves along bored piles considering modulus degradation.” *Journal of Geotechnical and Geoenvironmental Engineering*, 128(9): 764-774.

Zhao, C.F., Lu, J., Sun, Q.C., Zhu, T., and Li, S.F. (2009). “Experimental study of load transmission property of large-diameter bored cast-in-situ deep and long pile in different soil layers.” *Chinese Journal of Rock Mechanics and Engineering*, 28(5): 1020-1026. (In Chinese).

Zarnani, S., and Bathurst, R.J. (2007). “Experimental investigation of EPS geofoam seismic buffers using shaking table tests.” *Geosynthetics International*, 14(3):165-177.

Zarnani, S., and Bathurst, R.J. (2008). “Numerical modeling of EPS seismic buffer shaking table tests.” *Geotextiles and Geomembranes*, 26 (5): 371-383.

Zhang, Q.Q., Zhang, Z.M., and He, J.Y. (2010a). “A simplified approach for settlement analysis of single pile and pile groups considering interaction between identical piles in multilayered soils.” *Computers and Geotechnics*, 37(7-8): 969-976.

Zhang, Q.Q., Zhang, Z.M., Yu, F., and Liu, J.W. (2010b). “Field performance of long bored piles within piled rafts.” *Proceedings of the institution of Civil engineers: Geotechnical Engineering*, 163(6): 293-305.

Zhang, Z.M., Zhang, Q.Q., and Yu, F. (2011a). “A destructive field study on the behavior of pile under tension and compression.” *Journal of Zhejiang University-Science A*, 12(4): 291-300.

Zhang, Z.M., Zhang, Q.Q., Zhang, G.X., and Shi, M.F. (2011b). “Large tonnage tests on super-long piles in soft soil area.” *Chinese Journal of Geotechnical Engineering*, 33(4): 535-543. (In Chinese)

Zhang, Q.Q. and Zhang, Z.M. (2012). “A simplified nonlinear approach for single pile settlement analysis.” *Canadian Geotechnical Journal*, 49: 1256-1266.